Injection Moulding of Natural Fibre Reinforced Polypropylene: Process, Microstructure and Properties

Ahmed Abdennadher

▶ **To cite this version:**

HAL Id: tel-01299794
https://pastel.hal.science/tel-01299794

Submitted on 8 Apr 2016

ParisTech
INSTITUT DES SCIENCES ET TECHNOLOGIES
PARIS INSTITUTE OF TECHNOLOGY

MINES
ParisTech

École doctorale n° 364 : Sciences Fondamentales et Appliquées

Doctorat ParisTech

T H È S E

pour obtenir le grade de docteur délivré par

l'École nationale supérieure des mines de Paris

Spécialité « Mécanique Numérique et Matériaux»

présentée et soutenue publiquement par

Ahmed ABDENNADHER

le 01 Décembre 2015

Injection Moulding of Natural Fibre Reinforced-Polypropylene:

Process, Microstructure and Properties

Injection de Polypropylène Renforcé de Fibres Naturelles:

Procédé, Microstructure et Propriétés

Directrice de thèse : **Tatiana BUDTOVA**
Directeur de thèse : **Michel VINCENT**

Jury

Mme Anne BERGERET, Professeur, C2MA, Mines d'Alès   Rapporteur

M. Gilles AUSIAS, Maître de conférences, LIMATB, Université de Bretagne-Sud, Lorient   Rapporteur

M. Jörg MÜSSIG, Professeur, Université de sciences appliquées de Brème- Allemagne   Examinateur

M. Johnny BEAUGRAND, Maître de recherche, INRA, Université de Reims Champagne Ardenne   Examinateur

M. Jean-Jacques FLAT, Docteur, Arkema, CERDATO, Serquigny   Examinateur

M. Michel VINCENT, Directeur de recherche, CEMEF, Mines ParisTech, Sophia Antipolis   Examinateur

Mme Tatiana BUDTOVA, Directeur de recherche, CEMEF, Mines ParisTech, Sophia Antipolis   Examinatrice

T
H
E
S
E

MINES ParisTech
CEMEF-UMR CNRS 7635
Rue Claude Daunesse CS 10207 - 06904 Sophia Antipolis Cedex, France

Acknowledgements

Table of Contents

Articles & Communications

This work has led to an article that is published in an international journal and three others are under progress. Several communications (oral presentations and posters) were given in national and international conferences.

Articles

Abdennadher, A., Vincent, M. and Budtova, T, "Rheological properties of molten flax- and Tencel®-polypropylene composites: Influence of fibre morphology and concentration J. Rheol. 60, 191 (2016)

Oral presentations

Abdennadher, A., Vincent M. and <u>Budtova</u> T., Microstructure of injected natural fibre reinforced propylene, "Matériaux" conference, Montpellier, France (November 2014)

<u>Abdennadher</u>, A., Vincent M. and Budtova T., Microstructure of injected natural fiber-polymer composite, American Society for Composites, 29th Technical Conference and 16th US-Japan Conference on Composite Materials, San Diego, USA, September (2014)

Abdennadher, A., Budtova T. and <u>Vincent</u> M., «Rheological properties of flax and Tencel® fiber reinforced polypropylene, Polymer Processing Society conference, Cleveland, USA (June 2014)

<u>Abdennadher,</u> A., Budtova T. and Vincent M., Rheological properties of molten natural fibre-polymer composite: cases of flax and Tencel®, 3rd EPNOE Conference Nice, France (October 2013)

<u>Abdennadher</u>, A, Vincent M., Budtova T., Rheological properties of molten natural fiber-polymer composite: Cases of flax and Tencel®, 41st JEPO conference, Aussois, France (September 2013)

Posters

Abdennadher, A.,Vincent M. and Budtova T., Microstructure of injected natural fiber-reinforced polypropylene, Natural fibres composite Workshop, Sophia-Antipolis, France (February 2015)

Abdennadher, A., Vincent M. and Budtova T., Rheological properties of molten natural fibre-polymer composite: Cases of flax and Tencel®, Mecamat conference, Aussois, France (January 2014)

Extended abstract of the thesis in French

Résumé étendu de la thèse

Introduction générale

Le réchauffement climatique et l'ampleur de l'effet des déchets non-biodégradables sur l'environnement sont devenus des problématiques d'actualité sur lesquelles les industriels se sont penchés. Cela a généré la mise en place de stratégies de développement durable qui encouragent à chercher une alternative aux matériaux fossiles à la fois respectueuse de l'environnement et garante de performances similaires.

Dans ce contexte, les fibres naturelles ont reçues une grande attention au cours des deux dernières décennies pour remplacer les fibres de verre comme renfort dans les composites polymères. En plus de leur aspect écologique, les principales raisons qui incitent à l'utilisation des fibres naturelles dans les composites sont leur faible coût et le gain en poids toute en gardant des propriétés mécaniques similaires aux composites à fibres de verre. La faible densité des fibres naturelles attire particulièrement le secteur des transports (automobile, ferroviaire, aéronautique…) très sensible à la réduction de poids. Les composites à fibres naturelles sont utilisés dans les automobiles pour des pièces intérieures comme des revêtements, des garnitures de tableaux de bord, des panneaux de porte... D'autres secteurs d'application des composites à fibres naturelles sont apparus comme le sport et loisirs (ski, snowboard, vélo...) grâce à leurs bonnes propriétés d'amortissement, les instruments de musique et haut-parleurs en raison de leurs excellentes performances acoustiques, ou aussi l'ameublement (bureau, chaise...) en raison de leurs aspect lorsque les fibres sont mélangés avec une matrice translucide.

Les fibres naturelles techniques utilisées comme renfort des polymères sont soit des fibres ligno-cellulosiques, provenant de tiges de plantes comme les lin, chanvre, jute et kenaf ou de graines (coton) ou de feuilles (sisal), soit des fibres à 100 % cellulosiques filées telles que les fibres Tencel (procédé Lyocell) ou viscose. Dans ce travail, deux types de fibres naturelles ont été utilisés, le lin et Tencel avec une matrice polypropylène, avec pour objectif :

- d'étudier et de comprendre l'influence des différentes compositions et morphologies de fibres :
  - sur la microstructure des composites, c'est à dire la taille, l'orientation et la concentration de fibres,
  - sur les propriétés rhéologiques et mécaniques qui en résultent,
- de vérifier si les modèles développés pour les fibres de verre peuvent prédire la pression pendant le remplissage de moule en injection et l'orientation des fibres naturelles dans des pièces moulées.

Les fibres de lin et Tencel sont différentes. Les composants principaux du lin sont la cellulose (64-81 %), l'hémicellulose (11-17 %), la lignine (2-3 %) et la pectine (2 %) tandis que Tencel est basée sur de la cellulose pure. De plus, elles présentent une morphologie différente. Tencel est une fibre élémentaire mince et flexible avec un diamètre uniforme (dû au procédé de filage), tandis que le lin est un «mélange» de fibres élémentaires semi-rigides minces et de faisceaux épais et rigides composés de fibres élémentaires assemblées. Enfin, leurs propriétés mécaniques intrinsèques sont également différentes. Il est donc supposé que ces différences de propriétés des fibres auront une influence sur la microstructure et les propriétés des composites.

En France, le lin de haute qualité est aujourd'hui cultivé dans les régions du nord (Normandie, Picardie et Nord-Pas-de-Calais) en raison des conditions climatiques modérées et du savoir-faire des liniculteurs. Avant d'être en mesure de renforcer un polymère, les fibres de lin sont soumises à un long cycle d'extraction comprenant le rouissage, la rupture, le teillage et le peignage. Plus de 80 % de la production de lin est aujourd'hui tournée vers l'industrie textile qui est leur application historique et seulement 10 % sont dédiés à un usage technique.

Le principal producteur de fibres de Tencel est la société autrichienne Lenzing qui nous a les aimablement fournies. La cellulose de base des fibres Tencel est extraite de la pulpe

principalement trouvée dans les eucalyptus. La cellulose est dissoute dans du N-méthylmorpholine-N-oxyde monohydrate, puis filtrée, centrifugée, filée, coagulée et séchée. En plus de leur utilisation principale dans l'industrie textile, les fibres Tencel sont couramment employées pour la fabrication de cordes ou des filtres automobiles.

Nous nous intéressons dans ce travail au polypropylène renforcé de fibres discontinues de lin et Tencel. Le mélange fibre/matrice se fait par extrusion bivis pour produire des granulés, qui sont ensuite transformés par injection. D'autres façons de fabriquer des composites thermoplastiques existent comme, par exemple, le moulage par compression. L'injection reste la méthode préférée pour fabriquer des pièces de géométries complexes avec une haute cadence et un faible coût de production. Le marché du moulage par injection est en pleine croissance avec l'augmentation des domaines d'application pour les composites à fibres naturelles. Le potentiel de ces matériaux combiné à la productivité du procédé d'injection satisfait au défi environnemental et à la performance industrielle. Toutefois, en raison de la complexité de choix et de la variété des fibres naturelles plusieurs questions subsistent.

Dans ce contexte, cette thèse a été lancée en octobre 2012 au Centre de Mise en Forme de Matériaux (Cemef) de Mines ParisTech, dans le cadre de la Chaire Industrielle Bioplastiques. Cette chaire est cofinancée par Mines ParisTech et cinq entreprises: Arkema, L'Oréal, Nestlé, PSA Peugeot Citroën et Schneider Electric. C'est un grand projet de recherche de 7 ans qui comprend différents thèmes dont l'objectif est de soutenir le développement et les applications de divers matériaux bio-sourcés (bioplastiques, matériaux ligno-cellulosiques et composites polymères à fibres naturelles). Une précédente thèse s'est déroulée dans le cadre de cette chaire portant sur le comportement et la rupture de fibres cellulosiques lors de leur compoundage avec une matrice polymère. La présente thèse vient compléter ce travail et se concentre sur l'étude et la compréhension des propriétés d'un polypropylène renforcé de fibres naturelles en abordant certaines questions autours du moulage par injection.

Problématiques

Les polymères renforcés de fibres de verre discontinues ont été largement étudiés et optimisés. La question principale ici est de savoir si les résultats et approches peuvent être étendus aux fibres naturelles. Les fibres de verre sont rigides, de diamètre constant et de propriétés uniformes. Comme mentionné ci-dessus, les fibres de lin techniques sont un

mélange de fibres élémentaires et de faisceaux. Pendant la mise en œuvre, les faisceaux se dissocient en faisceaux plus minces voire même en fibres élémentaires. En fonction de leur diamètre et longueur, les fibres de lin peuvent se présenter comme semi-rigides ou rigides. En outre, les fibres de lin sont un produit d'agriculture dont les propriétés varient avec les conditions de culture et d'extraction et la variété dont elles proviennent. Tout cela fait que leur morphologie est très différente de celle des fibres de verre. L'autre type de fibres de cellulose utilisée dans ce travail est Tencel. Ces fibres sont filées à partir d'une solution de cellulose, et donc leur morphologie, composition et propriétés sont bien contrôlées. Cependant, leur morphologie est très différente non seulement du verre mais aussi du lin. La principale différence avec des fibres de verre est que les fibres Tencel sont très flexibles, ce qui, a priori, ne permet pas d'adopter les approches développées pour des fibres de verre. Considérant tout cela, les points suivants seront précisés :

1) L'effet du procédé sur les fibres naturelles (rupture, dissociation en faisceaux) est crucial pour la compréhension de la microstructure au sein des pièces moulées par injection. Quelle différence d'endommagement entre lin, Tencel et verre va en avoir lieu pendant la mise en œuvre ? Quelle est l'ampleur de la casse des fibres pendant l'injection ? Quel est l'effet de la concentration sur la rupture des fibres ?

2) Les propriétés rhéologiques des polymères thermoplastiques renforcés de fibres naturelles à l'état fondu sont très importantes pour la simulation du procédé d'injection. Ces propriétés sont assez bien connues pour les composites à fibres de verre. Le comportement rhéologique des composites à fibres naturelles est-il similaire à celui des fibres de verre ? Quelle est l'influence du type de fibre et de leur flexibilité sur les propriétés viscoélastiques du composite à l'état fondu ?

3) Etant donné que la morphologie des fibres naturelles est différente de celle des fibres de verre, l'extrapolation aux fibres naturelles des méthodes utilisées pour caractériser la microstructure des composites à fibres de verre semble être discutable. Si elle s'avère impossible, une nouvelle méthode pour l'analyse de la distribution et de l'orientation des fibres doit être développée.

4) Comme les propriétés mécaniques des composites sont en corrélation directe avec la microstructure, les relations microstructure-propriétés devraient être étudiées pour la compréhension et pour l'amélioration des performances.

5) Dans le but d'optimiser les conditions d'injection pour les composites à fibres naturelles, il est essentiel de vérifier si les modèles d'orientation des fibres et de simulation du procédé existantes pour les thermoplastiques renforcés de fibres de verre sont adaptés aux polymères renforcés de fibres naturelles.

Pour répondre à ces questions, après l'introduction générale (Chapitre 1), la thèse se compose des parties suivantes :

Chapitre 2, qui décrit les matériaux et les méthodes utilisés dans cette étude

Chapitre 3, où la distribution de taille des fibres est analysée,

Chapitre 4, où la microstructure (orientation, concentration, courbures) des fibres est analysée

Chapitre 5, où le comportement rhéologique est mesuré

Chapitre 6, consacré au comportement mécanique

Chapitre 7, sur l'analyse et la simulation du procédé d'injection

Dans la suite nous allons présenter l'objectif de chaque chapitre et les principaux résultats trouvés.

Chapitre 2 : Matériaux et méthodes

Ce chapitre décrit les matériaux utilisés dans ce travail ainsi que les méthodes de préparation et de caractérisation de composites. Bien que ce travail concerne principalement les polymères thermoplastiques renforcés de fibres naturelles, l'étude est étendue aux fibres de verre pour comparaison. A titre de référence, le polypropylène pur a été également étudié.

Dans la première partie de ce chapitre, les informations sur tous les matériaux utilisés dans la présente étude ont été détaillées. Ensuite, les deux étapes de mise en forme, l'extrusion bivis et l'injection, ont été présentées. Les techniques expérimentales utilisées pour évaluer la microstructure des composites (microscopie optique et électronique), leurs propriétés

rhéologiques (en mode dynamique et capillaire) et leurs performances mécaniques (en tension et choc) ont été également décrites.

Chapitre 3 : Analyse de taille de fibres

Les fibres de lin, Tencel et de verre ont été mélangées avec le polypropylène par extrusion bivis en plusieurs concentrations. Les différents composites ont été injectés dans un moule en forme de boîte. La distribution de tailles des fibres a été analysée après mélange et après injection, par dissolution du polypropylène et analyse par microscopie optique, cartographie et analyse d'images. Les fibres de verre ont été fortement cassées pendant le mélange et relativement peu endommagées lors du moulage par injection. La réduction de longueur est nettement moindre pour les fibres Tencel®. Les fibres de lin voient leur longueur et leur diamètre réduits au cours des deux étapes, les faisceaux étant dissociés. Le rapport de forme est donc constant. Quel que soit le type de fibres, la casse est plus importante lorsque la concentration augmente.

Chapitre 4 : Orientation et dispersion des fibres dans des pièces injectées

La complexité de la morphologie des fibres de lin et Tencel a nécessité une nouvelle approche de caractérisation permettant la quantification de leur orientation, distribution et courbure. Des surfaces de coupes parallèles au plan de la boite ont été obtenues par polissage pour plusieurs niveaux dans l'épaisseur. Des images de ces sections ont été ensuite prises par microscopie optique en mode réflexion et analysées par un logiciel de traitement d'image semi automatiquement.

En fonction de leurs formes apparentes, les fibres ont été classées en quatre catégories: droites, en forme de C, en forme de S et particules ou fibres hors-plan. Nous avons démontré qu'à cause de la différence de flexibilité, les fibres Tencel peuvent se courber en deux conformations: en forme de C ou en forme de S, tandis que les fibres de lin élémentaires se courbent seulement en forme de C.

Les fibres sont généralement alignées dans la direction d'écoulement à la surface de boite et perpendiculairement à cette direction dans le plan médian. Le nombre de fibres Tencel est trois fois plus grand que celui de lin pour la même concentration en volume. Cela a été

expliqué par la présence de faisceaux dans le lin qui persistent et n'arrivaient pas à se dissocier après l'injection. En outre, comme pour les fibres de verre, la concentration de lin augmente de la surface au plan milieu dans l'épaisseur, alors que la concentration Tencel est pratiquement indépendante de l'épaisseur.

Chapitre 5 : Propriétés rhéologiques des composites

Les propriétés des différents polypropylènes renforcés ont été étudiées en géométrie plan-plan en mode dynamique et en rhéométrie capillaire, pour des concentrations en fibres de 0 à 30 % en poids et des températures comprises entre 180 et 200 °C. Les mesures rhéologiques dynamiques ont montré que l'augmentation de la teneur en fibres et de la flexibilité de fibres (cas de Tencel) conduit à l'augmentation de la viscosité complexe et des modules élastique et visqueux. Une contrainte seuil apparente a été identifiée à basses fréquences lorsque la concentration volumique de fibres atteint le régime concentré. Cela est dû aux interactions entre fibres qui sont encore plus marquées lorsque la flexibilité de la fibre augmente. Pour la même concentration, les composites à fibres Tencel présentent une viscosité et une contrainte seuil apparente modérément plus élevées que celles des composites de verre et largement supérieures à celles du lin. Ceci est dû à la haute flexibilité et au plus grand nombre des fibres Tencel.

L'influence de la température sur la viscosité des composites a été analysée en utilisant la loi d'Arrhenius permettant le calcul de l'énergie d'activation. Pour les trois types de composites, l'énergie d'activation augmente quand la teneur en fibres augmente. L'ajout de fibres au polypropylène semble augmenter la "résistance" du composite à s'écouler. Les composites Tencel présentent une énergie d'activation plus élevée par rapport à celle du lin et du verre. Nous suggérons que des restrictions supplémentaires aux mouvements de chaînes de polymères peuvent être causées par la structure en réseau de fibres extrêmement flexibles.

La superposition rhéologie capillaire/dynamique obéit à la loi de Cox-Merz. Les courbes maitresses comprenant les mesures en dynamique et capillaire ont été modélisées par l'équation de Carreau-Yasuda à seuil. Le résultat obtenu donne l'évolution de la viscosité pour une large gamme de taux de cisaillement. Ce sera une donnée d'entrée importante pour le calcul numérique de la pression et de l'orientation des fibres (Chapitre 7).

Chapitre 6 : Propriétés mécaniques des composites

L'influence de la microstructure sur les propriétés en traction des composites a été étudiée dans des éprouvettes prélevées dans les boites injectées, à différents angles par rapport à la direction principale d'écoulement. Les échantillons alignés avec cette direction présentent de meilleures propriétés en traction que ceux orientés à 45 ° et 90 ° pour tous les composites étudiés. Les composites à base de verre présentent un module d'Young et une résistance à la traction supérieurs aux composites à fibres de lin et de Tencel, et ce quel que soit la concentration en fibres. Les composites Tencel montrent un plus grand allongement à la rupture par rapport aux composites de verre et de lin.

Les modèles de Cox-Krenchel et Kelly-Tyson ont été utilisés pour analyser la rigidité et la résistance à la traction, en utilisant des facteurs d'orientation améliorés et déterminés à partir des observations au Chapitre 4. Certains écarts se sont produits au niveau de la prédiction des propriétés de traction dans la direction principale d'écoulement. Ces écarts ont été associés à l'imprécision des valeurs de module de la fibre, à l'orientation des fibres hors plan, aux courbures des fibres et à la possibilité de présence d'une couche appauvrie en fibres vers la surface.

L'investigation des propriétés d'impact des composites sur des éprouvettes séparément injectées a montré que les composites à fibres Tencel ont la résistance à l'impact la plus élevée par rapport au polypropylène renforcé par des fibres de verre et de lin. Cela a été interprété par la flexibilité et le nombre important de fibres à fraction volumique identique qui peuvent former un réseau qui résiste à la propagation de fissures. L'analyse de la résistance à l'impact a été réalisée en utilisant le modèle de Thomason et Vlug. Il a été démontré que les prédictions sont en accord avec les résultats expérimentaux à l'exception des composites à faible concentrations.

Chapitre 7 : Simulation de la pression et de l'orientation de fibre : comparaison avec l'expérience

Lors des campagnes d'injection, les pressions sur des capteurs situés dans la cavité ont été mesurées. Le niveau des pressions mesurées pour les différents matériaux (concentration et types de fibres) est bien corrélé aux niveaux de viscosité mesurée au Chapitre 5.

La pression a été calculée pendant la phase de remplissage avec le logiciel Rem3D. L'accord avec l'expérience est correct. Il y a un écart essentiellement au début de l'évolution de la pression qui se réduit lorsque la matière fondue progresse dans la cavité. Ceci est vrai pour le polypropylène pur et pour tous les composites étudiés. Cette constatation pourrait être expliquée par l'imprécision des paramètres thermiques requis pour la mise en place des calculs.

L'orientation des fibres de verre calculée à la fin du remplissage avec Rem3D$^{®}$ est en accord avec l'expérience, sauf dans les couches à cœur où un écart est observé. Les erreurs peuvent être attribuées aux conditions aux limites thermiques, au modèle d'orientation et aux erreurs expérimentales.

La prédiction de l'orientation des fibres de lin et de Tencel dans les pièces injectées a été aussi réalisée. L'objectif était de savoir si le modèle d'orientation de fibres rigides peut être appliqué aux deux types de fibres naturelles bien que leurs structures soient très différentes de celles des fibres de verre rigides.

L'orientation calculée des fibres de lin correspond approximativement aux résultats expérimentaux. Des paramètres de calcul ajustés pourraient améliorer la précision des calculs. Cet accord satisfaisant peut s'expliquer par le fait que les fibres sont en partie sous forme de faisceaux rigides.

L'orientation calculée des fibres Tencel est extrêmement loin de ce qui a été obtenu dans l'expérience. Les fibres Tencel sont très flexibles et leur comportement pendant l'écoulement ne peut être estimé via un modèle de fibres rigides. Par conséquent, un modèle de fibre flexible serait nécessaire pour les thermoplastiques renforcés de fibres Tencel pour obtenir des résultats d'orientation adéquats. Cependant, cela ne semble pas si évident vu que le passage du régime dilue au régime concentré des modèles fibres flexibles n'est encore pas maitrisé.

Conclusions et perspectives

Le travail réalisé a fourni une analyse en profondeur de la relation procédé-microstructure-propriétés pour l'injection du polypropylène renforcé de fibres naturelles. Ce type de composites prend progressivement de l'ampleur car il présente des avantages par rapport aux composites à fibres de verre tels que la réduction de poids, le faible coût, l'aspect environnemental toute en gardant des propriétés mécaniques similaires.

Nous avons effectué nos travaux avec deux types de fibres naturelles, Tencel et lin qui ont différentes structures intrinsèques: le lin est un mélange de fibres élémentaires semi-rigides et de faisceaux épais et rigides, alors que les fibres Tencel sont individuelles et très flexibles. Les fibres de verre rigides ont été également utilisées pour la comparaison. Une variété de techniques expérimentales a été utilisée dont certaines ont été mises au point pour évaluer la microstructure, les propriétés mécaniques et rhéologiques des composites. Une simulation de la phase de remplissage lors de l'injection a été effectuée, ce qui a permis de comparer la pression et l'orientation des fibres calculées avec celles obtenues expérimentalement.

A la lumière de ce travail, plusieurs perspectives peuvent être envisagées. Une première est de développer une méthode automatique d'analyse de taille et d'orientation des fibres, ce qui aidera beaucoup à réduire le volume du travail expérimental. Une deuxième perspective est de tester différentes conditions d'injection, que ce soit au niveau de la forme de la cavité, de l'épaisseur et du type de seuil ou au niveau des conditions machines : débit, pression de maintien, température de moule. Une autre perspective qui parait importante est de tester d'autres fibres analogues au lin comme par exemple les fibres de chanvre ou de sisal, ou des fibres se rapprochant des fibres Tencel comme le coton pour vérifier les résultats obtenus. Enfin, l'amélioration des modèles d'orientation de fibres en prenant compte des particularités des fibres naturelles est une piste qui mériterait d'être envisagée.

Chapter 1

General Introduction

Global warming and enormous amount of non-biodegradable waste are current problems that have to be solved. This speeds up industries to replace the fossil-based materials by alternative eco-friendly ones, which should provide similar performances together with a minimum of environmental footprint.

Within this context, natural fibres have gained a great attention over the two past decades, aiming to substitute glass fibres as reinforcement for polymer composites. In addition to their renewability, the main reasons that make natural fibres useful when applied in composites are cost and weight saving, keeping similar composite mechanical properties compared to glass fibre filled polymers. The low density of natural fibres particularly attracts the automotive industry and gives solution to the weight reduction issue. Natural fibre composites are used in automotive industry for producing interior parts as trim parts in dashboards, door panels, parcel shelves, backrests and cabin linings. In 2013, 30,000 tons of natural fibres were used in the European automotive production [Dammer et al. (2013)]. For example, Mercedes-Benz used 46 kg of renewable materials including natural fibre composites in 87 components of the S-class cars (2013). For the same reasons as mentioned above, natural fibre composite were welcomed to be applied for interior cladding of railway carriages and aircraft bodies.

Some other applications have also emerged for natural fibres composites such sport and leisure (ski, snowboard, bicycle…) thanks to their good damping properties, or musical instrument and loudspeakers because of their excellent acoustic performances, or furniture (desk, chair,…) due to their exceptional optical properties when mixed with translucent matrix. Natural fibres composites as a whole thus account for around 15% of the volume of composites manufactured in Europe [Dammer et al. 2013].

Natural fibres used in field of polymer composites are either lignocellulose fibres extracted from wood, from the bast of plants (flax, hemp, jute, kenaf), from seeds (cotton), from leafs (sisal) and also man-made spun cellulose fibres such as Tencel from Lyocell process and viscose.

In this work, two types of cellulosic fibres were mixed with polypropylene: flax and Tencel. The reason was to study and to understand the influence of fibre composition, morphology and properties on composite structure and properties, starting from fibre breakage during compounding and injection moulding, to molten composite morphology, composite microstructure, composite mechanical properties and finally checking if models developed for glass fibres can predict fibre orientation in injection moulded parts with cellulosic fibres. Flax and Tencel are very different. First, they have different composition: the main component of flax is cellulose by 64-81 %, but hemi cellulose (11-17 %), lignin (2-3 %) and pectin (2 %) are also present [Baley (2002); Le Moigne (2014)], while Tencel is based on pure cellulose [Fink et al. (2014)]. Second, they have different morphology: Tencel is elementary thin and flexible fibre with uniform diameter (determined by spinning process) while flax is a "mixture" of thin semi-rigid elementary fibres and thick rigid bundles made of elementary fibres assembled together. Finally, their intrinsic mechanical properties are also different. It is thus supposed that these differences in fibres properties would influence composite microstructure and properties.

The use of natural fibres by humans, in particular flax (*Linum usitatissimum L.),* dates back the ancient Egyptian civilisation. It was imported in Europe by the Middle East Phoenician traders 2,000 years ago. The translation of its scientific name is "*linen most useful*", signing its importance in the world economy [Tortora and Collier (1997); Borland and Berglund (2002); Akin (2012)]. In France, high-quality flax is today cultivated in the northern regions (Normandie, Picardie and Nord Pas de Calais) due to the moderate climate conditions and the developed know-how. Before being able to reinforce composite, flax fibres undergo a long cycle of extraction that includes retting, breaking, scutching and hackling (see more details in Bos (2004) and Müssig (2010)). More than 80 % of flax production is today designated for textile industry that is their classical application, and only 10 % are dedicated for a technical use.

Tencel fibres are made via Lyocell process that was first commercialised in 1992 by Courtaulds. Today, the major producer of these fibres is the Austrian company Lenzing who

kindly provided these fibres for the current study. The cellulose for Tencel fibres is extracted from the pulp of hardwood trees, mainly eucalyptus. The cellulose is dissolved in N-methylmorpholine-N-oxide monohydrate, filtered, spun, coagulated and dried. In addition to their primary use in textile industry, Tencel fibres are commonly applied in ropes, automotive filters, abrasive materials and protecting suiting materials.

Natural fibres composites are generally manufactured under different processes either with thermoplastic or thermoset matrices. Thermoplastics are usually mixed with short natural fibres in twin-screw extruder to produce pellets that are in turn processed by injection moulding. Some other ways for producing composites are also possible such as compression moulding. Injection moulding is the preferred method to manufacture parts with a complex geometry at high production rate and low price. The market for injection moulding is constantly growing with increasing application areas for the natural fibre composites.

The potential of natural fibre composites together with the efficient productivity of injection moulding make clearly a balance between the environmental challenge and the industrial performance. However, because of the complexity and multiple choices of natural fibres some questions still need to be answered. Within this context, the present thesis was launched in October 2012 at the Centre for Material Forming (Cemef) of Mines ParisTech, in the frame of the Industrial Chair in Bioplastics. This Chair is co-financed by Mines ParisTech and five companies: Arkema, L'Oréal, Nestlé, PSA Peugeot Citroën and Schneider Electric. It is a 7-years large research project that includes different research topics, supporting the development and applications of various materials based on biomass polymer (bioplastics, lignocellulose, polymer composites with natural fibres). A previous thesis on natural fibre based composites in the frame of this Chair investigated the behaviour and rupture mechanisms of cellulosic fibres during their compounding with a polymer matrix [Le Duc (2013)]. The present thesis continues this topic and focuses on studying and understanding of the properties of natural fibre based composites particularly when processed by injection moulding.

Even though the understanding of natural fibre reinforced composites has recently been significantly improved, several issues related to injection moulding process remain unsolved. The main question here is if the approaches developed for rigid glass fibre based composites can be applied to composites with cellulosic fibres. Glass fibres are rigid with a uniform diameter and defined properties. As mentioned above, technical flax fibres are a mixture of

elementary fibres and bundles. During processing, bundles dissociate into thinner ones and/or into elementary fibres. Depending on their diameter and length, flax fibres and bundles can be semi-flexible or rigid. Flax fibres are agriculture based products; their properties depend on the cultivation and the extraction conditions. Flax fibres that are harvested from different varieties exhibit different properties. Their morphology is thus very different from that of glass fibres. The other type of cellulosic fibres used in this work is Tencel. They are spun cellulose fibres and thus of uniform and controlled morphology, composition and properties. However, their morphology is very different from glass fibres and also from flax. The main difference with glass fibres is that Tencel is very flexible, which may cause problems when using approaches developed for glass fibres.

Considering all said above, the following points should be clarified:

1) The effect of processing on natural fibres breakage and dissociation into bundles is crucial in terms of the understanding of composite microstructure within injection moulded parts. Are flax and Tencel breaken to the same extent? Is there a significant breakage during injection moulding? Does the fibre concentration influence the fibre breakage?

2) The rheological properties of molten composites are very important for predicting the outputs of the injection moulding process. They are reasonably well understood for glass fibre based composites. Are they similar or not to natural fibre reinforced composites? What is the influence, if any, of fibre type and flexibility on molten composite viscoelastic properties?

2) Since the morphology of natural fibres is different from glass fibres, the applicability of the methods used to characterize the microstructure of glass reinforced polymer on the microstructure characterisation of natural fibre composites is questionable. If not applicable, a new method for the analysis of fibre dispersion and orientation should be developed.

3) As the composite mechanical properties are directly correlated with the microstructure, the relationships microstructure-properties should be studied for understanding and for improving the performance of natural fibre based composites.

4) In order to optimise the injection moulding conditions for composites with cellulosic fibres, it is important to check if the existing fibre orientation models based on glass fibre-composite are able to simulate or not the natural fibre composites.

To answer these questions, the thesis is composed of seven chapters:

Chapter 1 is the general introduction (the current chapter), in which the context, the issues and the content of the thesis are presented.

Chapter 2 sums up all details of materials and processing steps used to make the fibre reinforced polypropylene, from compounding to injection moulding. The methods used to characterize the composite microstructure (optical and scanning electron microscopy) and properties (rheology and mechanical performances) are also presented in this chapter.

The five other chapters are divided into two main parts: the first part presents a literature review on the subtopic of the ongoing chapter and the second part shows the results obtained in this work. Below is a brief presentation of each chapter.

Chapter 3 is dedicated to the study of the influence of processing (extrusion and injection) and of fibre concentration on fibre size distributions. Both types of cellulosic fibres, flax and Tencel, and also glass fibres, were investigated. For flax fibres length and diameter were analysed. This was done by dissolving polypropylene matrix and using optical microscopy, cartography and image analysis to obtain length, diameter and aspect ratio distributions for each case.

Chapter 4 studies the microstructure of injection moulded polypropylene reinforced with 20.5 vol % of flax, Tencel and glass fibres. A sample is extracted from the injected box and polished at different depths. The microstructure is analysed using optical microscope in reflection mode. The differences in the microstructural features (orientation and dispersion) between glass and natural fibres are demonstrated, showing the impossibility of using approaches developed for glass fibres to quantify their orientation in composite. To quantitatively describe the microstructure of composites with cellulosic fibres, a new approach is suggested which divides fibres in four classes according to their curvature. The distribution of the fibres along the depth of composite and fibre orientation is quantified,

Chapter 5 presents the investigation of the viscoelastic properties of flax, Tencel® and glass based polypropylene composites, focusing on the effect of fibre type, concentration and flexibility. Correlations between the dynamic and capillary viscosity of composites are also presented and discussed.

Chapter 6 exhibits a correlation between fibre microstructure in the injection moulded parts and the tensile and impact properties of composites based on flax, Tencel and glass. For the

study of tensile properties, samples were cut from boxes with different orientations relative to the main flow direction: 0°, 45° and 90°. The experimentally obtained results are compared to models existing in literature.

Chapter 7 starts with the analysis of the experimental results of pressure recorded during the injection moulding of composites. Then pressure is calculated using Rem3D$^{\circledR}$ simulation software developed for glass fibre based composites and compared with the experimental results. Fibre orientation is also modelled using Rem3D$^{\circledR}$, and compared to the experimental orientation shown in Chapter 4. The applicability of this simulation tool to natural fibres is discussed in this chapter.

References

Akin, D. E. (2012). Linen most useful: perspectives on structure, chemistry, and enzymes for retting flax. ISRN biotechnology, 2013.

Baley, C. (2002). Analysis of the flax fibres tensile behaviour and analysis of the tensile stiffness increase. Composites Part A: Applied Science and Manufacturing, 33(7), 939-948.

Borland, V. S., & Berglund, D. R. (2002). From flower to fabric. Textile World, 52-55.

Bos, H. L. (2004). The potential of flax fibres as reinforcement for composite materials. Technische Universiteit Eindhoven.

Dammer, L., Carus, M., Raschka, A., & Scholz, L. (2013). Market Developments of and Opportunities for biobased products and chemicals. Nova-Institute for Ecology and Innovation.

Fink, H. P., Ganster, J., & Lehmann, A. (2014). Progress in cellulose shaping: 20 years industrial case studies at Fraunhofer IAP. Cellulose, 21(1), 31-51.

Le Duc, A. (2013). Comportement et rupture de fibres cellulosiques lors de leur compoundage avec une matrice polymère (Doctoral dissertation, Ecole Nationale Supérieure des Mines de Paris).

Le Moigne, N., Longerey, M., Taulemesse, J. M., Bénézet, J. C., & Bergeret, A. (2014). Study of the interface in natural fibres reinforced poly (lactic acid) biocomposites modified by optimized organosilane treatments. Industrial Crops and Products, 52, 481-494.

Müssig, J. (Editor) (2010). Industrial Applications of Natural Fibres - Structure, Properties and Technical Applications. Chichester, John Wiley & Sons, United Kingdom.

Tortora, P. G., & Collier, B. J. (1997). Understanding textiles. Prentice-Hall, Englewood Cliffs, New Jersey, United States.

Chapter 2

Materials & Methods

This chapter describes materials used in the study, methods to prepare composites and methods to characterize them.

Although this work primarily concerns natural fibre reinforced polypropylene, glass fibre reinforced polypropylene with the same fibre volume fractions were prepared and used for comparison. As a reference, neat polypropylene was also studied. The information on all the materials used in this study are given in this chapter.

The major part of this chapter provides the details of the processing steps used to make the composites, from extrusion to injection moulding. The detailed conditions for manufacturing injection moulded parts used in this study are given. The techniques used to assess the composite microstructure, rheology and mechanical performances are also described.

1. Materials

1.1. Polypropylene

The polypropylene used is PPH9020 homopolymer from Total Petrochemical. Table 2.1 shows characteristics given by the supplier.

Table 2.1 Characteristics of the polypropylene used in this study

	Method	*Unit*	*Value*
Melt Flow Index 230°C/2.16 kg	*ISO 1133*	*g/10 min*	*25*
Melting point	*ISO 3146*	*° C*	*165*
Density	*ISO 1183*	*g/cm^3*	*0.905*
Tensile Strength at Yield	*ISO 527-2*	*MPa*	*37*
Elongation at Yield	*ISO 527-2*	*%*	*8*
Tensile Modulus	*ISO 527-2*	*MPa*	*1700*
Flexural Modulus	*ISO 178*	*MPa*	*1600*
Izod Impact Strength (notched) at 23°C	*ISO 180*	*kJ/m²*	*4*
Charpy Impact Strength (notched) at 23°C	*ISO 179*	*kJ/m²*	*4.5*

1.2. Fibres

1.2.1. *Flax*

Flax fibres were supplied by Dehondt Technologies (France) as NATTEX roving which were harvested in 2010 from Drakkar variety (France). These rovings were cut to a length of 0.5 mm by the company Apply Carbon (France). After these transformations, fibres appear as a mixture of thin and rather flexible elementary fibres and thick rigid bundles composed of elementary fibres "glued" together (Figure 2.1a). Bundles were partially separated during compounding (Figure 2.1 b).
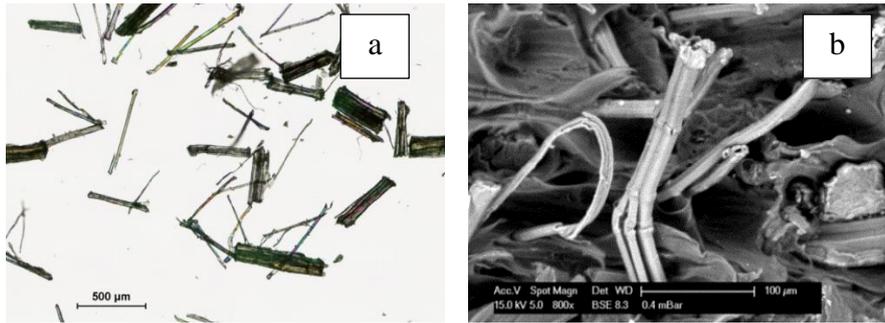
Figure 2.1

Flax fibres: "mixture" of bundles and elementary fibres a) as delivered and b) after compounding (in polypropylene matrix)

1.2.2. *Tencel*

These are man-made cellulose II fibres produced with Lyocell process, kindly provided by Lenzing AG (Austria). Tencel fibres are regenerated cellulose fibres formed in a wet fibre-formation process out of eucalyptus pulp dissolved in N-methylmorpholine-N-oxide monohydrate. They are individual flexible fibres with a diameter of 10 µm (Figure 2.2). Fibres with the average length of 500 µm (as given by the producer) were made from longer fibres by milling.
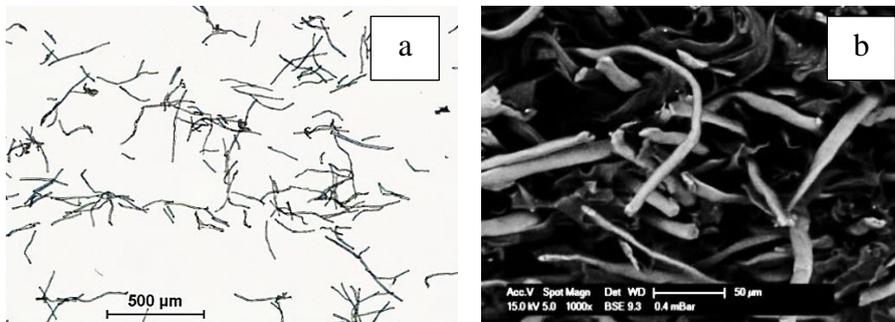

Figure 2.2

Tencel fibres a) as delivered and b) after compounding (in the matrix)

1.2.3. *Glass fibres*

Glass fibres were kindly provided by Arkema. Fibres are of 2 500 µm as initial average length, 10 µm as diameter, 2.5 g/cm^3 as density and 73 GPa as elastic modulus. Contrary to natural fibres, glass fibres show a straight shape (Figure 2.3.a) and a regular cross-section

(Figure 2.3.b). Moreover, the density of glass fibres is 70 % higher than that of flax and Tencel.
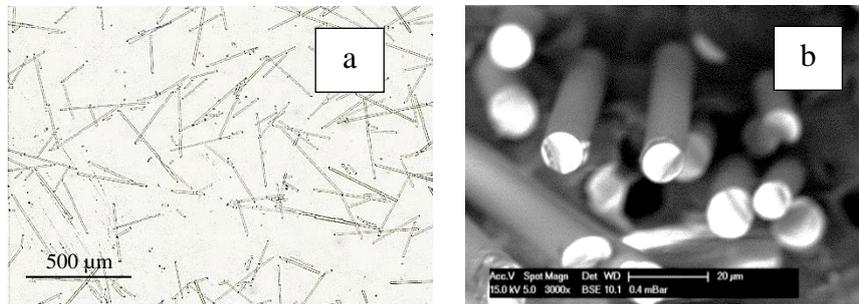
Figure 2.3

Glass fibres: a) as delivered and b) after compounding

Decalin (decahydronaphthalene) was purchased from Sigma-Aldrich and used to dissolve polypropylene for the measurements of fibre size distribution.

2. Processing: compounding and injection moulding

2.1. Compounding

2.1.1. *Principle*

The purpose of compounding is to enable a good dispersion of fibres throughout a polymer melt. The twin screw extruder is usually used for composite compounding. Basically, a twin screw extruder consists of two parallel screws turning within a 8-shaped housing barrel. The most industrially used one has a corotating and intermeshing screws configuration. Screws and barrel may be built up from different segments. Barrel wall is usually smooth, but it can be constructed with longitudinal or helical grooves, for particular applications requiring an intensive shear rate solicitation. The screws are designed as three main zones from the inlet to the die: melting zone, mixing zone and conveying zone (Figure 2.4.a). The screws can be adjustable depending on the particular configuration of each zone. Conveying elements are used in melting and conveying zones (Figure 2.4.b). They may have different pitches and spacing between flights. Mixing zone contains reverse flight screw elements or kneading elements for more intensive mixing (Figure 2.4.c and d).
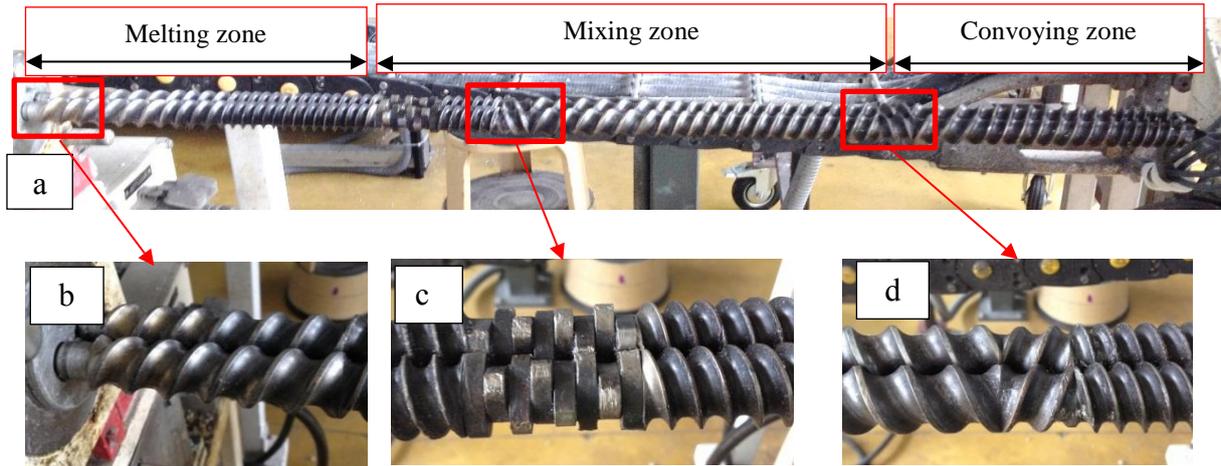
Figure 2.4

Twin screw configuration a) main zones of screws b) convoying elements c) kneading elements d) reverse flight elements

2.1.2. *Compounding conditions*

Four concentrations of fibres were prepared for each type of fibre, flax, Tencel and glass. Because of the difference in density ρ between glass and cellulosic fibres, it is the volume fraction that was chosen to be the same (Table 2.2).

Table 2.2 Composite formulations

Volume fraction, %	Weight fraction, %		
	Flax	Tencel	Glass
3.6	5	5	9.3
6.3	10	10	15.6
13.1	20	20	29.4
20.5	30	30	41.6

For a better understanding of composite rheology, no coupling agent was used in composite formulation, with the purpose of not modifying the matrix viscosity when varying fibre concentration [Le Moigne et al. (2013)].

Before compounding, fibres were dried at 105 °C for 2 hours. Clextral BC21 extruder (*Centre des Matériaux, Ecole des Mines d'Alès*) was used to prepare composites. It is a co-rotating twin screw extruder with a centreline distance of 21 mm and a screw length of 900 mm. The global flow rate was 7 kg/h and the screw speed was 200 RPM. A dedicated feeder was operated to control the fibre feed rate relatively to the one of matrix, which enables to get the desired concentration. The screw profile (Figure 2.3.a) was built in *Centre de Matériaux d'Ales* by combining conveying and mixing elements ensuring short residence time of fibres to protect them from temperature degradation and breakage. The barrel temperature was progressively increased throughout 12 zones from 60 ° C to 190 ° C, as shown in Figure 2.5. The matrix and fibres were fed from zones 1 and 7, respectively.

zone	1	2	3	4	5	6	7	8	9	10	11	12
T°C	60	80	120	140	190	190	190	190	190	190	180	190
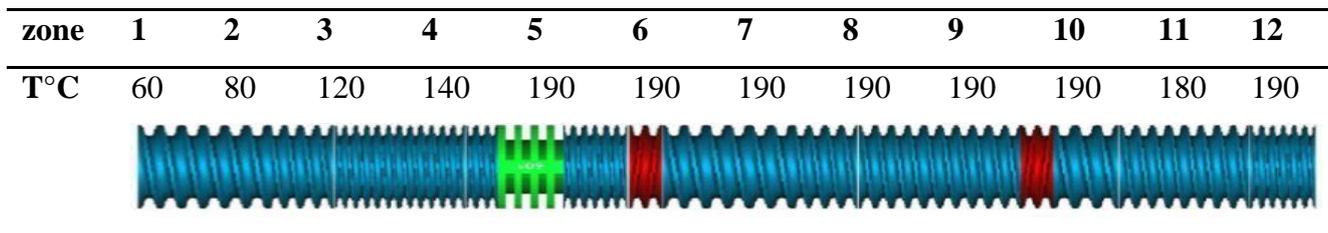
Figure 2.5

Screw profile used for composite compounding

At the die exit, composite was immediately quenched in water (Figure 2.6.a), then granulated into pellets whose size around 5 mm (Figure 2.6.a), as required by injection moulding processing. The maximum measured temperature was 195 °C. The relative rise in temperature with respect to the setting temperature is caused by the viscous heating.
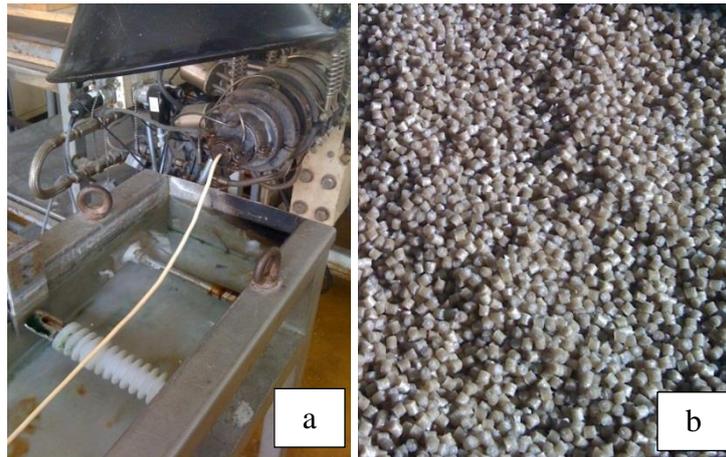
Figure 2.6

a) A water bath used for cooling compound after extrusion b) obtained granules after pellitisizing

2.2. Injection moulding

2.2.1. *Principle*

The injection moulding process has been essentially made for unfilled thermoplastic materials. The same machines are used to process reinforced thermoplastics. Injection moulding machine can commonly be divided into two units: an injection unit and a clamping unit, as shown in Figure 2.7.
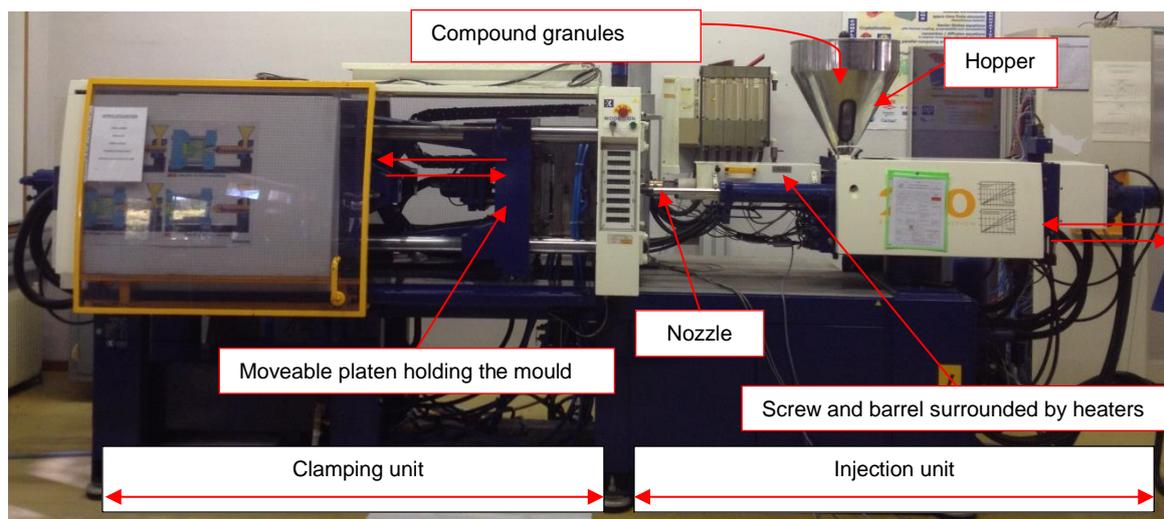
Figure 2.7

Injection moulding machine and its main constituents

2.2.2. *Clamping unit and mould*

The functions of the clamping unit are to open and to close the moveable platen that holds mould, and to eject components from the mould (Figure 2.8). Melts resin enters into mould from the sprue bushing which is directly connected with injection barrel by the nozzle. The sprue feeds the cavity through channels which are also referred as *runners* .The melt flows through the runners and arrives in the cavities by the gates. The entire design containing sprue, runners and cavities is machined out on the mould and the amount of melt needed to fill them is called "*shot*". Ejection is possible by a sprue puller and ejector pins, also known as knock out pins, located throughout the cavity and the runners. A cooling system is passing water through series of channels drilled and connected in the mould to form a continuous pathway. The role of water is to keep the mould at a desired temperature in order to solidify the polymer. The mould description here is primary and simple. More tools can be used for complex moulds with sophisticated design. For example, sliders enabling side-actions can be put on the mould when the part shows undercuts.
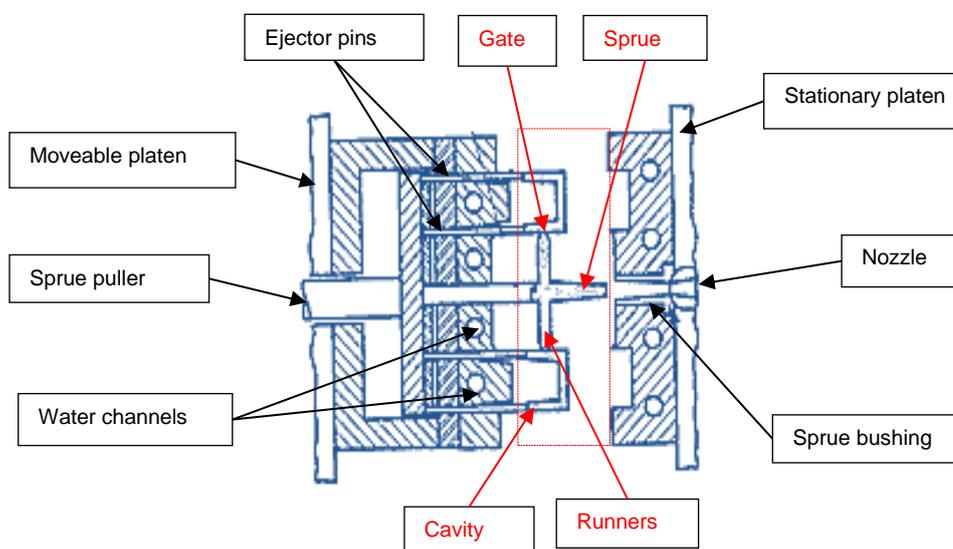

Figure 2.8

A typical two plate injection mould including a cavity and its system of injection (sprue, runners and gate framed with the dashed line red rectangle)

2.2.3. *Injection unit*

The injection unit functions are to plasticise material and to inject it into the mould. These functions are handled by a three-section-screw (feed, compression and metering) (Figure 2.9). Modern standard screws have an overall length of 20-23 D (length as a product of diameter). The length of the feed section is generally the half-length of the screw, while compression and metering sections accounting together the residual half-length and having approximately the same length. The *pitch* varies between 0.8-1 D from the feed to the metering zones across the screw *flights*.
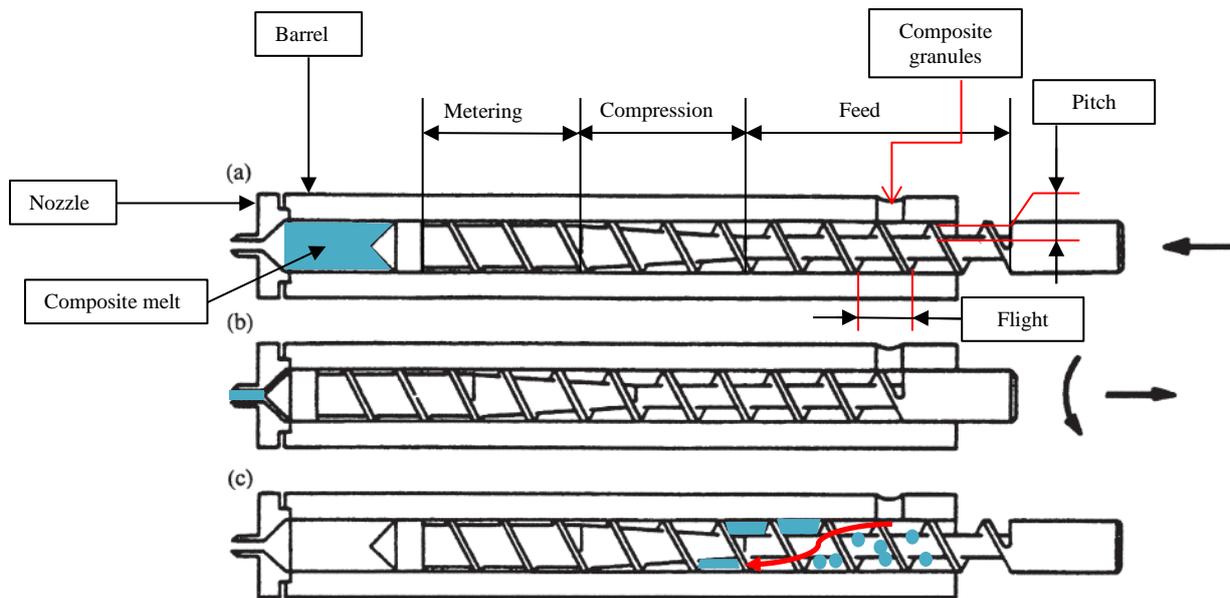
Figure 2.9

Screw in injection moulding machine and its sequence during the injection moulding cycle

[Rosoto et al. (2000)]

Figure 2.9 describes schematically the sequence of the screw along the cycle of injection moulding. At the beginning of cycle, the screw is at a retracted position in the barrel and the melt occupies the region between the screw tip and the nozzle (Figure.2.9.a). Then during injection the screw advances taking the function of piston when the mould halves closed and clamping force applied (Figure.2.9.b). This induces the material displacement through the nozzle and the filling of the mould cavity. Once the mould is filled, pressure is maintained in the injection cylinder till the material in the mould gates solidifies. During this holding stage,

an additional melt from the barrel compensates the polymer cooling shrinkage. After this stage a new dose of melt is prepared for the next injection cycle. The screw rotates enabling the material melting and mixing through its transfer from hopper to screw forward (Figure.2.9.c). Pressure generated in the melt transfer allows the retraction of screw in the barrel. This pressure can be varied by controlling the axial displacement of screw; this procedure is called the application of *back pressure*. Once the new dose is ready, the solidified part is ejected from the cavity and the mould is clamped again to start the subsequent cycle. As the screw comes forward, the melt can flow through its flights. A non-return valve is usually located to the front of the screw, preventing the melt backflow.

2.2.4. *Injection moulding conditions*

The granules of composites were further processed in DK Codim NGH 110/200 injection machine (Figure 2.6), with 28 mm as screw diameter and 84 cm^3 as practical shot volume. The injection moulded part is a "box" with dimensions of 175 mm x 71 mm x 59 mm (Figure 2.10). Table 2.3 regroups the injection moulding conditions.
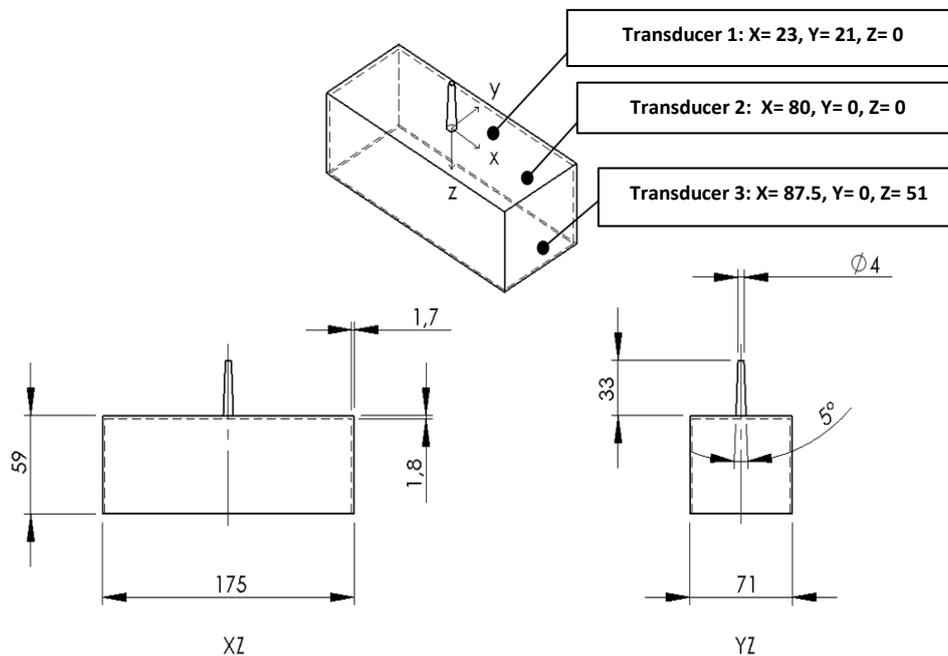
Figure 2.10

Injection molded box, all dimensions are in mm

Table 2.3 Injection moulding conditions

Injection temperature, °C	*190*	Cooling time, s	*10*
Mold temperature, °C	*30*	Holding time, s	*10*
Flow rate, cm³/s	*92.4*	Holding pressure, bar	*600*
Shot length, mm	*115*	Back pressure, bar	*0*
Clamping force, KN	*1100*	Screw speed, RPM	*120*

Several pressure and temperature sensors were placed in and around the mould. Five pressure transducers are used: three transducers are located in the mould as shown in Figure 2.10, one is before the mould entrance at the nozzle and another one is placed in the hydraulic cylinder behind the screw. A temperature sensor was installed in the mould located at 2 cm from the cavity surface.

3. Characterisation

3.1. Fibre size analysis

Fibre length and diameter after compounding and after injection were determined as following: the composite was diluted with Decalin® to get a fibre concentration in the mixture (polypropylene, fibres and Decalin®) lower than 10 %, which avoids fibre overlapping and facilitates a later fibre size measurement. As shown in Figure 2.11, the mixture is placed in a ball-flask immersed in an oil bath and gently stirred during 2h under 170 °C (see more details in ref. LeMoigne et al. (2011); LeDuc et al. (2011); Soccalingame et al. (2015)).

Figure 2.11

Extraction of fibres from composites under a gentle stirring

A few drops of polypropylene-Decalin-fibre suspension were deposited on a glass plate and analysed in transmission optical microscopy by using Leica DP 4500 optical microscope equipped with a high resolution 3-CDD numerical camera (JVC KY-F75U, 1 360 x 1 024 pixels). The glass slide is held by a microscope stage that can be displaced in *x* and *y* directions as described in Figure 2.12. This displacement is controlled by a handed stage driver. The displacement of the stage is monitored by a position detector related to a computer, in which was installed *Cartograph* (Microvision®). Images were taken by the camera at each position of the stage. The focus is adjusted by moving the stage in the *z* direction. *Cartograph* enables to assemble the different images with respect to their positions in the specimen. A real time homogenization between the elementary images was performed automatically by a dedicated tool in *Cartograph* software.

Figure 2.12

Leica DP 4500 optical microscope equipped with accessories dedicated to perform specimen cartographies

The analysis of fibre size was then performed using cartography of $\simeq$ 5 x5 mm² built-up from 50 elementary transmission images (830 μm x 640 μm) per composite formulation. The measurement of fibre size was done semi-automatically by *Archimed* (Microvision[®]), the image processing software dedicated to measurement. After selecting the fibre pattern "by hand", a numerical calliper integrated in the image acquisition software allowed the measurement of each fibre length and diameter (Figure 2.13). The statistical analysis was based on 200 fibres per sample. Each formulation was analysed at least three times, giving the difference in the size within an uncertainty interval of 10 %. The minimal size that was taken into account was 10 μm.

The non-processed (initial) fibre size was analysed in the same way by dispersing fibres on a glass slide and using the cartography approach.
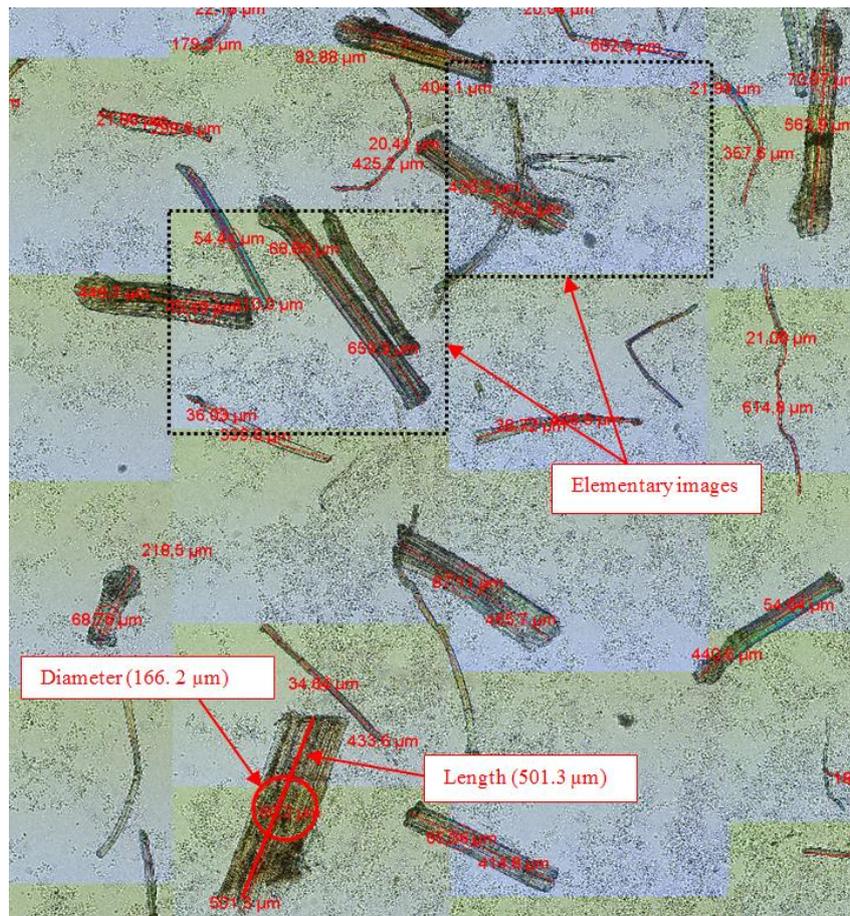
Figure 2.13

A part of a cartography of flax-based composite obtained by assembling elementary images (dashed rectangles), the red numbers correspond to the measurements of fibre size (lines for length and circle for diameter)

3.2. Microstructure analysis

A sample was cut at 70 mm from the gate in *xy*-plane of the injection moulded box as shown in Figure 2.14.a. It was then embedded with epoxy resin and polished to analyse the microstructure at different depths from the surface (Figure.2.14.b). Six layers down from the surface to the middle plane, at 100 µm, 200 µm, 400 µm, 600 µm, 800 µm and 900 µm (middle layer) were made, allowing the analysis of fibre orientation in planes parallel to the surface (*xy* plane in our case). We assumed the symmetric pattern of flow with respect to the middle plane. Two transverse cross sections in *zy* and *zx* planes were also analysed to have a 3D overview of the fibre orientation.

The preparation of the sample surface requires a great care to have a good image quality suitable for characterizing the fibre microstructure. The sample is firstly polished by abrasives, starting with coarse ones and finishing with fine ones, and secondly polished by diamond paste. At least a difference in depth of 100 μm was needed between two successive layers to avoid scratches and to get a polished surface plausible for analysing. The sample was analysed with optical microscopy in *reflection* mode, and 5 mm x 5 mm cartographies were recorded by assembling "elementary" images (Figure.2.14.c, see details in the section 3.1 Fibre size analysis). The obtained image was semi-automatically analysed by *Archimed* (Microvision[®]) software. Fully automatic measurements were not possible because of the variation of contrast within the fibres themselves and the irregularity of fibres shape. This aspect will be further discussed in Chapter 4.
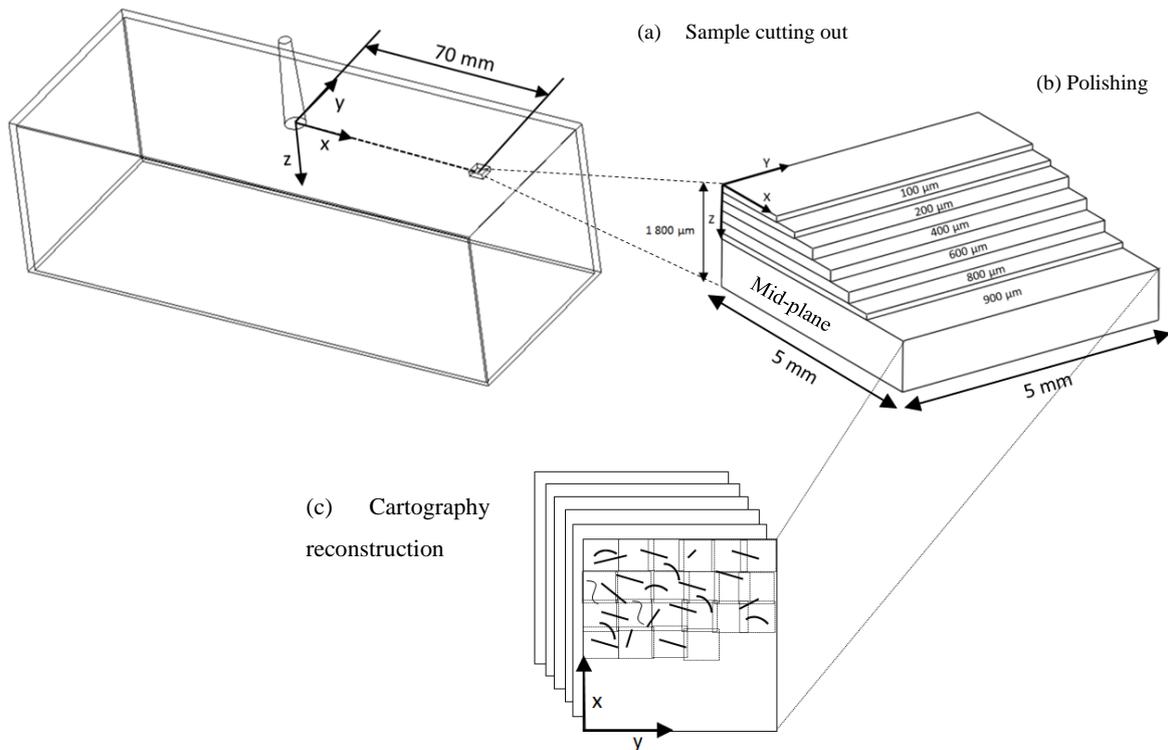

Figure 2.14

A schematic representation of a sample cut from the injected box and polished as 6 layers in the flow *xy*-plane

3.3. Rheology of molten composites

3.3.1. *Dynamic rheology*

Viscoelastic properties of molten composites were studied using oscillatory parallel plates rheometer that imposes on the sample a shear sinusoidal deformation with frequency ω and follows the resultant stress response. The typical experiment consists of placing a sample between two plates as shown in Figure 2.15.a. While the bottom plate remains fixed, a motor rotates the top one, inducing a time dependent strain given by:

$$\gamma(t) = \gamma_0 \sin(\omega t) \qquad\qquad\qquad \text{[Eq.2.1]}$$

Concurrently, the time dependent shear stress $\sigma(t) = \sigma_0 sin(\omega t + \delta)$ is deduced by measuring the torque that sample imposes on the bottom plate. For an elastic material, the stress is exactly in phase with the sinusoidal strain. For a purely viscous material, the applied strain and the measured stress are out of phase, with a phase angle $\delta = \pi/2$. Viscoelastic materials are in between with $0 < \delta < \pi/2$ (Figure 2.15.b). Storage modulus $G'(\omega)$ and loss modulus $G''(\omega)$ are the solid-like and liquid-like contributions to the measured stress response, respectively. Therefore, the stress of a viscoelastic material is given by

$$\sigma(t) = G'(\omega)\gamma_0 \sin(\omega t) + G''(\omega)\gamma_0 \cos(\omega t) \qquad\qquad \text{[Eq.2.2]}$$

Complex viscosity η^* is defined by as

$$\eta^*(\omega) = \frac{\sqrt{(G')^2 + (G'')^2}}{\omega} \qquad\qquad\qquad \text{[Eq.2.3]}$$

and phase angle δ by

$$\tan \delta = \frac{G''}{G'} \qquad\qquad\qquad \text{[Eq.2.4]}$$
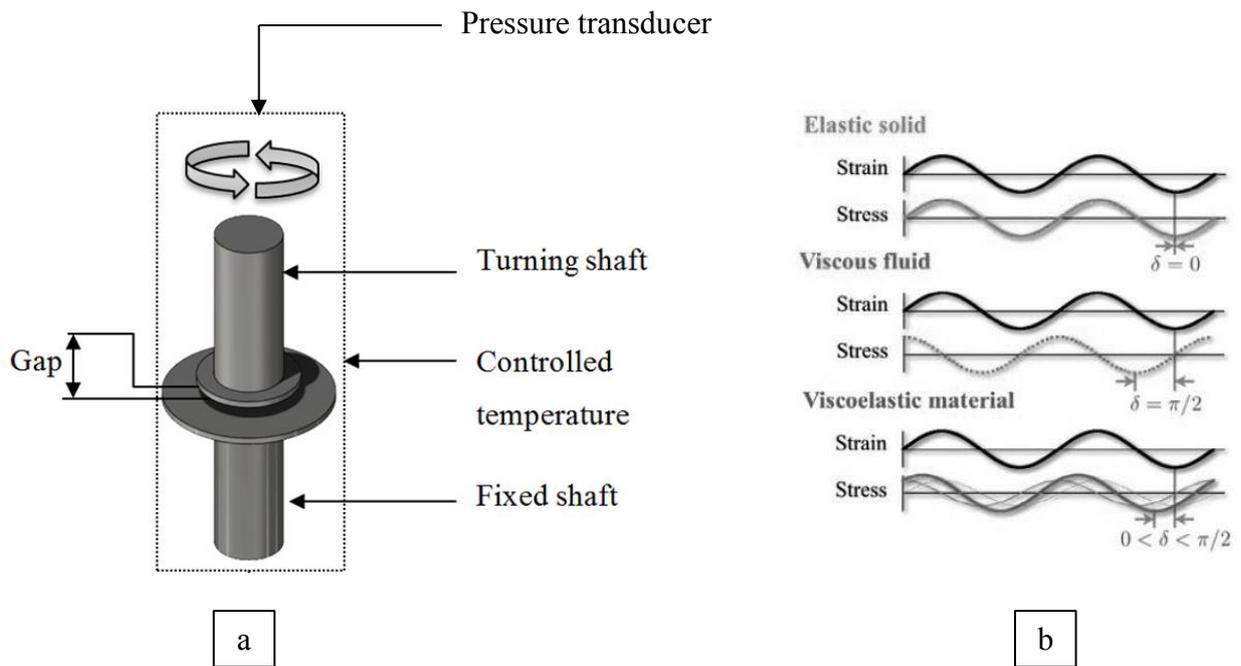
Figure 2.15

Dynamic rheology, a) schematic representation of the dynamic rheometer b) typical stress shear responses

In this study, the dynamic rheological measurements (small amplitude oscillatory shear) were performed on Anton Paar MCR302 rheometer, using parallel plate geometry with plates of 25 mm as diameter and 1 mm as gap. Samples were made with Minijet Themofisher® that is a lab scale injection moulding machine. The injection temperature, mould temperature, injection and holding pressures were respectively 190 °C, 50 °C, 500 bar and 100 bar.

Frequency sweep tests were performed from 100 to 0.1 rad/s at 180 °C, 190 °C and 200 °C. The strain was fixed at 1 % for the entire series of frequency sweep tests, ensuring that all composites are in a linear visco-elastic regime. The thermal stability of composites was also checked: no viscosity variation was recorded during 30 minutes within the experimental errors, which is much longer than the duration of frequency sweep experiment.

3.3.2. *Capillary rheology*

Capillary rheometer is designed to characterize polymer melts at high shear rates typically from 10 s^{-1} to 10 000 s^{-1}. Such shear rate can be reached in injection moulding process. The measurement principle consists of injecting a molten polymer into a capillary of a circular cross section and measuring the pressure drop for a given flow rate.

The capillary rheology measurements were performed with RheoArt rheometer at 190 °C using different extrusion speeds and die lengths (0, 4, 8 and 16 mm), constant die diameter (2 mm) and apparent shear rates ranging from 100 to 1 000 s^{-1}. The RheoArt is a capillary rheometer with a pre-shearing *Couette* chamber (Figure 2.16.a). After feeding (Figure 2.16.b), the material is first pre-sheared at a shear rate of 10 s^{-1} for 60 seconds (Figure 2.16.c). Then it is transferred in the bottom chamber and the central piston injects the polymer through the die (Figure 2.16.d, e and f).
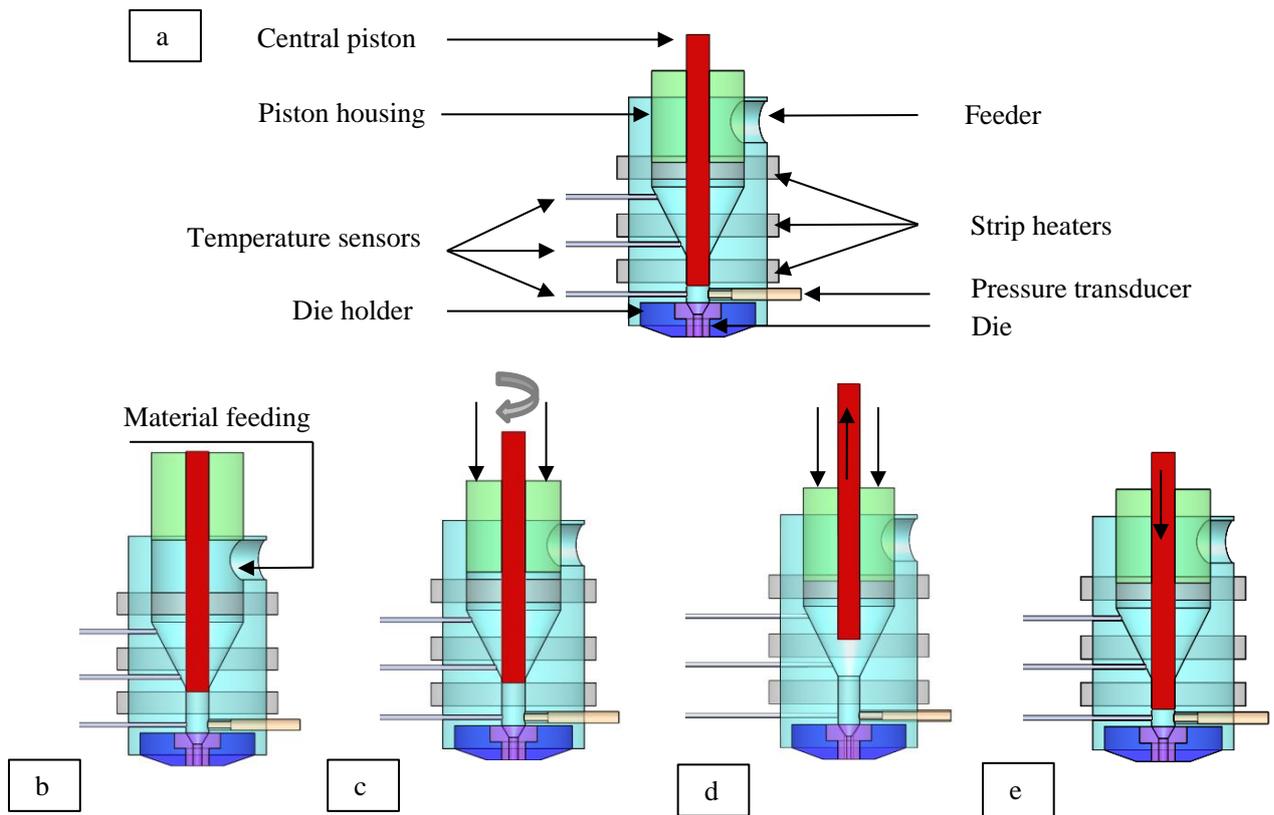
Figure. 2.16

Schematic representation of RheoArt capillary rheometer and the different sequences of the experiment, a) General description of the RheoArt rheometer, b) Material feeding, c) Couette Preshearing, d) the central piston mooves up and the housing piston moves down to compress the melt e) the central piston pushes the melt into the die

Figure 2.17 shows typical pressure plateaus at different piston speeds and different die lengths. Some oscillations in pressure curves can occur because fibres block the flow around the capillary entrance. The experiments were considered when the pressure plateaus are flat on average and a

steady state is reached to give plausible pressure values that can be considered for a further capillary rheology analysis.
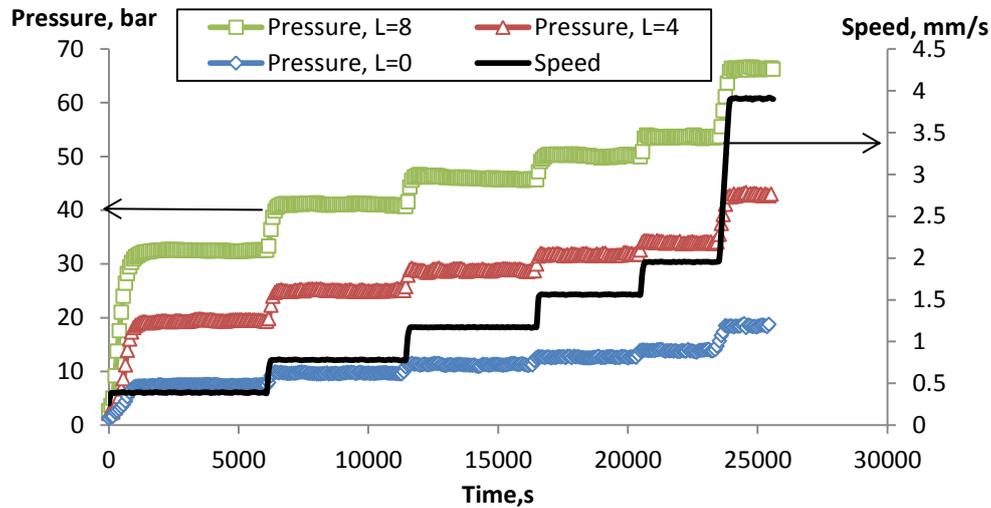
Figure 2.17

Typical pressure curves for different speeds and different die length, example of 20.% vol % Tencel/PP composite.

Figure 2.18 shows the average of pressure plateaus as function of the *L/D* of die for the different apparent wall shear rate values. The obtained plots are linear and their slopes increase when the shear rate increases, as expected. These are the Bagley plots that enable determining entrance and exit pressure losses. After these corrections, we can plot wall shear stress vs apparent shear rate, as shown in Figure 2.19 (20.5 vol % Tencel/PP was taken as an example). For all materials studied, these flow curves appear as a straight line, meaning that they follow a power law all over the shear rate range of the measurements, and then the power law index value can be determined.
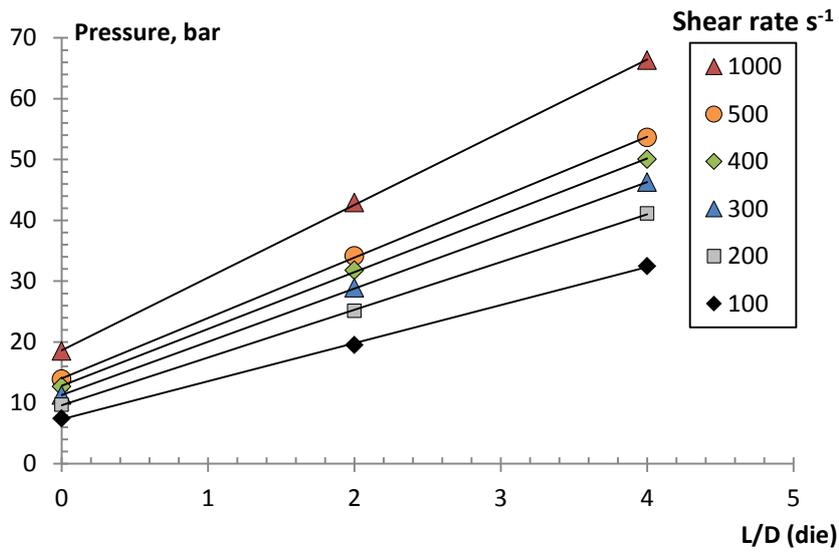
Figure 2.18

Pressure vs die aspect ratio for different apparent shear rate values from $100\ \text{s}^{-1}$ to $1\ 000\ \text{s}^{-1}$, for 20.5 vol % Tencel/PP
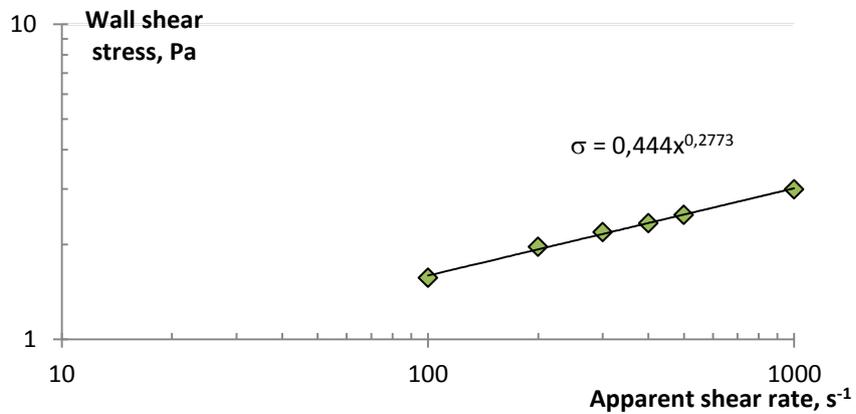
Figure 2.19

Shear stress versus the apparent shear rate, for 20.5 vol % Tencel/PP, $n = 0.277$

The Rabinowich correction enables determining the wall shear rate as a function of the apparent wall shear rate and of the power law index m. By knowing the wall shear stress and the wall shear rate, we can plot the viscosity curve as shown in Figure 2.20.
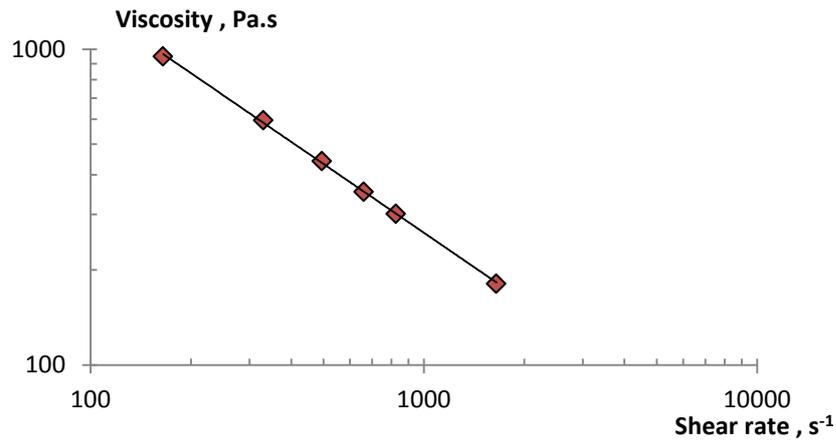
Figure 2.20

Final viscosity curve for 20.5 vol % Tencel/PP

3.4. Mechanical properties of composites

3.4.1. *Tensile test*

Tensile test set-up commonly involves fixing the sample by grips in the testing machine and extending it until failure. The elongation of the gauge section is recorded versus the applied force using a mechanical sensor. The elongational strain ε is calculated using the following equation:

$$\varepsilon = \frac{L-L_0}{L_0}$$
[Eq.2.5]

where $L - L_0 = \Delta_L$ is the change in gauge length, L_0 is the initial and L the final lengths, respectively. The force measurement is used to calculate the stress, σ, given by equation

$$\sigma = \frac{F}{S}$$
[Eq.2.6]

where F is the tensile force and S is the initial cross-section of the sample.

The apparent stress–strain curve can be plotted. Tensile properties can be deduced from that plot, such as Young's modulus, ultimate tensile strength and elongation at failure.

Tensile trials were performed with Erichsen machine equipped by 2 kN transducer. The tensile specimens were cut out from the moulded box at the location ($x = 70$ mm, $y = 0$ mm)

along three angles (0°, 45°, 90°) with respect to the flow direction *x* (Figure 2.21). The aim is to investigate the influence of fibre orientation on tensile properties. The dimensions of "dog bone" samples were according NF ISO527-25B standard: 30 mm x 4 mm x 1.8 mm. The tests were performed on three samples of each formulation.
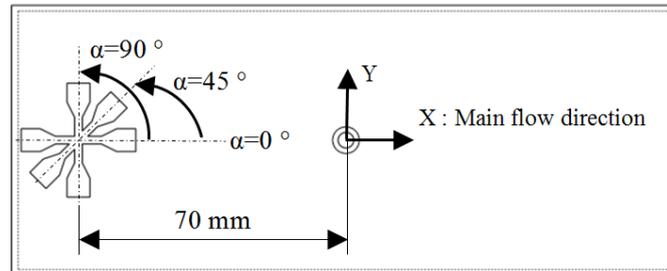
Figure 2.21

Schematic presentation of the position of tensile samples cut out from the injected box, with respect to *x*, the main flow direction

3.4.2. *Charpy Impact test*

Charpy impact test enables the determination of energy needed to fracture a material. The samples were moulded and designed following the ISO 179-1/1eA standard, using a mould with four cavities as drawn in Figure 2.22. The composite in granules was inserted in the same machine used to make the "boxes", DK codim NGH 110/200. Table 2.4 gives details of injection moulding conditions.

Sample after notching
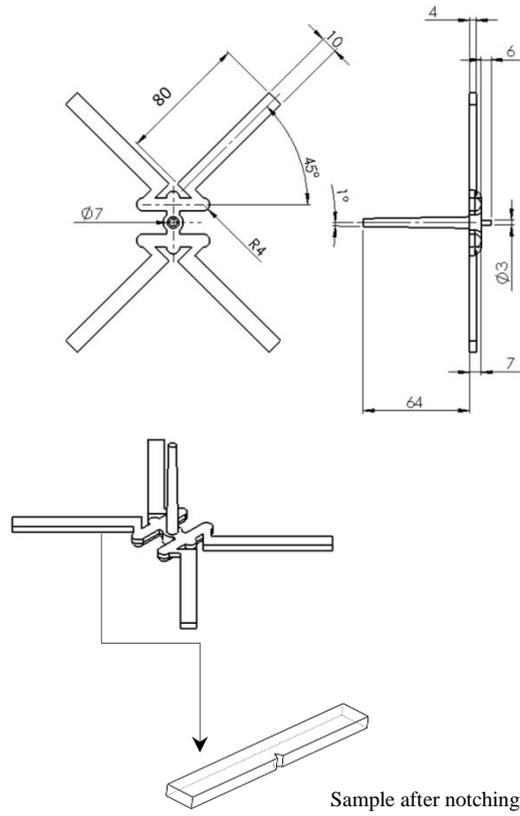
Figure 2.22

Injection molded impact cavity and dimensions of samples; all dimensions are in *mm*

Table 2.4 Injection moulding conditions for making impact bars

Injection temperature, °C	*190*	Cooling time, s	*10*
Mold temperature, °C	*30*	Holding time, s	*10*
Flow rate, cm^3/s	*94*	Holding pressure, bar	*270*
Shot length, mm	*48*	Back pressure, bar	*50*
Clamping force, KN	*1100*	Screw speed, RPM	*120*

Impact tests were performed on Instron Ceast 9050 under the following conditions: 1 J hammer, speed of 2.9 m.s^{-1}, temperature of 25 °C, with "A" notch type and a support of 60 mm.

3.5. Observation of composites morphology by Scanning Electron Microscopy (SEM)

The SEM enables images by scanning sample surfaces with a focused beam of electrons. The interactions between the sample and the electron beam provide electron loss energy shaped as a teardrop and called the interaction volume (Figure 2.23). We can distinguish two types of interactions: 1) elastic interactions with energy close to the incident one. The reflected electrons are called the backscattered electrons and give information about the material composition because they reach a deep level in the sample 2) inelastic interactions with lower energy than the elastic one and their corresponding electrons are called secondary electrons. They provide information about the topography.
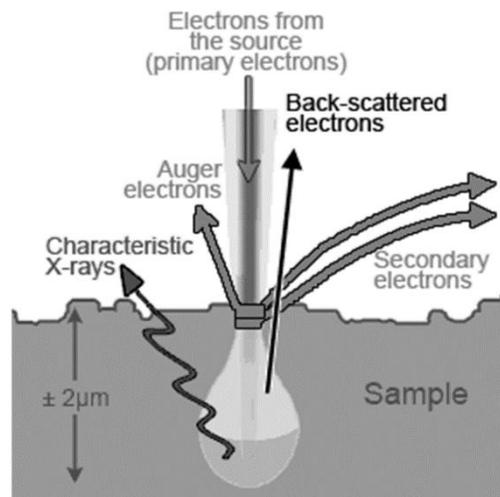
Figure 2.23

The interaction volume in SEM

SEM observations were performed on a XL30 ESEM by setting up the acceleration voltage at 15 keV and a diaphragm of 20 µm. The objective is to get a qualitative characterization of the topography (secondary electrons) in three cases 1) the rupture surfaces after tensile and impact testing, 2) the fibre microstructure in composites extruded in capillary rheometer, and 3) microstructure in the moulded part. The idea is to closely observe fibres, aiming to get the information complementary to the optical microscopy observations described in Section 4.2.

4. References

Fink, H. P., Ganster, J., & Lehmann, A. (2014). Progress in cellulose shaping: 20 years industrial case studies at Fraunhofer IAP. Cellulose, 21(1), 31-51.

Charlet, K., Jernot, J. P., Breard, J., & Gomina, M. (2010). Scattering of morphological and mechanical properties of flax fibres. Industrial Crops and Products, 32(3), 220-224.

Charlet, K., Jernot, J. P., Breard, J., & Gomina, M. (2010). Scattering of morphological and mechanical properties of flax fibres. Industrial Crops and Products, 32(3), 220-224.

Le Duc, A., Vergnes, B., & Budtova, T. (2011). Polypropylene/natural fibres composites: analysis of fibre dimensions after compounding and observations of fibre rupture by rheo-optics. Composites Part A: Applied Science and Manufacturing, 42(11), 1727-1737.

Le Moigne, N., den Oever, M., & Budtova, T. (2013). Dynamic and capillary shear rheology of natural fiber-reinforced composites. Polymer Engineering & Science, 53(12), 2582-2593.

Le Moigne, N., van Van Den Oever, M., & Budtova, T. (2011). A statistical analysis of fibre size and shape distribution after compounding in composites reinforced by natural fibres. Composites Part A: Applied Science and Manufacturing, 42(10), 1542-1550.

Rosato 3rd, D. V. (2000). Injection Molding Handbook 3rd Edition Kluwer Academic Publishers Norwell.

Soccalingame, L., Bourmaud, A., Perrin, D., Bénézet, J. C., & Bergeret, A. (2015). Reprocessing of wood flour reinforced polypropylene composites: Impact of particle size and coupling agent on composite and particle properties. Polymer Degradation and Stability, 113, 72-85.

Vincent, M., Giroud, T., Clarke, A., & Eberhardt, C. (2005). Description and modeling of fiber orientation in injection molding of fiber reinforced thermoplastics. Polymer, 46(17), 6719-6725.

Chapter 3

Fibre size analysis

during processing

The mechanical properties of composites generally depend on fibres size (aspect ratio), fibre dispersion in the matrix and fibre-matrix adhesion. As glass fibres, natural fibres are broken when mixed with polymer and when injected into a mould. Studying and understanding the evolution of fibre size during processing is thus extremely important.

The first part of this chapter is dedicated to the state of the art on the fibre size evolution during processing for glass fibre- and natural fibre-reinforced thermoplastics. The second part focuses on the results of the statistical analysis of fibre size performed on all studied composites, at each processing step, from the initial fibres to their size after extrusion and finally after injection. The aim is to show the influence of each process step and also of the fibre concentration on the fibre size. A comparison between glass and natural fibre cases is discussed.

1. The state of the art

The technique usually used to investigate the fibre size consists of separating fibres from the polymer matrix either by burning matrix when it is possible (in the case of glass fibre, for example) or by dissolving it with an appropriate solvent. Recently, [Shen et al. (2004), Bernasconi et al. (2012); Tausif et al. (2014); Thi et al. (2015)] a non-destructive technique that is X-ray µCT (Micro Computed Tomography) has been used to analyse the microstructure of composites, in particular the fibre size. The statistical analysis of fibre dimensions are based on the number-average of fibre length L_n, diameter D_n and aspect ratio $(L/D)_n$, and weight-average fibre length L_w, diameter D_w and aspect ratio $(L/D)_w$ defined as follows:

$$P_n = \frac{\sum_i n_i P_i}{\sum_i n_i} \qquad \text{[Eq 3.1]}$$

$$P_w = \frac{\sum_i n_i P_i^2}{\sum_i n_i P_i} \qquad \text{[Eq 3.2]}$$

n_i is the number of fibres and P_i can be L_i as fibre length or D_i as fibre diameter or $(L/D)_i$ as fibre aspect ratio.

1.1. Glass fibre reinforced thermoplastic

Yilmazer and Cansever (2002) investigated the breakage of glass fibre in polyamide-6 based composites and demonstrated that compounding highly reduces the fibre length and additional fibre breakage can be caused by injection moulding. The initial glass fibre length was 4 500 µm. This value decreased to L_n = 122-195 µm and L_w = 406-496 µm after extrusion and further decreased to L_n = 104-141 µm and L_w = 206-302 µm after injection moulding. The extent of decrease in L_w is larger that of L_n, meaning that long fibres remained after extrusion are broken during injection moulding. L_w was reduced by 90 % in twin screw extruder and it was further reduced by 37 % after injection molding. The extent of fibre breakage after compounding decreased with the increase of the screw speed and slightly increased with the feed rate. Inceoglu et al. (2011) reported similar findings in what concerns compounding of 30 wt % glass fibre reinforced polyamide-12.

Fu et al. (1999) reviewed the main aspects of design and process for glass fibre reinforced thermoplastics, influencing fibre rupture during compounding and injection moulding (Table 3.1). For compounding, in addition to the aspects mentionned earlier (lower screw speed and higher feed rate), a higher barrel temperature can reduce the glass fibre breakage, due to the lower resultant viscosity and stress. For injection moulding, a higher back pressure has more dramatic effect on the fibre breakage than a higher injection moulding speed. The back pressure value is directly related to the extent of the shot plasticizing in the barrel-screw system (similar to extrusion system), before being injected into the cavity. Increasing fibre content leads also to more fibre breakage, which was explained by more intense fibre-fibre and fibre-wall interactions. In addition, Turkovich and Erwin (1983) demonstrated that longer intial fibre leads to longer fibre length in the final part for the injection moulding of glass fibre reinforced polyamide 6-6 composite. However, Akay and Barkley (1991) showed that only a slight effect of the intial fibre length can be observed in the residual fibre length after processing for the case of glass fibre reinforced polypropylene. Reprocessing composites causes a further rupture of fibres.

Table 3.1 Influence of design/fabrication factors on final fibre length in short fibre reinforced polymer composite [Fu et al. (1999)]

Design /fabrication factors		*Average fibre length*
Compounding	*Lower* screw speed	Higher
	Higher barrel temperature	
	Lower mixing times	
Injection Molding	*Lower* back pressure	Higher
	Lower injection speed	
	More generous gate & runners dimensions	
Lower fibre content		Higher
Larger original fibre		Higher
Reprocessing		Lower

Lafranche et al. (2006) measured the evolution of glass fibre length along the injection molding screw, the non-return valve, nozzle and cavity. Almost 70 % of fibre breakage happens at the compression section of the screw.

Ramini et al. (1995) investigated the evolution of glass fibre length in SPS (syndiotatic polystyrene) matrix for three extrusion-screw designs, and for different locations in the injection-moulded part (A, B and C) (Figure. 3.1.a). The composite was moulded with zero back pressure and low injection molding speed to avoid fibre breakage. Figure 3.1.b shows that whatever the screw design, L_n decreases from the sprue to the end of the cavity.
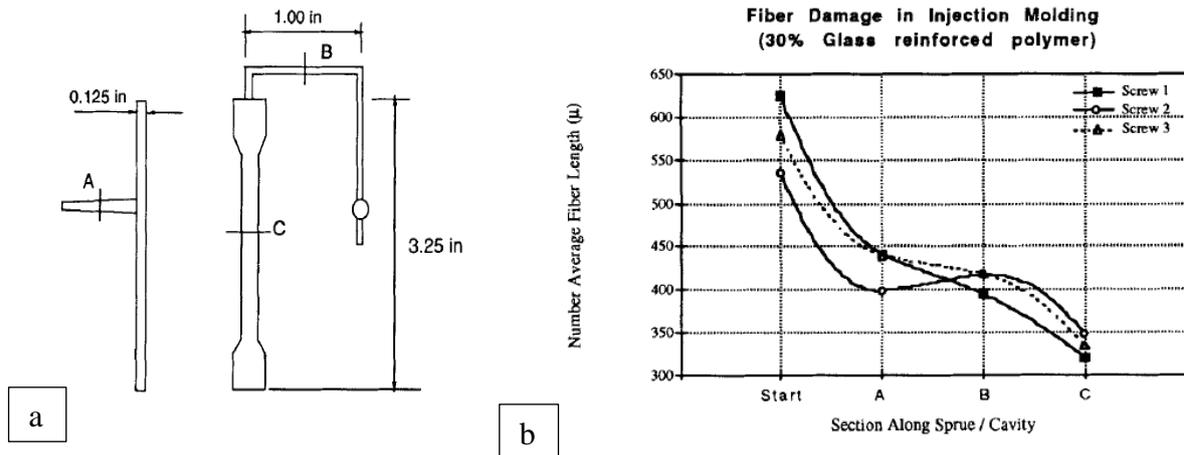
Figure 3.1

a) Injection moulded tensile bar showing positions of samples A,B and C in which fibre lengths were measured b) The number-average of glass fibre length L_n as a function of the position in the moulded part [Ramini et al. (1995)]

1.2. Natural fibre reinforced thermoplastic

It was recently demonstrated that the breakage mechanism of natural fibres is different from glass fibres [Le Duc et al. (2011); Le Duc (2013)]. Flax and Tencel fibres were observed using a rheo-optical equipment. It was shown that Tencel fibre is broken after accumulation of fatigue at the points where fibre bends (Figure.3.2.a). The flax bundles were firstly dissociated into elementary fibres that were in turn broken at defects (kink bands) because of the cumulated fatigue (Figure.3.2.b). The kink bands appear during the extraction of fibres from the stems [Le Duc et al. (2011)].
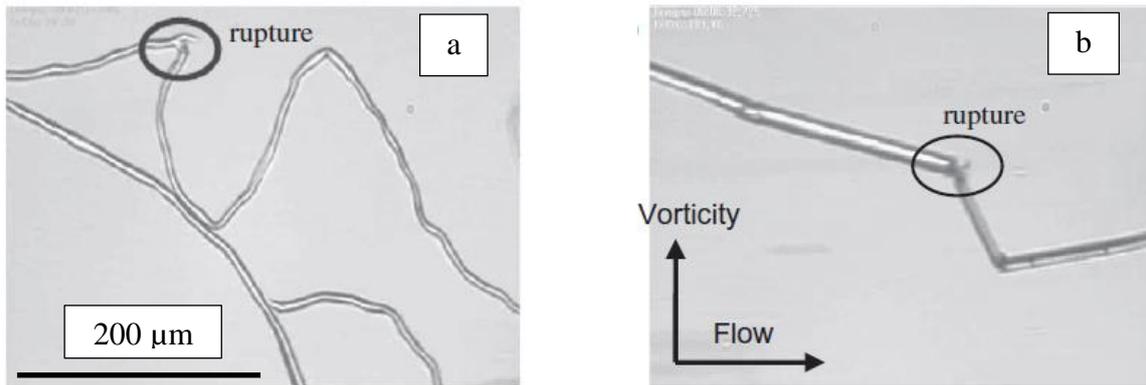
Figure 3.2

Fibre breakage observed by rheo-optic a) Tencel fibre b) elementary flax fibre [Le Duc et al. (2011)]

As mentioned above, flax fibres usually appear as bundles of elementary fibres. To obtain the longest possible aspect ratio, bundles should be dissociated without the breakage of the elementary fibres. Using rheo-optics, Le Duc et al. (2011) demonstrated that the dissociation of flax bundles happens under flow for various cumulated strains (Figure 3.3). Bundles dissociation increases with increasing the cumulated strain.
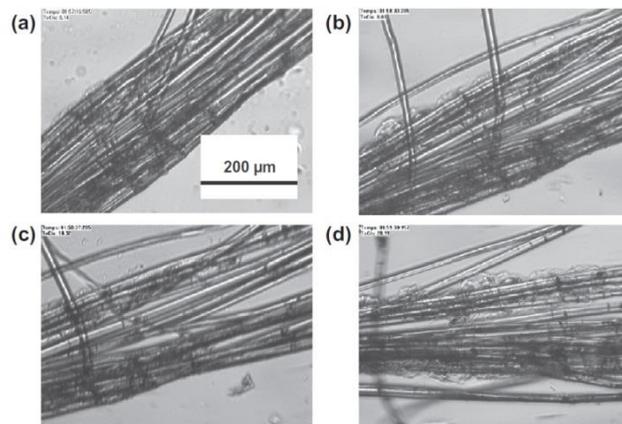
Figure 3.3

Rheo-optical images of flax bundles dissociation under flow at various cumulated strains γ, (a) γ = 0.2 (b) γ = 110 (c) γ = 180 (d) γ = 970 [Le Duc et al. (2011)]

Moreover, Le Moigne et al. (2011) showed that when fibre is initially structured in bundles, it tends to be divided into elementary fibres, thus diameter decreases, while when fibre is already elementary before processing, diameter remains constant and length decreases (Figure 3.4). The mechanism of rupture of glass fibres is different and simpler than that of natural fibres. Glass fibres have a constant diameter and their rupture occurs when the surrounding stress overcomes a critical value [Tukovich and Erwin (1983)].
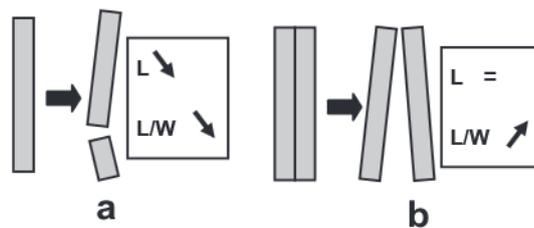
Figure 3.4

Schematic representation of the evolution of fibre length and aspect ratio with increasing fibre concentration associated to (a) breakage of the elementary fibres into smaller particles and (b) delamination of the bundles into elementary fibres [Le Moigne et al. (2011)]

Beaugrand and Berzin (2012) showed that the presence of moisture in hemp fibres when added to polycaprolactone (PCL) can lead to higher bundles dissociation, which seems contrarily to what is normally expected. This was explained by the role of water for reducing the softening of fibres and for resisting against the defects induced by processing, which causes weakness points initiating fibre fracture. The authors showed also that an increase in temperature can reduce the obtained aspect ratio after extrusion, which is in disagreement with what is known for glass fibres literature [Fu et al. (1999)]. Beaugrand and Berzin (2012) argued this by the possible degradation of some fibre components such as lignin up to 160 °C. These results were obtained with a particular biodegradable matrix (PCL) with low melting temperature (60 °C) and must be checked with other current thermoplastic matrices such as polypropylene or polyethylene. Berzin and Beaugrand (2012) and Berzin et al. (2014) showed that lower screw speed and higher flow rate during extrusion lead to lower hemp fibre breakage during compounding, which is in agreement with the glass fibre case [Yilmazer and Cansever (2002); Inceoglu et al. (2011); Fu et al. (1999)]. It was shown by Berzin et al. (2014) for hemp fibre reinforced polycaprolactone and LeDuc (2013) for flax fibre reinforced polypropylene that upon a critical value of Specific Mechanical Energy (SME), the fibre

breakage is excessive; this is also in agreement with the results of Inceoglu et al. (2011) in case of glass fibre reinforced polyamide. SME is a significant parameter that can assess the fibre breakage due to the cumulative strain involved during compounding.

Keller (2003) investigated the size of hemp fibres in PEA (co-polyesteramide) and PHBV (poly(3-hydroxybutyrate-co3hydroxyvalerate)) matrices after compounding and after injection moulding. Two types of hemp fibres differently extracted from the plants were studied: BIA (fibre degummed by the biological separation process) and DDA (fibres separated by the steam explosion process) with two different initial number-average lengths $L_n = 8$ mm and $L_n = 15.2$ mm and number-average diameters $D_n = 23 \pm 6$ µm and $D_n = 25 \pm 8$ µm, respectively. A particular screw configuration was used for each system and the moulded parts were shaped as tensile bars. The fibre length dramatically decreased: the residual L_n in the moulded tensile bar was 530 µm for PEA/DDA hemp and 100 µm for PEA/BIA hemp. However, no variation of fibre diameter even after injection has been shown, which seems somewhat ambiguous. Berzin et al. (2014) demonstrated that the breakage of natural fibres can be partially limited by optimizing the screw profile during compounding.

Contrarily to glass fibre case, when the screw configuration was the same, Keller (2003) found that the length distribution of the resultant hemp fibre (type DDA) in the granules was independent on the fibre content (Figure 3.5).
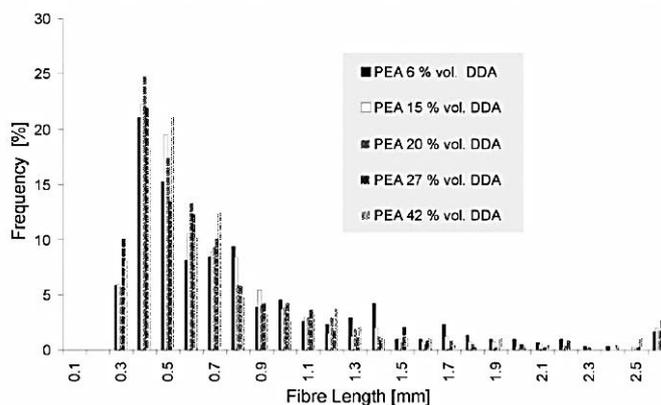
Figure 3.5

DDA-hemp length distribution for granules compounded with PEA for different concentration [Keller (2003)]

In addition, injection moulding did not cause a further shortening of hemp fibres in DDA/PEA composites (Figure 3.6).
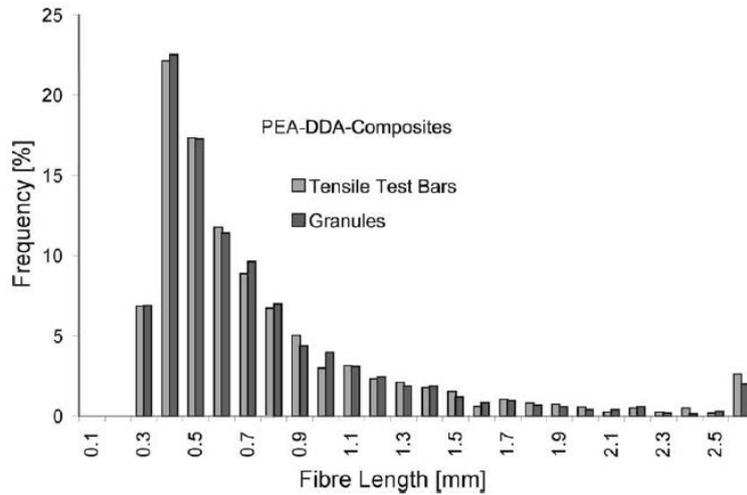
Figure 3.6

Comparison between DDA-hemp fibre length distribution at granules after compounding and at tensile test bars after injection moulding, the matrix is PEA [Keller (2003)]

Barkoula et al. (2010) studied the fibre size evolution during compounding and injection moulding of flax fibre reinforced polypropylene. They demonstrated that a further fibre shortening happens during injection moulding. The distribution of fibre length given in Figure 3.7 shows that the amount fibre length $\geq$ 0.8 mm decreases from 88 % after compounding to 55 % after injection and the maximum length reduced from 2.4 mm after compounding to 2 mm after injection.
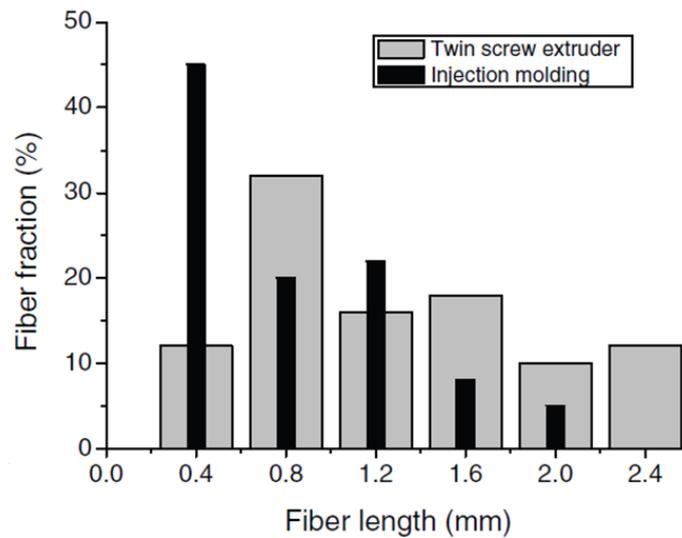
Figure 3.7

Comparison between length of fibre for 28 wt % flax reinforced-polypropylene after compounding and after injection moulding [Barkoula et al. (2010)]

The variation of fibre diameter of flax fibres during compounding and injection moulding was not taken into account despite of the "obvious" distribution of diameter observed in injection moulded part as shown in Figure 3.8.
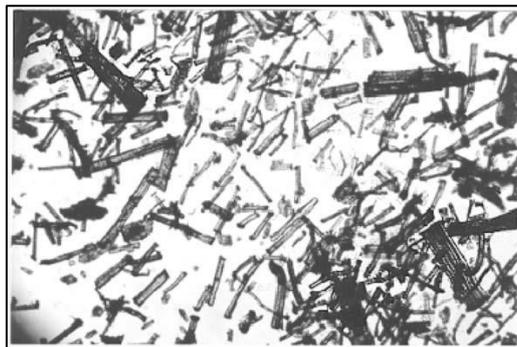
Figure 3.8

Image of flax fibres extracted from flax/PP composites after injection moulding [Barkoula et al. (2010)]

Using the X-ray tomography technique, Alemdar et al. (2008) investigated the fibre length and diameter of wood-reinforced polypropylene before and after processing (including compounding and injection moulding). Before processing, the length range of almost 80 % of

wood fibres is between 316 μm and 600 μm. It decreases after processing, giving a length average of 238 μm and 285 μm for wood/PP with and without coupling agent, respectively. The diameter of wood fibres was reduced by 61 % and 69 % for wood/PP with and without coupling agent, respectively [Alemdar et al. (2008)]. For the same system (wood/PP), by using SEM cross-section analysis, Soccalingame et al. (2015) showed that thick fibres/particles are more sensitive to breakdown and processing has no effect under a critical diameter. Moreover, the authors concluded that adding coupling agent does not show any influence on the fibre breaking during processing.

1.3. Conclusion

The mechanism of breakage of glass fibres in a thermoplastic matrix during twin screw compounding and injection moulding processes is rather well understood. The key parameters influencing the breakage of a glass fibre during compounding and injection moulding were investigated in details. The comparison between glass fibre and natural fibre breakage cases enables to conclude, on the one hand, some similarities under particular process conditions, such as the decrease of fibre breakage with increasing the feed rate and decreasing the screw speed at compounding step, and on the other hand, some differences such as the evolution of fibre length with increasing fibre content and the additional breakage of fibre after injection. The main reason behind these dissimilarities is probably the difference of morphology between natural fibres and glass fibres. An adequate comparison between glass fibre and natural fibre breakage during process would have more credibility and precision under the same process conditions.

2. Results and discussions

The aim of this section is to show a comparative study among flax-, Tencel- and glass-fibre size distributions, after compounding and after injection moulding, in a polypropylene matrix. All composites were processed under the same conditions and with the same polypropylene matrix, as described in Chapter 2. A statistical analysis of fibre size (length *L*, diameter *D* and aspect ratio *L/D*) is performed for different fibre types (Tencel, flax and glass), after compounding and injection, and for different fibre concentrations (from 3.6 vol % to 20.5 vol %). We will firstly present separately the case of each type of fibre, and then examine the effect of the fibre type on the fibre size.

2.1. Glass fibres

2.1.1. *Effect of processing*

Figure 3.9 shows a comparison between the length distribution of glass fibres as delivered, after compounding and after injection for the example of 20.5 vol %. The initial length distribution is bimodal with a minor peak around 1 500 µm and a sharper one around 3 000 µm. After compounding the length distribution becomes unimodal with a peak around 400 µm, indicating a strong fibre breakage. This peak is then marginally shifted to shorter lengths after injection moulding.
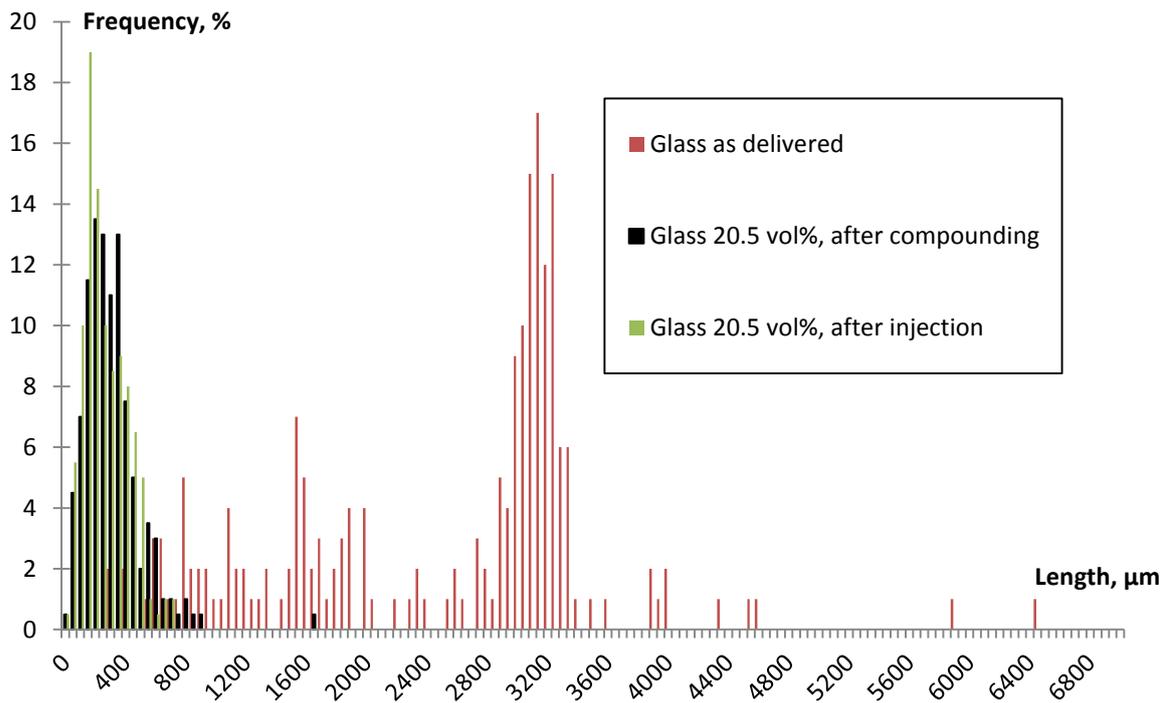
Figure 3.9

The evolution of glass fibre length distribution during compounding and injection for 20.5 vol % glass/PP composite

Table 3.2 shows that fibres are shortened by 80 % during compounding. Injection moulding causes a further fibre breakage by 20 %. In addition, after injection, L_n is slightly shortened while L_{max} is nearly two times reduced, which means that long fibres keep breaking during injection. This seems similar to the results of Yilmazer and Cansever (2002).

Table 3.2 Glass fibre sizes as delivered, after compounding and after injection

	As delivered	*After compounding*				*After injection moulding*			
Wt %	-	9.4	15.6	29.4	41.6	9.4	15.6	29.4	41.6
Vol %	-	3.6	6.3	13.1	20.5	3.6	6.3	13.1	20.5
L_n	2512	618	498	391	330	495	379	302	286
L_w	2941	858	607	571	438	719	502	412	361
L_{max}	6475	2550	2498	2353	1659	2066	1170	1035	715
L_{min}	317	87	64	43	49	30	39	30	44
$(L/D)_n$	251	62	50	39	33	49	38	30	29
$(L/D)_w$	294	86	61	57	44	72	50	41	36

2.1.2. *Influence of fibre concentration*

Figure 3.10 shows the influence of fibre content on fibre length distribution after injection. The length distibution in 3.1 vol % glass/PP is a large distribution, extending over a wide length range from 20 µm to 2 000 µm. The length distribution of composite with 20.5 vol % presents a sharper peak around 200 µm, and the range of sizes is reduced to 20-700 µm. We can conclude that glass fibre length decreases with the increase of fibre content, which seems in agreement with Fu et al. (1999) results.
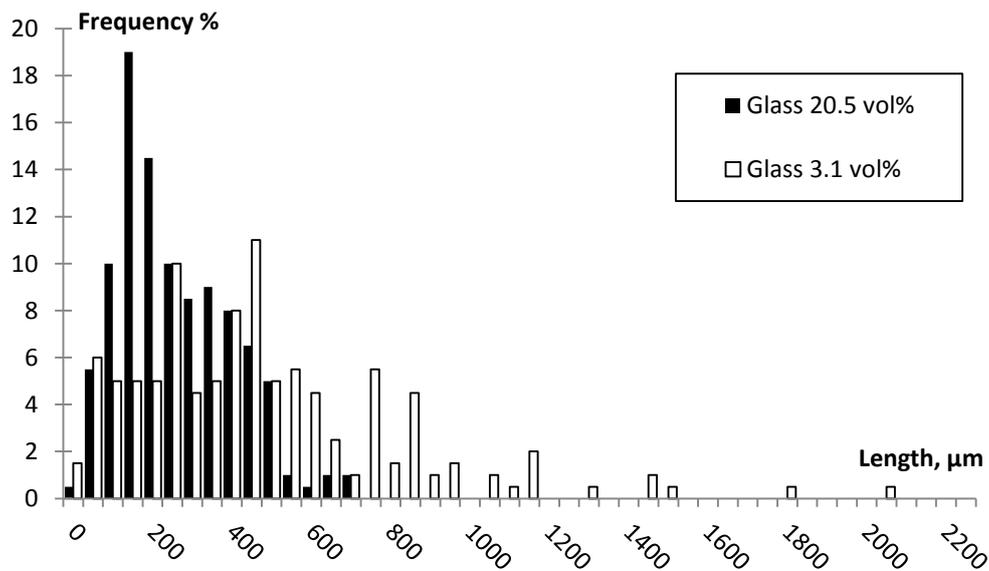
Figure 3.10

Glass/PP composite: influence of fibre content on the fibre length distribution after injection

2.2. Tencel

2.2.1. *Influence of processing*

Figure 3.11 shows a comparison between the length distribution of Tencel fibres as delivered, after compounding and after injection, for the volume fraction of 20.5 vol %. The length distributions after compounding and after injection are similar and no significant difference can be distinguished. Both distributions are slightly shifted to shorter lengths compared to the distribution of the initial fibres.
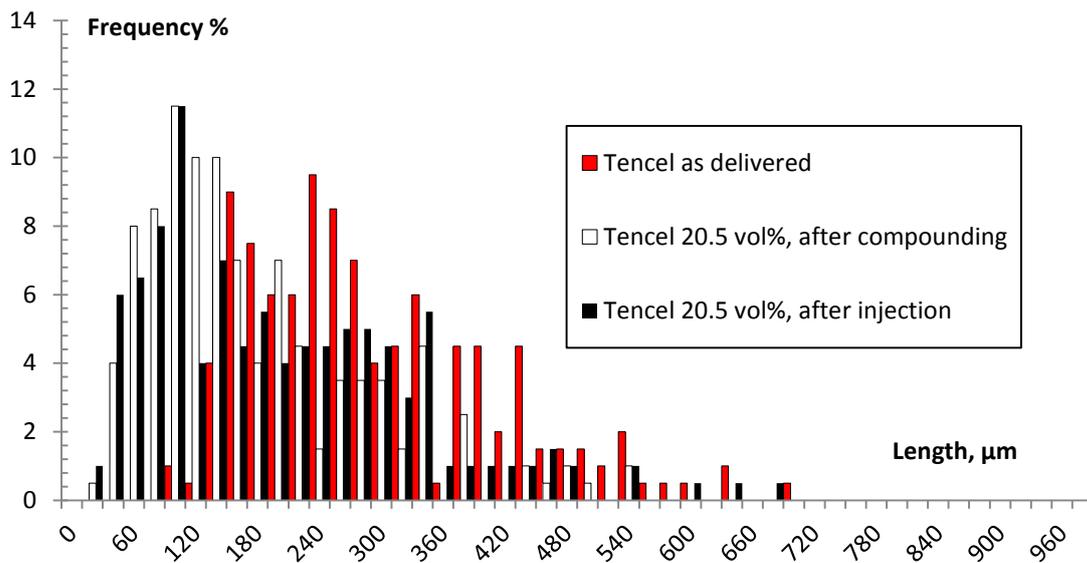
Figure 3.11

The evolution of Tencel fibre length distribution at different processing steps in the composite for 20.5 vol % Tencel/PP

Contrarily to the glass fibre case, Table 3.3 shows that injection moulding did not cause an additional length reduction for Tencel fibres. The difference in length between after compounding and after injection moulding lies in the error experimental range 10 % (as mentionned in Chapter 3, Section 3.1 Fibre size anlysis).

Table 3.3 Sizes of Tencel fibres: as delivered, after compounding and after injection moulding

	As delivered	*After compounding*				*After injection moulding*			
Wt %	-	5	10	20	30	5	10	20	30
Vol %	-	3.6	6.3	13.1	20.5	3.6	6.3	13.1	20.5
L_n	300	240	242	237	195	262	255	230	202
L_w	338	294	318	306	264	342	277	290	287
L_{max}	714	680	793	656	820	738	627	562	688
L_{min}	113	53	30	29	34	50	50	46	21
$(L/D)_n$	30	24	24.2	23.7	19.5	26.2	25.5	23	20.2
$(L/D)_w$	33.8	29.4	31.8	30.6	26.4	34.2	27.7	29	28.7

2.2.2. *Influence of concentration*

Table 3.3 shows that fibre length practically does not change with the increase of fibre concentration from 3.6 to 13.1 vol % after compounding. However, a considerable fibre breakage can be observed at 20.5 vol %. Figure 3.12 presents the influence of fibre content on the fibre length distribution after injection for Tencel/PP composites. The distribution peak is progressively moved to shorter length values and the distribution gets sharper with the increase of the fibre concentration. This results in L_n reduction from 255 µm for 6.5 vol % concentration to 202 µm for 20.5 vol % concentration, as shown in Table 3.3. Fibre concentration has a stronger influence on fibre size than processing.
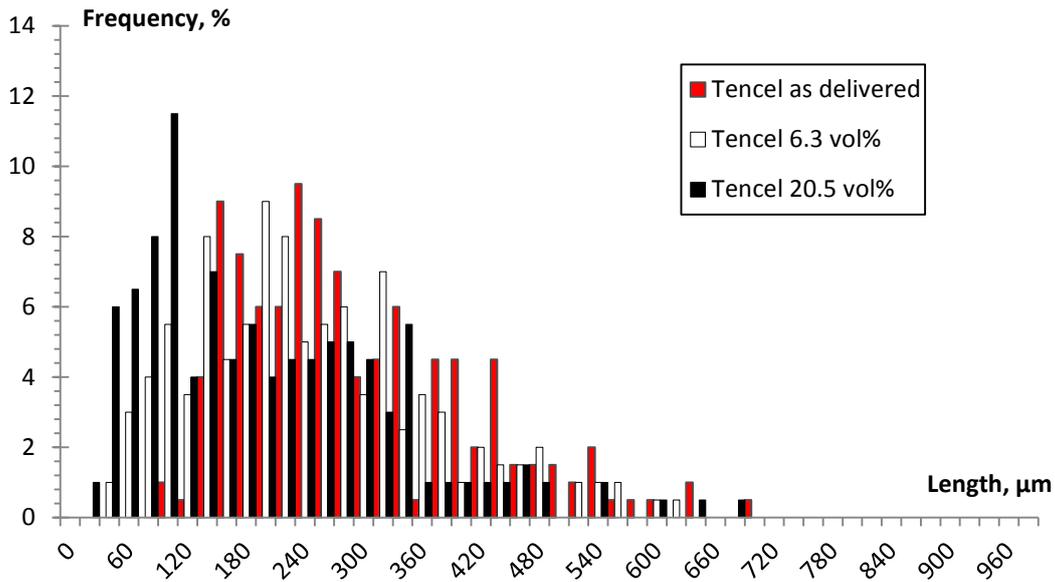
Figure 3.12

Influence of fibre content on Tencel fibre length distribution after injection moulding

As man-made fibres, the aspect ratio of Tencel is the length over a constant diameter, meaning that the aspect ratio has the same variation of the length. This is also the case of glass fibre but not that of flax fibres that will be shown in the next section.

2.3. Flax

The analysis of flax fibres size consists of studying the evolution of two variables: length and diameter. Table 3.4 regroups all these measurements.

Table 3.4 Flax fibre sizes as delivered, after compounding and after injection moulding

	As delivered	*After compounding*				*After injection moulding*			
Wt %	-	5	10	20	30	5	10	20	30
Vol %	-	3.6	6.3	13.1	20.5	3.6	6.3	13.1	20.5
L_n	450	433	415	434	422	428	407	420	388
L_w	458	478	472	469	477	464	446	458	433
L_{max}	1020	1028	1150	874	1116	855	827	922	863
L_{min}	211	53	64	60	74	98	85	71	81
D_n	48	35	34	39	39	34	36	32	28
D_w	84	46	49	60	54	46	54	43	34

D_{max}	238	133	151	254	143	126	168	101	119
D_{min}	10	9	11	12	11	14	11	11	13
$(L/D)_n$	14.8	14.9	15.7	14.6	13.5	15.3	14.4	15.9	15.1
$(L/D)_w$	20	18	21	18	17	19	18	20	18
$(L/D)_{max}$	50	52	52	40	43	39	36	56	44
$(L/D)_{min}$	2	2	1	2	2	2	2	4	3

2.3.1. *Influence of processing*

Figure 3.13 a, b and c shows the length, diameter and aspect ratio distributions of flax fibres, respectively, for three states of fibres: as delivered, after compounding and after injection moulding, and this for the concentration of 20.5 vol %. The initial fibres reveal a unimodal length distribution with a sharp peak around 400 µm and an overall range between 200 µm and 1 000 µm. The distributions of fibre length after compounding and after injection are similar, exhibiting a wide peak also around 400 µm and a range of length between 50 µm and 800 µm (Figure 3.13. a). This means that fibres were broken during processing and thus L_n decreases from 450 µm, as delivered, to 422 µm after compounding and 388 µm after injection moulding.
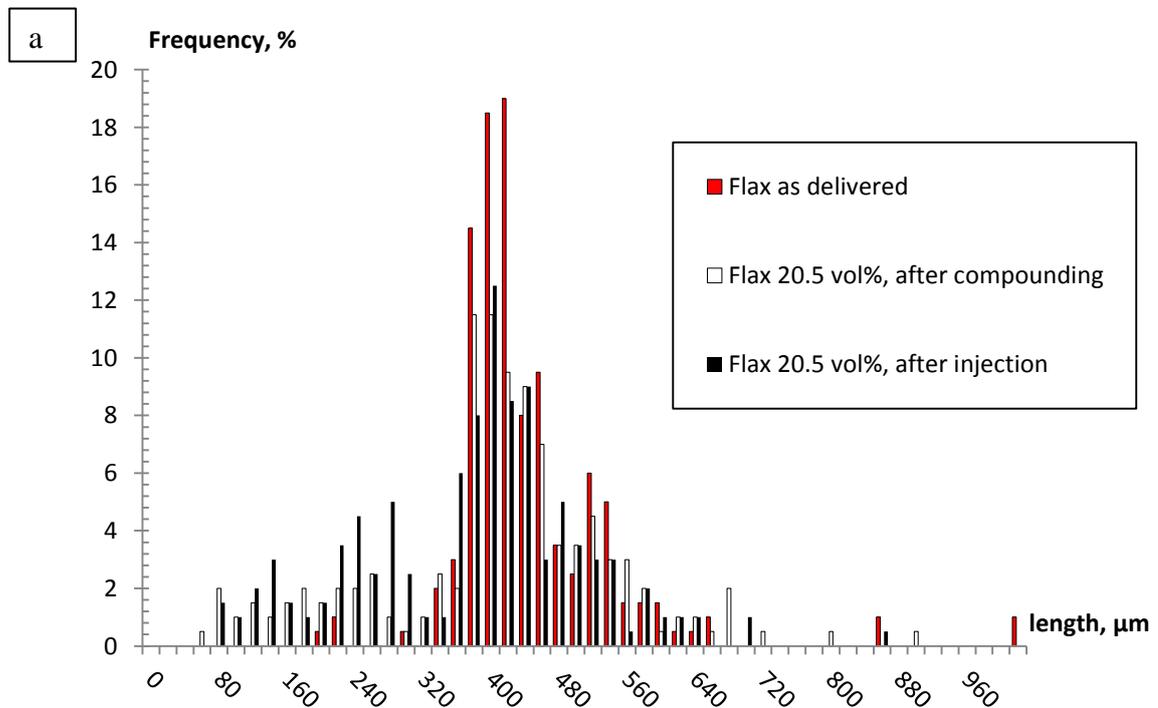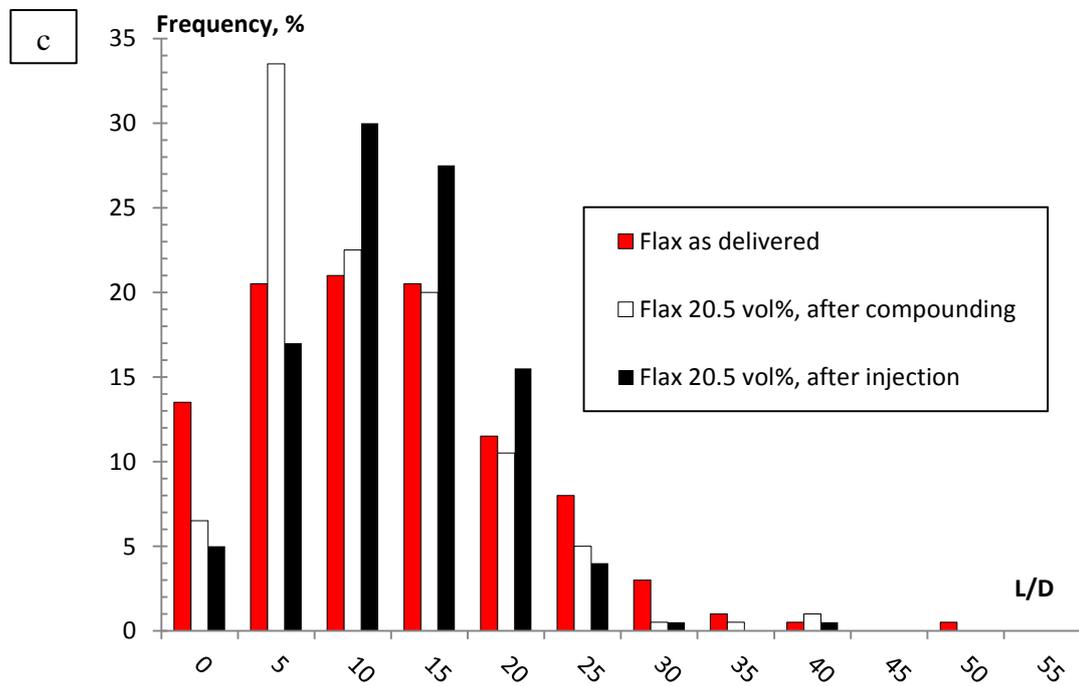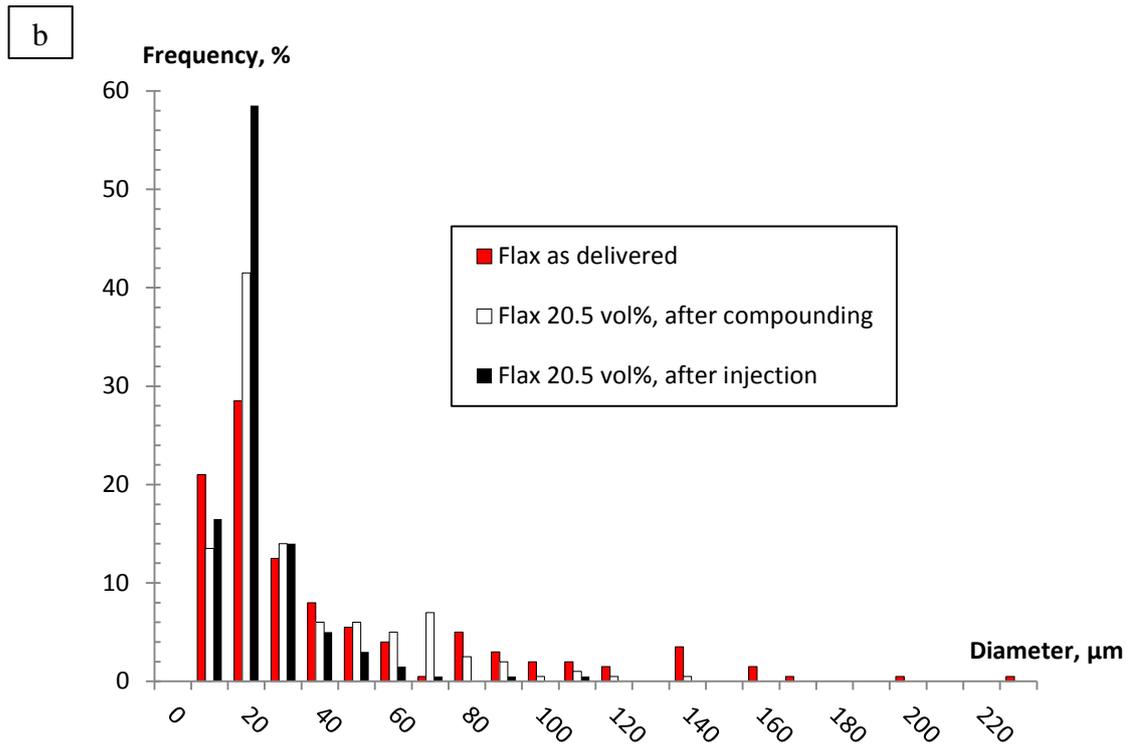
Figure 3.13

The evolution of distributions of (a) fibre length, (b) fibre diameter and (c) aspect ratio, along processing for 20.5 vol % flax/PP

The diameter distribution in Figure 3.13 b shows that, on the one hand, $D_n \geq 160$ µm disappear after compounding and 120 µm $\leq D_n \leq 160$ µm disappear after injection, and on the other hand, the frequency of fibres with the diameter of 20-40 µm increases progressively along the process, from fibres as delivered to fibres after injection. D_n and D_w decrease from 48 µm and 84 µm as delivered to 39 µm and 54 µm after compounding, and to 28 µm and 34 µm after injection, respectively. This means that not only the length is reduced during processing but also the diameter, due to the bundles' dissociation.

The distribution of the aspect ratio is similar for all steps of processing (Figure 3.13.c). Because the extent of length decrease is nearly equal to the extent of diameter decrease (Table 3.4), $(L/D)_n$ is almost unchanged during processing. However, the initial fibres are thick and long while the final fibres are thin and short (Figure 3.14).
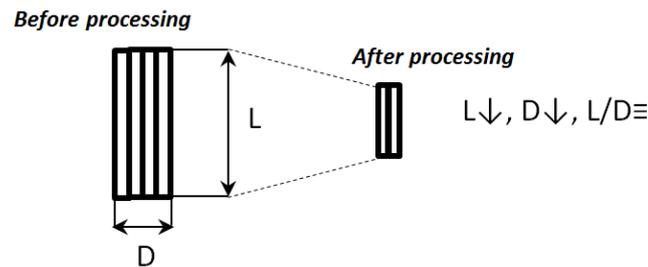
Figure 3.14

Schematic representation of the degradation of flax fibres during processing

2.3.2. *Influence of concentration*

Figure 3.15 a, b and c shows a comparison between length, diameter and aspect ratio distributions in composites with 20.5 vol % and 3.1 vol % of flax, respectively. Some long fibres ($L_n \geq 740$ µm) with low frequencies ~ 1 % disappear and the frequency of some short fibres ($L_n \leq 300$ µm) increases when concentration increases from 3.1 % vol. to 20.1 vol % , hence L_n and L_w slightly decrease from 428 µm and 464 µm to 388 µm and 433 µm, respectively. However, there is almost no difference in length between 3.1 vol %, and 13.1 vol %, according to Table 3.4, which means that the major fibre breakage happens when the concentration reaches 20.5 vol %. A similar statement for diameter distribution can be concluded (Figure 3.15.b). This leads to a decrease of D_n and D_w from 34 µm and 46 µm to 28

and 34 μm, respectively, when increasing concentration from 3.1 vol % to 20.5 vol %. However, the diameter remains constant between 3.6 vol % and 13.1 vol % as shown in Table 3.4. Figure 3.15.c provides the distribution of the aspect ratio that remains moderately unchanged with the increase of fibre concentration. $(L/D)_n$ and $(L/D)_w$ remain constant around 15 and 18-19, respectively, as given in Table 3.4.
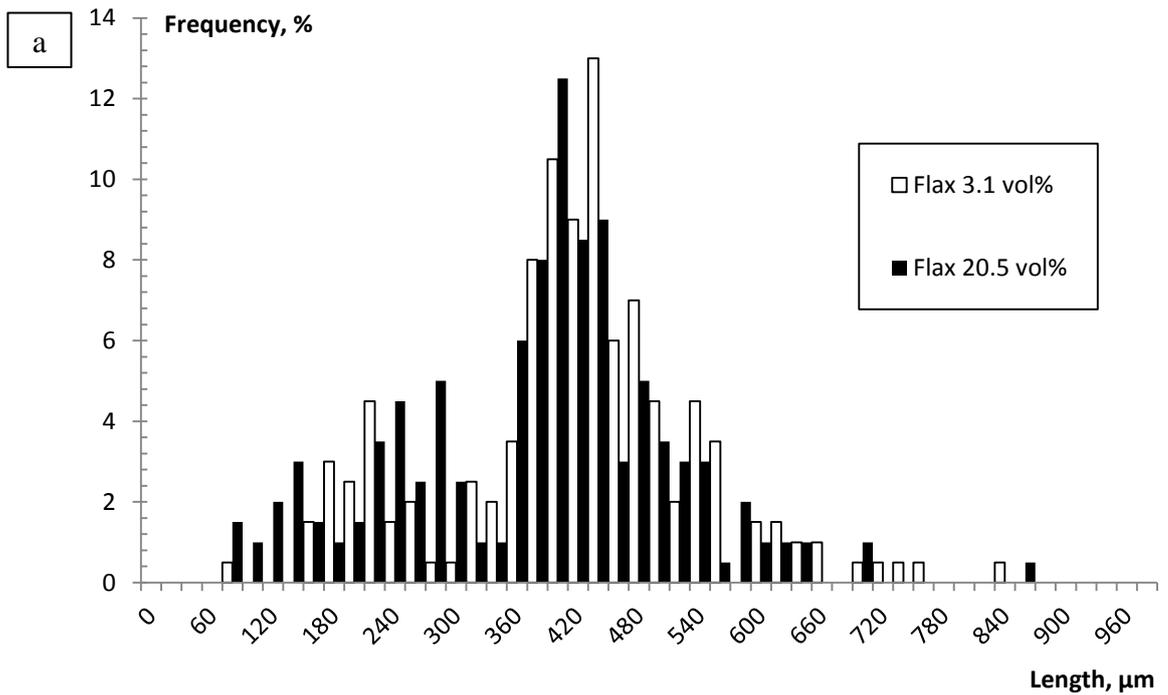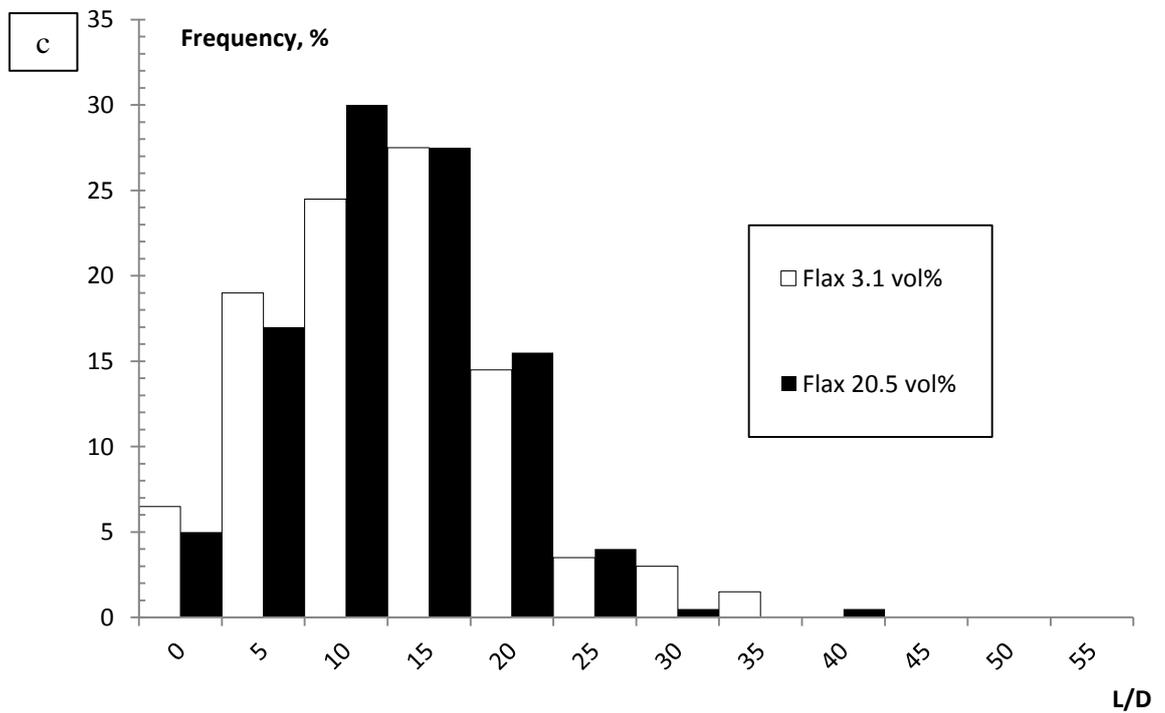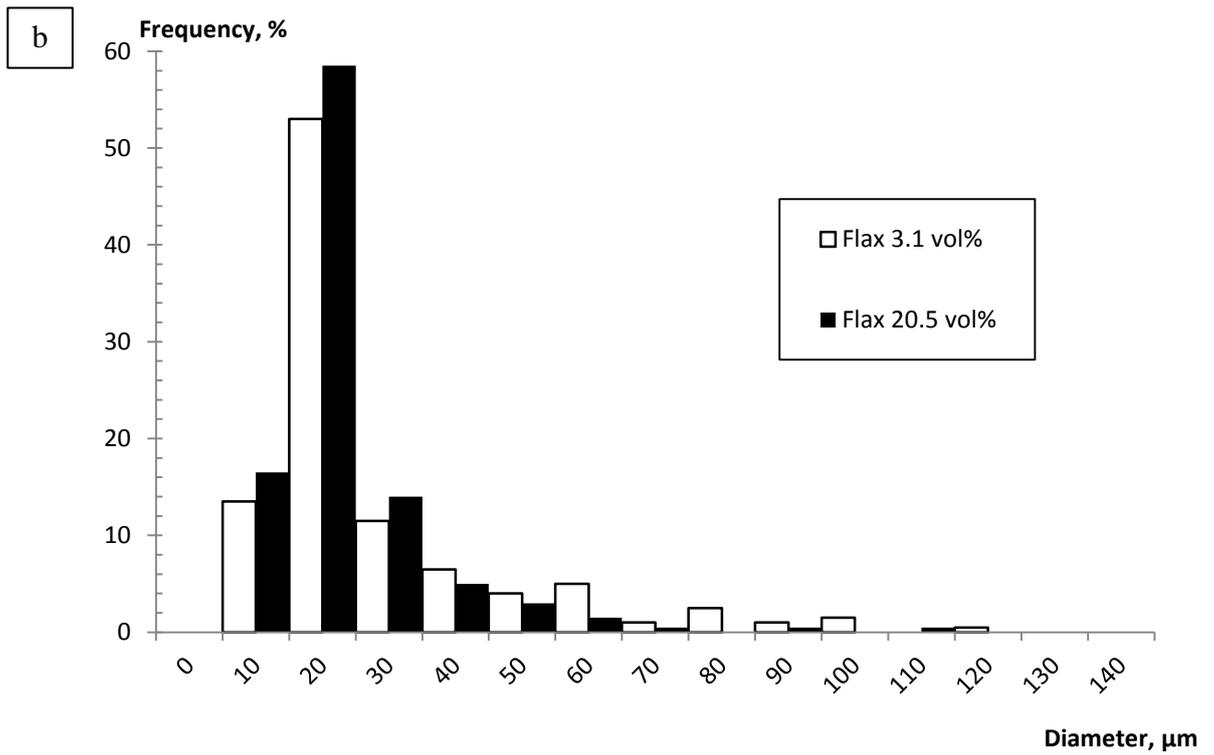
Figure 3.15

Influence of fibre content on flax fibre (a) length (b) diameter and(c) fibre aspect ratio

distributions after injection

2.4. Comparison between fibre types

Figure 3.16 shows L_n evolution with the fibre content, for glass, Tencel and flax composites during processing. Glass fibre length dramatically decreases by almost 80 %, from the unprocessed fibres to fibres in the 3.1 vol % composite after compounding. For the concentration between 3.1 vol % and 20.5 vol %, fibre length remains decreasing with a much lower rate compared to concentration between zero (unprocessed fibres) and 3.1 vol %. Injection moulding causes an additional glass fibre breakage. The difference of length between fibres after compounding and fibres after injection moulding decreases when fibre content increases. For flax and Tencel fibres, most of length reduction occurs from the initial fibres to after compounding fibres. While L_n of Flax fibres marginally decreases as the fibre content gets higher after injection moulding, that of Tencel remains unchanged. Considering that L_n of glass fibres keeps decreasing with a higher slope than flax fibres, flax fibres becomes progressively longer than glass ones. Tencel fibres are initially shorter than flax and glass ones. Because Tencel fibre length evolution with fibre content is similar to the flax one, the difference between Tencel and flax fibre length is almost constant all over the studied concentrations (about 120-150 µm). However, the difference of fibre length between Tencel and glass fibres decreases from 260 µm at 3.1 vol % to 80 µm at 20.5 vol % after injection moulding.
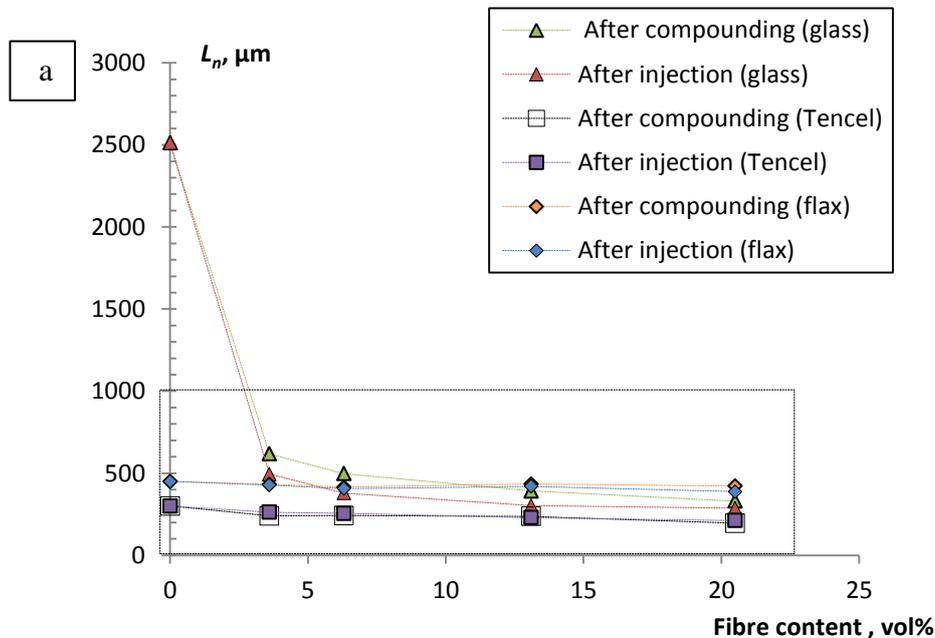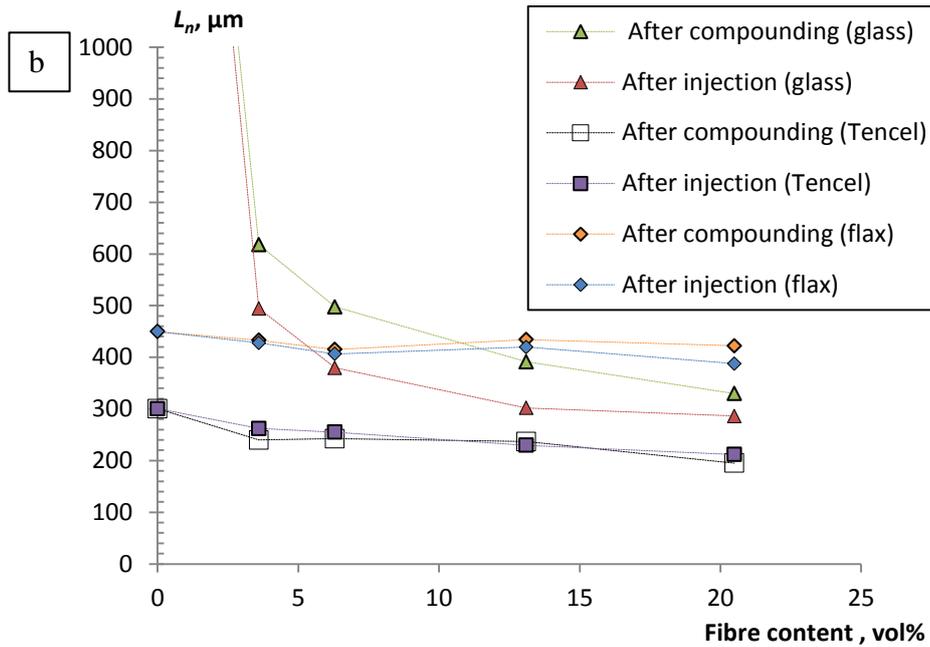
Figure 3.16

a) L_n evolution with the fibre content; zero volume fraction corresponds to the initial fibres (unprocessed), b) zoom of the figure "a" in the dashed line rectangle

Figure 3.17. presents D_n of flax fibre as a function of the fibre content, after compounding and after injection. The unprocessed fibres show a $D_n = 48$ µm. Considering that D_n of elementary fibres is 10-15 µm, the number-average of the elementary fibres per bundle is about 3-4. The reduction from $D_n = 48$ µm for fibres as delivered to $D_n = 34$ µm for fibres in the 3.1 vol % composite after compounding, corresponds to a dissociation of one elementary fibre from a bundle of four elementary fibres, which results in bundle of three elementary fibres. Compounding reduces the diameter with lower extent for 13.1 and 20.5 vol % when compared to 3.6 and 6.3 vol %. However, after injection moulding, D_n progressively decreases from 48 µm as delivered until 28 µm at 20.5 vol %, which corresponds on average to a bundle of two elementary fibres.
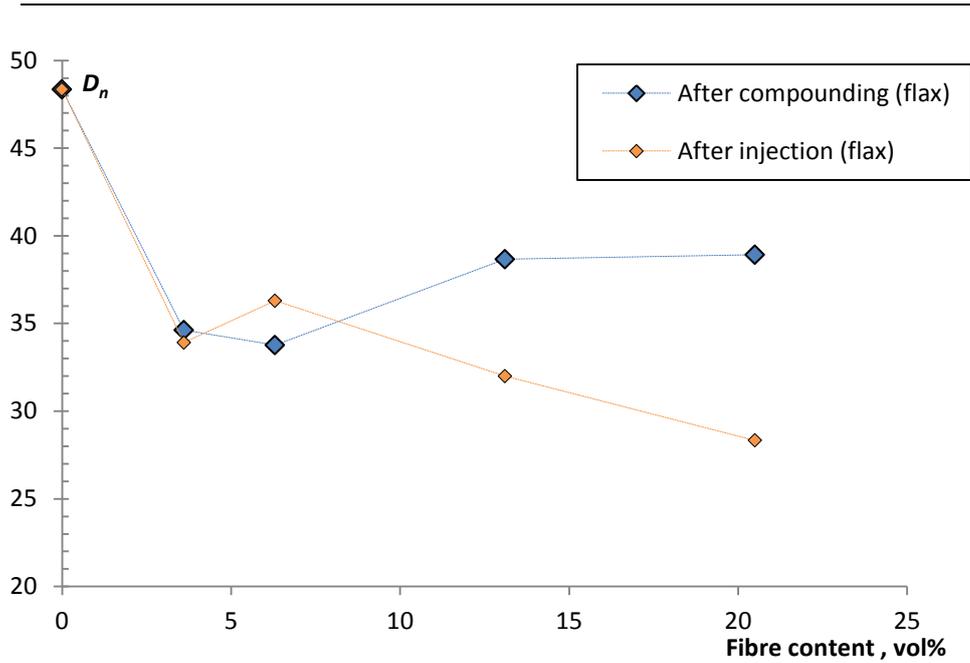
Figure 3.17

Evolution of flax D_n with the fibre content; zero volume fraction corresponds to the initial

fibres (unprocessed)

Figure 3.18 shows $(L/D)_n$ evolution with fibre content for glass, Tencel and flax fibre composite during processing. Because the diameter of glass and Tencel fibres is constant (10 µm), $(L/D)_n$ presents the same evolution as their L_n but divided by ten. For flax fibre, the aspect ratio is unchanged either by increasing concentration or by the injection moulding. This is the result of the simultaneous dissociation of bundles and the diminution of length as explained in Figure 3.17. In conclusion, the final aspect ratio after injection moulding can be organized in descendant order 1) glass 2) Tencel 3) flax.
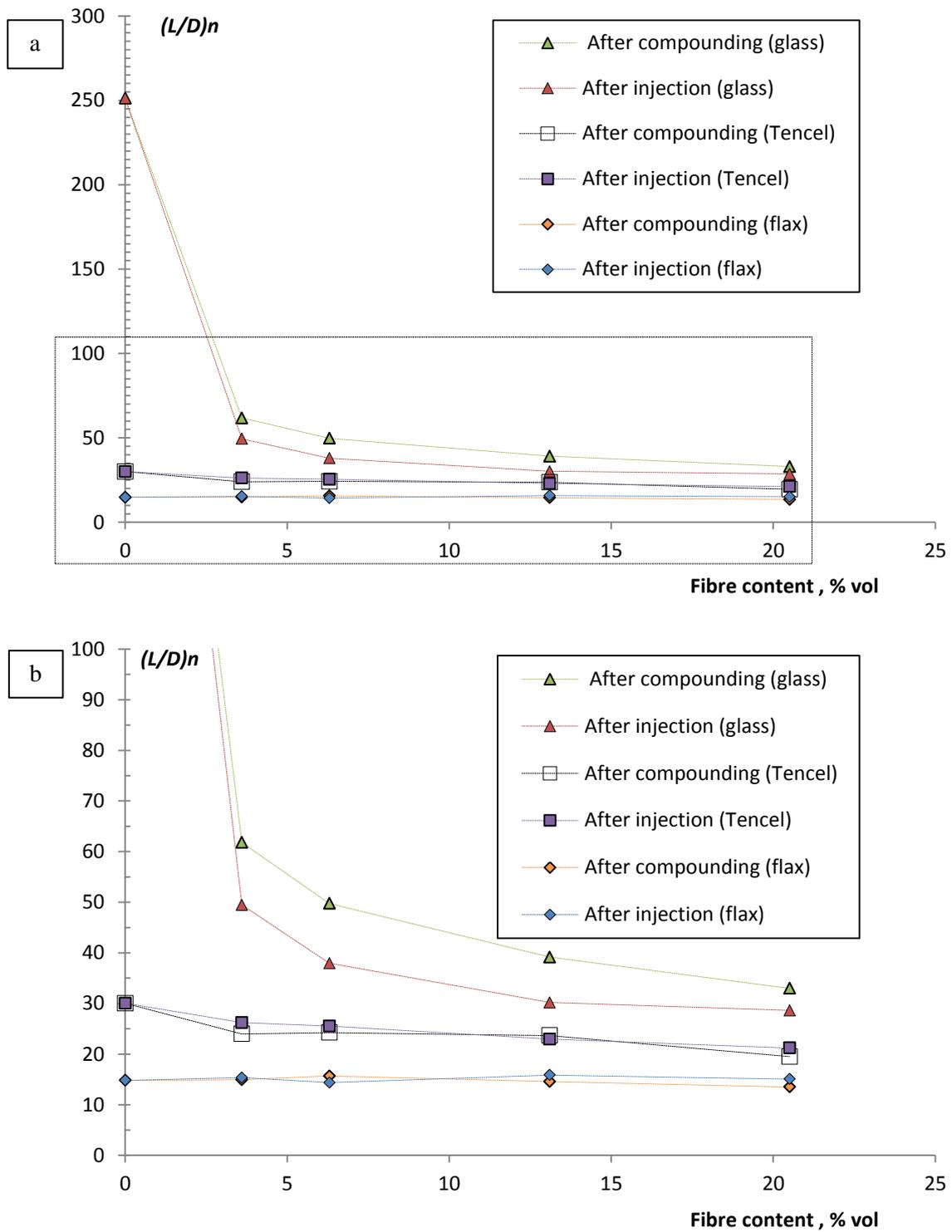
Figure 3.18

a) $(L/D)_n$ evolution with the fibre content; zero volume fraction corresponds to the initial fibres (unprocessed) b) zoom of the figure (a) within the dashed rectangle

2.5. Conclusions

A substantial investigation of fibre rupture was performed along the entire process, from the initial fibres to those in the moulded part. The breakage of glass fibres is different from flax and Tencel fibres ones.

The influence of compounding and injection moulding, and the concentration of fibres were investigated. Glass fibres are initially longer than flax and Tencel fibres. Glass fibres undergo an intensive breakage during compounding and an additional slight one during injection moulding. The increase of fibre content shortens fibres to some extent. This was in agreement with the state of the art. The breakage of Tencel fibres is much smaller on average as compared to glass fibres. The maximum of Tencel fibre breakage is around 30 % at high concentration after injection moulding. The length of flax fibre is reduced. Because of the decrease of flax diameter, its aspect ratio does not vary, becoming lower than those of Tencel and glass. This behaviour is completely different from the glass fibre rupture during processing, which reflects the specificity of natural fibres made of bundles.

The mechanical properties of the final moulded parts depend not only on fibre length or aspect ratio but also on other microstructure features such as orientation and dispersion. This will be detailed in the next chapter.

3. References

Akay, M., & Barkley, D. (1991). Fibre orientation and mechanical behaviour in reinforced thermoplastic injection mouldings. Journal of materials science, 26(10), 2731-2742.

Alemdar, A., Zhang, H., Sain, M., Cescutti, G., & Müssig, J. (2008). Determination of Fiber Size Distributions of Injection Moulded Polypropylene/Natural Fibers Using X-ray Microtomography. Advanced Engineering Materials, 10(1-2), 126-130.

Barkoula, N. M., Garkhail, S. K., & Peijs, T. (2009). Effect of compounding and injection moulding on the mechanical properties of flax fibre polypropylene composites. Journal of reinforced plastics and composites.

Bernasconi, A., Cosmi, F., & Hine, P. J. (2012). Analysis of fibre orientation distribution in short fibre reinforced polymers: A comparison between optical and tomographic methods. Composites Science and Technology, 72(16), 2002-2008.

Berzin, F., Vergnes, B., & Beaugrand, J. (2014). Evolution of lignocellulosic fibre lengths along the screw profile during twin screw compounding with polycaprolactone. Composites Part A: Applied Science and Manufacturing, 59, 30-36.

Fu, S. Y., Hu, X., & Yue, C. Y. (1999). Effects of fiber length and orientation distributions on the mechanical properties of short-fiber-reinforced polymers. 材料, 48(6Appendix), 74-83.

Franzen, B., Klason, C., Kubat, J., & Kitano, T. (1989). Fibre degradation during processing of short fibre reinforced thermoplastics. Composites, 20(1), 65-76.

Inceoglu, F., Ville, J., Ghamri, N., Pradel, J. L., Durin, A., Valette, R., & Vergnes, B. (2011). Correlation between processing conditions and fiber breakage during compounding of glass fiber-reinforced polyamide. Polymer Composites, 32(11), 1842-1850.

Keller, A. (2003). Compounding and mechanical properties of biodegradable hemp fibre composites. Composites Science and Technology, 63(9), 1307-1316.

Lafranche, E., P. Krawczak, A. Coulon, J.P. Ciolczyk and J.Maugey (2006). Processing-dependent microstructure of long glass fibre reinforced polyamide 6-6 injection moulding and related mechanical properties. The 8th International conference on flow processes in composites materials (FPCM8). Douai, France.

Le Duc, A., Vergnes, B., & Budtova, T. (2011). Polypropylene/natural fibres composites: analysis of fibre dimensions after compounding and observations of fibre rupture by rheo-optics. Composites Part A: Applied Science and Manufacturing, 42(11), 1727-1737.

Le Duc, A. (2013). Comportement et rupture de fibres cellulosiques lors de leur compoundage avec une matrice polymère (Doctoral dissertation, Ecole Nationale Supérieure des Mines de Paris).

Le Moigne, N., van Den Oever, M., & Budtova, T. (2011). A statistical analysis of fibre size and shape distribution after compounding in composites reinforced by natural fibres. Composites Part A: Applied Science and Manufacturing, 42(10), 1542-1550.

Shen, H., Nutt, S., & Hull, D. (2004). Direct observation and measurement of fiber architecture in short fiber-polymer composite foam through micro-CT imaging. Composites Science and Technology, 64(13), 2113-2120.

Shon, K., & White, J. L. (1999). A comparative study of fiber breakage in compounding glass fiber-reinforced thermoplastics in a buss kneader, modular Co-rotating and counter-rotating twin screw extruders. Polymer Engineering & Science, 39(9), 1757-1768.

Soccalingame, L., Bourmaud, A., Perrin, D., Bénézet, J. C., & Bergeret, A. (2015). Reprocessing of wood flour reinforced polypropylene composites: Impact of particle size and coupling agent on composite and particle properties. Polymer Degradation and Stability, 113, 72-85.

Tausif, M., Duffy, B., Grishanov, S., Carr, H., & Russell, S. J. (2014). Three-Dimensional Fiber Segment Orientation Distribution Using X-Ray Microtomography. Microscopy and Microanalysis, 20(04), 1294-1303.

Thi, T. B. N., Morioka, M., Yokoyama, A., Hamanaka, S., Yamashita, K., & Nonomura, C. (2015). Measurement of fiber orientation distribution in injection-molded short-glass-fiber composites using X-ray computed tomography. *Journal of Materials Processing Technology*, *219*, 1-9.

Von Turkovich, R., & Erwin, L. (1983). Fiber fracture in reinforced thermoplastic processing. Polymer Engineering & Science, 23(13), 743-749.

Yilmazer, U., & Canserver, M. (2002). Effects of processing conditions on the fiber length distribution and mechanical lproperties of glass fiber reinforced nylon-6. Polymer composites, 23(1), 61.

Chapter 4

Fibre orientation and dispersion in injection-moulded parts

Rupture of fibre during processing severely limits the mechanical properties of the injection moulded component. An unfavourable orientation and dispersion during the flow in the mould cavity can have a similar effect on composite mechanical properties. The set of fibre size, orientation and dispersion is commonly called microstructure in the field of fibre-reinforced thermoplastics. We analysed in Chapter 3 the fibre size that is one of the important microstructural features. In injection moulding process, the fibre orientation and dispersion are induced by the flow. While very little is known about the microstructure of natural fibre reinforced thermoplastic, the case of glass fibre is more mature and well-studied.

In this chapter, we begin by the state of the art in order to understand the difference between glass and natural fibres related to the flow induced orientation and dispersion. We suggest a method of characterization of natural fibres orientation, enabling to take into account some of their inherent features. A major part of the results and discussions section is concerned with the microstructure of natural fibre reinforced polypropylene; the case of glass fibre microstructure is also investigated for comparison.

1. State of the art

1.1. Characterization techniques and approaches in fibre orientation characterisation

1.1.1. *Dispersion*

The dispersion of fibres consists of investigating the volume fraction distribution in the injection-moulded part. The most used technique is to determine the density of composite across the thickness by grinding sample to an appropriate thickness. Reproducing this experiment in several locations in the injection-moulded part enables to map out the distribution of the fibre volume fraction all over this part.

In order to evaluate the extent of the density variation, the experimental measurements are compared with the reference density. The latter is calculated by the mixing rule equation defined as:

$$\rho_c = \rho_f f + \rho_m (1 - f) \qquad \text{[Eq.4.1]}$$

were ρ_c , ρ_f and ρ_m are the densities of composite, fibres and matrix, respectively. f is the volume fraction of fibre.

The matrix is usually assumed to keep the same density throughout the thickness. This leads to a small error because it is expected that matrix increases in crystallinity and thus in density nearby the mid-plane of the studied part. Nevertheless, when the fibres are much denser than matrix this error can be neglected [Sphar et al. (1990)].

1.1.2. *Orientation*

1.1.2.1. *Glass fibres*

The technique classically used to analyse the orientation of glass fibre reinforced polymers (Figure 4.1) consists of observing a cross-section in the part thickness either with optical microscope in reflected light mode or with Scanning Electron Microscope (SEM). An example of a cross-section is given in Figure 4.1.

x :the   main
flow direction
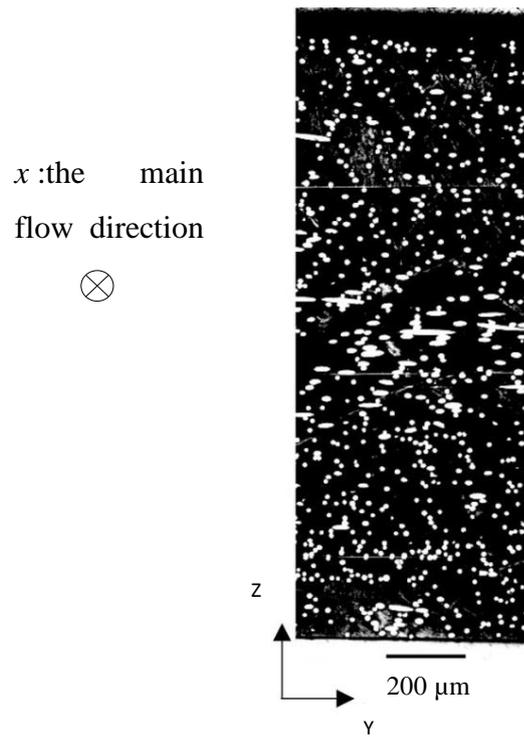
Figure 4.1

Example of a polished surface perpendicular to the main flow direction observed by scanning electron microscopy [Vincent et al. (2005)]

Both angles ϕ (in *xy*-plane) and θ can define the fibre orientation as presented in Figure 4.2
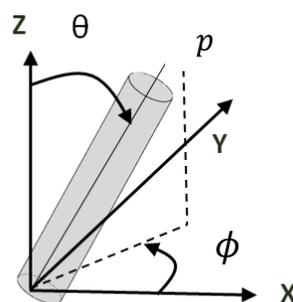
Figure 4.2

Definition of the angles θ and ϕ, p is the unit vector associated to fibre

We outline that we will consider that x is the flow direction, xy is the plane of the moulded parts and z is the thickness axis, in all the following sections.

Assuming that all fibres have the same diameter, cylindrical glass fibres meet the polished surface either as circles (with diameter equal to the fibre diameter) or as ellipses (with minor axis equivalent to the fibre diameter) (Figure 4.3.b). When a fibre is perfectly perpendicular to the cross-section, the apparent shape result is circular. When a fibre makes an angle with respect to a cross-section, the minor and the major axis of ellipses determine the orientation angle ϕ of a fibre with respect to the cross section, and the orientation of the ellipse gives the angle θ (Equation. 4.2) [Vincent et al. (2005)]. Therefore, the full 3D orientation can be determined (except indeterminacy between ϕ and $\pi-\phi$).

$$\theta = cos^{-1}\left(\frac{Q}{J}\right)$$
[Eq. 4.2]

where "J" is the major axis and "Q" is the minor of the ellipse (Figure 4.3b)
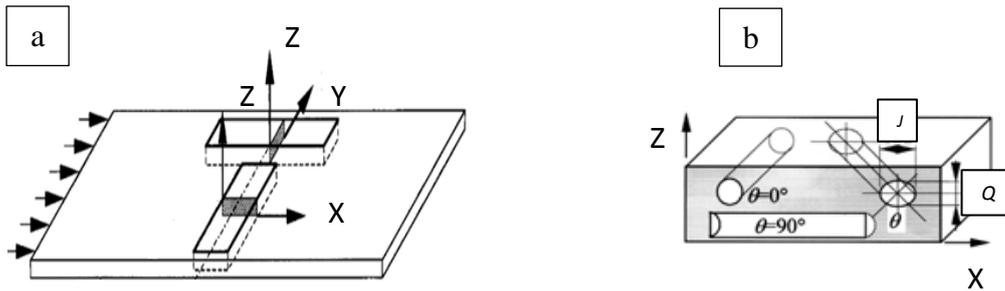
Figure 4.3

(a) fibre cross-section perpendicular to *xy*-plane and (b) ellipses method for quantification of fibre orientation [Neves et al. (1998)]

Advani and Tucker (1987) defined an orientation tensor, assuming that fibres are rigid cylinders, their section is circular and their concentration is spatially uniform, given by:

$$a_{ij} = \int_p p_i p_j \psi(\boldsymbol{p}) d\boldsymbol{p}$$
[Eq. 4.3]

where $\boldsymbol{p}$ is the unit vector associated to fibre whose component p_i are function of the angles θ and ϕ (Figure 4.2) and $\psi(\boldsymbol{p})$ is the distribution function, such that $\psi(\theta,\phi)\,sin\theta\,d\theta\,d\phi$ indicates the probability that fibres are between θ and $\theta + d\theta$ and ϕ and $\phi + d\phi$.

Aligned along in x axis $\qquad$ Aligned along y axis $\qquad$ Random in *xy* -plane

$a_{xx} = 1$, others are zero $\qquad$ $a_{yy} = 1$, others are zero $\qquad$ $a_{xx} = a_{yy} = 0.5$, others are zero
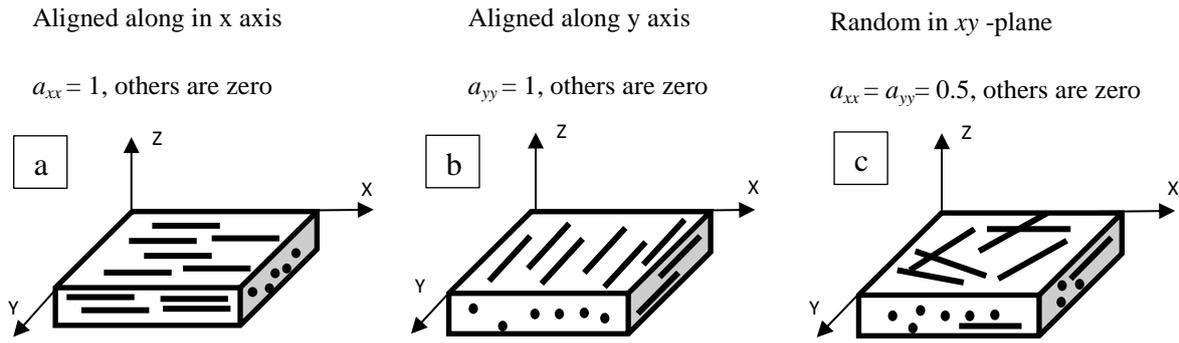
Figure 4.4

(a) aligned fibres along *x*-axis, (b) aligned fibres along *y*-axis and (c) random orientation in

xy-plane

The long fibres and the fibres oriented perpendicular to the main flow direction have a higher probability to appear in the cutting section. Furthermore, fibre oriented with (θ, ϕ) and $(\pi - \theta, \phi + \pi)$ are undistinguishable. This must be counterbalanced by the function $F(\theta)$ as defined by Bay and Tucker (1992) and reported later by Vincent et al. (2005):

$$\frac{F(\theta)}{F(90)} = \frac{1}{\frac{L}{D}\cos\theta + \sin\theta} \qquad \text{[Eq. 4.4]}$$

where $F(90)$ is the weighting function for $\theta = 90°$, L is the fibre length and D is the fibre diameter. The average of a_{ij} of n fibres of orientation p_i^k becomes:

$$a_{ij} = \frac{1}{n}\frac{\sum_{k=1}^{n} p_i^k p_j^k F(\theta_k)}{\sum_{k=1}^{n} F(\theta_k)} \qquad \text{[Eq. 4.5]}$$

X-ray computed microtomography (µCT) is another technique that has been used to characterize the orientation of glass fibre reinforced polymer in injection moulded parts [Shen et al. (2004); Bernasconi at al. (2012); Tausif et al. (2014); Thi et al. (2015)]. This technique enables not only the study of fibre orientation but also a complete description of microstructure including fibre length and dispersion. Some results of fibre size analysis obtained by using this technique were already presented in the Chapter 3. This technique consists of slicing a sample into thin sections and imaging it from multiple rotation angles. The multitude of images is processed by sophisticated computer algorithms, providing a three dimensional reconstruction of the microstructure of fibres. An example of a three dimensional representation of a glass fibre reinforced polypropylene is shown in Figure 4.5.
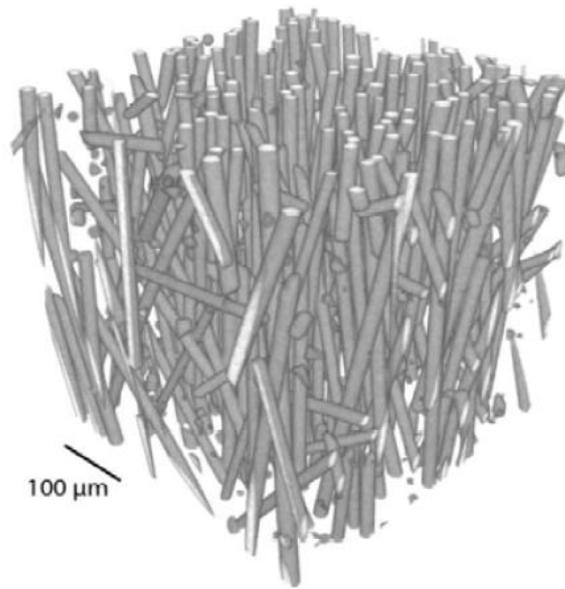
Figure 4.5

Three-dimensional representation of a sample taken from injection moulded part of glass reinforced polypropylene [Kastner et al. (2012)]

1.1.2.2. Natural fibres

The ellipses method used to quantify the glass fibre orientation by analysing cross sections cannot be extended to the natural fibre case because the apparent sections of fibres are irregular. Figure 4.6 presents an example of two images taken by optical microscopy in reflection, which correspond to *xz* and *yz* planes of a tensile bar with 20 wt % flax/starch acetate [Peltola et al. 2011]. Figure 4.7 shows another example of *yz*-plane of tensile bar of 30 wt % pulp fibre reinforced polypropylene [Nystrom (2007)]. The quantification of orientation by ellipses method showed previously for glass fibres requires some assumptions such as the fibre rigidity and a circular fibre cross-section, which is not the case of natural fibre morphology. Natural fibres contain bundles and elementary fibres all of non-circular section.
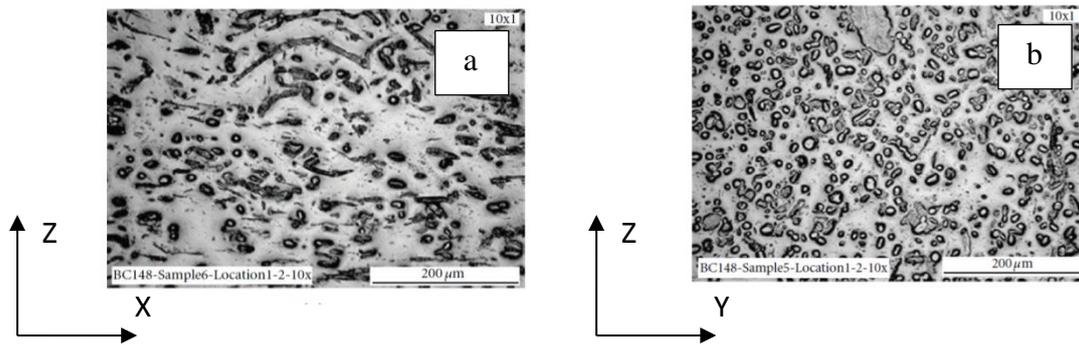
Figure 4.6

xz (a) and *yz* (b) planes with *x* the main flow direction
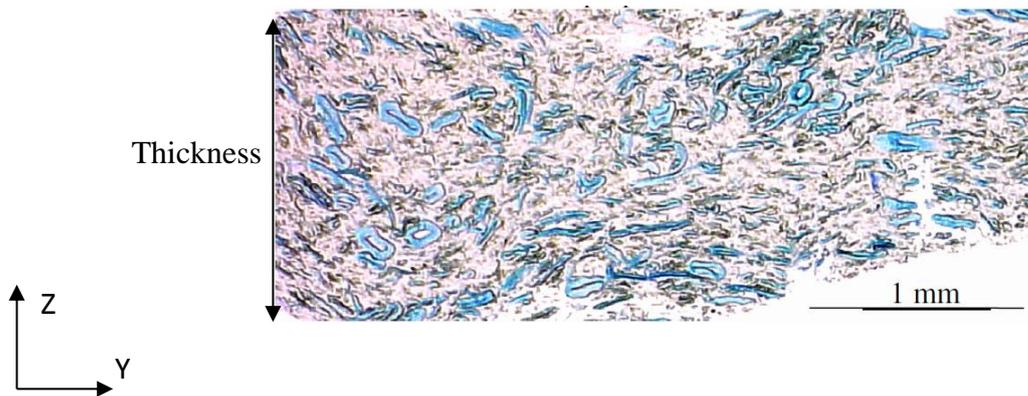
Figure 4.7

A surface of 30 wt % pulp reinforced polypropylene obtained using polarized light

microscopy [Nystrom (2007)]

In most studies dealing with natural fibres the *xy*-plane at different levels of thickness is observed. The observations may be done by optical microscopy in transmission and reflection or by SEM. Hornsby et al. (1997) observed flax straw fibres reinforced polypropylene by *optical microscopy in reflection* in *xy*-plane of the injection-moulded part. Figure 4.8 shows two cross sections nearby surface and at the mid-plane of the part.
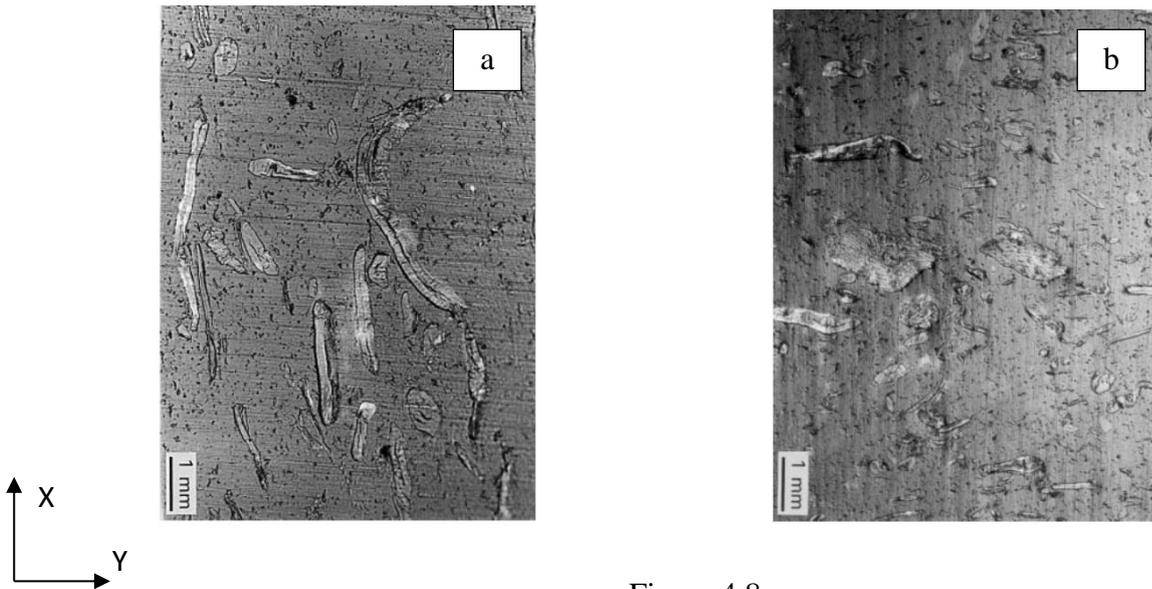
Figure 4.8

Cross sections in *xy*-plane (a) near surface and (b) at the mid-plane, *x* is the main flow direction [Hornsby et al. (1997)]

Aurich and Mennig (2001) observed injection moulded plaque based on 30 wt % flax reinforced polypropylene by *optical microscopy in transmission*. An example of two cross sections at 0.02 and 0.2 mm from the surface in *xy*-plane is presented in Figure 4.9.
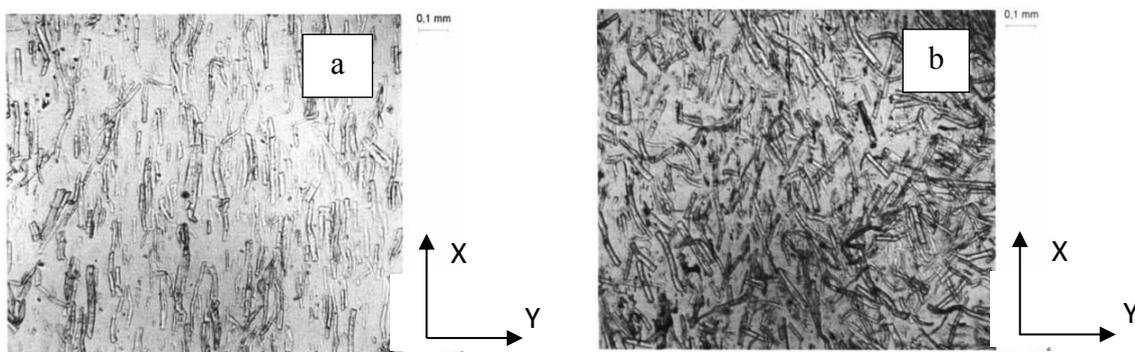
Figure 4.9

xy-cross section at two different levels in thickness: at 0.02 mm (a) and at 0.2 mm (b) from the surface, 2 mm is the entire thickness and *x* is the main flow direction [Aurich and Mennig (2001)]

Similar observations of the same *xy*-plane with the same system (flax fibre-reinforced polypropylene) were performed by Bourmaud et al. (2013) on a tensile test bar at 0.1 mm and 1 mm from the surface of the part using SEM (Figure 4.10)
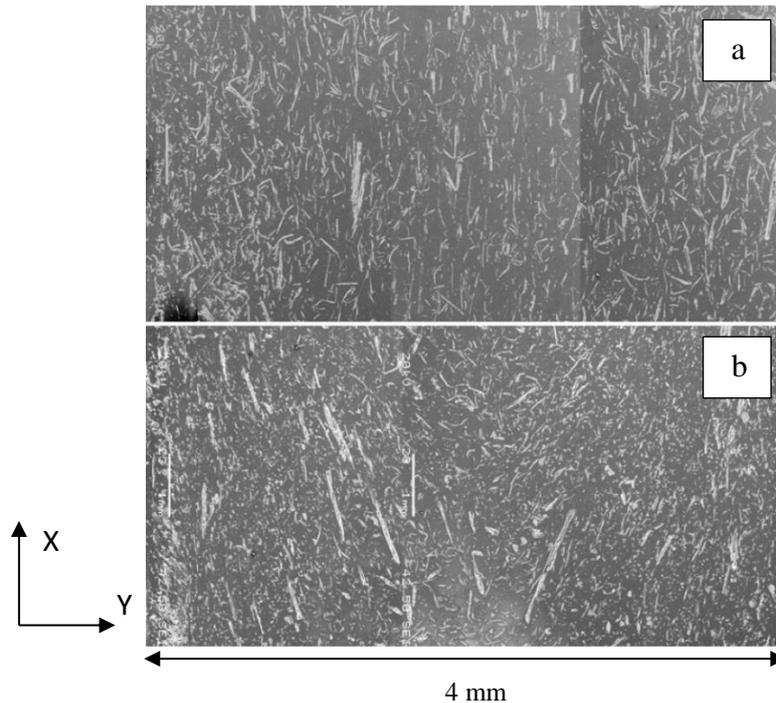
Figure 4.10

Cross sections at 0.1 mm (a) and 1 mm (half-thickness) (b) from the surface 20 wt % of flax fibre- reinforced polypropylene, *x* the main flow direction [Bourmaud et al. (2013)]

The surfaces in *xy* planes shown in Figures 4.8, 4.9 and 4.10 seem suitable to quantify the orientation of natural fibres in injection-moulded parts, whatever the microscopy technique used for observations. However, the quantification of fibre orientation in *xy*-plane requires more experimental work because sections at different levels in thickness are needed to obtain the orientation state across thickness. By using ellipses method, only one cross section perpendicular to *xy*-plane is performed to characterize the orientation state of glass fibres.

Other studies have focused on the X-ray µCT as an experimental technique to assess the orientation of natural fibre-reinforced thermoplastic. However, this technique has its limitations because if high resolution is needed only small field of view is possible. Because the conservation of small details is important for the understanding of the microstructure of natural fibres (irregular shape, fibre curvature), a high resolution is required to detect the exact fibre cross section. Therefore, observations are limited to samples not large enough to establish analyses of fibre orientation in the scale of injected-moulded parts. Furthermore, the density of natural fibres ($\rho \approx 1.5$ g/cm^3) is close to the one of thermoplastic matrix ($\rho \approx 0.9$-1.2 g/cm^3), which makes the X-ray attenuation coefficient low and materials

undistinguishable. Presently, many researchers work on improving this technique and recently some progress have been made in the determination of the fibre length distribution [Alemdar et al. (2008), Joffre et al. (2014)], but fibre orientation distribution in a wide region of observation with high resolution and 3D reconstruction, such as the glass fibre case, is not yet reached. Figure 4.11 presents two examples of a 3D reconstruction in µCT of wood fibre- and hemp fibre-reinforced polypropylene. Only qualitative observations were carried out and a statistical analysis of fibre orientation was not possible.
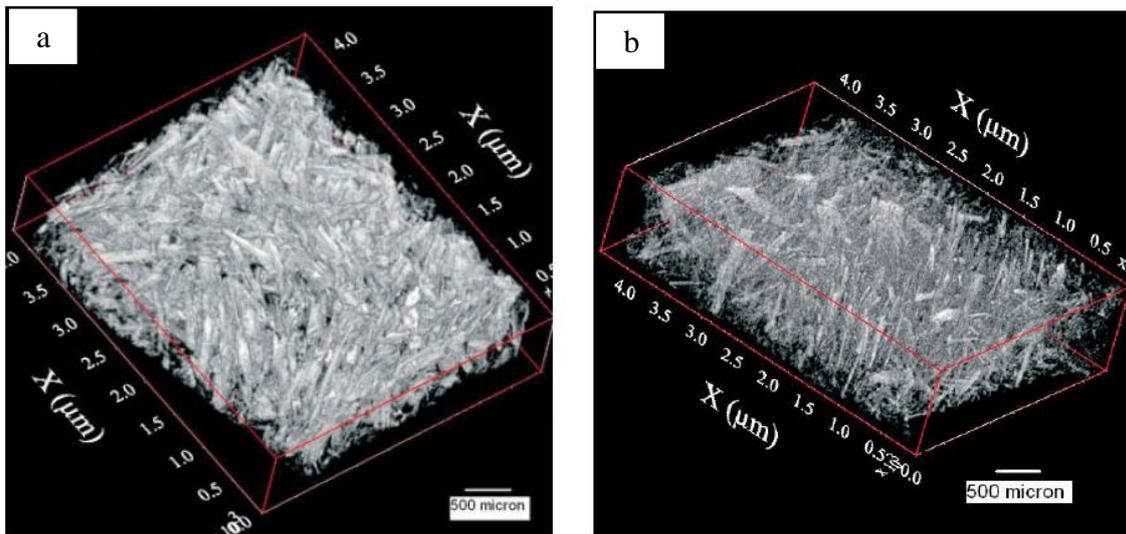
Figure 4.11

3D visualization of the fibre structure in the polypropylene (a) wood fibres and (b) hemp fibres reinforced composites [Alemdar et al. (2008)]

1.2. Fibre orientation results

1.2.1. *Glass fibres*

An example of the evolution of a_{xx} as a function of thickness from the surface of injection-moulded part for glass fibre reinforced PAA (polyacrylamide)) is presented in Figure 4.12. A symmetric orientation with respect to the mid-plane is typically obtained with a_{xx} close to zero at the core (0.2 here) and a_{xx} close to one at surface (0.8 here), concluding that orientation of fibre changes across the thickness from surface to the mid-plane.
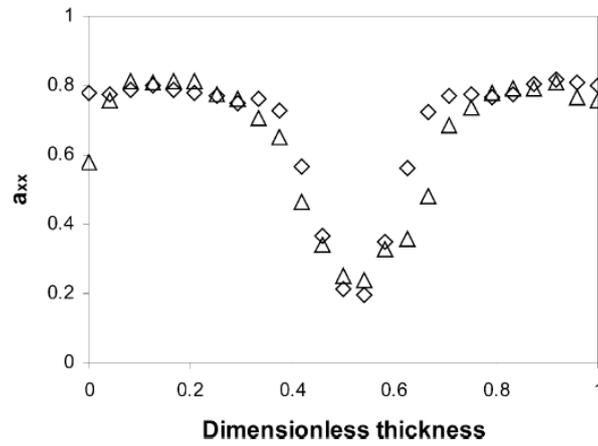
Figure 4.12

Evolution of a_{xx} along the thickness of injected part for glass reinforced PAA with 50 wt % (triangle) and 30 wt % (square) fibres [Vincent et al. (2005)]

Bay and Tucker (1992) predicted by computation and observed experimentally five main layers: two skin layers (which are the thinnest and the least oriented ones), two shell layers and one core layer. Intermediate layer can exist between shell and core layers, but it is usually ignored and added to core layer as one continuous layer.

The typical fibre orientation in an edge-gated part is shown in Figure 4.13. In the shell layers fibres are oriented in the flow direction and in the core layer perpendicular to the flow direction. The shell layer is located in a zone were shear is dominant (Figure 4.13). The skin layer resulting from the fountain flow exhibits a random orientation and its thickness depends on the cooling and the filling times. Greatz number (Gz) gives the range of the skin layer thickness:

$$Gz = \frac{4e^2}{\alpha.t_{fill}}$$
[Eq.4.6]

where $2e$, α and t_{fill} are the cavity thickness, the thermal diffusivity of the melt and the mould filling time, respectively. The thickness of the skin layer increases with Gz increasing, however Bay and Tucker (1992) proposed that no skin can appear if $Gz > 100$.
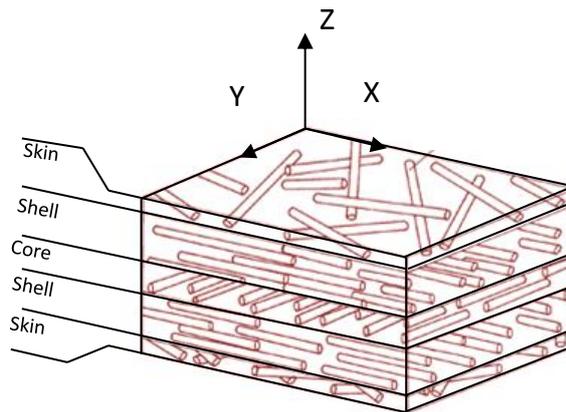
Figure 4.13

Typical three-dimensional orientation with the different possible layers, *x* is the main flow direction

The entrance of the cavity that is the junction between feeding channel or sprue and the cavity itself is usually a divergent because the section of the channel is much smaller than the section of the cavity. Therefore, the flow is highly extensional at the centre, thus fibres get oriented perpendicular to the flow direction. Near the surface, a shear flow is predominant, and fibres are mostly oriented along the flow direction. Fibres located very close to the surface (skin region) were submitted to the fountain flow ([Tadmor 1974], Figure 4.14). The complex flow with extensional deformations (but not only) leads to a random or slight orientation at the flow direction. This orientation state is rapidly frozen very close to the cold mould walls.
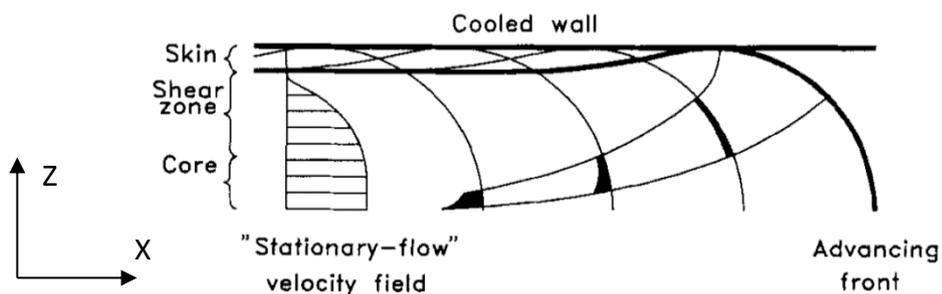
Figure 4.14

A typical flow in a cavity channel. The shaded areas show schematically the transport of material from the centre to the wall [Toll and Anderson (1993)]

It was also shown that the thickness of the core layer may also depend on fibre length and concentration. Spahr et al. (1990) investigated the concentration of glass fibres across the thickness of injection-moulded plaques. Two different lengths of fibres (*long fibres L_n= 3-4 mm* and *short fibres $L_n \leq 1$ mm*) and four concentrations from 10 wt % to 40 wt % of glass fibres were investigated. Figure 4.15 shows the ratio core thickness/part thickness that is plotted as a function of the volume fraction. The core thickness increases by increasing the fibre concentration and the fibre length.
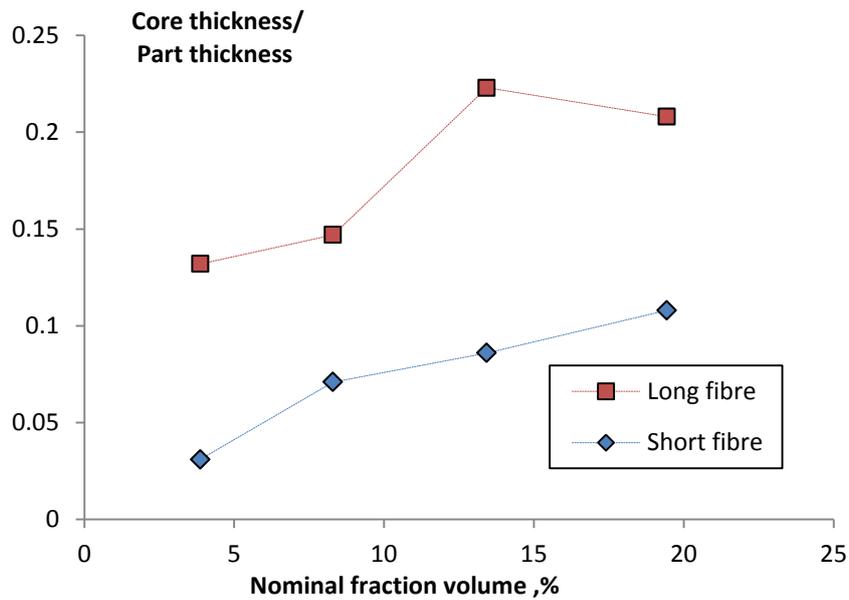
Figure 4.15

Change in core thickness with fibre volume fraction for long and short glass fibre reinforced polypropylene [Spahr et al. (1990)]

Figure 4.16 shows the local volume fraction of glass fibres in shell and core layers as a function of the overall volume fraction. The core layer is denser than the shell one by increasing the fibre concentration. The difference in the local concentration induced by long and short fibres is higher at the core as compared to the shell, when the overall concentration increases.
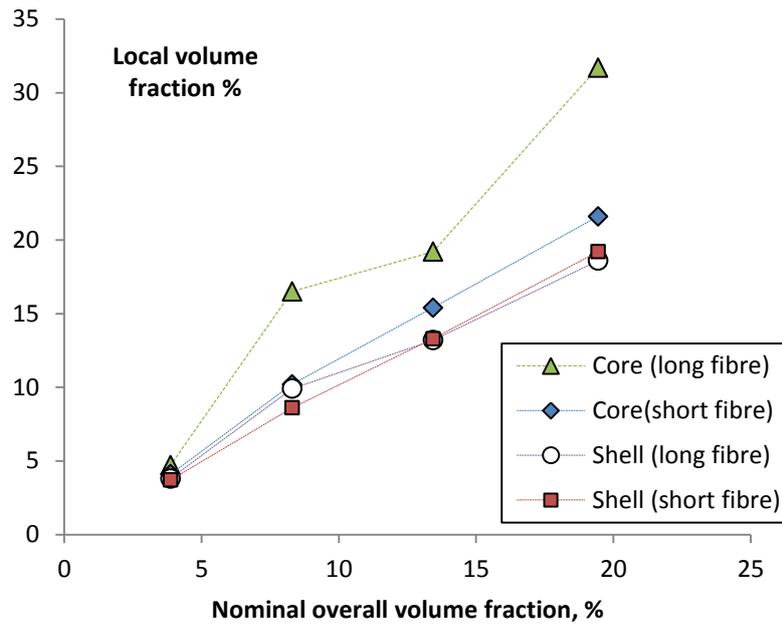
Figure 4.16

Difference between shell- and core- local fibre volume fraction as a function of the nominal overall fibre volume fraction for long and short glass fibre reinforced polypropylene [Spahr et al. (1990)]

Spahr et al. (1990) calculated the fibre orientation factor $f_p = 2a_{xx} - 1$, considering that $a_{xx} \geq 0.5$ when fibres are in the shell layer resulting in $f_p \geq 0$ and $a_{xx} \leq 0.5$ when fibres are in the core layer resulting in $f_p \leq 0$. Moreover, when fibres are strongly aligned along the flow direction (*x*) or along the direction perpendicular to the flow (*y*), f_p is close to 1 or -1, respectively. Figure 4.17 shows f_p vs the overall volume fraction for short and long fibres. Fibres in both shell and core layers become more aligned when the fibre volume fraction increases. Short fibres are more oriented than the long ones. Based on SEM images in *xz* and *yz* cross sections, the orientation of long fibres was measured by two methods: i) personal evaluation or "by hand" (unfilled symbol) and ii) image analysis. However, short fibre orientation was only measured by "hand".
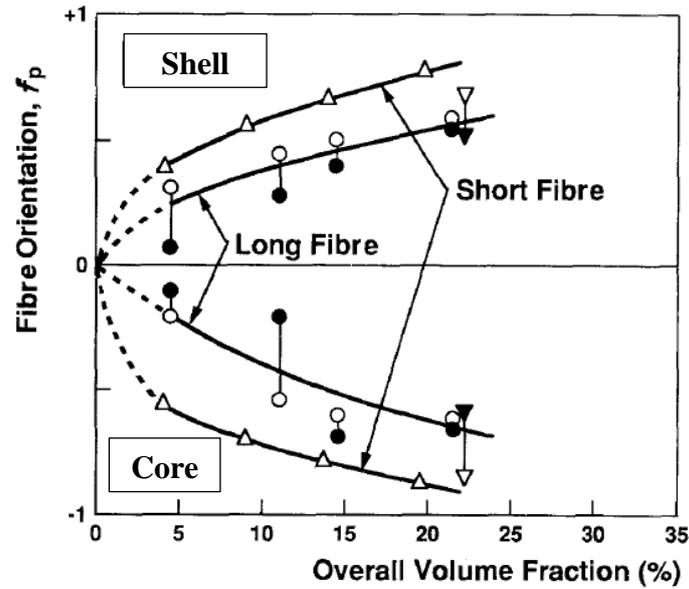
Figure 4.17

f_p as function of overall volume fraction of long and short fibres [Spahr et al. (1990)]

Understanding which factors can influence dispersion and orientation of fibres is important to control the mechanical properties of the moulded part. The main key factors are the injection conditions such as the injection speed, the packing holding and cooling time, the geometry of cavity and the melt rheology. Many studies have investigated the influence of these factors on the alignment of fibres or the thickness of skin, shell and core layers. The results are summarized in Table 4.1.

Table 4.1 Factors influencing the orientation and dispersion of glass fibre in thermoplastic composites, GF means glass fibres

Factors		*System* (GF: glass fibres)	*Observations (orientation with respect to the main flow direction)*	*References*
Gate	Point-centre gate	GF reinforced - nylon and - polypropylene	Perpendicular core	Bay and Tucker 1992)
	Film-sprue gate	GF reinforced nylon 66	Aligned core	Darlington and Smith (1987)
		GF reinforced polypropylene		Sanou et al. (1985)
Injection speed	Faster	GF reinforced polypropylene	Ticker and perpendicular core	Akay and Barkley (1991)
	Slower	GF reinforced polypropylene	Thinner and perpendicular core	Bright et al. (1978)
Thicker cavity	-	- GF reinforced polypropylene - Glass-flake filled polypropylene	Thicker and perpendicular core	Bouti et al. 1989 Fisa and Rahmani (1991) Gillepsie et al. (1985) Gupta and Wang (1993)
Colder walls	-	GF reinforced polypropylene	Thinner and perpendicular core + thicker skin layers	Vincent and Agassant (1986) Akay and Barkley

				(1991) Gupta and Wang (1993)
Lower power law index (more shear-thinning)	-		Thicker and perpendicular core	Darlington and Smith (1987) Bay and Tucker 1992)
Edges effect	Closer to the edge	GF reinforced polypropylene	Thinner and perpendicular core	Kenig (1986) Akay and Barkley (1991)
Fibre depletion and fibre segregation		Glass bead filled polypropylene	Gradual depletion of fibre from the core to the skin	Shmidt (1977)
		Fibre reinforced polypropylene/polyamide		Bright et al. 1987 Akay and Barkley (1991) Helger and Mennig (1985) Singh and Kamal (1989)
	-	Short/ Long GF reinforced polypropylene		Sphar et al. 1990 Akay and Barkley (1991)
		GF reinforced Vertron resin		Bailey and Rzepka (1991)
Packing and holding	Without	GF reinforced PET	Aligned core	Malzahn and Schultz (1986)
	With		Perpendicular core	

	Increase	Long fibre reinforced Vertron resin	- Thinner and perpendicular core - The longer the time of maintaining pressure, the more aligned fibres (in the transition core/shell area)	Bailey and Rzepka (1991)
Higher aspect ratio of fibres	-	GF reinforced polypropylene or other polymers	- Thicker core - Less fibre mobility at the melt front - Higher depletion from the core to the skin - Lower degree of orientation in both shell and core layers - Possibility of fibre bending - Jetting and irregular filling - Higher fibre wall interaction	Spahr et al. (1990) Bailey and Rzepka (1991) Blanc et al. (1987) McLelland and Gibson (1990) Truckenmuller and Fritz (1991)
Higher fibre concentration	-	GF reinforced polypropylene Glass-flake filled polypropylene	-Thicker core -Flatter velocity profile -Clamping force increases quadratically with fibre volume fraction	Spahr et al. (1990) Bouti et al. (1989)

1.2.2. *Natural fibres*

Whereas the microstructure of glass fibre-reinforced thermoplastic reached a good understanding, the literature of natural fibre case is not yet mature and a lack of information still exists. The dispersion of natural fibres in injection-moulded parts was not previously studied and most of the studies dealing with fibre orientation have been limited to some qualitative observations. All the *xy*-plane observations shown in Chapter 4, section 1.1.2.2 Natural fibres, indicate a considerable change of orientation of fibres nearby surface compared to the core, which seems similar to the core-shell structure seen earlier for glass fibres. The main study, in which a significant quantification of flow-induced orientation was performed, is the one of Aurich and Mennig (2001). They quantified the orientation of 30 wt % flax fibre-reinforced polypropylene by optical microscopy in *transmission*. They observed and quantified the orientation in *xy*-plane for 11 cross sections with different levels across thickness and for four locations in a film-gated plaque, as shown in Figure 4.18. In each cross section, 600 fibres were characterized. Unfortunately, the method of the fibre orientation measurement was not detailed enough. Furthermore, only the average of fibre aspect ratio was provided (*L/D*= 13), whereas flax fibres contain bundles and their length and diameter are critical parameters to consider when analysing a composite microstructure.
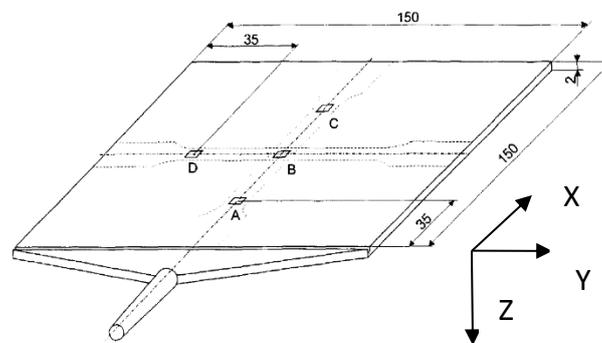
Figure 4.18

Injection moulded plaque with locations of orientation; all dimensions are in mm [Aurich and Mennig (2001)]

Despite of the lack of some microstructural information, Aurich and Mennig (2001) demonstrated that a core-shell structure appears in flax fibre composites. At 0.1 mm from the plaque surface, the fibre orientation distribution presents a unimodal distribution peaking

around the *x*-direction (0° angle) (Figure 4.19.a). At *z*= 0.5 mm the distribution becomes bimodal (Figure 4.18.b) and their maxima moved and fused with the perpendicular flow direction +/- 90° when approaching to the mid-plane (*z*= 1 mm, Figure 4.19.c).
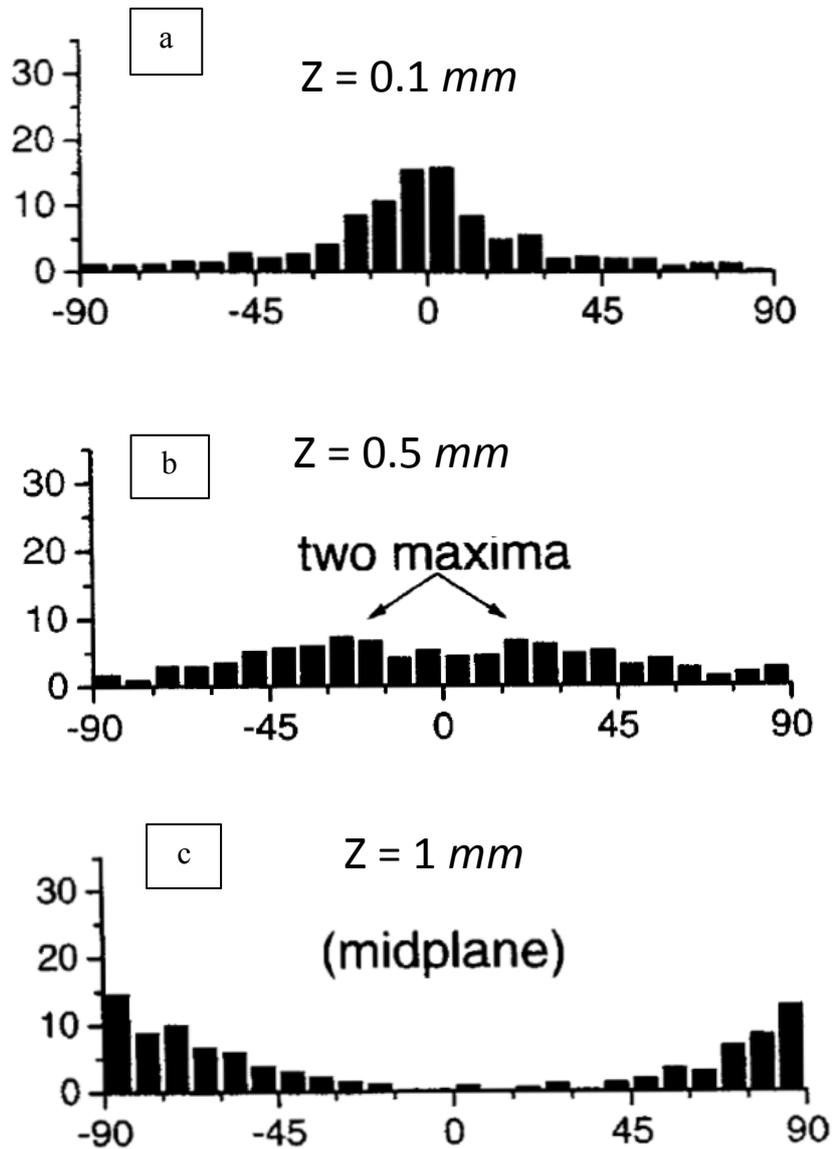
Figure.4.19

Fibre orientation distribution with respect to *x*-direction at location A (see figure 4.17) for three levels in the thickness (a) 0.1 mm, near to the surface (b) 0.5 mm, intermediate layer, and (c) 1 mm mid-plane[Aurich and Mennig (2001)]

Aurich and Mennig (2001) used the tensor components without the correction of the distribution function $F(\theta)$ as defined by

$$a_{ij} = \frac{1}{n}\sum_{k=1}^{n} p_i^k p_j^k \qquad\qquad \text{[Eq. 4.7]}$$

This leads to three main components of orientation

$$a_{xx} = < sin^2\theta\ cos^2\phi > \qquad\qquad \text{[Eq. 4.8]}$$

$$a_{xy} = < sin^2\theta\ cos\phi\ sin\phi > \qquad\qquad \text{[Eq. 4.9]}$$

$$a_{yy} = < sin^2\theta\ sin^2\phi > \qquad\qquad \text{[Eq.4.10]}$$

Considering that the orientation is planar, some simplifications take place as $\theta = 90°$ (Figure 4.3), so $sin\theta = 1$:

$$a_{xx} = < cos^2\phi > \qquad\qquad \text{[Eq. 4.11]}$$

$$a_{xy} = < cos\phi\ sin\phi > \qquad\qquad \text{[Eq. 4.12]}$$

$$a_{yy} = < sin^2\phi > \qquad\qquad \text{[Eq. 4.13]}$$

Figure 4.20.a shows that at the location A, a_{xx} increases from 0.6 at *z* = 0.02 mm to 0.9 at *z* = 0.2 mm, indicating a strong alignment along *x*-direction. It then decreases until 0.2 at *z* = 0.9 mm and remains almost constant at the mid-plane *z* = 1mm, which is again a sign of strong fibres alignment but along *y*-direction. A similar trend was noticed for B and C locations. However, for location D closer to the plate edge (Figure 4.20.b), at *z* = 0.2 mm the orientation is quite similar to that of location A, but at the mid-plane instead of decreasing till 0.2, a_{xx} decreases only until 0.7, signifying that fibres in the core are more aligned to *x*-direction than to *y*-direction. Moreover, a_{xy} of location D is not close to zero compared to location A, meaning that the direction of the principal orientation at location D is different to *x*-direction or *y*-axis [Tucker (1988)]. According to authors, an "uneven flow velocity" close to the edge is behind this orientation. Compared to the edge effect shown in Table 4.1, this seems in disagreement with glass fibre reinforced polypropylene studies [Kenig (1986), Akay and Barkley (1991)] in which, even closer to the part edges, a perpendicular core was kept with thinner thickness than at a middle part location.
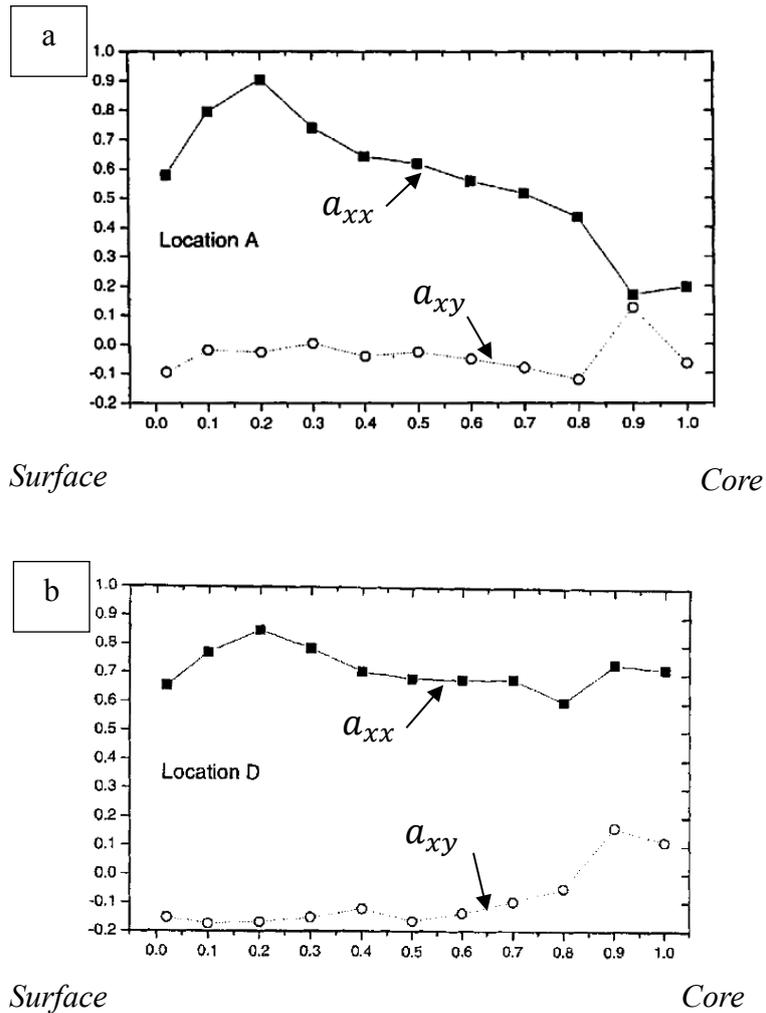
Figure. 4.20

Components of orientation tensors at location "A" (a) and location "D" (b) [Aurich and Mennig (2001)], see the text for more details

Recently, Lafranche et al. (2013) investigated the orientation of flax fibre-reinforced polypropylene. The studied sample was taken from the middle of a tensile bar. Using microtome, the flow plane was observed by the optical microscopy in *reflection mode* at different levels across thickness and 150 measurements of fibre orientation were carried out for each layer by a dedicated image processing software. Figure 4.21 shows a_{xx} evolution across the thickness for different volume fractions. Starting from 10 % in depth from the surface, fibres become quite aligned in the main direction of flow (a_{xx}= 0.9) and keep the same orientation toward the core, except the highest fibre concentration of 22 vol % for which fibres are less aligned near the surface (a_{xx}= 0.6-0.7) and are rather randomly oriented (a_{xx}

= 0.5-0.6) at the core. The core-shell structure here is not well pronounced. The reason is probably related to the moulding conditions and the shape of the gate, as mentioned in Table 4.1. Lafranche et al. (2013) investigated the orientation state with increasing fibre concentration, providing results from large number of analysed layers. Nevertheless, neither details about the method of fibre orientation measurement nor images of the cut surfaces were provided.
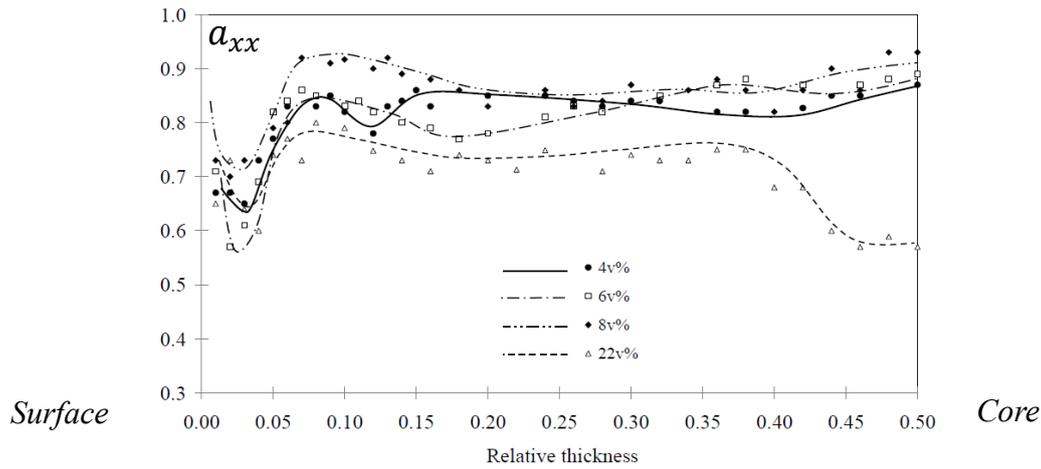
Figure 4.21

The orientation state regarding the main flow direction across the thickness for different fibre concentrations [Lafranche et al. (2013)]

1.3. Conclusions

The fibre orientation and dispersion are important factors to control the final properties of injection-moulded parts. A good understanding of these parameters has been built up for glass fibre reinforced composites. A typical orientation of core-shell structure was observed, characterized and modelled. The dispersion of fibre across thickness was correlated to fibre orientation, length and concentration. Furthermore, most factors that can influence the orientation and the dispersion of glass fibre in a thermoplastic polymer have been studied in details such as the injection conditions, the mould geometry and the rheology of melt.

Two possible techniques of fibre orientation characterization that are the microscopy (either optical or scanning electron) analysis of cross section *perpendicular* to *xy*-plane (*xz* or *yz*) and X-ray micro-tomography, were presented. Each one has its limitations when it is related to natural fibres, whereas it is going thoroughly with glass fibres. Until now, most studies on

natural fibres have been limited to qualitative observations. Only few studies have been dealing with the orientation quantification of natural fibres in cross sections parallel to the part plane (*xy*). A core-shell structure similar to glass fibre composites has been observed for the natural fibres case. However, these studies did not take into account their specific features (flexibility, bundles structure). Moreover, the dispersion of natural fibres in injection-moulded parts is not yet investigated and correlated to fibre orientation. In the following section, we suggest a new method of microstructure characterization based on the cross section analysis, dealing with the specific features of natural fibres. This method enables to investigate the fibre dispersion, orientation and bending.

2. Results and discussion

2.1. Qualitative observations

Figure 4.22 shows two cross sections in *xz*-plane and *yz*-plane of 20.5 vol % flax/PP. The location of both sections in injection-moulded box is presented in the same figure. The orientation of fibre changes across the thickness from surface to core. A core-shell structure similar to that observed for glass fibre composites is obtained. While fibres are aligned along *x*-direction close to surface in *xz*-plane, they are aligned along *y*-direction around the core in *yz*-plane. The magnified image shown in Figure 4.22 confirms that the cross section of flax fibre is irregular. The reason is that the majority of flax fibres consist of bundles in which elementary fibres are "glued" together in an asymmetrical way. The number of elementary fibres in a bundle varies from few to several tens, giving 3-4 elementary fibres per bundle on average (as measured in Chapter 3, section 2.3. Flax) and they are assembled in different ways.

X : Main flow direction

Z

Thickness =1800 μm

Y

Z

X= Main flow direction
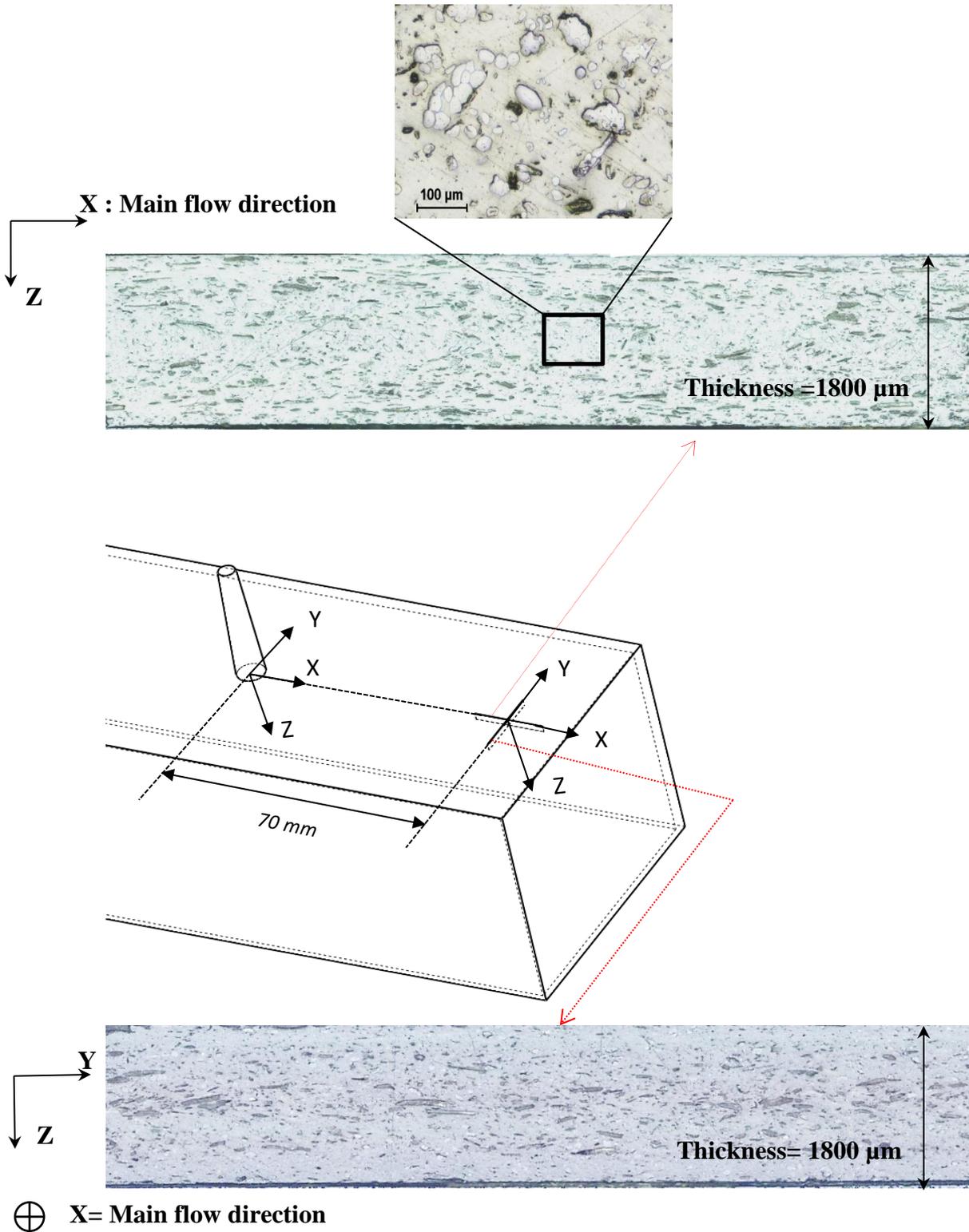
Figure 4.22

Two cross sections in *xz*-and *zy*-planes and their positions in the injection-moulded box.

Figure 4.23 shows a comparison between glass and Tencel fibre cross sections in *xz*-plane nearby surface. Because of their "slenderness", Tencel fibres do not have a circular cross-section like glass fibres, even if their equivalent diameter seems almost constant.
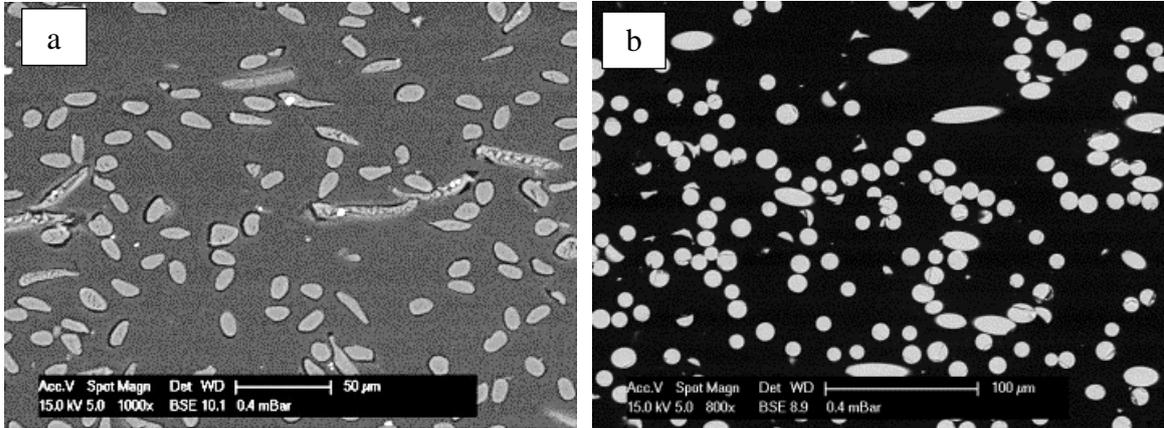
Figure 4.23

SEM images of cross sections of (a) 20.5 vol % Tencel/PP and (b) 20.5 vol % glass/PP at *xz*-plane around core (same position of the zoomed image in Figure 4.21)

Moreover, Tencel fibres are very flexible, making the notion of orientation questionable, as schematically shown in Figure 4.24.
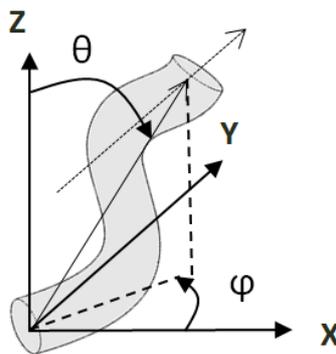
Figure 4.24

Schematic representation of Tencel fibre orientation, analysing the apparent ellipses of cross section gives the dashed line vectors, whereas the solid line vector represents the real orientation.

In summary, the approach of analysing fibres cross sections in *xz*-and *yz*-planes developed to determine the orientation of glass fibres in a polymer matrix cannot be applied for Tencel and flax, which is in agreement with what we concluded from the state of the art section.

*We suggest then to investigate the microstructure of fibres in **xy-plane**,* as it was done in the study of Aurich and Mennig (2001) presented in the state of art section. Figure 4.25 shows how the sample was cut from the moulded box and observed in *xy*-plane (same location to Figure 4.21 but different observation plane).
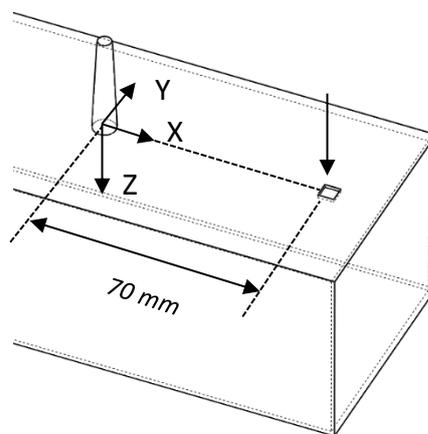
Figure 4.25

Location of sample used for *xy*-plane observation in the moulded box

First, a suitable way for the analysis of fibre orientation in composites had to be found. Optical microscopy images in transmission and reflection modes of cross-sections of flax/PP composites were performed (Figure 4.26). In general, the transmitted light technique provides more information of fibres' spatial position than the reflected one. In transmission, the entire fibres can be seen even if they are positioned "below" the surface. However, because of fibres overlapping the analysis of fibre dimensions from the images made in transmission mode seems very complicated and may lead to artefacts. Moreover, with transmitted light, only a thin layer (< 100 µm) of composite sample must be prepared, which causes practical problems in samples preparation.
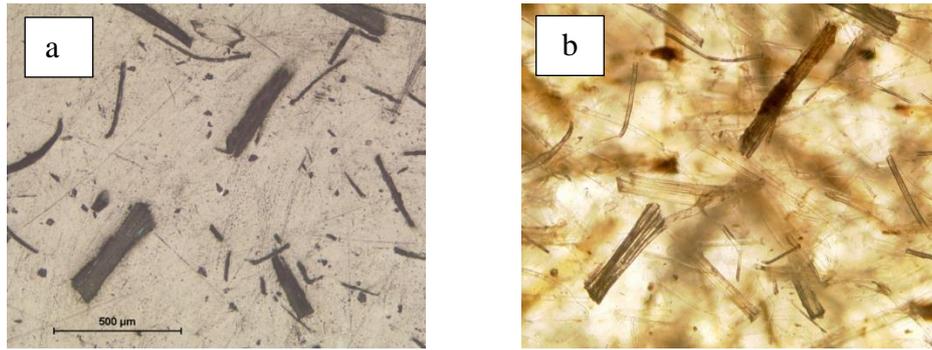
Figure 4.26

xy cross section of flax/PP composite, fibre concentration is 6.3 vol %: comparison between optical microscopy image in reflection (a) and in transmission (b) modes; the scale is the same for both images.

The reflected light technique is simpler than the transmitted one because only the surface matters, so the sample thickness is not critical. In addition, reflected light technique enables a good contrast, so that a quantitative image analysis can be performed. Hence, the optical microscopy in reflection was chosen to analyse fibres orientation. Surfaces in *xy*-plane at different levels across thickness are then required to quantify orientation, as mentioned in Section 1.1.2. As a representative concentration of fibres, 20.5 vol % was chosen for all composites (flax, Tencel and glass).

It should be noted that three fibre orientations are possible with respect to *xy*-plane: i) fibres are fully "in-plane", i.e. an orientation angle θ with respect to the *xy*-plane is 90° (see Figure 4.2), ii) fibres form a certain (large) angle with *xy*-plane, i.e. an orientation angle θ with respect to the *xy*-plane between 0° and 90°, meaning that only an apparent shape of fibres can be seen in *xy*-plane) and iii) fibres are almost perpendicular to *xy*-plane (i.e. θ = 0°). The first two cases cannot not be distinguished when analysing the images taken in *xy*-plane and thus both will be considered together. We shall say that fibres are out of *xy*-plane when their width (or diameter) is comparable with their length on the cross section.

Figure 4.27 provides the flax fibre orientation state in *xy*-plane (at location shown in Figure 4.25: *x* = 70 mm, *y* = 0 mm) at six different levels across the thickness from *z* = 100 μm (~shell) to *z*= 900 μm (core). We remind here that observed surfaces have dimension of 5 x 5 mm², made by bringing 50 reflected optical microscopy images together into one cartography (see Chapter 2). Whereas fibres show a parallel orientation to *x*-axis in the shell region at *z* =

100 µm and $z = 200$ µm), they are mainly aligned perpendicular to x-axis in the core region at $z = 800$ µm and $z = 900$ µm. The transition region i.e. between the shell and the core (from 400 µm to 600 µm) shows a random orientation, which is in agreement with the finding of Aurich and Mennig (2001). Figure 4.28 shows a similar orientation state for Tencel fibres. However, the number of Tencel fibres per cartography is higher as compared to that of flax.

X= **Main flow direction**
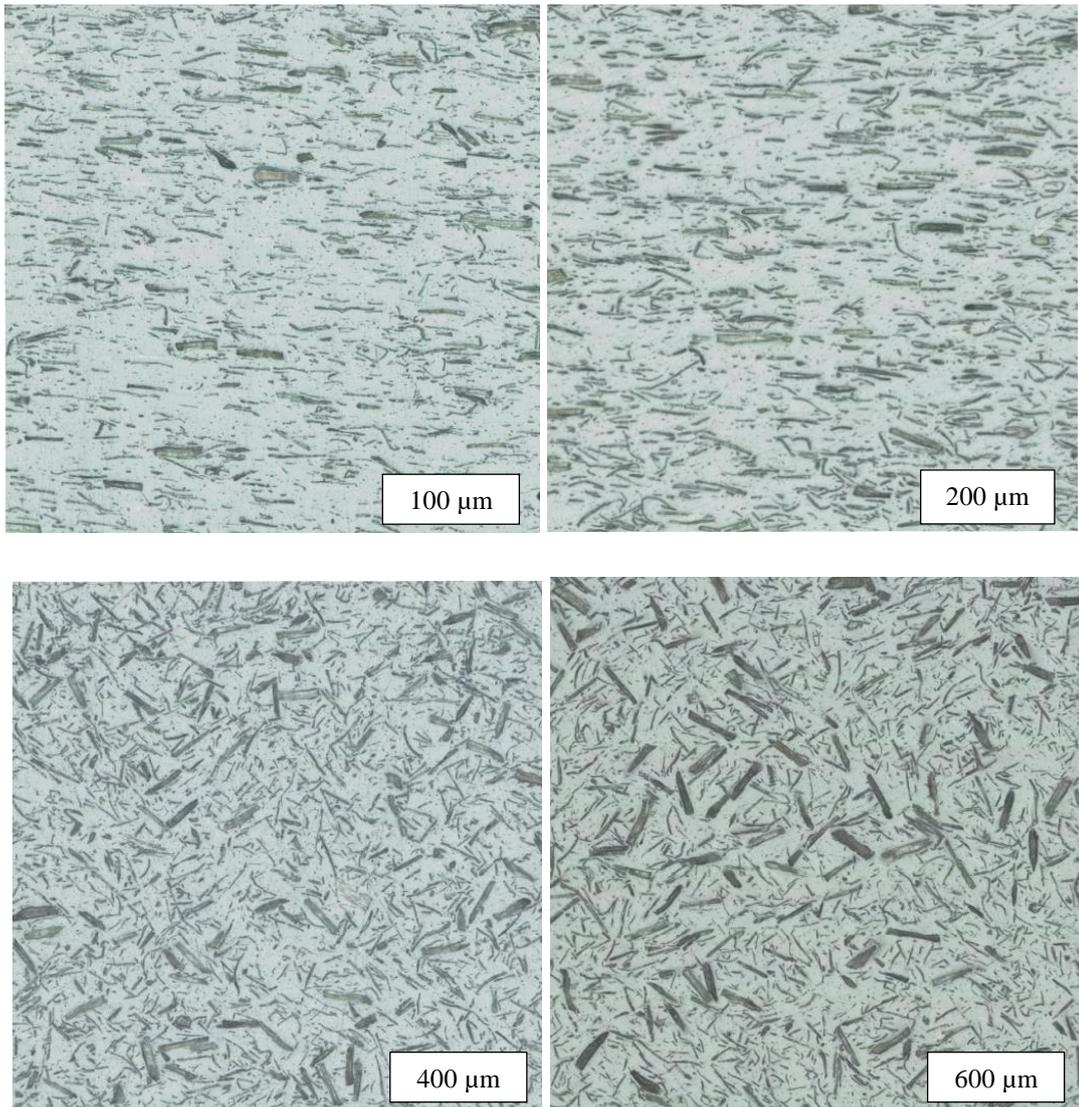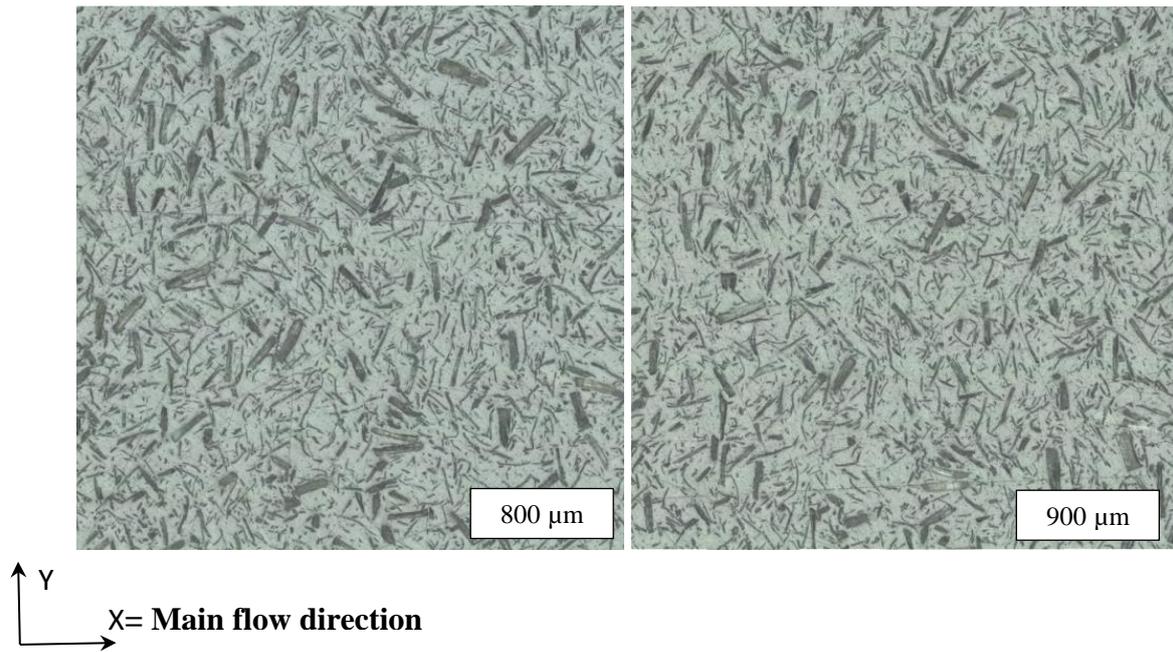
Figure 4.27

Microstructure (optical microscopy in reflected light) of 20.5 vol % flax reinforced polypropylene; 5 x 5 mm² polished surfaces in *xy*-plane across the thickness from sample's surface to core
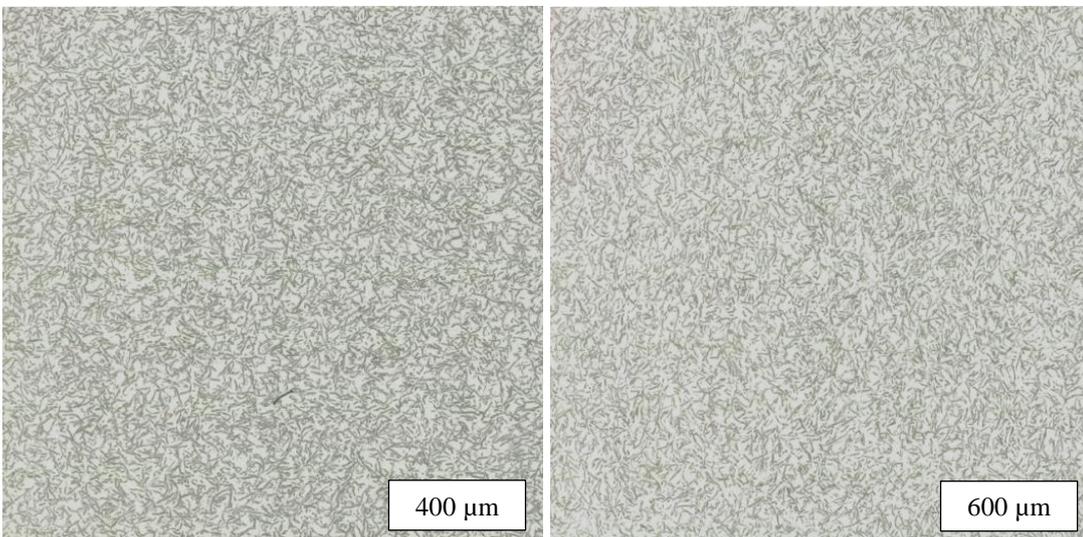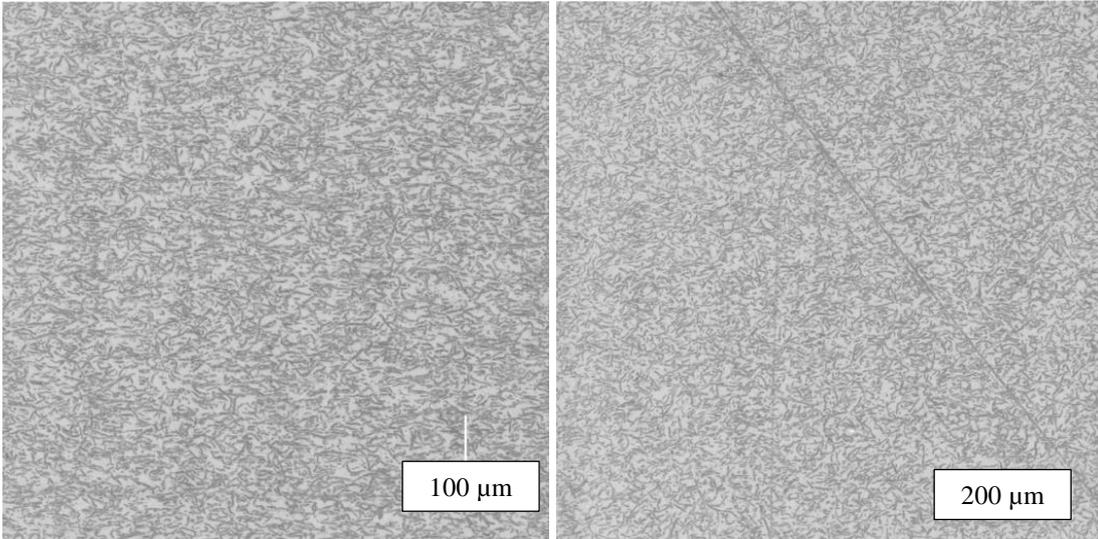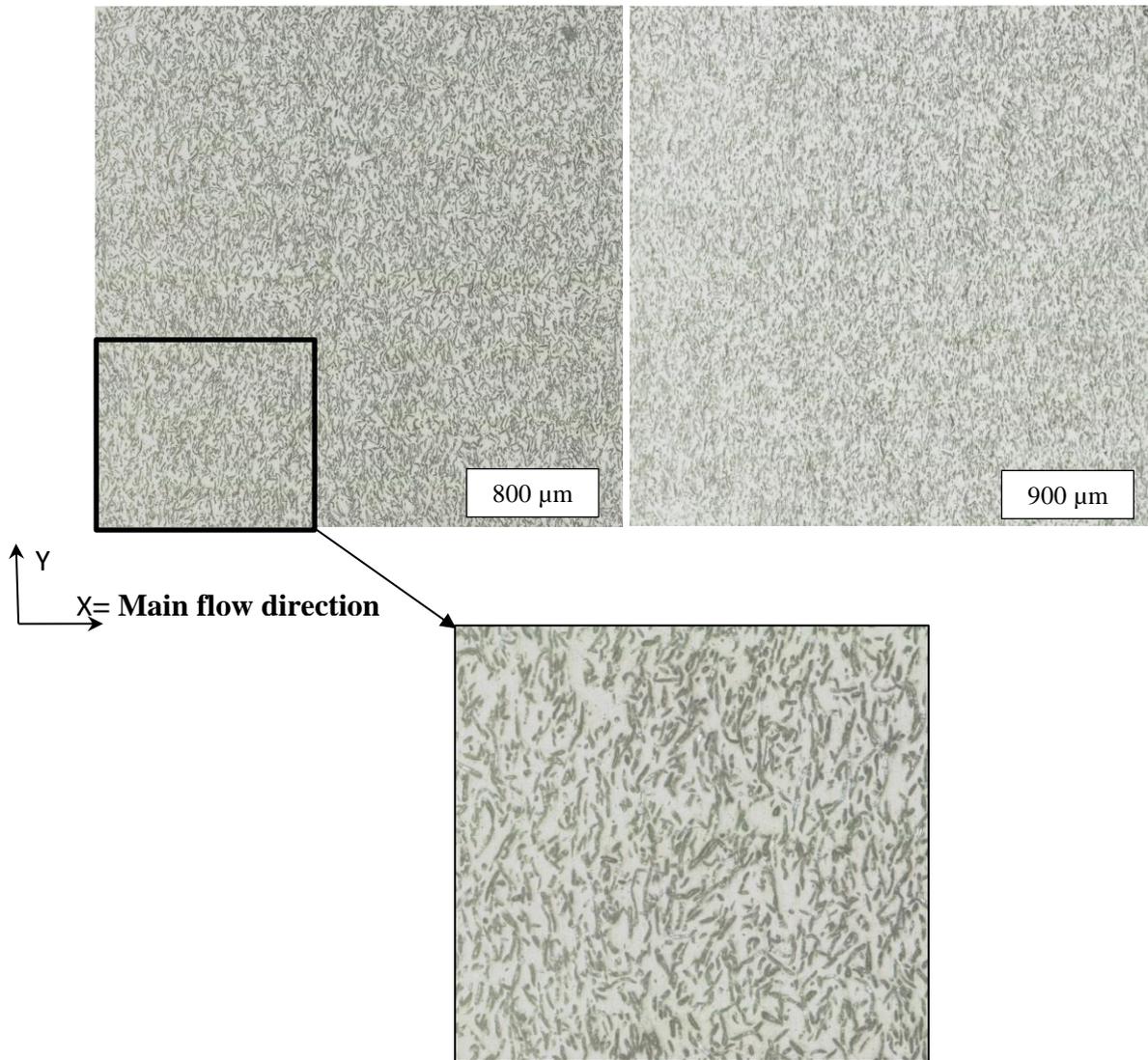
Figure 4.28

Microstructure (optical microscopy in reflected light) of 20.5 vol % Tencel reinforced polypropylene; 5 x 5 mm² polished surfaces in *xy*-plane across the thickness from sample's surface to core

To compare Tencel- and flax-based composites with glass fibre ones, *xy*-cross sections of glass fibre composites were also prepared (Figure 4.29). We limited our observations to three representative layers: in the shell region, in transition zone (between shell and core) and in the core region; they correspond to the position $z = 100$ µm, $z = 600$ µm and $z = 900$ µm, respectively (Figure 4.29). A succession of parallel-random-perpendicular orientation regarding the main flow direction can be attributed to glass fibres. This core-shell structure

111

seems to be common for all types of fibres. Nevertheless, the alignment in each fibre type appears different. This will be further detailed in the next section in which the fibre orientation is quantified.
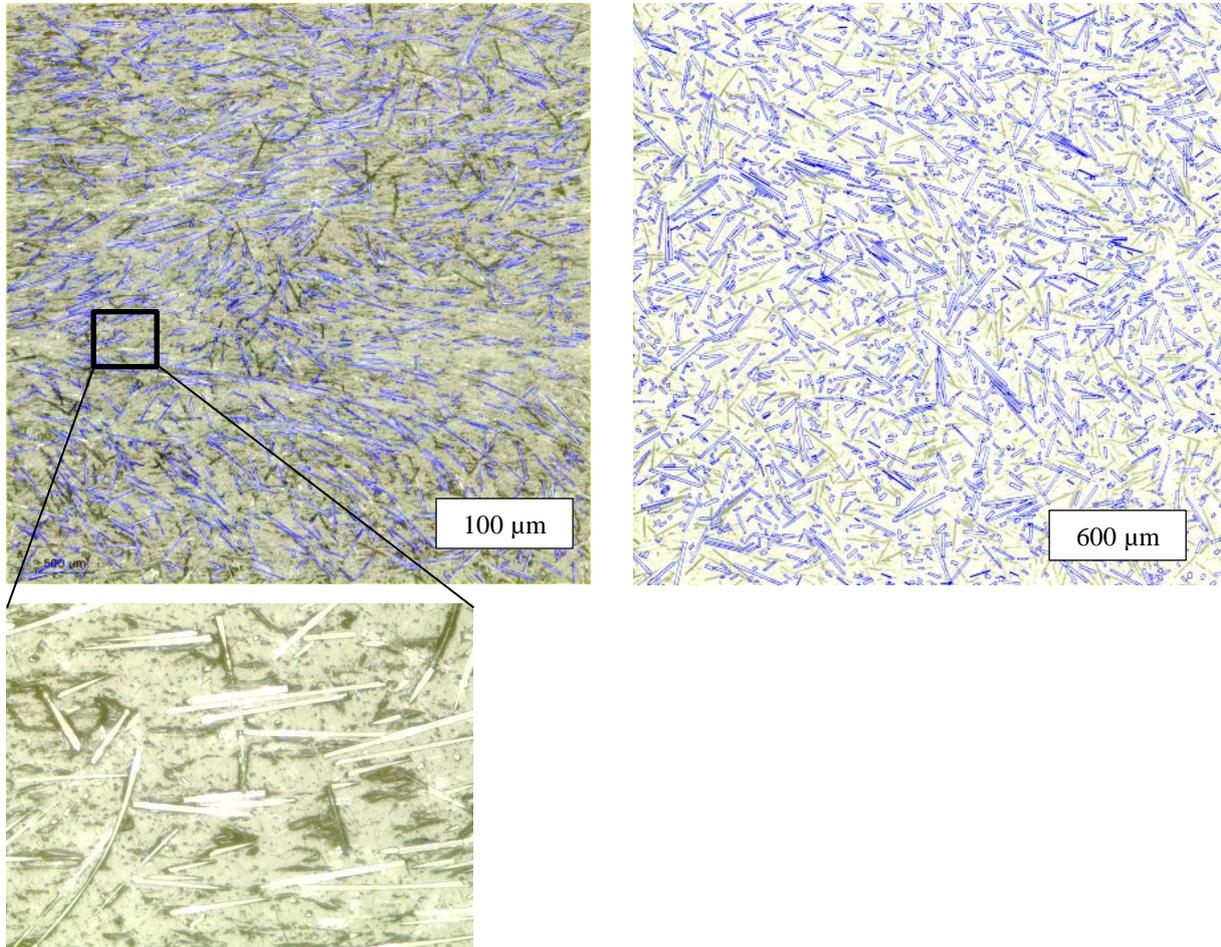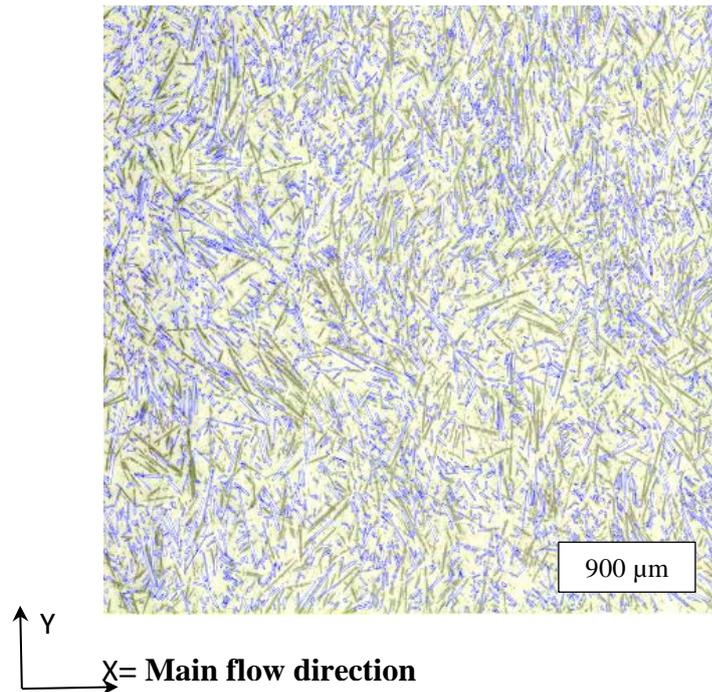
Figure 4.29

Microstructure (optical microscopy in reflected light) of 20.5 vol % glass reinforced polypropylene; 5 x 5 mm² cross sections in *xy*-plane across the thickness from sample's surface to core. Blue colour represents rectangles fitting the glass fibres used for quantifying the microstructure and helping to clarify the cartography regarding the optical artefacts which come from polishing (black area surrounding fibres) as shown in the zoomed image.

To quantify the microstructural features in *xy*-plane, we suggest to approximate fibre by a rectangle. We measure its width (b), length (a) and orientation angle (ϕ) relative to *x*-axis (Table 4.2). We suggest four fibre categories depending on their apparent shape (Table 4.2): straight fibres, C-shaped, S-shaped and "particles" (width is comparable to length). The latter category can be made of two classes of fibres: those which are out-of-plane (orientation angle θ close to 0 °) and simply small particles that appear during fibre breakage. We suppose that when a "particle" is an "agglomerate" of smaller ones, as shown in Figure 4.22, it is a bundle of flax that is out-of-plane. However, it is difficult to distinguish between a simple small particle and an elementary fibre that is out-of-plane and gives a similar apparent shape. Here, it is again another example of the difficulty arising during the analysis of natural fibre based composites, as far as flax fibres can make a "dust" due to breakage into small pieces and fibrillation [Le Moigne et al. (2014)]. Category 4 was characterised by the equivalent diameter D_a approximated by Huebscher formula [Huebscher (1948)]. The bending angle β

and the extended-fibre length average L_{cn} and L_{sn} were deduced from the rectangle dimensions by approximating fibres as a bent rod (or "C-shaped fibre") for category 2 and "S-shaped" rod for category 3. In the cartographies, the apparent objects that are represented by rectangle dimensions under 10 μm x 10 μm were not taken into account.

Table 4.2 Approach to quantify the dimensions and orientation of natural fibres in composites

In-plane fibres			Particles/out-of-plane fibres
Category 1 **Straight fibres**	**Category 2** **C-shaped fibres**	**Category 3** **S-shaped fibres**	**Category 4**
This category is related to bundles and short elementary fibres not long enough to be bent	Extended fibre length average $$L_{cn} = 2\sqrt{b^2 + \left(\frac{a}{2}\right)^2}$$	Extended fibre length average $$L_{sn} = 4\sqrt{\left(\frac{b}{2}\right)^2 + \left(\frac{a}{4}\right)^2}$$	$$D_a = 1{,}3 \left[\frac{(ab)^5}{(a+b)^2}\right]^{\frac{1}{8}}$$ (Huebscher formula)
ϕ = orientation angle a = fibre apparent length b = fibre apparent diameter	$$\beta = \frac{2\,b}{a}$$ a = end to end vector b = bending Fibre diameter= elementary fibre diameter (10 μm)		
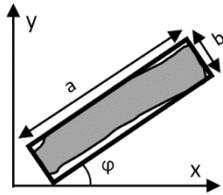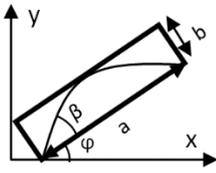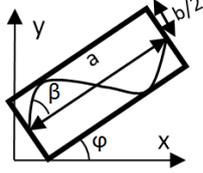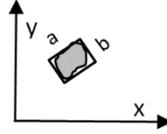
2.2. Distribution of fibre concentration throughout the thickness

Figure 4.30.a, b and c represents the distribution of flax, Tencel and glass fibres across the thickness for different fibre categories, respectively. We consider that glass fibres are fully straight, and even if some particles appear at the cross section, they are usually under our critical size of measurement (10 x 10 μm²). The quantification of the number of fibres per

cross section was possible because all cartographies have the same size (5 x 5 mm²). Figure 4.30.a shows that the total number of flax fibres increases twice from $z = 100$ µm to $z = 400$ µm, and it remains almost constant up to the core layer ($z = 900$ µm). The dominant category is the straight fibres; they make around 60 % of the total number of fibres, followed by the particles/out-of-plane category with 30 % and C-shaped category with around 10 %. S-shaped category does not appear in the case of flax fibres, which is probably due to their high stiffness and low aspect ratio.
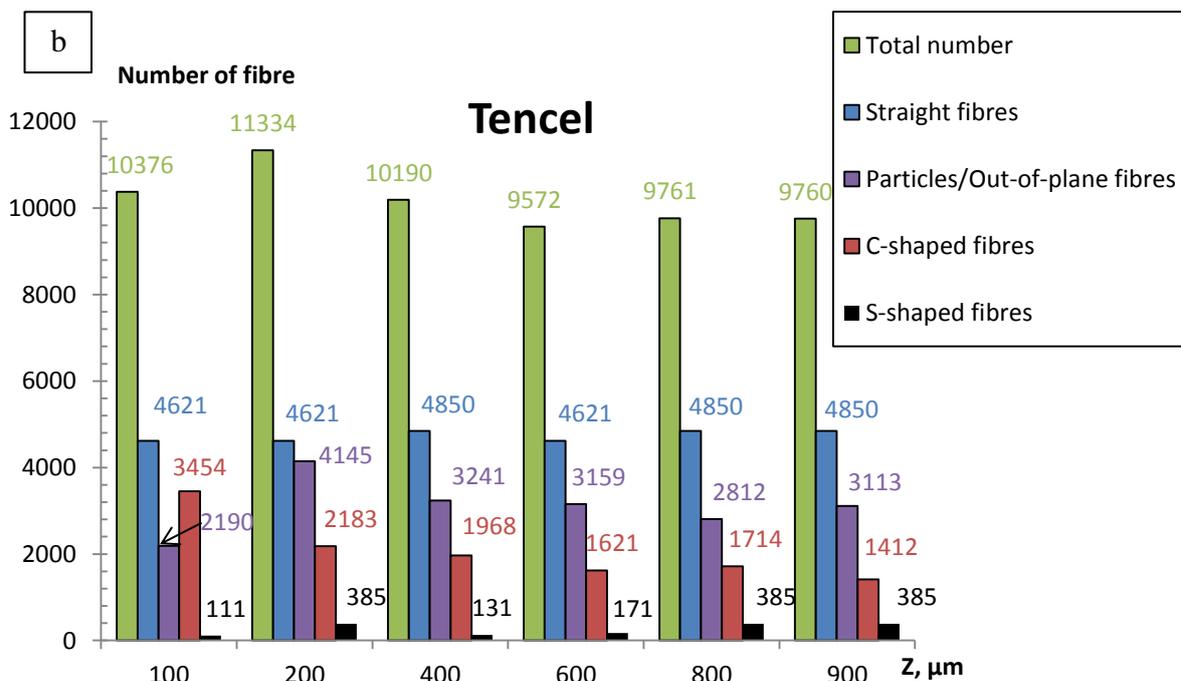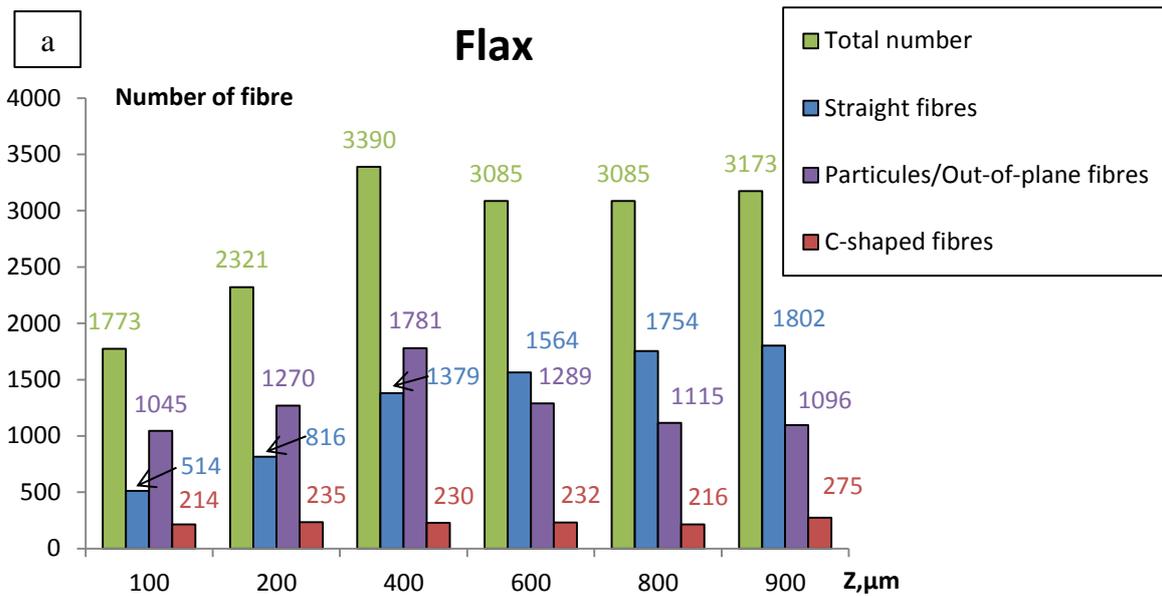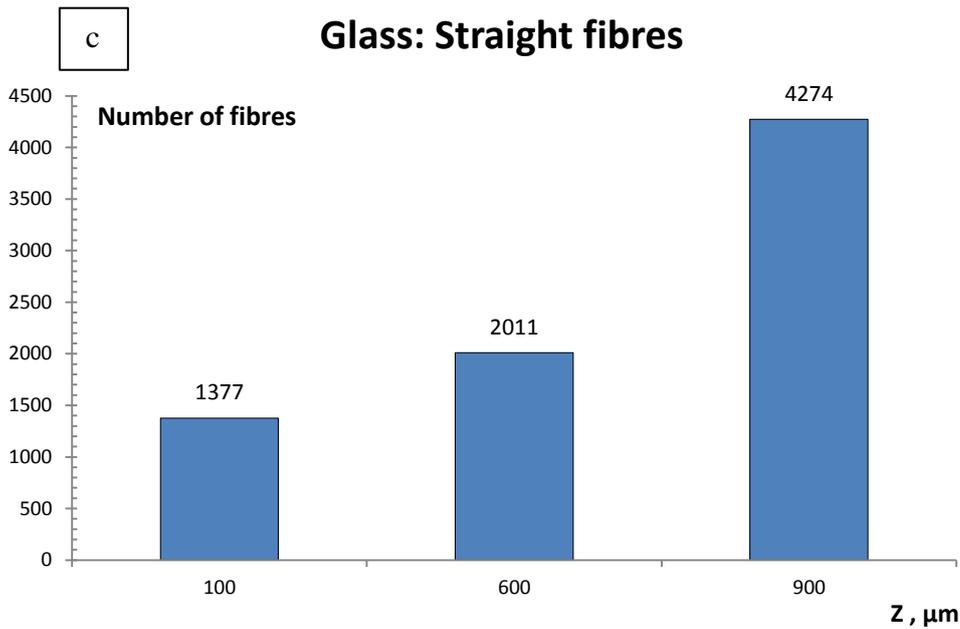
Figure 4.30

Distribution of the different categories of fibres (straight, C-shaped, S-shaped and particles/out-of-plane) for (a) flax, (b) Tencel and (c) glass across the thickness of sample. For glass fibres only one category (straight) is considered

Concerning the evolution of flax fibre number across sample thickness, the total number of fibres increases from 100 to 400 µm and remains almost constant from 400 µm to 900 µm. The straight fibres category keeps increasing from surface to core. Taking into account that most of straight fibres are in bundles, two assumptions are possible i) bundles are transferred toward the core, escaping high shear zones and ii) bundles are dissociated into elementary fibres or thinner bundles on high shear zone close to surface and "new" fibres are then transferred to the core. For glass fibres case (only rigid straight fibres) presented in Figure 24.c, their number is three time higher at the core ($z = 900$ µm) than near the surface ($z = 100$ µm). This is in agreement with results of Spahr et al. (1990) showing that core layer contains more fibres than shell layer. Moreover, the number of fibres at the core compared to surface is higher for glass than for flax fibres. This can be explained by the higher aspect ratio of glass fibres as demonstrated in Chapter 3 (see the influence of a higher aspect ratio in Table 4.1, section 1.2 [Spahr et al. (1990); Bailey and Rzepka (1991); Blanc et al. (1987); McLelland and Gibson (1990); Truckenmuller and Fritz (1991)]. Another reason is that when flax fibres are

broken, they leave away more "dust" or small particles that decrease the amount of straight fibres obtained after breakage.

The total number of Tencel fibres is almost three times greater than that of flax fibres (compare Figure 4.30.a and 4.30.b). This is also illustrated in Figure 4.30 that compares two cross sections of flax and Tencel composites taken at the same position from sample surface, $z = 400$ µm. Figure 4.31 demonstrates that this difference is caused by the effect of bundles that are present in flax fibres even after processing. Furthermore, the total number of Tencel fibre remains almost constant across composite thickness, which seems different from glass case for which core contains more fibres. Tencel fibres may disobey the dispersion trends in the cavity because of their higher flexibility compared to flax and glass fibres. While around 50 % of Tencel fibres are straight (most of them have short aspect ratio), 30 % are particles/out-of-plane and the rest are curved in which less than 4 % are S-shaped fibres. The latter category appears only in Tencel, which may be also caused by the high flexibility of these fibres. The number of C-shaped category of Tencel decreases almost twice from surface to core. The most probable reason is that a lower shear is produced at core as compared to surface, leading to less curved fibre at core.
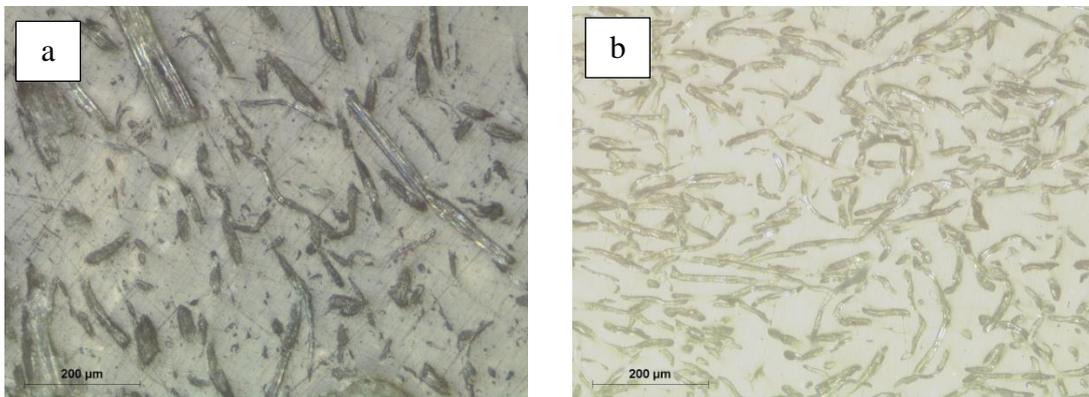
Figure 4.31

Comparison between flax (a) and Tencel (b) fibres dispersion (at the same location and position in thickness, $z = 400$ µm), number of Tencel fibres is much higher than that of flax which are partially structured in bundles

2.3. Distribution of fibre orientation throughout the thickness
- *In-plane orientation*

Figure 4.32.a, .b and .c presents the distribution of fibre orientation, i.e. angle ϕ towards the main flow direction in *xy*-plane (see Figure 4.2), for the cases of straight flax, Tencel and

glass fibres, respectively. We selected three representative layers corresponding to three main regions in thickness (shell, transition and core regions). Figure 4.32.a demonstrates that flax fibres in the shell region ($z= 100$ μm) are mostly oriented around 0 °, i.e. along the main flow direction. In the transition region ($z= 600$ μm), fibre orientation shows two large peaks at ± 40 °. The maxima of these peaks move towards ±80 ° in the core region ($z= 900$ μm), indicating the orientation perpendicular to the flow direction; this is in agreement with the finding of Aurich and Mennig (2001).
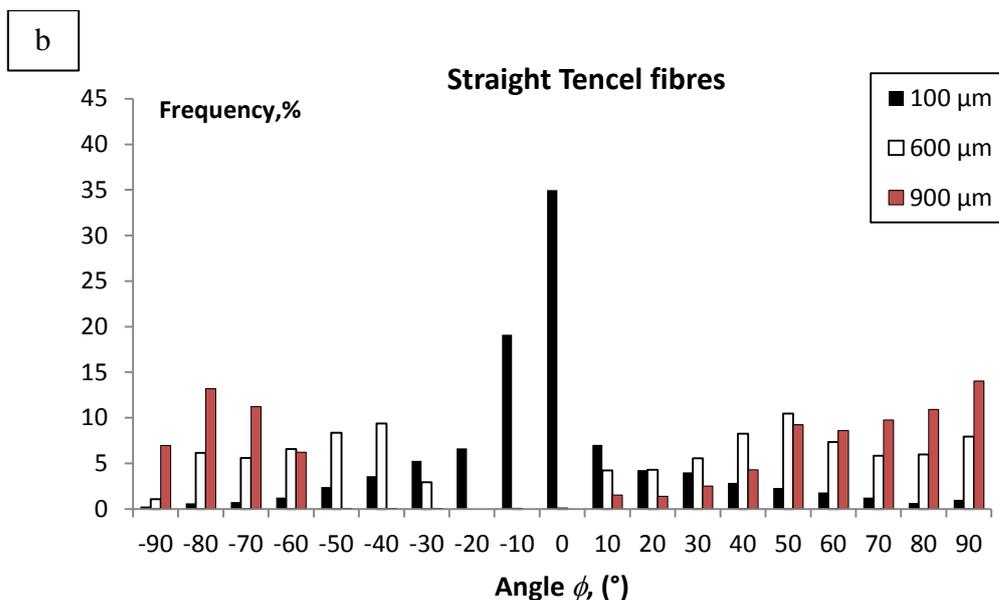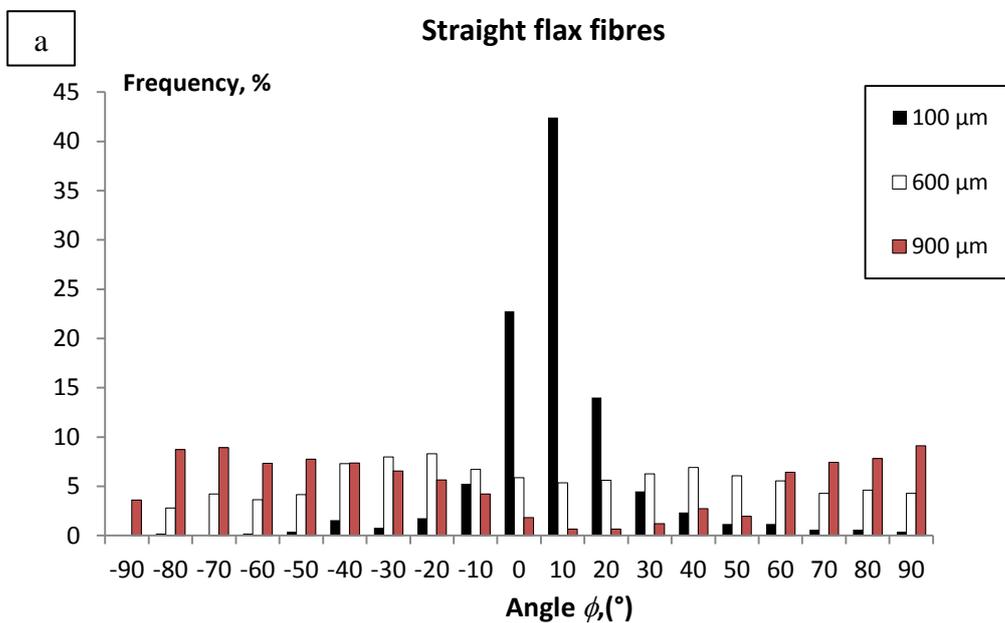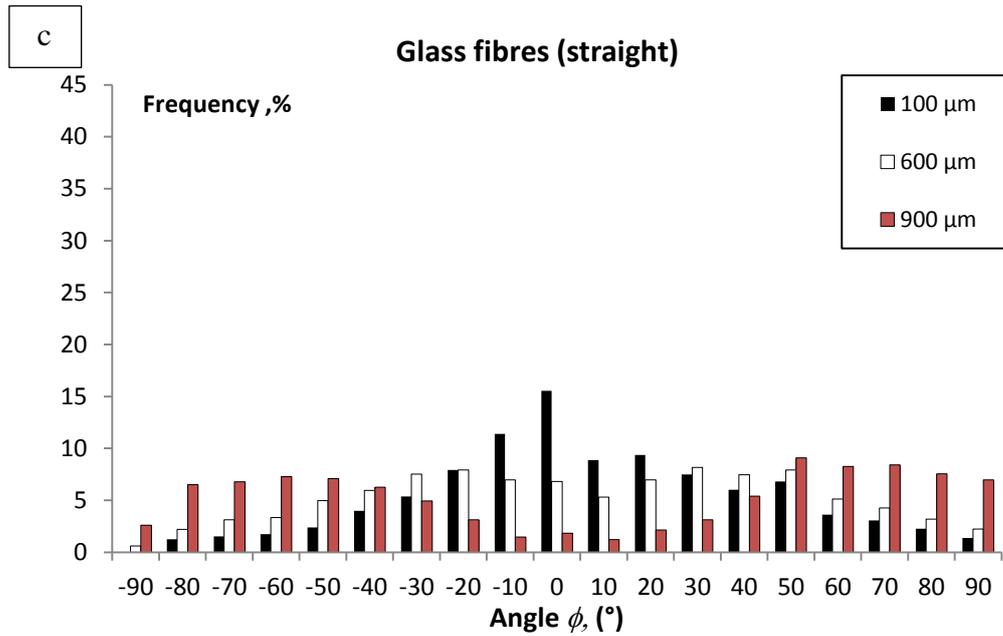
Figure 4.32

Distribution of orientation angle ϕ (in *xy*-plane, towards the main flow direction) for the category of straight fibres, for 900 μm, 600 μm and 100 μm of depth from surface for (a) flax (b) Tencel and (c) glass.

The global pattern of the fibre orientation distribution is almost the same for flax and Tencel. However, the sharpness of peaks varies with fibres type, indicating the difference in the alignment regarding the main flow direction. This difference is probably due to the difference in aspect ratio, flexibility and interactions between fibres during the flow, which leads in turn to a different melt viscosity between each fibre-type composite. It is known that a variation of aspect ratio results in a different composite rheology [Darlington and Smith (1987); Bay and Tucker (1993)]. Consequently, depending on the melt viscosity, a flatter or a sharper melt front during flow leads to a change in fibre orientation. For example, a higher fibre concentration leads to more interactions between fibres, and thus to flatter velocity profile during flow, so a different orientation in core and shell layers (see Table 4.1, section "influence of higher fibre concentration" [Spahr et al. (1990); Bouti et al. (1989)]. A similar analogy can be considered when we compare Tencel to flax. The local concentration of fibres is higher for Tencel than for flax, leading to more interactions between Tencel fibres than between flax ones, and thus a different orientation of fibres. Moreover, according to Table 4.1, a higher aspect ratio causes a lower degree of orientation in both core and shell layers (Table 4.1). This matches well with glass fibre as far as they present a higher aspect ratio than

flax and Tencel fibres (Figure 4.32.c). More details on the correlation between the morphology of fibres and composite viscosity will be provided in the next chapter.

For curved fibres, Figure 4.34 shows the case of Tencel C-shaped fibres, the result is similar to that of straight fibres (we remind here that the orientation of curved categories is represented by the orientation of the end-to-end vector).
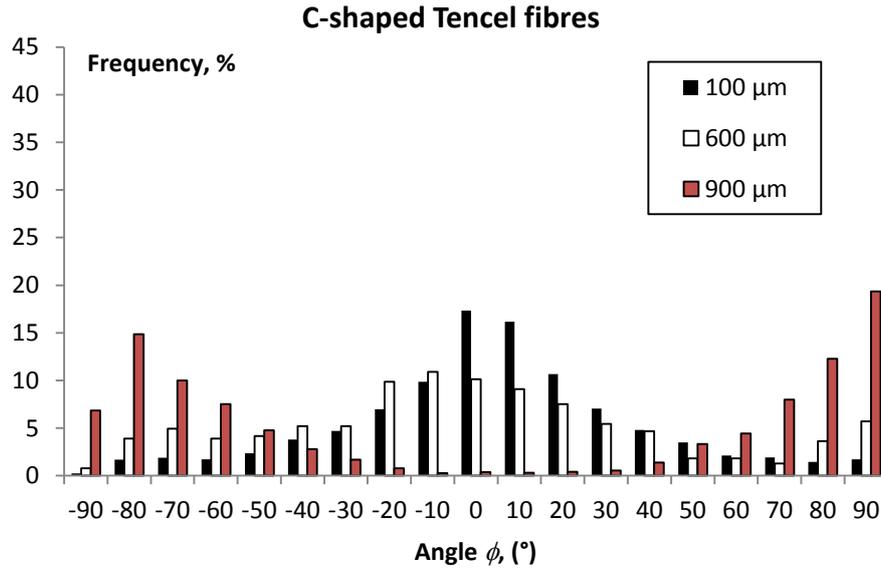
Figure 4.34

Distribution of orientation angle ϕ (in *xy*-plane, towards main flow direction) for C-shaped category of Tencel for 900 μm, 600 μm and 100 μm of depth from surface

Another way to describe the orientation of fibres in *xy*-plane across thickness from surface to core is to use the first component of the orientation tensor a_{xx}. The latter varies from 1, when fibres are parallel to *x*-axis, to 0, when fibres are perpendicular to this direction i.e. oriented along *y*-axis (see Figure 4.4).

Figure 4.34.a presents the evolution of a_{xx} for straight and C-shaped flax fibres across thickness from surface to core. Both categories are well aligned along *x*-direction from *z*= 100 μm to *z*= 200 μm (the shell layer) with $0.8 < a_{xx} < 0.9$, whereas their orientation from *z*= 400 μm to *z*= 900 μm is almost isotropic, showing $0.3 < a_{xx} < 0.6$.

Figure 4.34.b shows the evolution of a_{xx} of straight, C-shaped and S-shaped Tencel fibres across thickness from surface to core. The three categories are aligned to *x*-direction in the

layers $z= 100$ μm and $z= 200$ μm, showing $0.75 < a_{xx} < 0.85$. From $z= 400$ μm to $z= 600$ μm, they show an isotropic orientation with $0.4 < a_{xx} < 0.65$. At core, from $z= 800$ μm to $z= 900$ μm, all fibres are aligned along *y*-direction with $0.15 < a_{xx} < 0.25$, except the S-shaped ones with $a_{xx} \approx 0.5$.
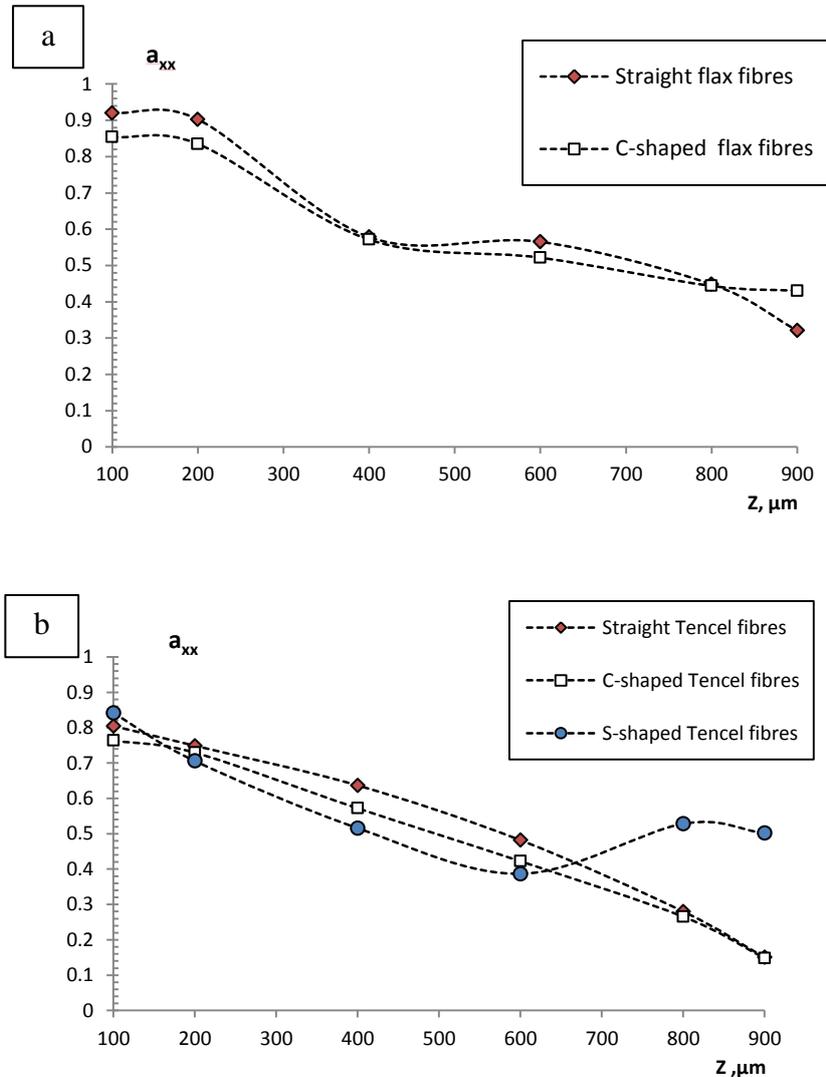
Figure 4.34

a_{xx} orientation component across the thickness from shell to core, for various fibre categories (straight, C-shaped and S-shaped fibres) for (a) flax and (b) Tencel

Next, we "mix" all categories *except particles/out-of-plane category* for which a description of fibre orientation cannot be considered, aiming to get a single generalised a_{xx} value. The contribution of each category in the entire orientation depends on its proportion relative to the total number of fibre. Therefore, to obtain a global interpretation of the orientation state a_{xx}

was weighted by the number of fibres in each category. Figure 4.35 presents the result of this approach for flax and Tencel superposed on the orientation curve of glass fibre (for which only one category, the straight fibres, is present). In shell region, flax fibres are most aligned, followed by Tencel and glass that are the least aligned fibres. In the core, Tencel fibres tend to be aligned perpendicular to the flow (along *y*-direction), whereas flax and glass fibres are randomly oriented.
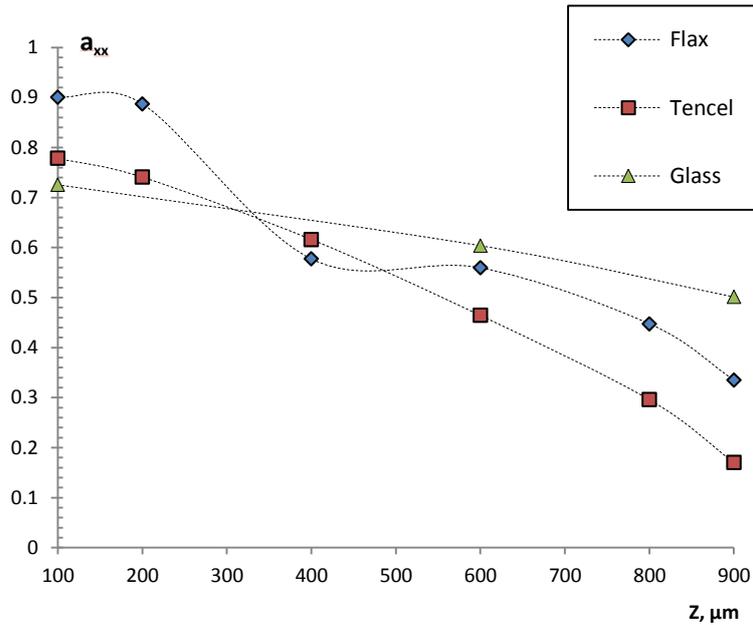
Figure 4.35

Generalised a_{xx} (in-plane categories) of flax, Tencel and glass as a function of the sample thickness from surface to core

- ▪ *Influence of out-of-plane orientation*

It is know that glass fibres make a small angle (angle θ, see Figure 4.2) regarding *xy*-plane [Phelps and Tucker (2009)]. In our study, this orientation can be observed in Figure 4.26 that exhibits a comparison between optical microscopy images in reflection and in transmission modes. As seen by transmission light observation, some fibres are in *xy*-plane but some others continue "under" the surface. Therefore, in *xy*-plane they appear shorter than they really are. It is thus interesting to compare how fibre length and diameter measured from the cross sections ("apparent length" and "apparent diameter", see Table 4.2) correlate with real fibre dimensions measured in Chapter 3.

Figure 4.36 shows the number average of the apparent length and diameter of the straight fibres category of flax across the thickness. Flax apparent average length is almost constant (180- 200 μm) along sample thickness. The apparent average diameter increases from 26 at z = 100 μm to 40 at z= 900 μm. Hence, the resultant aspect ratio decreases from 8.6 to 5.3 (not shown in Figure 4.36).
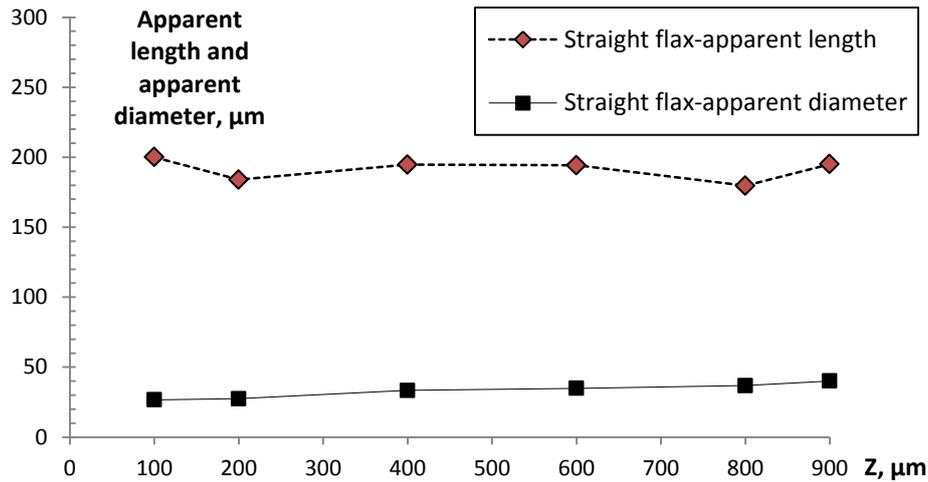
Figure 4.36

The evolution of the apparent average length and diameter of the straight flax fibre category across sample thickness from surface to core

The results of the fibre size analysis presented previously in Chapter 3 show that after injection flax fibre is characterised by L_n= 388 μm, D_n= 28 μm, and $(L/D)_n$= 16 for the concentration of 20.5 vol %.; the sample analysed was taken from the same location as used for the analysis of microstructure in the injected box). The "real" length of fibres seems to be twice greater than the apparent one. This seems surprising but it can be justified: according to equation 4.2 (J and Q are the apparent L and D, respectively), we plotted in Figure 4.37 a theoretical correlation between the apparent aspect ratio and the angle regarding xy-plane. Let us consider a rigid fibres with a constant diameter (case of glass), when θ= 0°, Q=J=D and θ= 90° Q=D and J=L, the real dimensions of the fibre, but 0°<θ< 90°, the apparent fibre length is smaller than L, so that the apparent L/D (J/Q) is smaller than the real L/D. For low apparent aspect ratio fibres, a deviation of small angle regarding the xy-plane, leads to a higher decrease in aspect ratio than what is expected. For example, to reduce the aspect ratio from fifteen in the real dimension to five as appearing in the cross section, the fibre must make an

angle of 4~5° to the cross-section. This angle deviation is quite small but its influence on the apparent length in the cross section is great, and this is in agreement with literature in glass fibres [Phelps and Tucker (2009)].
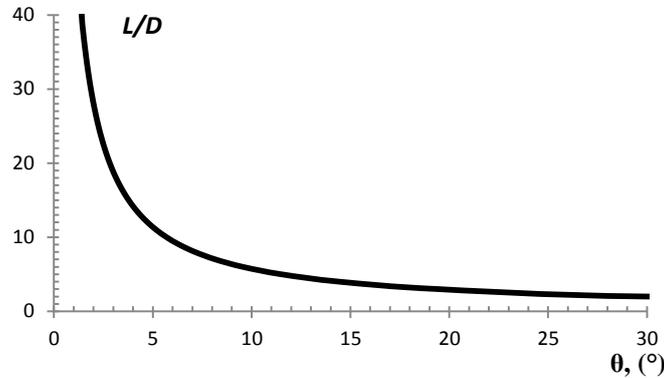
Figure 4.37

The apparent aspect ratio as function of the angle to *xy*-plane

2.4. Fibre bending

Figure 4.38 shows that the average of angle β (bending angle, see Table 4.2) is ranging between 20° and 30°, remaining almost constant between 100 μm and 900 μm of depth. For C-shaped category, the "Extended fibre length average" L_{cn} (see Table 4.2) of flax fibres are apparently longer than Tencel ones (Figure 4.39). As seen before, this can be explained by the fact that flax fibres are stiffer than Tencel ones ($E_{flax} > E_{Tencel}$, see Chapter 2, Section 1. Materials), thus flax has to be longer to recover some flexibility and to bend like Tencel. The "Extended fibre length average" L_{sn} of S-shaped Tencel fibre is slightly higher than that of C-shaped category L_{cn} (Figure 4.39). S-shaped fibres form different conformation while for C-shaped practically only one angle of bending was observed. Forgacs and Mason (1959) studied the motion of a flexible fibre in shear flow when they rotate. Stiff fibres rotate with orbits as predicted by Jeffry (1922). When fibres are less stiff, they rotate as springy orbits i.e. fibres slightly buckle and then become straight as they realigned along flow direction. Increasing flexibility, fibres showed different conformations called "snake-turn", "S-turn" or other complex shape, and this seems to be similar to what we observed for C-shaped and S-shaped categories.
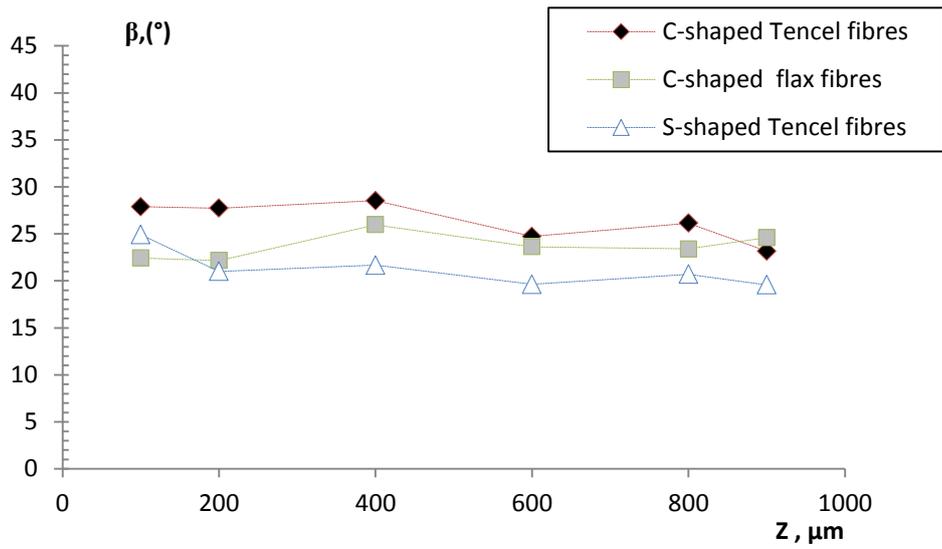
Figure 4.38

The evolution of the bending angle β across the thickness for C-shaped and S-shaped categories of Tencel and for C-shaped category of flax
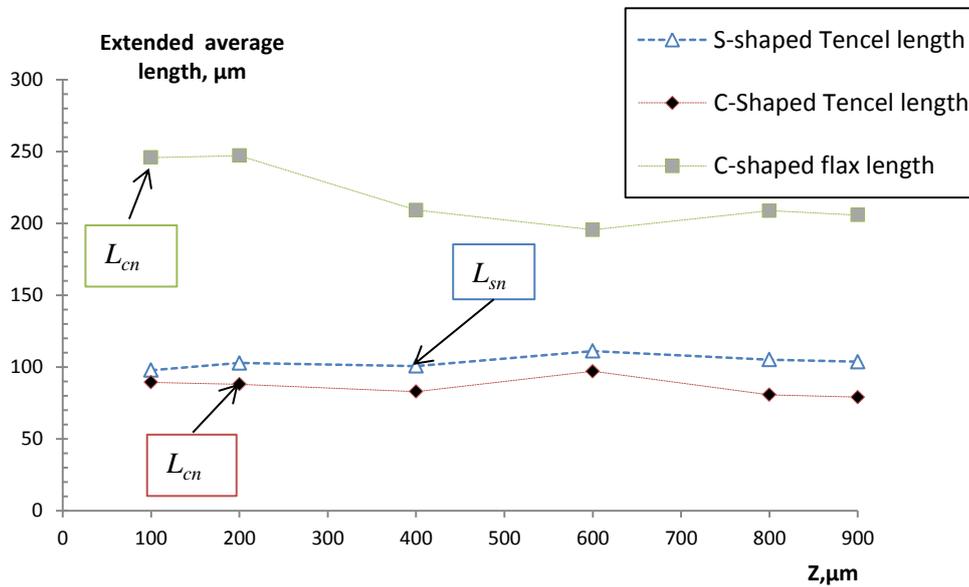
Figure 4.39

The evolution of the extended fibre average length across thickness for C-shaped and S-shaped categories of Tencel and for C-shaped category of flax

2.5. Conclusions

A novel experimental approach have been suggested to study in details the microstructure of the injection moulded flax -and Tencel- reinforced polypropylene. The orientation and dispersion (number of fibre per layer) were quantified, using optical microscopy in reflection mode and image analysis. Cross sections performed by polishing a sample cut for the moulded box in *xy*-plane, for several levels in thickness from shell to core region. Fibres were classified into four categories depending on their apparent shapes: straight, C-shaped, S-shaped and particles/out-of-plane fibres. Because of flexibility difference between flax and Tencel (typically proportional to aspect ratio over Young modulus), Tencel fibres can be bent in two conformations: C-shaped and S-shaped, whereas elementary flax fibres can be bent only in one conformation that is C-shaped .

The *xy*-cross sections were carefully analysed in terms of fibres distribution and fibre orientation across the sample thickness for each category. The following conclusions can be drawn from this study:

- Flax and Tencel fibres exhibit a core-shell structure in the moulding, being similar to what was reported for glass fibres reinforced polymer. While the shell fibres are aligned along the flow direction, the core ones are perpendicular.

- The distributions over the sample thickness of flax and Tencel fibres are different: as for glass fibres, the concentration of flax increased from surface to core, whereas that of Tencel was practically unchanged.

- Another difference between flax and Tencel was observed in term of fibre dispersion throughout thickness: the number of Tencel fibres was three times larger than that of flax. This difference was explained by the fact that even after injection, a lot of flax fibres remained in bundles. For glass fibres, the change of concentration per layer was important as the number of fibres was lower than that of flax at surface and become larger at core.

- The alignment of fibres with respect to the main flow direction depends on the fibre type. Flax, Tencel and glass fibres show a_{xx} near surface-core of 0.9-0.3, 0.8-0.2 and 0.7-0.5, respectively.

- Finally, the fibre apparent length measured at the cross section is smaller than the true one obtained in Chapter 3 via matrix dissolution. This was explained by out-of-plane orientation.

Concluding, this chapter shows certain similarities and differences in the microstructure of Tencel-and flax-based composites compared to glass fibre ones. Fibre flexibility plays an important role in microstructure and has to be taken into account when predicting and modelling injection moulding process. The influence of fibre flexibility on the rheological properties of composites will be presented in the next chapter.

3. References

Advani, S. G., & Tucker III, C. L. (1990). Closure approximations for three-dimensional structure tensors. Journal of Rheology (1978-present), 34(3), 367-386.

Akay, M., & Barkley, D. (1985). Processing-structure-property interaction in injection moulded glass-fibre reinforced polypropylene. Composite structures, 3(3), 269-293.

Akay, M., & Barkley, D. (1991). Fibre orientation and mechanical behaviour in reinforced thermoplastic injection mouldings. Journal of materials science, 26(10), 2731-2742.

Alemdar, A., Zhang, H., Sain, M., Cescutti, G., & Müssig, J. (2008). Determination of Fiber Size Distributions of Injection Moulded Polypropylene/Natural Fibers Using X-ray Microtomography. Advanced Engineering Materials, 10(1-2), 126-130.

Aurich, T., & Mennig, G. (2001). Flow-induced fiber orientation in injection molded fit fiber reinforced polypropylene. Polymer composites, 22(5), 680-689.

Bailey, R., & Rzepka, B. (1991). Fibre orientation mechanisms for injection molding of long fibre composites. International Polymer Processing, 6(1), 35-41.

Bay, R. S., & Tucker, C. L. (1992.a). Fiber orientation in simple injection moldings. Part I: Theory and numerical methods. Polymer composites, 13(4), 317-331.

Bay, R. S., & Tucker, C. L. (1992.b). Fiber orientation in simple injection moldings. Part II: Experimental Results. Polymer composites. 4, 332-341.

Bernasconi, A., Cosmi, F., & Hine, P. J. (2012). Analysis of fibre orientation distribution in short fibre reinforced polymers: A comparison between optical and tomographic methods. Composites Science and Technology, 72(16), 2002-2008.

Blanc. R., S.Philipon, M. Vincent, J.F Agassant, H. Alglave, R.Muller and D. (1987). Froelich. Injection molding of reinforced thermosets. Internat.polym. Process. 2, 21-27.

Bourmaud, A., Ausias, G., Lebrun, G., Tachon, M. L., & Baley, C. (2013). Observation of the structure of a composite polypropylene/flax and damage mechanisms under stress. Industrial Crops and Products, 43, 225-236.

Bouti, A., Vu-Khanh, T., & Fisa, B. (1989). Injection molding of glass flake reinforced polypropylene: flake orientation and stiffness. Polymer composites, 10(5), 352-359.

Bright, P. F., Crowson, R. J., & Folkes, M. J. (1978). A study of the effect of injection speed on fibre orientation in simple mouldings of short glass fibre-filled polypropylene. Journal of Materials Science, 13(11), 2497-2498.

Darlington, M. W., & Smith, A. C. (1987). Some features of the injection molding of short fiber reinforced thermoplastics in center sprue-gated cavities. Polymer composites, 8(1), 16-21.

Fellahi, S., Meddad, A., Fisa, B., & Favis, B. D. (1995). Weldlines in injection-molded parts: A review. Advances in polymer technology, 14(3), 169-195.

Forgacs, O. L., & Mason, S. G. (1958). The flexibility of wood-pulp fibers. Tappi, 41, 695-704.

Gillespie, J. W., Vanderschuren, J. A., & Pipes, R. B. (1985). Process induces fiber orientation: Numerical simulation with experimental verification. Polymer composites, 6(2), 82-86.

Gupta, M., & Wang, K. K. (1993). Fiber orientation and mechanical properties of short-fiber-reinforced injection-molded composites: Simulated and experimental results. Polymer Composites, 14(5), 367-382.

Hegler, R. P., & Mennig, G. (1985). Phase separation effects in processing of glass-bead-and glass-fiber-filled thermoplastics by injection molding. Polymer Engineering & Science, 25(7), 395-405.

Hornsby, P. R., Hinrichsen, E., & Tarverdi, K. (1997). Preparation and properties of polypropylene composites reinforced with wheat and flax straw fibres: Part II Analysis of composite microstructure and mechanical properties. Journal of Materials Science, 32(4), 1009-1015.

Huebscher, R. G. (1948). Friction equivalents for round, square and rectangular ducts. ASHVE Transactions (renamed ASHRAE Transactions), 54, 101-118.

Jeffery, G. B. (1922, November). The motion of ellipsoidal particles immersed in a viscous fluid. In Proceedings of the Royal Society of London A102:161. The Royal Society.

Joffre, T., Miettinen, A., Berthold, F., & Gamstedt, E. K. (2014). X-ray micro-computed tomography investigation of fibre length degradation during the processing steps of short-fibre composites. Composites Science and Technology, 105, 127-133.

Karmaker, A. C., & Youngquist, J. A. (1996). Injection molding of polypropylene reinforced with short jute fibers. Journal of Applied Polymer Science, 62(8), 1147-1151.

Kastner, J., Plank, B., & Salaberger, D. (2012, April). High resolution X-ray computed tomography of fibre-and particle-filled polymers. In 18th World Conference on Nondestructive Testing, Durban, South Africa (pp. 16-20).

Kenig, S. (1986). Fiber orientation development in molding of polymer composites. Polymer composites, 7(1), 50-55.

Lafranche, E., Martins, C. I., M Oliveira, V., & Krawczak, P. (2013, July). Prediction of tensile properties of injection moulding flax fibre reinforced polypropylene from morphology analysis. In Key Engineering Materials (Vol. 554, pp. 1573-1582).

Le Moigne, N., Longerey, M., Taulemesse, J. M., Bénézet, J. C., & Bergeret, A. (2014). Study of the interface in natural fibres reinforced poly (lactic acid) biocomposites modified by optimized organosilane treatments. Industrial Crops and Products, 52, 481-494.

Malzahn, J. C., & Schultz, J. M. (1986). Transverse core fiber alignment in short-fiber injection-molding. Composites science and technology, 25(3), 187-192.

McClelland, A. N., & Gibson, A. G. (1990). Rheology and fibre orientation in the injection moulding of long fibre reinforced nylon 66 composites. Composites manufacturing, 1(1), 15-25.

Neves, N. M., Isdell, G., Pouzada, A. S., & Powell, P. C. (1998). On the effect of the fiber orientation on the flexural stiffness of injection molded short fiber reinforced polycarbonate plates. Polymer composites, 19(5), 640-651.

Nyström, B. (2007). Natural fiber composites optimization of microstructure and processing parameters. Thesis in Lulea University of Technology.

Peltola, H., Madsen, B., Joffe, R., & Nättinen, K. (2011). Experimental study of fiber length and orientation in injection molded natural fiber/starch acetate composites. Advances in Materials Science and Engineering, 2011.

Phelps, J. H., & Tucker, C. L. (2009). An anisotropic rotary diffusion model for fiber orientation in short-and long-fiber thermoplastics. Journal of Non-Newtonian Fluid Mechanics, 156(3), 165-176.

Rose, W. (1961). Fluid-fluid interfaces in steady motion. Nature, 191, 242-243.

Sanou, M., Chung, B., & Cohen, C. (1985). Glass fiber-filled thermoplastics. II. Cavity filling and fiber orientation in injection molding. Polymer Engineering & Science, 25(16), 1008-1016.

Shen, H., Nutt, S., & Hull, D. (2004). Direct observation and measurement of fiber architecture in short fiber-polymer composite foam through micro-CT imaging. Composites Science and Technology, 64(13), 2113-2120.

Singh, P., & Kamal, M. R. (1989). The effect of processing variables on microstructure of injection molded short fiber reinforced polypropylene composites. Polymer composites, 10(5), 344-351.

Spahr, D. E., Friedrich, K., Schultz, J. M., & Bailey, R. S. (1990). Microstructure and fracture behaviour of short and long fibre-reinforced polypropylene composites. Journal of Materials Science, 25(10), 4427-4439.

Tadmor, Z. (1974). Molecular orientation in injection molding. Journal of Applied Polymer Science, 18(6), 1753-1772.

Tausif, M., Duffy, B., Grishanov, S., Carr, H., & Russell, S. J. (2014). Three-Dimensional Fiber Segment Orientation Distribution Using X-Ray Microtomography. Microscopy and Microanalysis, 20(04), 1294-1303.

Thi, T. B. N., Morioka, M., Yokoyama, A., Hamanaka, S., Yamashita, K., & Nonomura, C. (2015). Measurement of fiber orientation distribution in injection-molded short-glass-fiber composites using X-ray computed tomography. Journal of Materials Processing Technology, 219, 1-9.

Toll, S., & Andersson, P. O. (1993). Microstructure of long-and short-fiber reinforced injection molded polyamide. Polymer composites, 14(2), 116-125.

Truckenmüller, F., & Fritz, H. G. (1991). Injection molding of long fiber-reinforced thermoplastics: A comparison of extruded and pultruded materials with direct addition of roving strands. Polymer Engineering & Science, 31(18), 1316-1329.

Tucker III, C. L. (1988). Predicting Fiber Orientation in Short Fiber Composites. The Manufacturing Science of Composites, TG Gutowski, ed., ASME, New York.

Vincent, M., & Agassant, J. F. (1986). Experimental study and calculations of short glass fiber orientation in a center gated molded disc. Polymer composites, 7(2), 76-83.

Vincent, M., Giroud, T., Clarke, A., & Eberhardt, C. (2005). Description and modeling of fiber orientation in injection molding of fiber reinforced thermoplastics. Polymer, 46(17), 6719-6725.

Chapter 5

Rheological properties of composites

The flow behaviour of molten composites is directly correlated to their microstructure. As seen in the previous chapter, the pattern of the melt front during cavity filling controls and designs the dispersion and the alignment of fibres. Therefore, assessing the composite rheology is required to correlate the microstructure with the results obtained during injection moulding process. Moreover, rheology experiments provide input data to simulate the filling stage, which enables to optimize modelling assumptions and also to predict the mechanical properties of the moulded part.

In the following chapter, we firstly present the state of the art on dynamic and capillary rheology of glass fibre- and natural fibre- reinforced thermoplastics. Then the results of this work about the viscoelastic properties of flax, Tencel and glass based composites are provided and discussed, focusing on fibre morphology and flexibility. The effect of fibre content and aspect ratio on rheology of composites will be demonstrated. Furthermore, the correlations between the dynamic and capillary viscosity will be assessed.

1. State of the art

1.1. Dynamic rheology

1.1.1. *Influence of fibre concentration and aspect ratio*

Recently, some considerable studies of dynamic rheology of natural fibre-reinforced thermoplastics have emerged in literature. Twite-Kamamba et al. (2009) studied hemp-reinforced polypropylene, Le Moigne et al. (2013) flax- and sisal-reinforced polypropylene and Sojoudiasli et al. (2014) flax -reinforced polypropylene. All these studies showed that increasing fibre content leads to an important change in the rheological behaviour of composites. We are going to focus on the study of Le Moigne et al. (2013) to describe this change. Figure 5.1 shows the evolution of complex viscosity η^* versus frequency ω for neat matrix with or without compatibilizer and two concentrations 20 wt % and 50 wt % of flax-reinforced polypropylene. The influence of compatibilizer will be discussed in section 1.1.2 (Influence of compatibilizer). At low frequencies, compared to neat matrix showing a Newtonian plateau, the complex viscosity of 20 wt % flax/PP composites keeps increasing when decreasing the frequency. By increasing the fibre content until 50 wt %, the slope of the viscosity rise becomes sharper. At high frequencies, the complex viscosity of 20 wt % merges to the matrix one, whereas that of 50 wt % follows a similar shear thinning slope to matrix at a greater magnitude. The complex viscosity evolution is essentially related to the viscous (G'') and elastic (G') moduli. Figure 5.2 shows G' and G'' versus frequency curves, for neat PP and for two concentrations of flax-reinforced polypropylene (30 wt % and 50 wt %). According to authors, viscous modulus of neat polypropylene is higher in magnitude than the elastic one, and the slopes of both elastic and viscous moduli at low frequencies are almost 1.3 and 0.8, respectively. The addition of fibres increases the magnitude of viscous and elastic moduli and reduces their slopes at low frequencies, showing plateau-like (slope≈ 0) for 50 wt % fibre content. The difference in magnitude between viscous modulus and elastic modulus becomes lower as fibre content increases. Above 20 wt %, the elastic modulus value overtakes the viscous one. Such a rheological response is similar to that of glass fibre reinforced thermoplastic. [Greene et al. (1995); Thomasset et al. (2005); Eberle et al. (2008)].
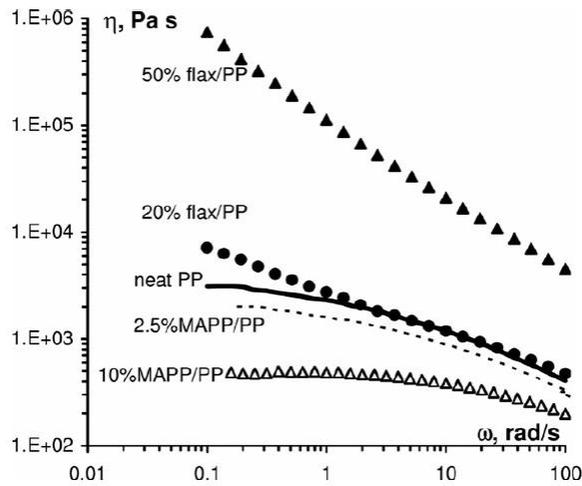
Figure 5.1

Dynamic viscosity of 20 and 50 wt % flax /PP and their corresponding MAPP/PP matrices, 2.5 % MAPP/PP (calculated) and 10 % MAPP/PP (experimental). Solid line corresponds to neat PP (experimental) [Le Moigne et al. (2013)]
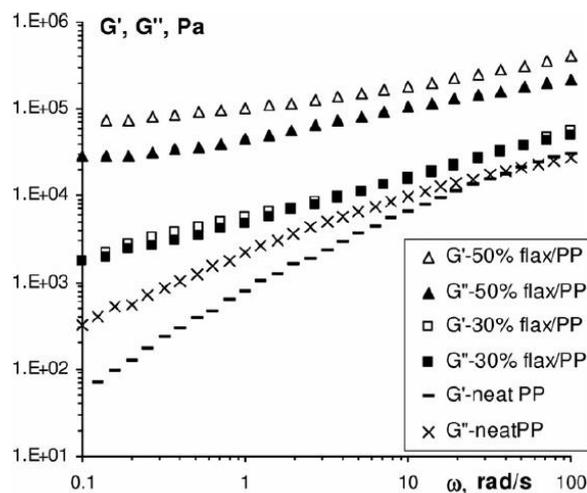
Figure 5.2

Elastic and viscous moduli versus frequency for 30 wt % and 50 wt % flax reinforced polypropylene [Le Moigne et al. (2013)]

Le Moigne et al. (2013) showed that increasing fibre content has a larger impact on complex viscosity and G' and G'' moduli at concentrated regime as compared to dilute and semi dilute regimes. The transition from semi-dilute to concentrated regime occurs when volume fraction is

higher than the inverse of the fibre aspect ratio $(L/D)^{-1}$. By increasing the aspect ratio, the transition semi-dilute /concentrated moves to lower concentrations. This means that the viscosity rise at low frequencies becomes greater when fibre aspect ratio increases, at the same fibre concentration. Authors concluded that the transition between semi dilute and concentrated regimes is a sign of the commencement of fibre-fibre interactions, becoming larger either by increasing fibre content or fibre aspect ratio. The fibre-fibre interactions lead to build a network-like structure at low frequencies, which lets the molten composite owning more elasticity. This is a typical solid-like behaviour indicating the presence of an apparent yield stress at low frequencies.

In order to assess the apparent yield stress, Le Moigne et al. (2013) and previously Twite-Kamamba et al. (2009) fitted the experimental curves with the modified Carreau-Yusuda model described by:

$$\eta_{(\omega)} = \frac{\sigma_0}{\omega} + \eta_0 \left[1 + \lambda\omega^a\right]^{\frac{(n-1)}{a}} \qquad \text{[Eq.5.1]}$$

where σ_0 is the apparent yield stress, η_0 is the zero shear viscosity, λ is the material characteristic time, a is the Yasuda parameter, ω is the frequency and n is the power-law index.

Using an approach of suspensions of solid particles [Heymann et al. (2002); Mueller et al. (2010)], Le Moigne et al. (2013) suggested apparent yield stress versus fibre volume fraction dependence similar to Krieger-Dougherty model

$$\sigma_0 = \sigma^* \left(\left(1 - \frac{f}{f_m}\right)^{[\eta]f_m} - 1\right) \qquad \text{[Eq.5.2]}$$

where σ^* is a fitting parameter related to the size of fibres , $[\eta]$ is the intrinsic viscosity, f is the volume fraction and f_m is maximal packing volume fraction that depends on fibre aspect ratio and size polydispersity. Two semi-empirical equations were used to asses f_m

$$f_m = 0.54 - 0.0125 \left(\frac{L}{D}\right) \text{ [Kitano et al. (1981)]} \qquad \text{[Eq.5.3]}$$

$$f_m = \frac{2}{0.32\left(\frac{L}{D}\right)+3.02} \text{ [Mueller et al. (2010)]} \qquad \text{[Eq.5.4]}$$

Figure 5.3 shows that σ_0 keeps gradually increasing with fibre content up to a critical concentration above which the increase becomes very steep. This critical concentration

corresponds to the transition from semi-dilute to concentrated regime. By comparing sisal/PP with $(L/D)_n = 2.6$ and flax/PP with $(L/D)_n = 5.5$ at the same concentration (0.303 vol % = 40 wt %), the authors concluded that the apparent yield stress decreases when L/D decreases.
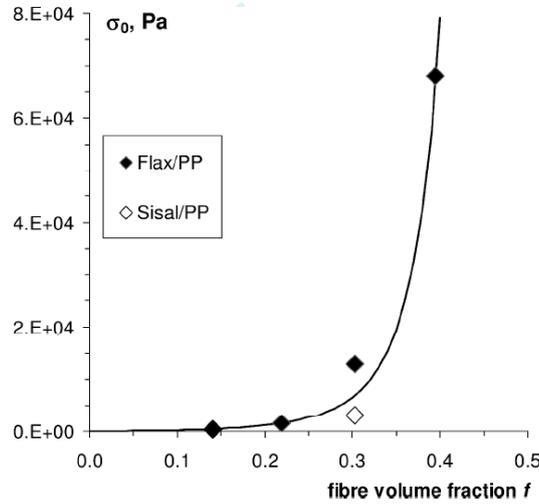
Figure 5.3

Apparent yield stress as function as the volume fraction f, for flax/PP and sisal/PP composites. Solid line for Eq 5.2 for flax with f_m, $[\eta]f_m = 4.58$ and $\sigma^* = 164$ Pa, $(L/D)_n$ varies between 2.8 and 5.5 [Le Moigne et al. (2013)]

The apparent yield stress was differently interpreted by Kerekes et al. (1985) and Bennington et al. (1990) for pulp and synthetic fibres immersed in water based liquids. They defined the apparent yield stress that is due to the presence of fibre network-like structure, taking into account the Young's modulus of fibres (E_f) as well as the fibre aspect ratio and the fibre content as follows:

$$\sigma_0 = a \left(E_f\right)^c \left(\tfrac{L}{D}\right)^d f^b \qquad\qquad \text{[Eq.5.5]}$$

where a, b, c and d are constants for a given fibre type and f the volume fraction.

Bennington et al. (1990) derived a theory for evaluating the apparent yield stress based on elastic fibre bending that induces frictional resistance at fibre contact points. They obtained Eq.5.5 with theoretical exponents $b = 3$, $c = 1$ and $d = 2$, a being an adjustable value.

Figure 5.4 shows the log-log plot of apparent yield stress versus fibre volume fraction for three types of pulp fibre suspension (Semi-Bleached Kraft: SBK, Stone Ground Wood: SGW

and Themo-Mechanical Pulp: TMP). The correlation between power law predictions and Eq.5.5 enables to assume that the apparent yield stress depends on the volume fraction raised to almost the third power (b = 2.72-3.56), which is approximately in agreement with Bennington et al. (1990). In addition, the apparent yield stress is greatly dependent on the aspect ratio and the Young's modulus fibre ($a\left(E_f\right)^c\left(\frac{L}{D}\right)^d = 3.82.\ 10^5$- $2.63\ .10^6$). However, no exact dependence can be made to estimate a, c and d.
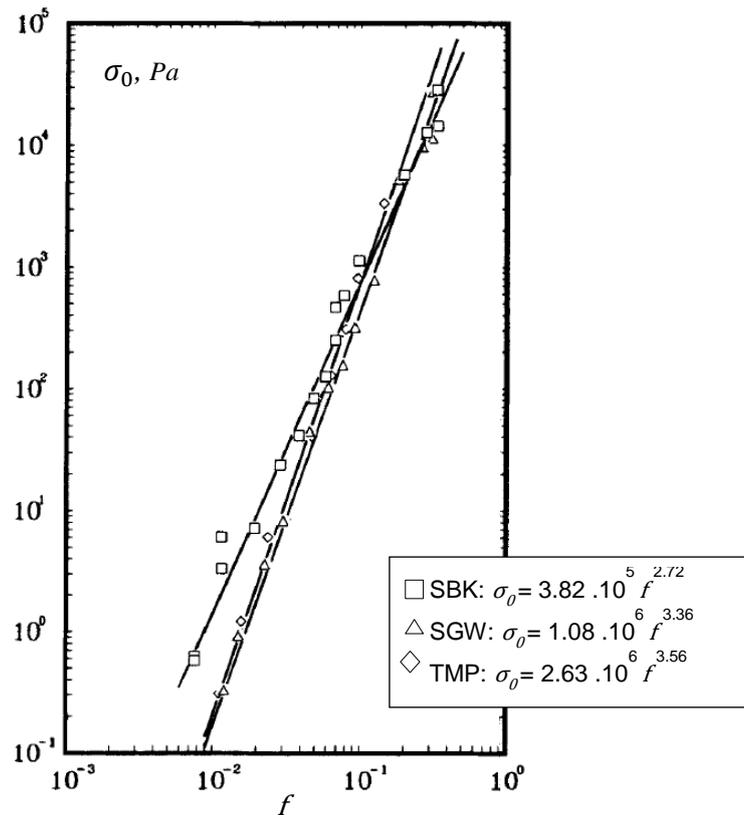
Fibre 5.4

The apparent yield stress as function of fibre volume fraction for pulp fibre suspensions, SBK (*L/D* = 64.7-93.7, E_f = 35.2 MPa), SGW (*L/D* = 20.3, E_f = *923* MPa, TMP (*L/D* = 38.7, E_f = 1080 MPa), power law predictions are shown in solid lines, the coefficient of variation of yield stress measurement is $\pm$10 % [Bennington et al. (1990)]

1.1.2. *Influence of compatibilizer and composition*

Adding compatibilizer to natural fibres based composite improves the adhesion between matrix and fibres. Maleic Anhydride grafted Polypropylene (MAPP) is suitable for natural fibre reinforced polypropylene. According to Gauthier et al. (1998), the key parameters of

using MAPP are the degree of grafting (Maleic Anhydride (MA) content) and the length of the grafted chains (PP chains). When MA content in MAPP increases, the interactions between MA and the fibre surface get larger. However, the possibility of the presence of free MA in composites is higher. Concerning chains of PP in MAPP, an easier entanglement with the fibre surface is possible, when they are long.

 A decrease in viscosity is observed upon the addition of MAPP (Eastman G-3015, 3.1 % MA) to the neat polypropylene, as shown in Figure 5.1 [LeMoigne et al. (2013)]. This effect is then counterbalanced when fibres are added. Similar results were found by Twite-Kabamba et al. (2009) who studied hemp/PP composites.

Sojoudiasli et al. (2014) investigated the effect of two different MAPP compatibilizers (Epolene E43 (MA 3.8 wt %) and Orevac 18729 (MA 1 wt %)) on flax reinforced polypropylene composite. The decrease in complex viscosity is higher for MAPP with higher MA content (Epolene E43) at the same composite formulation.

Le Moigne et al. (2014) showed that using flax treated with an organosilane coupling agent can significantly improve the fibre-matrix adhesion for flax/ PLA (poly (lactid acid)) composites.

1.1.3. *Influence of temperature and activation energy*

The determination of temperature-dependent viscoelastic properties requires applying the time-temperature superposition principle. This principle typically involves the following steps: 1) experimental determination of viscosity versus frequency curves at several temperatures and a fixed frequency range 2) selection of a reference temperature T_0 3) all viscosity vs frequency curves corresponding to different temperatures are shifted along both vertical and horizontal axis, fitting the reference viscosity curve (η_{T_0} versus ω_{T_0}) 4) considering the temperature shift factor a_T , the obtained master curve at the reference temperature is a plot of the shifted viscosity $a_T \eta_{T0}$ as function of the shifted frequency ω_{T_0}/a_T

The shift factor a_T is usually correlated to the activation energy E_a using an Arrhenius-type equation as follows

$$a_T = exp\left[\frac{E_a}{R}\left(\frac{1}{T} - \frac{1}{T_0}\right)\right]$$ [Eq.5.6]

where R is the universal gas constant, T is the temperature in K and T_0 is the reference temperature.

The influence of fibre concentration on the activation energy of molten composites seems to be an opened question. In some studies E_a is dependent on fibre content, while in some others, it is independent and remains constant when compared to matrix E_a.

Islam and Begum (2015) showed that E_a of coir/PP composite increases from about 40 kJ/mol for neat PP to about 80 kJ/mol for 30 wt % concentration (Figure 5.5). According to authors, this was interpreted by the additional energy needed to drag fibres into the fluid-motion, when compared to flowing without fibres.
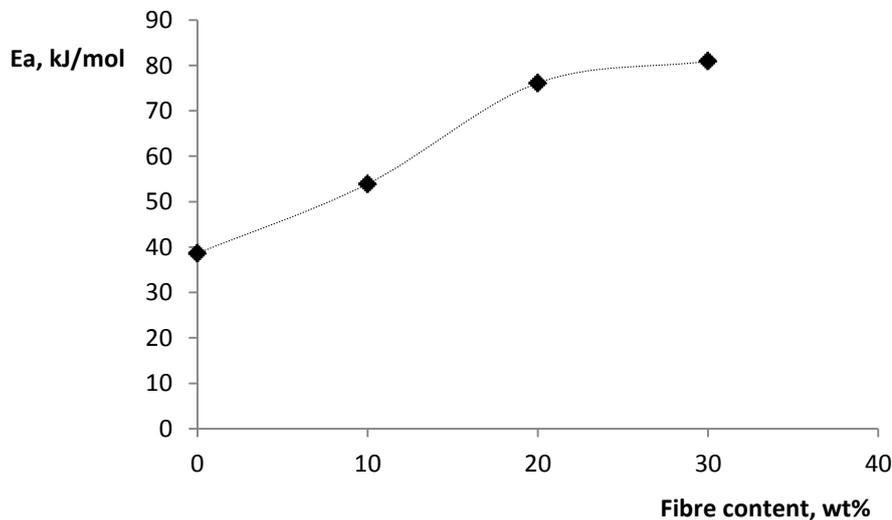
Figure 5.5

E_a of coir/PP as function of fibre content [Islam and Begum (2015)]

Herrera (2014) found a similar result showing that E_a of PLA increases from 74 to 82 kJ/mol by adding 5 wt % of flax fibre.

Nevertheless, some other authors found that activation energy decreases by increasing the fibre content: this was the case for sisal fibre/poly(butylene succinate) composites (E_a decreased from 35 kJ/mol for the neat polymer to 1-2 kJ/mol for 50 wt % sisal composite) [Feng et al. (2011)] and for glass fibres/PP composites (from 10 kJ/mol for the neat PP to 6 kJ/mol after adding 30 wt % glass fibres) [Tiptipakorn et al. (2009)]. The reason of this decrease may be that E_a was calculated within the shear thinning regime.

Laun (1984) studied the activation energy of 30 wt % glass fibre-reinforced for different matrices (PP, HDPE, LDPE, and PA6) in steady state mode. E_a of 30 wt % glass/PP (82± 3.2 kJ/mol) and 30 wt % glass/HDPE (34.9± 1.4 kJ/mol), are slightly higher than that of neat PP (44 kJ/mol) and neat HDPE (28 kJ/mol). Whereas, E_a is not affected by fibres in case of LDPE (51 kJ/mol for neat LDPE versus 48.7± 3.6 for 30 wt % glass/LDPE) and PA6 (80 kJ/mol for neat PA6 versus 82± 3.2 kJ/mol).

1.1.4. *Influence of fibre flexibility*

To interpret the rheological properties of a suspension of flexible fibres, Switzer et al. (2003) used the criterion of flexibility F that couples fibre Young's modulus and aspect ratio with the shear stress $\eta_m \, \dot{\gamma}$ surrounding fibres:

$$F = \frac{64}{\pi} \left(\frac{L}{D}\right)^4 \frac{\eta_m \, \dot{\gamma}}{E_f} \qquad\qquad\qquad [Eq.5.7]$$

η_m is the matrix viscosity. When $F \to \infty$, fibres are perfectly flexible threads; when $F \to 0$, fibres become rigid. Keshtkar et al. (2008) applied this criterion to study the dynamic rheology of model synthetic (Polyacrylate and Nylon) fibres dispersed in silicone oil. Figure 5.6.a shows that higher complex viscosity and elastic modulus were obtained at the same fibre concentration (6.5 vol %) either for fibres with lower Young's modulus at the same the same fibre aspect ratio or for fibres with higher aspect ratio at the same Young's modulus. This means that complex viscosity and elastic modulus of suspensions are larger as fibre flexibility increases (lower Young's modulus and higher aspect ratio). The difference in complex viscosity and elastic modulus between suspensions becomes progressively smaller as the frequency increases. This trend was more pronounced for composites with higher fibre concentrations. They concluded that with more flexible fibres a "stronger structure" is formed due to larger number of fibre-fibre interactions. The authors outlined that the complex viscosity does not depend on the fibre stiffness (fibre Young's modulus) after a high pre-shearing of 5 s^{-1} (results presented in Figure 5.6 were made after a pre-shear of 0.1 s^{-1}).
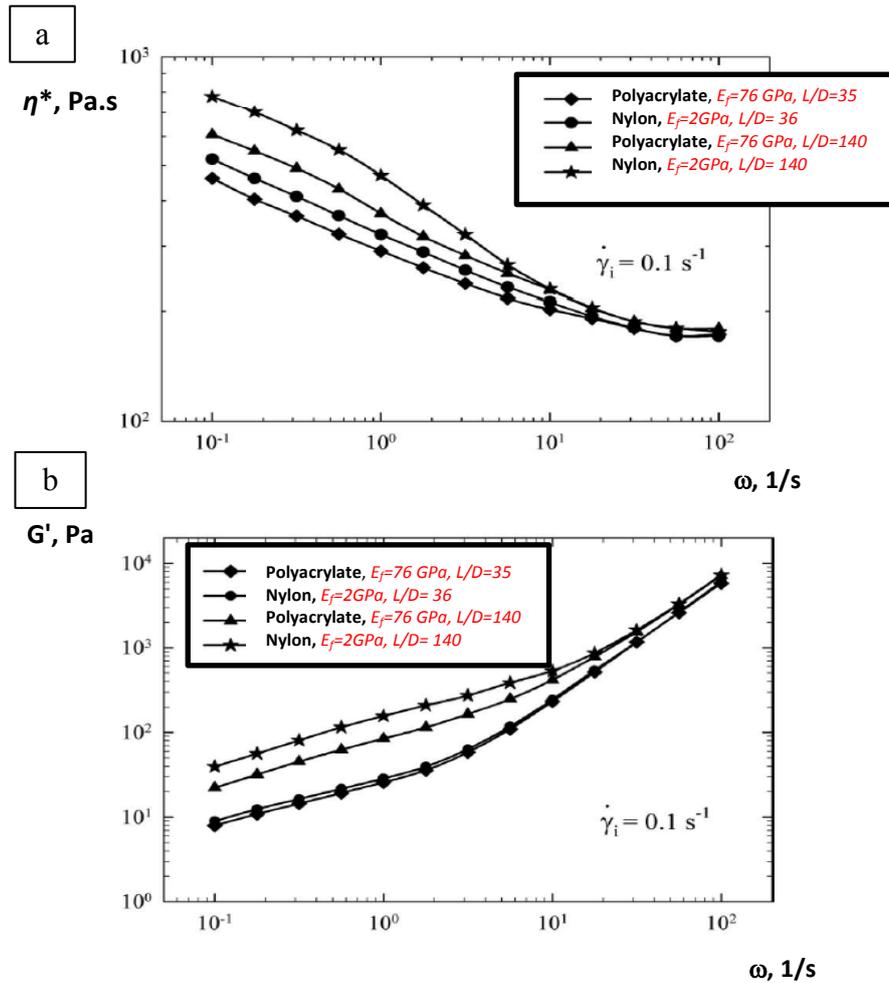
Figure 5.6

Complex viscosity (a) and elastic modulus (b) of Polyacrylate- and Nylon fibres-silicone oil suspensions with different aspect ratio and fibre stiffness, after pre-shearing at 0.1 s^{-1} [Keshtkar et al. (2008)]

1.2. Capillary rheology and comparison with dynamic

The capillary rheology of natural fibre composite was investigated by Basu et al. (1992), comparing jute fibre- to glass fibre-reinforced polypropylene. The initial fibre length of glass and jute fibres is 4.7 mm and 1-5mm, respectively. Figure 5.7 shows that the viscosity of both composite systems increases as fibre content increases, for a shear rate ranging from 60 s^{-1} to 4000 s^{-1}. The increase of viscosity becomes smaller when the shear rate gets higher. Considering that jute and glass fibres do not possess the same density, the comparison at the same weight fraction (so different volume fraction) between jute and glass fibre composites is difficult. The same volume fraction is needed to obtain a plausible comparison.

144
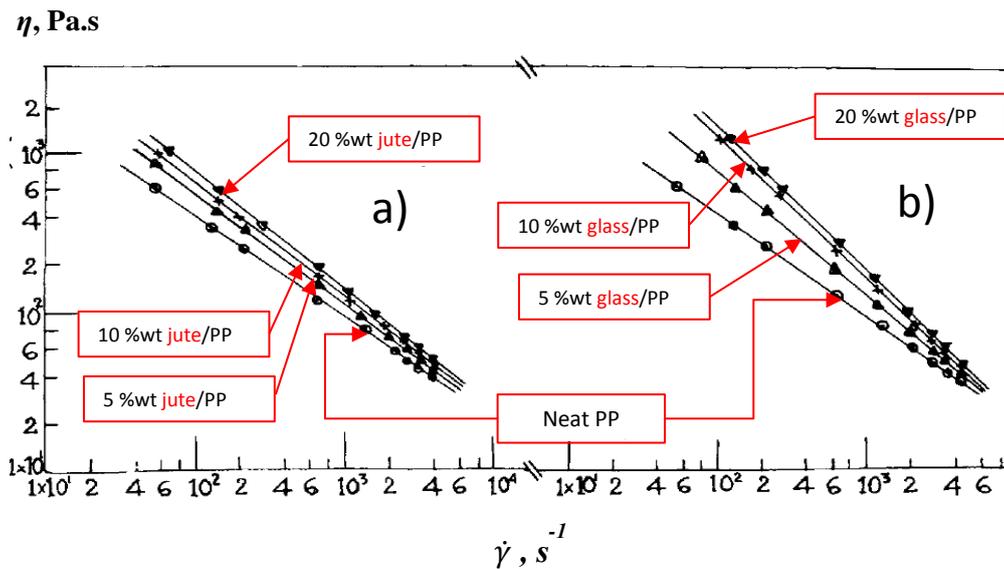
Figure 5.7

Variation of melt viscosity with shear rate at 210 °C for neat PP and for composites with 5, 10 and 20 wt % (a) jute/PP and (b) glass/PP [Basu et al. (1992)]

Le Moigne et al. (2013) investigated also the capillary rheology of flax fibre based composites (Figure 5.8). Similar results to that of Basu et al. (1992) were obtained. They showed that the viscosity obtained from dynamic and capillary experiments did not follow the Cox-Merz rule (Eq.5.8): capillary viscosity was lower than that obtained in dynamic mode.

$$\eta(\gamma) = |\eta^*(\omega)|_{\omega=\dot{\gamma}} \qquad\qquad [Eq.5.8]$$

Le Moigne et al. 2013 argued this deviation by the difference in the orientation of fibres in oscillatory shear experiments (fibres are randomly oriented) and capillary mode (fibres are well aligned along the flow direction). Mobuchon et al. (2005) observed a less pronounced deviation for 30 wt % glass fibre reinforced polypropylene. Laun (1984) found that glass fibre- reinforced polyethylene were following Cox Merz rule (Figure 5.9).
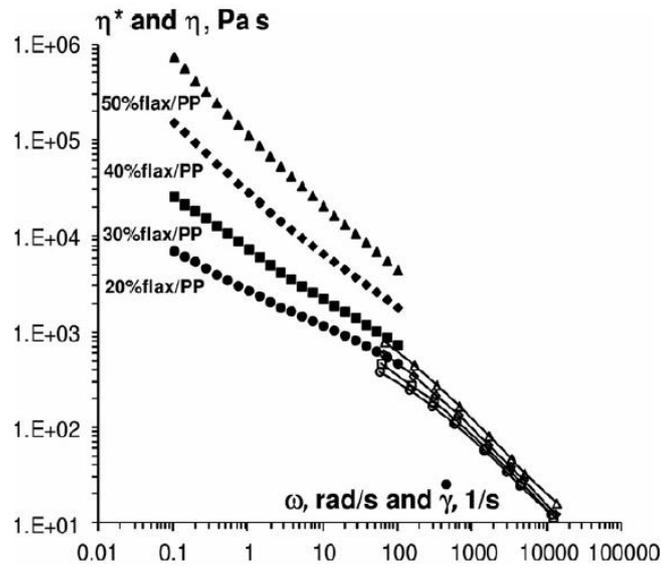
Figure 5.8

Cox-Merz plot for the viscosity of flax/PP composites obtained from dynamic measurements (filled symbols), and capillary measurements (open symbols). Lines for capillary data are given to guide eye [Le Moigne et al. (2013)]
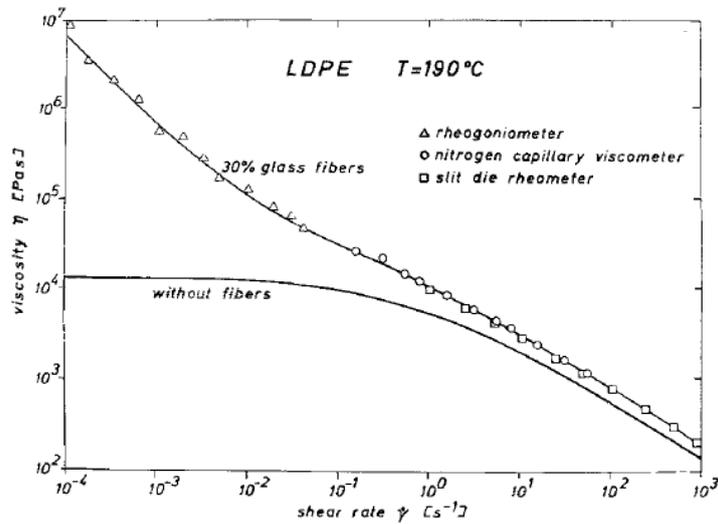
Figure 5.9

Viscosity versus shear for high density polyethylene melt without fibres and with 30 wt % glass fibres [Laun (1984)]

1.3. Conclusions

A brief review of literature on the rheological properties of fibres suspended in a fluid under simple shear showed that viscoelastic properties depend on fibre concentration, aspect ratio, flexibility and also on the presence of compatibilizer. Natural fibres have much complex morphology compared to glass fibres; they can be rigid or flexible (or semi-rigid) and can consist of elementary fibres and/or bundles in which fibres are "glued" together. The rheology of such composites is more complex and strongly depends on fibre type, in addition to all other "classical" parameters. In the next section, we describe the results obtained for flax and Tencel-based polypropylene composites and compare them with the viscoelastic properties of glass fibre based composites, all obtained in the same conditions.

2. Results and discussion

2.1. Dynamic rheology results

We remind that *no compatibilizer* was used in this study in order not to modify matrix viscoelastic properties. The correlation between volume and weight concentrations is presented in Chapter 2, Table 2.3.

2.1.1. *Influence of fibre concentration on composite viscoelastic properties*

Figures 5.10 and 5.11 show complex viscosity η^* and $\tan\delta = G''/G'$ as a function of frequency ω at 190 °C for the neat polypropylene and composites with 6.3 and 20.5 vol % of flax, Tencel and glass. The results obtained for other fibre concentration (3.1 vol % and 13.1 vol %) are not shown in order not to overload the graphs. Polypropylene shows a classical rheological behaviour with a Newtonian plateau at low frequencies and shear thinning at higher frequencies. The increase of fibre concentration leads to a viscosity rise and the disappearance of the Newtonian plateau, which is in agreement with literature Le Moigne et al. (2013) Sojoudiasli et al. (2014)
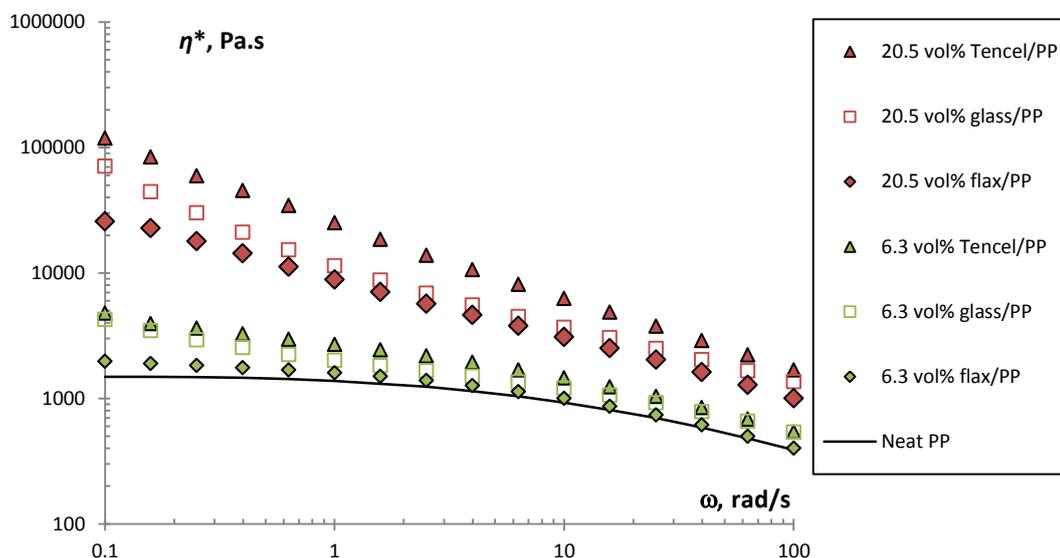
Figure 5.10

Complex viscosity of neat PP, flax/PP, Tencel/PP and glass/PP composites with 6.3 and 20.5 vol % of fibres at 190 °C.

The tangent of phase angle δ represents to what extent the system is more viscous or more elastic. For all studied systems, tanδ is greater than 1 overall studied frequencies, which is expected for the case of neat PP (Figure 5.11). The lower the frequency, the higher tanδ. The increase of fibre concentration leads to a decrease of tanδ, indicating a greater elasticity of the system that is particularly pronounced at low frequencies. For 20.5 vol % concentration of Tencel/PP and flax/PP composites, tanδ is around 2 at low frequencies and around 1 at high frequencies. tan$\delta > 1$ was also obtained for glass fibre based composites, as already reported in literature [Kitano et al. (1984); Drozdov et al. (2003); Mobuchon et al. (2005); Guo et al. (2005)].
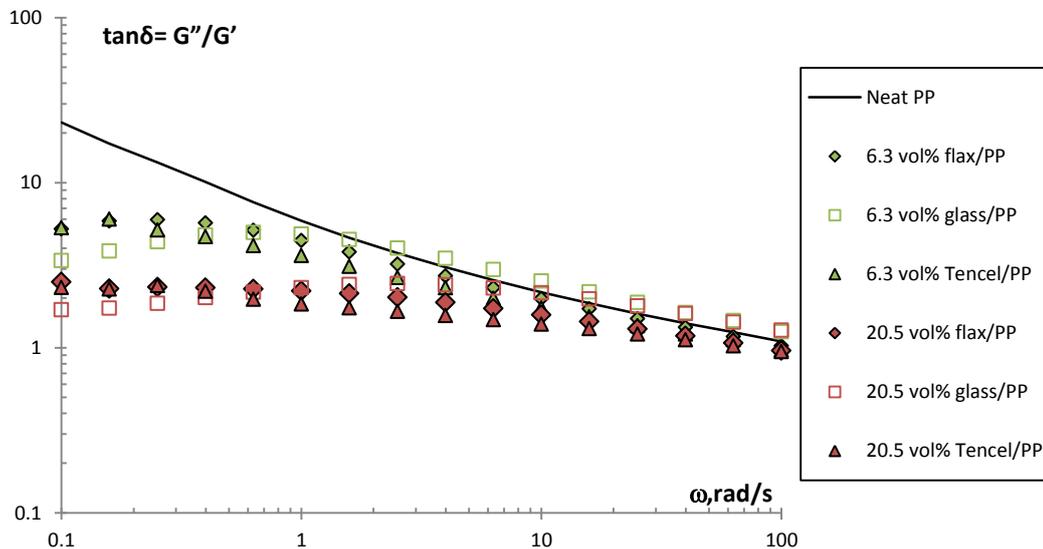
Figure 5.11

tanδ = G''/G' of neat PP, flax/PP, Tencel/PP and glass/PP composites with 6.3 and 20.5 vol % of fibres at 190 °C

Figure 5.12a and 5.12.b show G' and G'' of neat PP and of composites with 6.3 vol % and 20.5 vol % of Tencel, glass and flax. The higher the fibre concentration is, the higher the moduli are. This effect is more pronounced at low frequencies and for Tencel-based composite, followed firstly by glass and then by flax-based composites. According to Maxwell model of viscoelastic fluids, G' and G'' are power-law dependent on frequency with exponents being $u = 2$ and $v = 1$ at low frequencies, respectively. The obtained u and v exponents are regrouped in Table 5.1. For the neat polypropylene $u = 1.6$ and $v = 0.98$; the deviation of u exponent from the model value may be due to the polydispersity of the polymer

chains[Le Moigne et al. (2013)]. Both exponents decrease when fibre concentration increases. At high fibre concentration strong elasticity is developed, signifying the appearance of a plateau-like region.
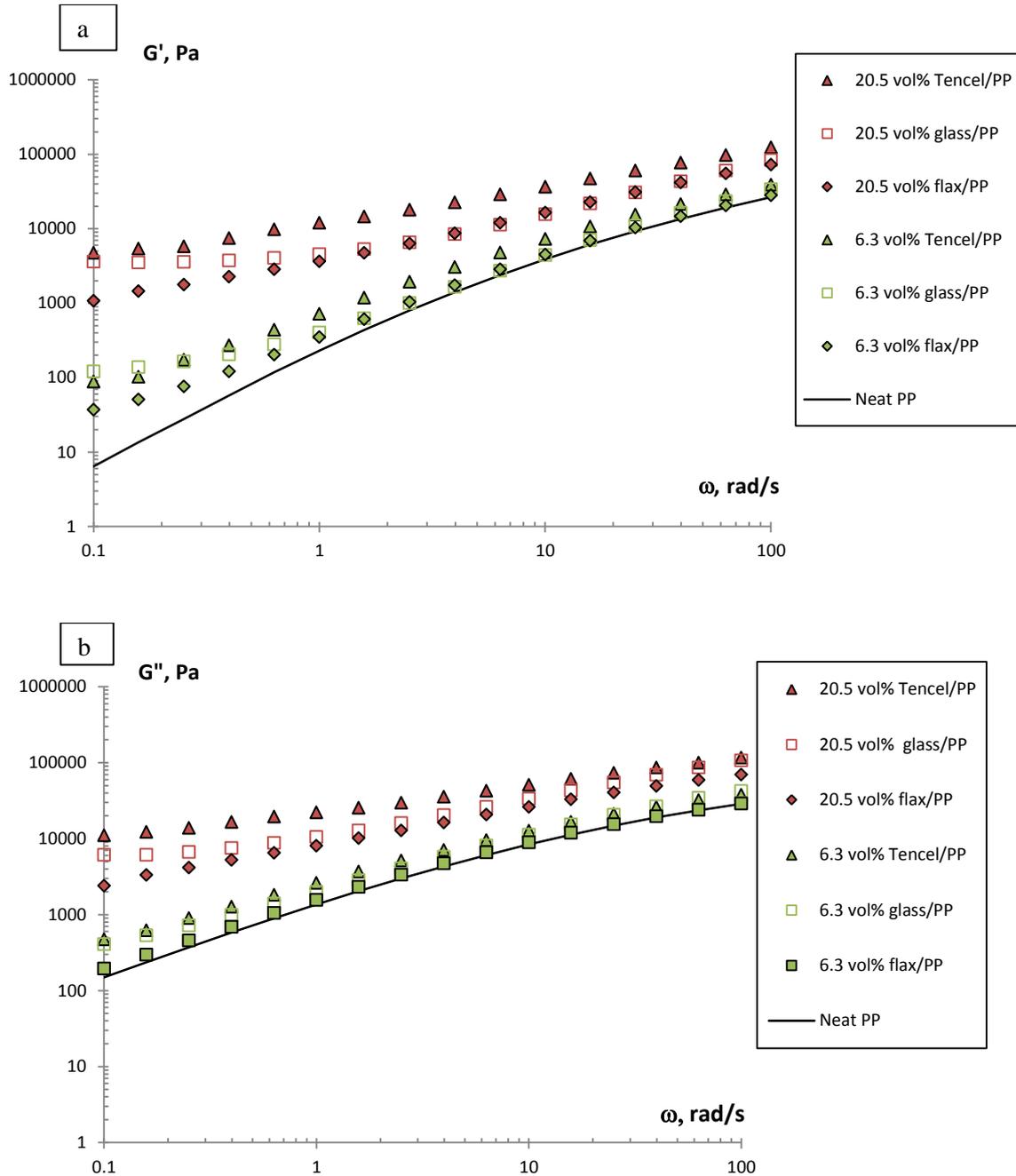
Figure 5.12

Elastic G' (a) and viscous (G") (b) moduli vs frequency at 190 °C for the neat PP and 6.3 and 20.5 vol % of fibres for Tencel/PP, flax/PP and glass/PP composites

Table 5.1 G' and G'' power-law exponents, *x* and *y,* respectively, at low frequencies

	vol %	*u*	*v*
Neat PP	0	1.59	0.98
Tencel/PP	6.3	0.84	0.73
flax/PP	6.3	0.86	0.92
glass/PP	6.3	0.38	0.64
Tencel/PP	20.5	0.32	0.29
flax/PP	20.5	0.53	0.56
glass/PP	20.5	0.02	0.15

Figure 5.13 shows shear stress-frequency dependence of Tencel/PP, glass/PP and flax/PP at 190 °C for two fibre concentrations, 6.3 and 20.5 vol %. The shear stress is defined by $\sigma = G^* \times \gamma$, where $G^* = \eta^* \times \omega$ is the norm of complex modulus and *γ* is the strain. At the same fibre concentration, Tencel-based composites have higher shear stress than glass and flax based composites at low frequencies; however at high frequencies all curves merge together.
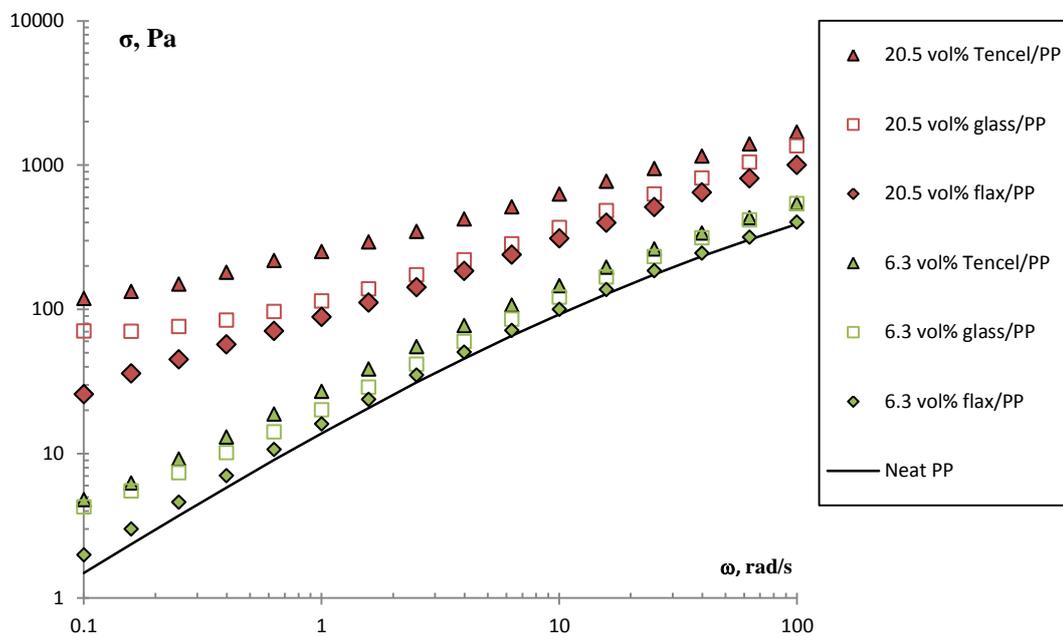
Figure 5.13

Stress shear vs frequency of flax/PP and Tencel/PP composites with 6.3 and 20.5 vol % of fibres at 190 °C

The apparent yield stress σ_0 for each composite at each temperature was determined by the following steps: 1) plotting the σ (the shear stress) versus frequency in a conventional plot (not log-log plot) 2) fitting the low frequency-end of curve by a linear model ($\sigma = a\,\omega + b$) 3) "b" gives the shear stress at zero frequency "σ_0" that corresponds to the apparent yield stress. Figure 5.14 gives examples of calculation of σ_0 of 20.5 vol % of Tencel, flax and glass composites, respectively
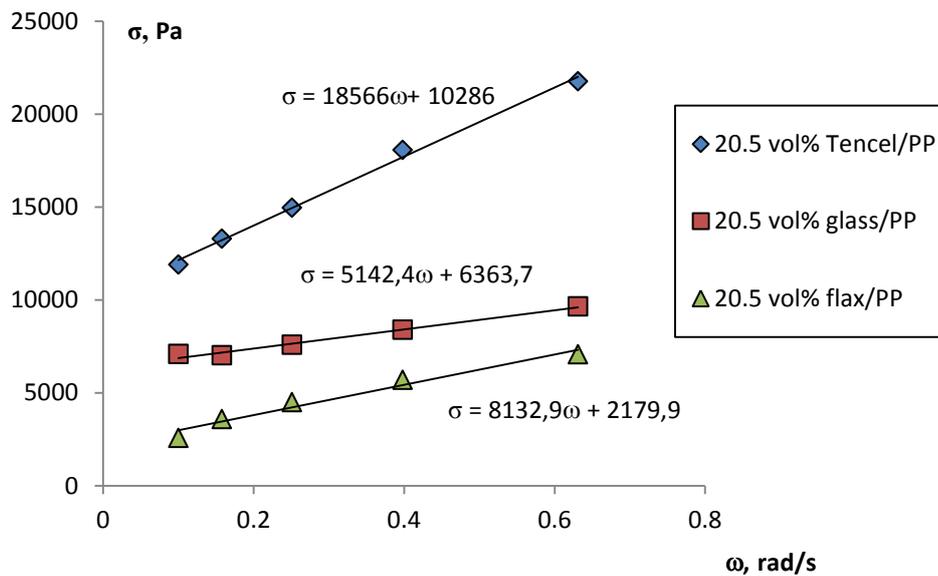
Figure 5.14

Shear stress vs frequency for 20.5 vol % composites with different fibre types

Figure 5.15 demonstrates the influence of fibre type, concentration and temperature on σ_0. The higher the concentration is, the higher the σ_0 is, being higher for Tencel-based composites and glass and lower for flax. Moreover, increasing temperature leads to decrease σ_0. Measured flax and Tencel yield stress-concentration dependences were fitted with power law, shown as solid lines in Figure 5.14. In all cases studied the yield stress is proportional to fibre volume fraction to the power 3 within 20 % of deviation, as predicted at Bennington et al. (1990) study. It is difficult to predict the other exponents in Eq. 5.5 as far as there are too many variables and the influence of temperature on fibre Young's modulus is not known.

$\sigma_0 (\text{Tencel}, 180\ °C) = 8\ 605.2\ f^{2,8239}$

$\sigma_0 (\text{glass}, 180\ °C) = 3\ 310.5\ f^{2,5538}$

$\sigma_0 (\text{flax}, 180\ °C) = 3\ 036.6\ f^{2,9981}$

$\sigma_0 (\text{flax}, 190\ °C) = 2\ 341.8\ f^{3,0432}$

$\sigma_0 (\text{flax}, 200\ °C) = 819.76\ f^{2,7776}$
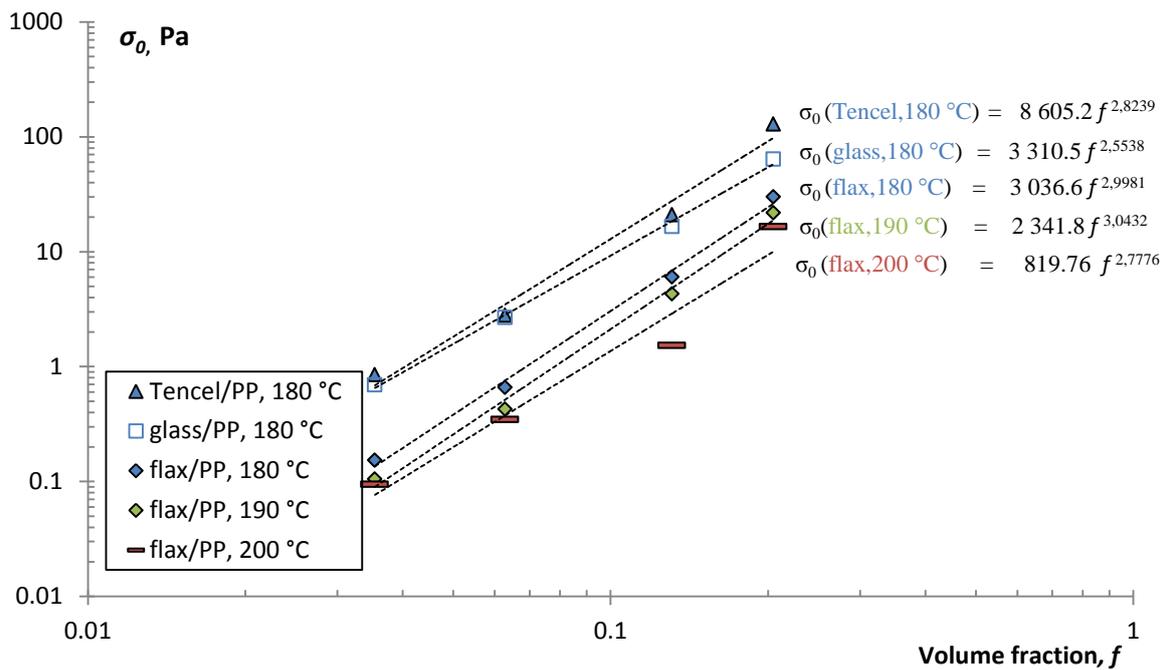
Figure 5.15

Apparent yield stress evolution with fibre volume fraction for Tencel/PP, flax/PP and glass/PP composites at 180 and 200 °C; lines are power law approximations

2.1.2. *Viscosity-temperature dependence*

Figure 5.16 shows an example of complex viscosity-frequency dependence for the case of the neat polypropylene and 20.5 vol % flax and Tencel composite at different temperatures (180, 190 and 200 °C). Similar results were obtained for other fibre concentrations and for glass fibre based composite (not shown). As expected, viscosity decreases as temperature gets higher, for all studied systems. Master plots were built using time-temperature superposition principle and shift factors a_T for each composite were determined, as explained in Section 1.1.3 (Influence of temperature and activation energy). The examples for the neat PP and 20.5 vol % composites with flax/PP, Tencel/PP and glass/PP are shown in Figures 5.15 and 5.16.
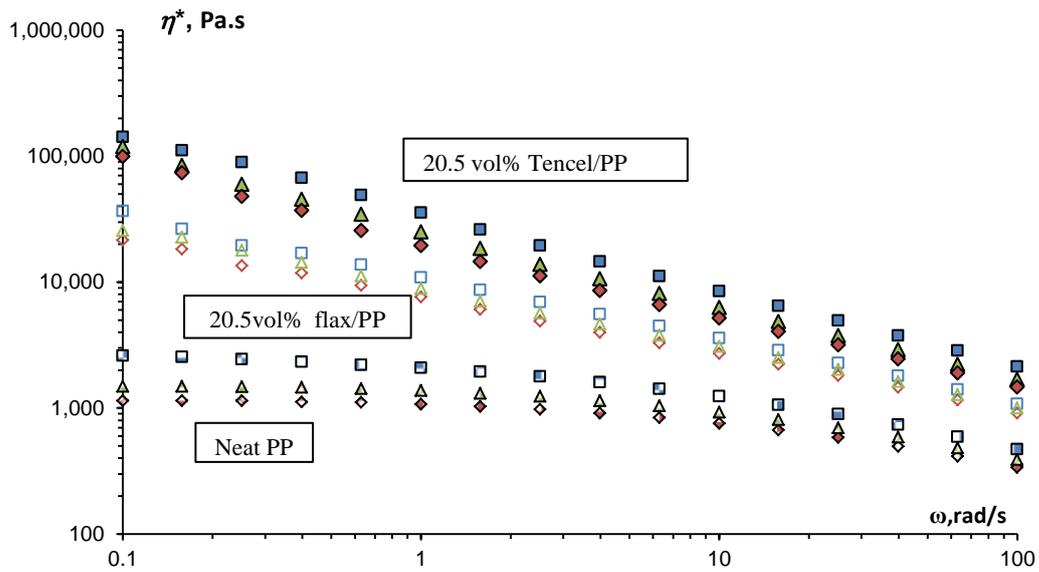
Figure 5.16

Viscosity vs frequency for the neat PP and 20.5 vol % flax/PP and Tencel/PP composite at three temperatures (from top to bottom): 180 (blue), 190 (green) and 200 (red) °C
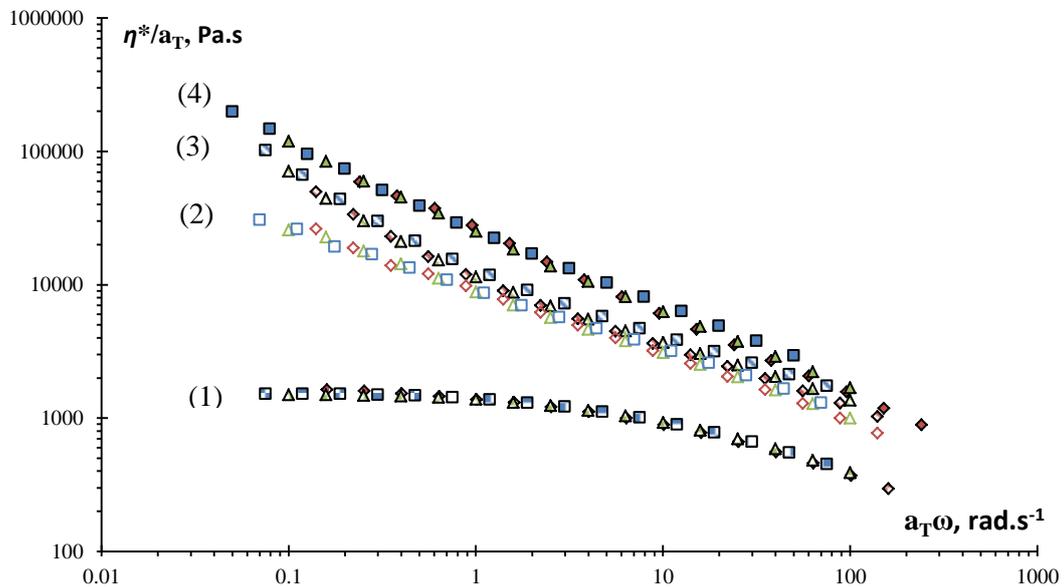
Figure 5.17

Master plots of the neat PP (1) and 20.5 vol % flax/PP (2), glass/PP(3) and Tencel/PP (4) composites at the reference temperature 190 °C

Figure 5.18 shows Ln (a_T) versus (1/T)-(1/T$_0$) of neat PP and Tencel/PP composite. Similar results were obtained for flax and glass based composites (not shown here). The shift factor a_T seems to obey to Arrhenius law (Eq. 5.4). The slope of the curve enables to assess E_a.
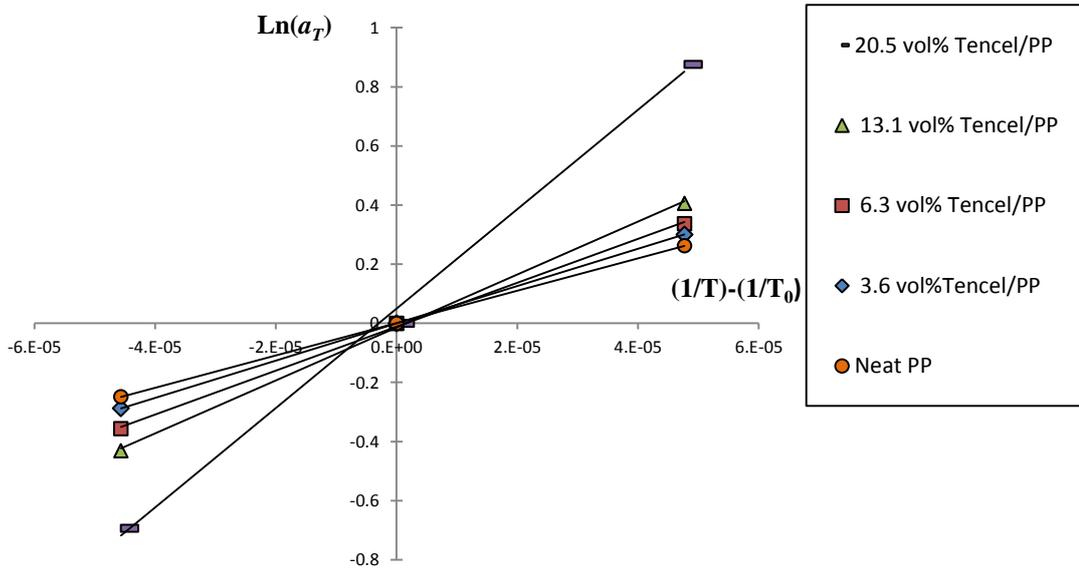
Figure 5.18

Ln (a_T) versus (1/T)-(1/T$_0$), for neat PP and Tencel/PP for different concentrations, the reference temperature (T$_0$) is 463 K = 190 °C.

Figure 5.19 shows the activation energy for all composites studied as a function of fibre concentration. E_a increases with fibre content for all types of fibres. Below 5 vol %, the composites with different types of fibres show very similar activation energy. From 5 vol % to 13 vol % Tencel and flax based composites have similar evolutions, while E_a of glass fibre composites shows a smaller increase. A steep increase in the activation energy for Tencel based composites occurs between 13 and 20.5 vol % while flax and glass based composites' activation energies are almost constant and very close. Our results are in agreement with the studies of Islam and Begum (2015) and Herrera (2014) showing that an increase of fibre concentration in composites leads to enhance the activation energy. We suppose that fibres prevent polymer chains to move as they would do without them. The increase of fibre concentration also leads to increase interactions between fibres (friction, overlapping, etc.) and between fibres and matrix, requiring an additional energy to flow. A quantitative

interpretation of the influence of fibre concentration on the activation energy of viscous flow of composites requires a separate study.
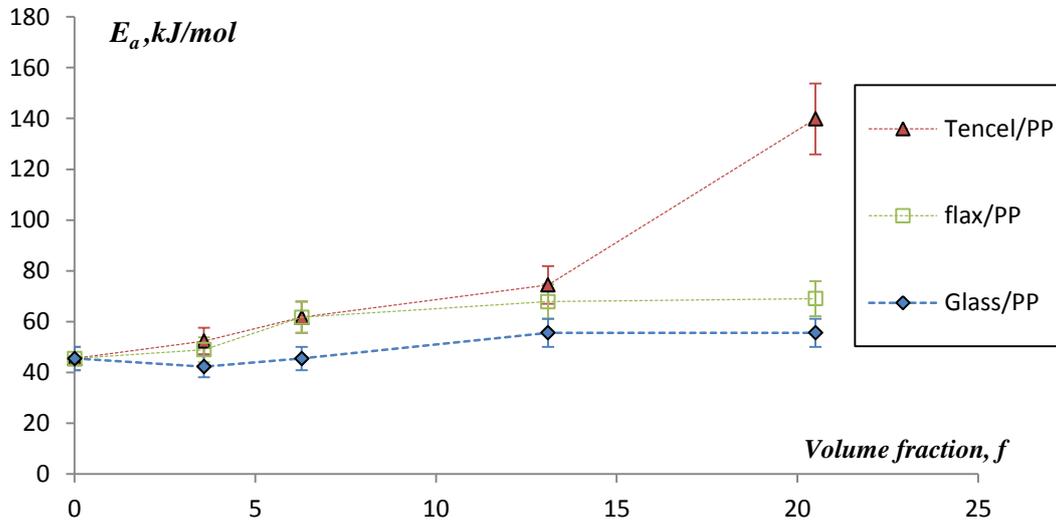
Figure 5.19

Activation energy evolution with fibre concentration for Tencel/PP, flax/PP and glass/PP composites; zero fibre content corresponds to the neat polypropylene

2.1.3. *Correlation between composite rheology and microstructure*

All results presented above demonstrate that composites with Tencel fibres show higher viscosity, elasticity, apparent yield stress and activation energy as compared to glass- and flax-based composites at the same fibre concentration. Several reasons can be given to explain this finding. The first one is related to the number of fibres N_i per 1 mm^3 of 30 wt % flax and Tencel$^®$ composites, calculated as follows:

$$N_i = \frac{4f}{\pi L_i D_i^2}$$
[Eq.5.9]

where subscript "*i*" is "*n*" or "*w*" corresponding to length and diameter weighted either in number or in weight.

For example, for 20.5 vol % fibre concentration, the number of Tencel fibres N_n and N_w is almost 10 times higher than the corresponding numbers for flax and 1.5- 2 times higher than for glass fibres.

Table 5.2 Microstructural features of fibres at 20.5 vol % and corresponding flexibility of at ω = 0.1 rad/s(low frequency)

Fibre type	E_f (GPa)	$(L/D)_n$ (20.5 vol %)	$(L/D)_w$ (20.5 vol %)	N (20.5 vol %)		$f(sd/c)$ (vol %)	$(\eta_m\dot{\gamma})$ (Pa) (ω = 0.1 rad/s)	F (ω = 0.1 rad/s)	
				N_n	N_w			F_n	F_w
Tencel	10-15	20 (D_n = 10 µm)	26 (D_w = 10 µm)	13392	9891	3-4	119	$2.6\ 10^{-2}$- $3.8\ 10^{-2}$	$7.4 10^{-2}$- $1.1\ 10^{-1}$
Glass	73	33 (D_n = 10 µm)	44 (D_w = 10 µm)	7913	5962	2-3	70.8	$2.3\ 10^{-2}$	$7.3\ 10^{-2}$
Flax	30-110	14 (D_n = 29 µm)	17 (D_w = 54 µm)	1586	1013	6-7	25.7	$2\ 10^{-3}$- $7\ 10^{-4}$	$1.4\ 10^{-3}$- $4\ 10^{-4}$

-*L/D:* fibre aspect ratio $(L/D)_w$ averaged in **w**eight, $(L/D)_n$: averaged in number

-*E_f.***f**ibre Young's modulus

-*N* = **N**umber of fibres per unit volume,: N_w average in weight, N_n: average in number

-*f(s-d/c)* = volume fraction of the transition semi-dilute/concentrated regime

-*F*: **F**lexibility [Eq 5.7], F_n average in **n**umber, F_w average in **w**eight

The second reason is that the transition from the semi-dilute to concentrated regime *f(s-d/c)* occurs at different concentrations depending on the type of fibre: *f(s-d/c) (glass) < f(s-d/c) (Tencel) < f(s-d/c) (flax)*, due to the difference in *(L/D)* values (Table 5.2). High dispersion in fibre dimensions (See Chapter 4, Section 2) and wide *L/D* distribution do not enable to calculate the exact value of this concentration. However, Figure 5.10 shows that for the concentration of 6.3 vol % a yield-like stress occurs at low frequency in case of Tencel and glass, signing that fibre-fibre interactions get already larger and a concentrated regime is well established. However, at the same concentration, the flax curve viscosity looks similar to that of polypropylene with a slight increase of viscosity at low frequencies, which means that fibre-fibre interactions just started to take place and the *f(s-d/c)* may be not reached. This is in agreement with the estimation of *f(s-d/c)* presented in Table 5.2.

 It should also be taken into account that glass fibre aspect ratio strongly decreases when fibre concentration increases. If fibre aspect ratio was the only parameter controlling composite viscosity and yield stress (at a given fibre concentration), it would be glass fibre based

composite and not Tencel-based that should have the highest values. However, the number of glass fibres is lower than that of Tencel, and thus the third fact, which is the fibre flexibility, has to be taken into account, as discussed below.

To illustrate the influence of fibre flexibility, we calculated the flexibility F (Eq.5.7) for fibre concentration of 20.5 vol % and frequency of $\omega = 0.1$ rad/s. Moreover, we used both aspect ratios, $(L/D)_n$ and $(L/D)_w$, to give the interval of flexibility values that we call F_n and F_w, respectively. The results are presented in Table 5.2. We approximate that the shear stress surrounding fibres is the same applied to the melt composite at a given frequency. Because it is impossible to prepare glass, flax and Tencel-based composites with the same fibre aspect ratio keeping the same processing conditions, the flexibility F reflects the influence of both fibre aspect ratio and Young's modulus. The flexibility of Tencel fibres is slightly higher than that of glass fibres and more than two orders of magnitude higher than for flax fibres.

As discussed in the state of the art section, flexible fibres (here the most flexible is Tencel) flow in a different way compared to the rigid ones (here glass fibres and flax bundles). Flexibility makes fibres turning under shear as S-turn or C-turn, which leads to shorter effective aspect ratio [Forgacs and Mason (1959)]. This will induce quicker rotation compared to rigid fibres, increasing the probability of fibre-fibre interactions, creating a larger normal stresses and longer time not aligned in the flow direction. All these factors contribute to the additional dissipation of viscous energy, higher yield stress, viscosity and elasticity of Tencel-based composites.

 Although, glass fibres have higher aspect ratio, Tencel based composites show higher viscosity, elasticity and higher yield stress (at a given fibre concentration). The specificity of cellulosic fibres has thus to be taken into account: if comparing Tencel and flax based composites, the number of fibres per volume unit is much higher for Tencel than for flax. The reason is that a major part of flax fibres are in bundles, and in addition Tencel is more flexible than flax. The understanding of fibre morphology and the adequate analysis of the distributions of both fibre length and diameter in natural fibre based composite are thus the key points for the interpretation of composite rheological properties.

2.2. Capillary rheology and comparison with dynamic

Figure 5.20 shows a superposition of viscosity values obtained with capillary and dynamic rheology for neat PP and Tencel/PP composites for all studied concentrations, 3.6, 6.3, 13.1

and 20.5 vol %. Contrary to Le Moigne et al. (2013), the Cox-Merz rule applies reasonably well. By increasing the shear rate, the curves corresponding to different concentrations tend to merge. For each concentration, the entire viscosity curve comprising dynamic and capillary measurements is fitted with the modified Carreau-Yasuda model (solid line) [Eq. 5.1].
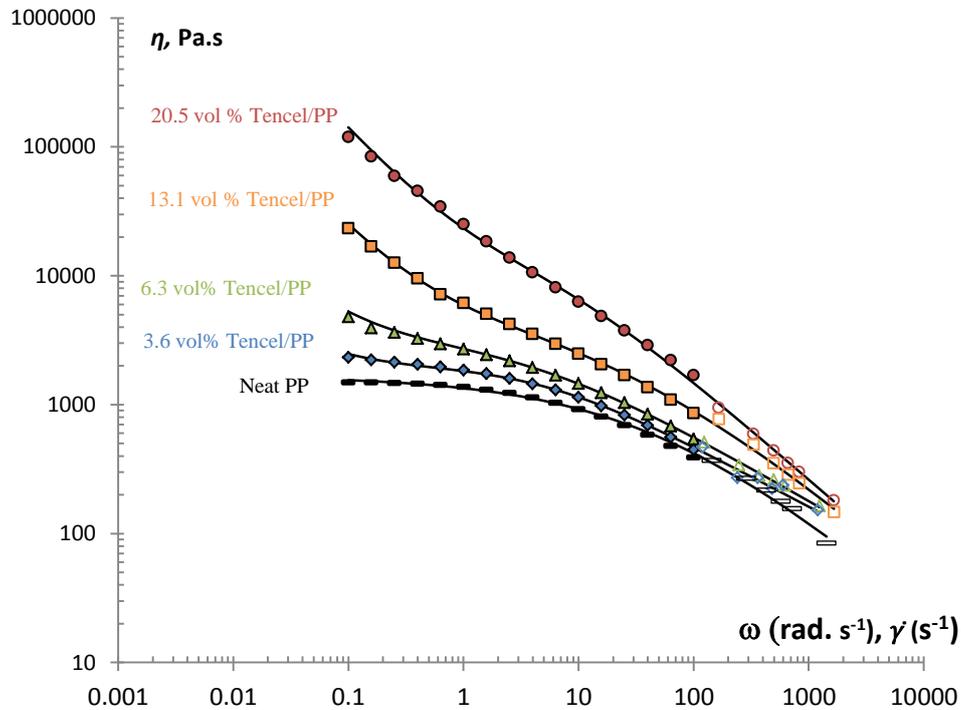
Figure 5.20

Dynamic (filled symbols) and capillary (open symbols) viscosity curves, for neat PP and Tencel/PP composites with 3.6, 6.3, 13.1 and 20.5 vol % at 190 °C. The solid lines correspond to fits with modified Carreau-Yasuda model

Figure 5.21 shows a comparison among Tencel, glass and flax composites with 20.5 vol % and neat PP. At high shear rate, the curve of glass based composite merges with the one of Tencel, while flax and PP curves remain decreasing parallel to Tencel's curve.
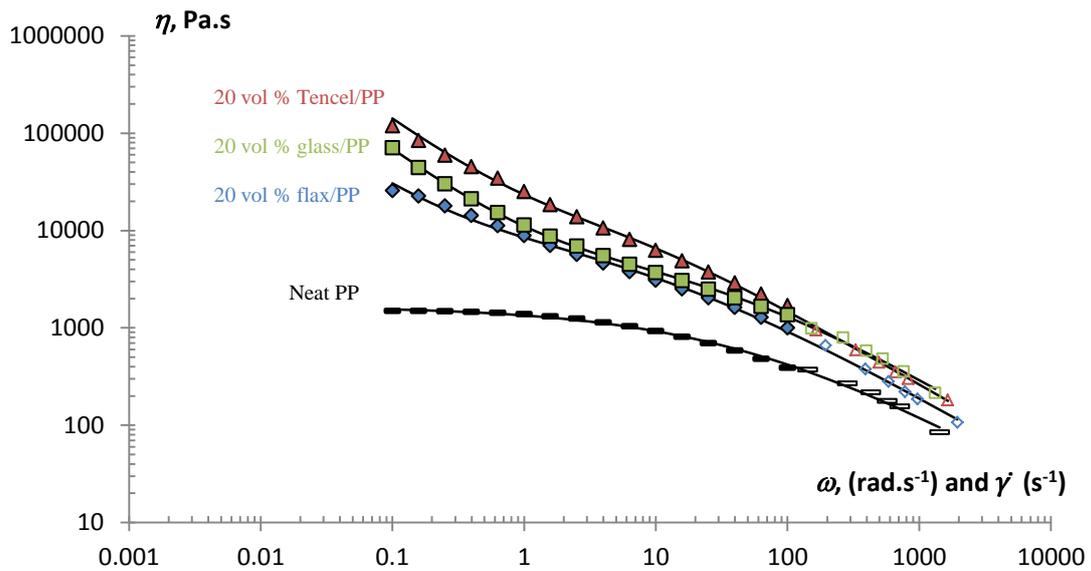
Figure 5.21

Dynamic (filled symbols) and capillary (open symbols) viscosity curves, for neat PP and composites with 20.5 vol % for Tencel/PP, glass/PP and flax/PP at 190 °C. The solid line represents the fitting according to the modified Carreau-Yasuda model

All curves including capillary and dynamic viscosity were fitted with the modified Carreau-Yasuda model at 190 °C, as shown in figure 5.20 and 5.21. The fitting results are summarized in Table 5.3.

Table 5.3 Fitting results of the modified Carreau-Yasuda model

	Vol %	σ_0	η_0	λ	n	a
Neat PP	0	0.0	1201	0.04	0.38	0.85
Tencel	3.6	53	2003	0.20	0.53	0.85
	6.3	227	2702	0.19	0.48	0.85
	13.1	2032	3457	0.04	0.23	0.85
	20.5	10285	12025	0.15	0.23	0.85
glass	3.6	61	1597	0.20	0.55	0.85
	6.3	257	2000	0.20	0.53	0.85
	13.1	1278	3492	0.14	0.39	0.85
	20.5	6435	3968	0.02	0.12	0.85
flax	3.6	11	1500	0.05	0.40	0.85
	6.3	43	15115	0.05	0.35	0.85
	13.1	431	3056	0.07	0.30	0.85
	20.5	2180	6173	0.09	0.21	0.85

Table 5.3 shows that σ_0 increases with the fibre content whereas n decreases. At low concentration (3.6 and 6.3 vol % for Tencel and glass, 3.6 vol % for flax) n is larger for the composite than for the PP. For the highest concentration, the values of λ (that is the characteristic time corresponding to the transition from Newtonian plateau to shear thinning) and of η_0 (that is zero shear rate viscosity) have to be taken with care as far as these composites show apparent yield stress and no Newtonian plateau is detectable. To set up the fitting of the experimental curves by Carreau-Yasuda model we have dealt with parameters as follows

- The apparent yield stress σ_0 we used the method described in Section 2.1.1.

-"n" was determined by fitting the end (high shear rate) of viscosity-shear rate curve, respectively

- "a" is calculated from the neat PP curve and fixed for all composites. This parameter defines the shear rate length of the transition between the Newtonian plateau (without considering the yield stress) and the power law region at high shear rate. According to Figure 5.21, the shear

thinning part of Tencel composites curves is connected to the Newtonian plateau in the same shear rate range as the one of the neat PP. This is also true for glass and flax composites that are not presented in Figure 5.21. This approach was already used by Lertwimolnun (2006) for nanocomposites of clay reinforced polypropylene with similar rheological behaviour.

- "λ" and " η_0" were calculated using Microsoft Solver[©] in Excel[©].

Figure 5.22 shows SEM images of cross sections of Tencel, glass and flax fibre based composites with 20.5 vol %. Most glass fibres appear aligned in the flow direction. Most Tencel fibres seem to be perpendicular which is unexpected. The number of flax fibres seems to be much lower than that of the two other composites. This is in agreement with the number of fibres per unit volume given in Table 5.2. Glass fibres appear as straight rods, whereas and Tencel are curved. Flax fibres appear as elementary semi-rigid fibres and as thick bundles.
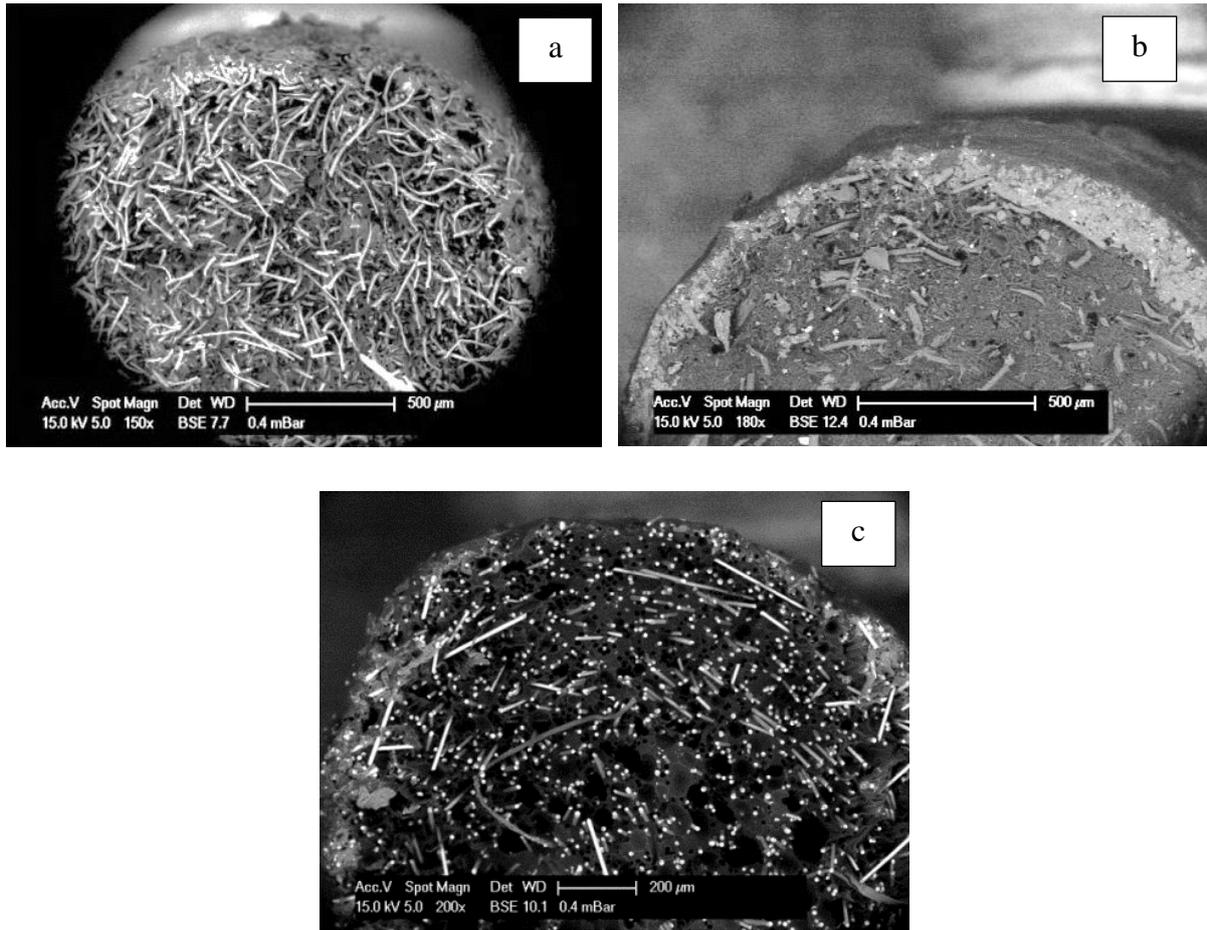
Figure 5.22

SEM images of cross sections of composite extruded from capillary rheometer with 20.5 vol % for (a) Tencel/PP (b) flax/PP (c) glass/PP

The increase of viscosity with fibre content can be evaluated by shifting curves to a reference concentration. Considering the concentration shift factor a_f, the obtained master curve at the reference concentration is a plot of the shifted viscosity $a_f \eta_f$ as function of the shifted frequency ω_f / a_f. Figure 5.23 shows the master plot of viscosity as a function of the frequency (for dynamic mode) and shear rate (for capillary mode). At high shear rates all curves merge into a master curve. At low shear rates, the superposition does not work because of the yield stress. To get a master curve on all the shear rate range, it would be necessary to apply a shift factor on the yield stress.
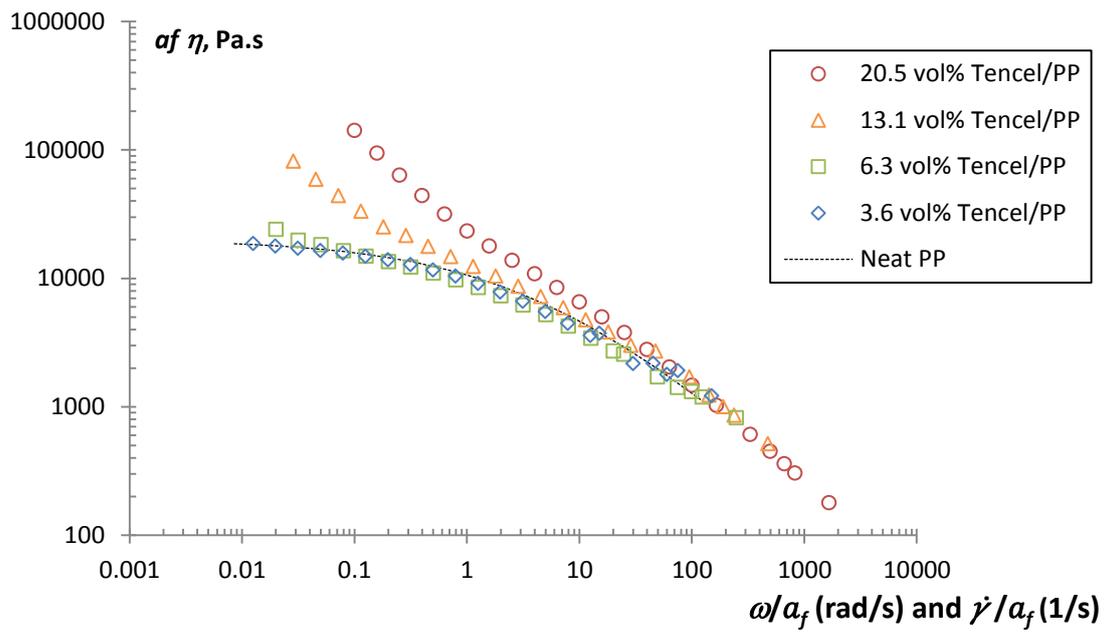
Figure 5.23

Master plot of dynamic and capillary viscosity vs frequency and shear rate at 20.5 % the reference concentration

Figure 5.24 presents the evolution of a_f with fibre content f for all studied composites and neat PP. $a_f = 1$ for 20.5 vol %, the reference concentration. For each composite a_f was fitted with exponential function: $a_f = A\,e^{-Bf}$ where A and B are adjustable constants. a_f does not follow Arrhenius-type equation as a_T (Eq. 5.5) . The couple of variables (A,B) increases from (9.34, 11.01) for flax/PP to (10.89, 11.89) for glass/PP and to higher values (12.25, 12.25) for Tencel/PP.
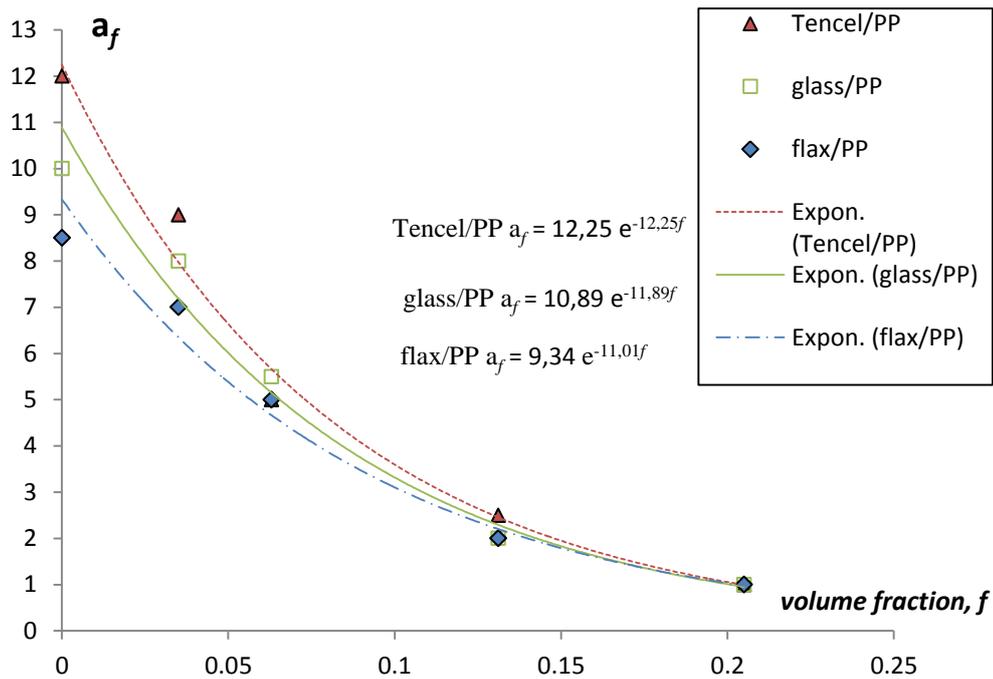
Figure 5.24

Concentration shift factor vs fibre volume fraction at 190 °C for Tencel, glass and flax composites. Zero concentration corresponds to the neat polypropylene. Equations in the graph correspond to the fitting of the plotted curves

2.3. Conclusions

Viscoelastic properties of molten polypropylene cellulose (Tencel) and natural fibre (flax) based composites were studied and compared with glass fibre composites prepared in the same conditions. Oscillatory and dynamic rheology was used. Fibre concentration was varied from 3.6 to 20.5 vol % and composite temperature from 180 to 200 °C. To correlate the rheological properties with fibre size and morphology, the analysis of fibre dimensions in composites already presented in Chapter 3 was used.

For dynamic rheology, we showed that complex viscosity, viscous and elastic moduli increase especially at low frequencies, when the fibre aspect ratio, flexibility and concentration increase. An apparent yield stress at low frequencies was evaluated and correlated with the fibre content. We interpreted the apparent yield stress by the enhancement of fibre-fibre interactions, which leads to network-like structure when volume fraction reaches the concentrated regime. The influence of temperature was modelled by Arrhenius law enabling

to evaluate the composite activation energy. The latter increases as fibre content gets higher. Tencel composites showed higher activation energy as compared to flax and glass ones. This was explained by reducing the polymer chains mobility when fibres are added to polymer. The fibre-fibre and fibre-matrix interactions increase when fibre content is greater, which needs more energy to let polymer chains flow.

The superposition dynamic/capillary rheology obeyed the Cox-Merz approximation. The overall curves including dynamic and capillary measurement were fitted with the modified Carreau-Yasuda model. The obtained results are plausible to be as inputs rheological data for further injection moulding process simulation. This will be the aim of Chapter 7. Finally, the increase in viscosity due to the concentration enhancement is evaluated by a concentration shift factor following an exponential evolution as a function of fibre concentration.

3. References

Azizi, H., & Ghasemi, I. (2009). Investigation on the dynamic melt rheological properties of polypropylene/wood flour composites. Polymer Composites, 30(4), 429-435.

Baley, C. (2002). Analysis of the flax fibres tensile behaviour and analysis of the tensile stiffness increase. Composites Part A: Applied Science and Manufacturing, 33(7), 939-948.

Basu, D., Banerjee, A. N., & Misra, A. (1992). Comparative rheological studies on jute-fiber- and glass-fiber-filled polypropylene composite melts. Journal of applied polymer science, 46(11), 1999-2009.

Bennington, C. P. J., Kerekes, R. J., & Grace, J. R. (1990). The yield stress of fibre suspensions. The Canadian journal of chemical engineering, 68(5), 748-756.

Charlet, K., Eve, S., Jernot, J. P., Gomina, M., & Breard, J. (2009). Tensile deformation of a flax fiber. Procedia Engineering, 1(1), 233-236.

Charlet, K., Jernot, J. P., Breard, J., & Gomina, M. (2010, a). Scattering of morphological and mechanical properties of flax fibres. Industrial Crops and Products, 32(3), 220-224.

Charlet, K., Jernot, J. P., Eve, S., Gomina, M., & Bréard, J. (2010, b). Multi-scale morphological characterisation of flax: From the stem to the fibrils. Carbohydrate Polymers, 82(1), 54-61.

De Guzmán, J. Relación entre la Fluidez y el Calor de Fusion, Anales de la Sociedad Española de Fisica y Quimica. 11, 353-362 (1913).

Doi, M., & Edwards, S. F. (1988). The theory of polymer dynamics (Vol. 73). oxford university press : New York.

Drozdov, A. D., Al-Mulla, A., & Gupta, R. K. (2003). The viscoelastic and viscoplastic behavior of polymer composites: polycarbonate reinforced with short glass fibers. Computational materials science, 28(1), 16-30.

Eberle, A. P., Baird, D. G., & Wapperom, P. (2008). Rheology of non-Newtonian fluids containing glass fibers: A review of experimental literature. Industrial & Engineering Chemistry Research, 47(10), 3470-3488.

Eyring, H. (1935). The activated complex in chemical reactions. The Journal of Chemical Physics, 3(2), 107-115.

Eyring, H. (1936). Viscosity, plasticity, and diffusion as examples of absolute reaction rates. The Journal of chemical physics, 4(4), 283-291.

Feng, Y. H., Zhang, D. W., Qu, J. P., He, H. Z., & Xu, B. P. (2011). Rheological properties of sisal fiber/poly (butylene succinate) composites. Polymer testing, 30(1), 124-130.

Forgacs, O. L., & Mason, S. G. (1959). Particle motions in sheared suspensions: IX. Spin and deformation of threadlike particles. Journal of colloid science, 14(5), 473-491.

Gassan, J., Chate, A., & Bledzki, A. K. (2001). Calculation of elastic properties of natural fibers. Journal of materials science, 36(15), 3715-3720.

Greene, J. P., & Wilkes, J. O. (1995). Steady-State and dynamic properties of concentrated fiber-filled thermoplastics. Polymer Engineering & Science, 35(21), 1670-1681.

Guo, R., Azaiez, J., & Bellehumeur, C. (2005). Rheology of fiber filled polymer melts: Role of fiber-fiber interactions and polymer-fiber coupling. Polymer engineering and science, 45(3), 385-399.

Harris, S. M. (2007). Dynamics of semi-flexible fibres in viscous flow (Doctoral dissertation, University of Leeds).

Herrera, A. M. (2014). Development of natural fiber reinforced polylactide-based biocomposites. Doctoral thesis, Université de Montréal, Génie Chimique.

Islam, M. A., & Begum, K. (2015). Rheological behavior of coir-fiber-filled polypropylene composites at constant shear stress. Polymer Composites, 36(1), 51-61.

Keshtkar, M., Heuzey, M. C., & Carreau, P. J. (2009). Rheological behavior of fiber-filled model suspensions: effect of fiber flexibility. Journal of Rheology (1978-present), 53(3), 631-650.

Kitano, T., Kataoka, T., & Nagatsuka, Y. (1984). Shear flow rheological properties of vinylon-and glass-fiber reinforced polyethylene melts. Rheologica acta, 23(1), 20-30.

Laun, H. M. (1984). Orientation effects and rheology of short glass fiber-reinforced thermoplastics. Colloid and Polymer Science, 262(4), 257-269.

Le Duc, A., Vergnes, B., & Budtova, T. (2011). Polypropylene/natural fibres composites: analysis of fibre dimensions after compounding and observations of fibre rupture by rheo-optics. Composites Part A: Applied Science and Manufacturing, 42(11), 1727-1737.

Le Moigne, N., den Oever, M., & Budtova, T. (2013). Dynamic and capillary shear rheology of natural fiber-reinforced composites. Polymer Engineering & Science, 53(12), 2582-2593.

Le Moigne, N., Longerey, M., Taulemesse, J. M., Bénézet, J. C., & Bergeret, A. (2014). Study of the interface in natural fibres reinforced poly (lactic acid) biocomposites modified by optimized organosilane treatments. Industrial Crops and Products, 52, 481-494.

Le Moigne, N., van Den Oever, M., & Budtova, T. (2011). A statistical analysis of fibre size and shape distribution after compounding in composites reinforced by natural fibres. Composites Part A: Applied Science and Manufacturing, 42(10), 1542-1550.

Lertwimolnun, W. (2006). Réalisation de nanocomposites polypropylene/argile par extrusion bivis (Doctoral dissertation, École Nationale Supérieure des Mines de Paris, Sciences et Génie des Matériaux).

Mobuchon, C., Carreau, P. J., Heuzey, M. C., Sepehr, M., & Ausias, G. (2005). Shear and extensional properties of short glass fiber reinforced polypropylene. Polymer composites, 26(3), 247-264.

Mohanty, S., Verma, S. K., & Nayak, S. K. (2006). Rheological characterization of PP/jute composite melts. Journal of applied polymer science, 99(4), 1476-1484.

Sojoudiasli, H., Heuzey, M. C., & Carreau, P. J. (2014). Rheological, morphological and mechanical properties of flax fiber polypropylene composites: influence of compatibilizers. Cellulose, 21(5), 3797-3812.

Switzer III, L. H., & Klingenberg, D. J. (2003). Rheology of sheared flexible fiber suspensions via fiber-level simulations. Journal of Rheology (1978-present), 47(3), 759-778.

Thomasset, J., Carreau, P. J., Sanschagrin, B., & Ausias, G. (2005). Rheological properties of long glass fiber filled polypropylene. Journal of non-newtonian fluid mechanics, 125(1), 25-34.

Tiptipakorn, S., Rimdusit, S., Kitano, T., & Damrongsukkul, S. (2009). Thermomechanical and rheological behaviours of waste glass fibre-filled polypropylene composites. Engineering Journal, 13(3), 45-59.

Twite-Kabamba, E., Mechraoui, A., & Rodrigue, D. (2009). Rheological properties of polypropylene/hemp fiber composites. Polymer Composites, 30(10), 1401-1407.

Chapter 6

Mechanical properties of composites

Mechanical properties of short fibre reinforced thermoplastics strongly depend on the microstructure established during processing. As seen in the previous chapters, the flow-induced microstructure in injection moulded parts leads to a multilayer-structure in which fibres are usually oriented parallel to the flow direction near the surface and perpendicular to the flow direction at the mid-plane. Therefore, injection moulded parts can be considered as anisotropic materials. The mechanical behaviour of such materials is dependent on the dispersion, size and orientation of fibres and the reinforcement is expected from the fibres aligned along the load direction.

The aim of this chapter is to correlate fibre microstructure in the injection moulded parts with the tensile and impact properties of composites. First, we present the state of the art related i) to the mechanical properties of natural fibre- and glass fibre-reinforced thermoplastics, focusing on the correlations with composite microstructure and ii) to the existing models classically used to predict their mechanical properties. We present then the experimental results of tensile tests performed on samples that were cut out from the moulded "box" along three different directions with respect to the main flow direction. The correlation with the microstructure was possible since tensile samples have been cut from the same location as the samples used for the microstructure analysis. The data that were obtained from the quantification of orientation in Chapter 4 and from fibre size analysis in chapter 3 will be used to model the tensile properties of composites. Moreover, an investigation of the impact properties made with impact bars injected separately will be presented and analysed. A comparison between experimental and theoretical results predicted by models will be discussed.

173

1. State of the art

1.1. Tensile properties

1.1.1. *Experimental results*

Many studies report on the mechanical properties of natural fibre reinforced thermoplastics, but only few studies correlate them with the microstructure in injection moulded parts. Aurich and Mennig (2001) studied the stiffness of 30 wt % flax reinforced polypropylene with fibre aspect ratio being 13 and with 2 wt % of MAPP added to improve adhesion. Tensile specimens were taken in parallel and in perpendicular directions to the main flow direction; the obtained elastic moduli were 3020 MPa and 2200 MPa, respectively. The authors explained the difference between elastic moduli in the parallel and the perpendicular directions by the different fibre alignment in the core and shell regions. The orientation component a_{xx} (with respect to the main flow direction) was 0.9 at the sample surface and 0.2 at the core in the central area of the plaque, and 0.6-0.9 close to the lateral border. The fibres are more aligned close to surface as compared to core. Similar results were found by Neves et al. (1998) for glass fibre-reinforced polycarbonate. The main factors influencing fibre alignment, and shell and core layers thickness were pointed out at Chapter 3 (State of the art section).

Bourmaud et al. (2013) investigated the stiffness of 13.7 vol % flax-reinforced polypropylene. To understand the difference in tensile properties between core and shell layers, a dog-bone sample with thickness of 4 mm was cut into 3 samples of the same shape such as the thickness of each was 1 mm (Figure 6.1). The samples from the shell layer were taken at a distance of 0.1 mm from the surface and the core sample was taken from the mid-plane. The tensile test was performed on the entire 4 mm thick sample and for the core and the shell samples of 1 mm thick each.
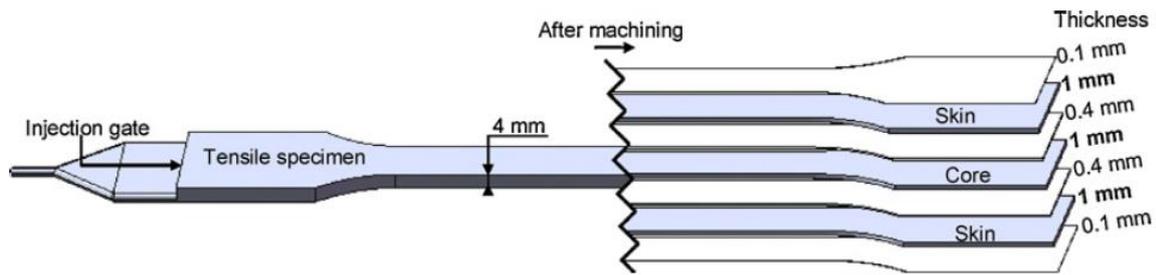
Figure 6.1

Sampling of the shell and core of the tensile specimen [Bourmaud et al. (2013)]

Figure 6.2 shows the stress-strain curves of the flax/PP core (a) and shell (b) specimens and their corresponding scans showing the presence of fibre aggregates (white areas). Three samples were tested for each core and shell regions. All samples were scanned before and after testing, using a scan micrograph. The purpose is to show the influence of fibre dispersion on the tensile properties. According to authors, the bundles' concentration is greater at the core than at the shell. For the core stress-strain curves (a), authors concluded that samples 3 and 2 contain larger bundles' size than the sample 1. The breakage occurs earlier as the bundles' size is larger, leading to a lower elongation at break. The strength also decreases as the bundles size is greater. For the shell stress-strain curves (b), the cross-sections show a lower bundles amount than at the core sample, explained by the higher shear close to the dog-bone surface. Only sample 1 in Figure 6.2.b has a bundle in the effective cross-section, which led to a premature breaking compared to the shell samples 2 and 3. In addition, whatever the sample is cut from shell or core, the presence of bundles does not affect the Young's modulus. The authors observed also cross sections of samples (parallel to the dog-bone plane) by SEM and showed that flax fibres are more aligned in the shell than in the core, the reason explaining the difference in term of strength and stiffness between core and shell samples. However, the microstructure investigation was limited to a qualitative observation and no quantitative analysis of fibre orientation was performed.
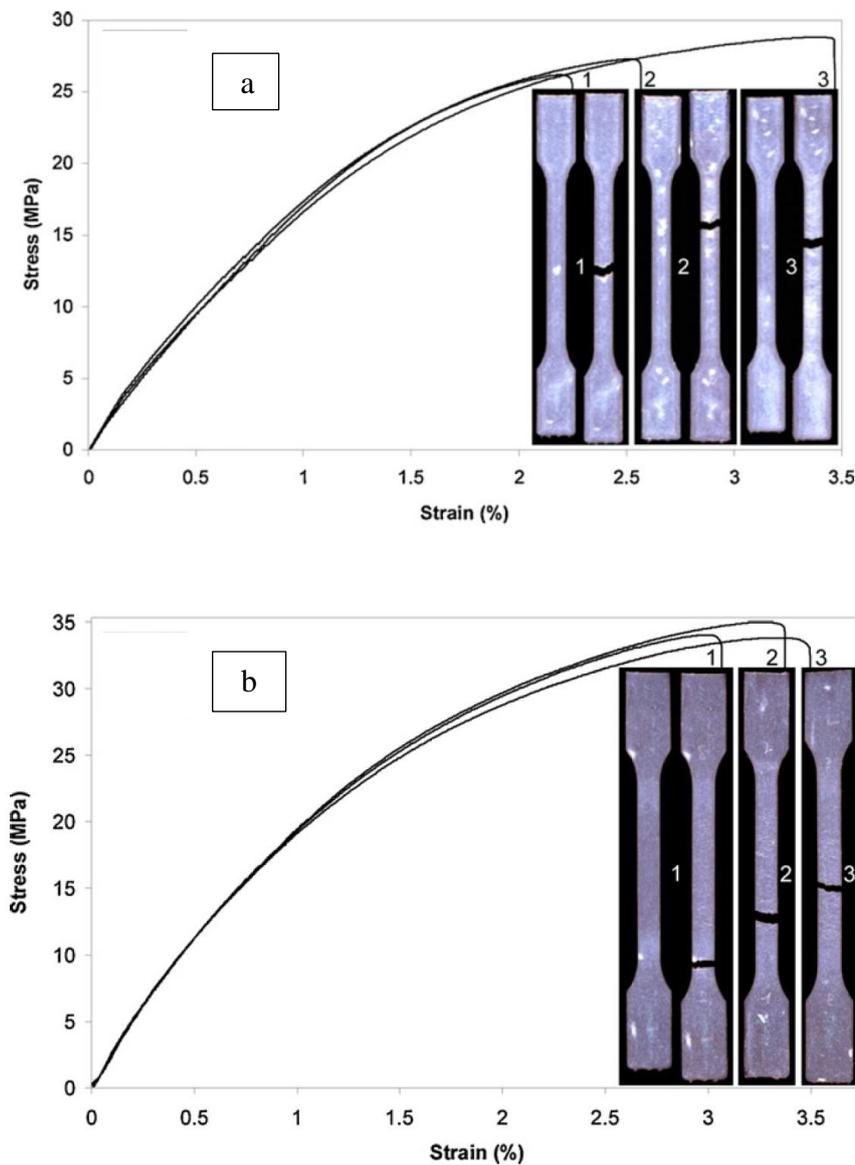
Figure 6.2

Stress-strain curves of the flax/PP of core samples (a) and shell samples (b) and the corresponding image obtained by micrograph scanning, before and after testing [Bourmaud et al. (2013)]

Bourmaud et al. (2013) observed also the breakage of the core sample during testing by a SEM micrograph. During the extension of the sample, the crack is initiated at the bundles, which make angle to the cross section plane (Figure 6.3). The authors considered that these bundles should present weakness areas that affect the composite properties. Therefore, improving bundles' dissociation could result in better tensile properties.
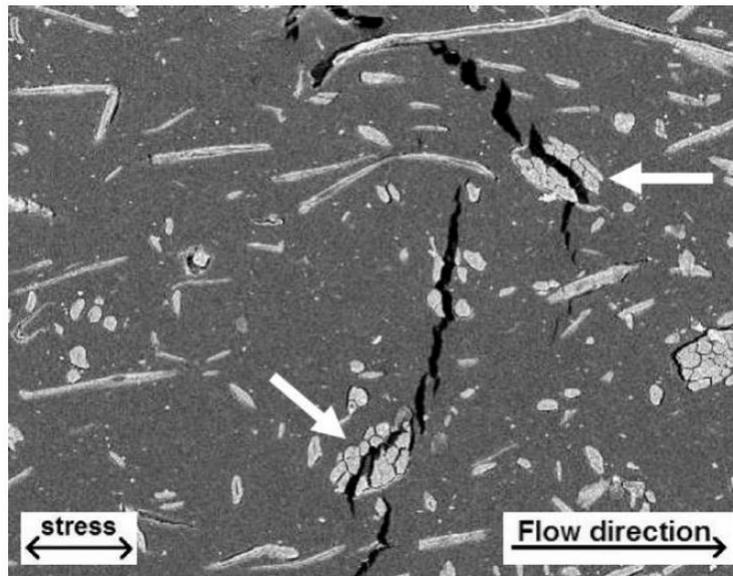
Figure 6.3

 SEM micrograph of a core 13.7 vol % flax/PP during tensile testing [Bourmaud et al. (2013)]

Figure 6.4 presents a comparison between flax fibre- and glass fibre-reinforced polypropylene at the same volume fraction 13.7 vol % [Bourmaud et al. (2013)]. With the same volume fraction, the weight fractions are different because of the difference in fibre density. In addition, 4 wt % of MAPP was added in the case of natural fibre composite. A considerable difference in stiffness and strength at break is observed between shell and core specimens, for each type of composite. The shell samples show a much higher Young's modulus as compared to core ones, by +69 % and +24 % for glass and flax based composites, respectively. The shell samples exhibit also a larger strength at break as compared to the core ones, by +81 % and +21 %, for glass and flax based composites, respectively. The glass fibre based composites reveal more important stiffness and strength at core and shell samples as compared to the flax based. The authors explained this by the higher stiffness of glass fibres, in addition to the bundle structure of flax that limits their dispersion in matrix and orientation in the tensile direction. Moreover, in a previous study of Bourmaud and Baley (2010), nano-indentation measurements demonstrated that the mechanical properties of the cell wall of flax fibres decrease after compounding and injection moulding, which changes their structure, composition, cohesion and water content. Bourmaud et al. (2013) did not focus on the influence of the fibre size on the tensile properties. The difference of properties between glass and flax based composites can be related to the difference of fibre size in composites, in

addition to the other reasons (fibre properties and orientation). It is known that fibre size decreases by processing and the mechanism of rupture of flax fibre is dissimilar to the glass one. Therefore, a difference of size of flax fibres compared to glass ones is expected after the injection moulding of composites (See Chapter 3, Section 2.4. Comparison between fibre types). The elongation at break is about 2.2-3.4 % for both types of composites. The neat polypropylene has an elongation at break of 3.4 % at the core and 11.2 % at the shell (not shown in Figure 6.4). Whereas, the elongation at break of composites considerably decreases at the shell samples compared to the neat PP, it remains almost constant at the core samples.
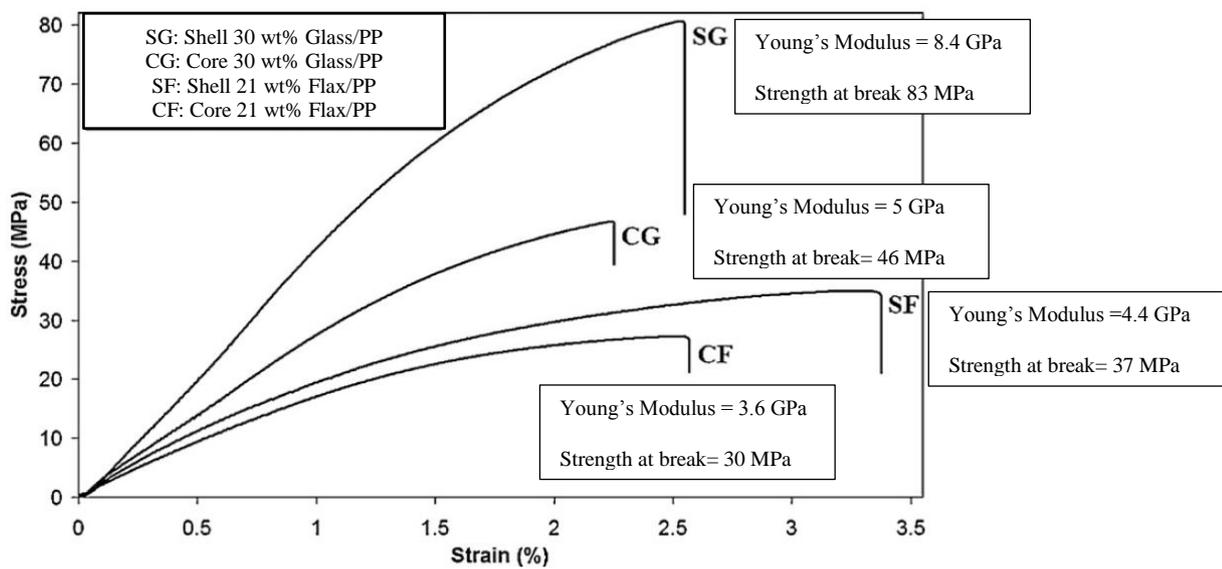
Figure 6.4

Stress-strain curves of the core and shell of glass and flax based composites at the same volume faction 13.7 vol % and different weight fraction (30 wt % Glass/PP and 21 wt % Flax/PP) [Bourmaud et al. (2013)]

Many authors studied the influence of various parameters, else than fibre orientation and dispersion, on the mechanical properties of composites. By analysing the influence of length and concentration on the stiffness of glass/PP composites [Thamason and Vlug (1996,a,b)] and flax/PP composites [Nechwatal et al. (2005)], it was shown that the fibre length needed to reach the maximum stiffness is much lower than that needed to reach the maximum strength. For glass/PP, a fibre length higher than 0.8 mm is enough to make the stiffness of a short fibre composite equivalent to 90 % of the stiffness of a continuous fibre composite, whereas 90 % of strength requires at least a fibre length of 13 mm [Thamason and Vlug (1996,a)]. For

flax/PP composites the equivalent length enabling a maximum stiffness is 1 mm, which is 8 times shorter than the length needed for a maximum strength [Nechwatal et al. (2005)]. Peijis et al. (1998), Van Den Oever et al. 2000, Gharkhail et al. (2000), Karmaker et al. (1996) and Barkoula et al. (2010) showed that MAPP improves the composite strength but has almost no effect on the stiffness for flax fibres based systems. Ganster and Fink (2006) focused on the mechanical properties of composite reinforced with man-made cellulose fibres. Figure 6.5 shows a comparison among composites with several types of man-made fibres and jute; all of them were made with 25 wt % of fibres and 1 wt % of MAPP. Tencel/PP composites show the highest Young's modulus. All composites show reduced elongations at break compared to the neat polypropylene.
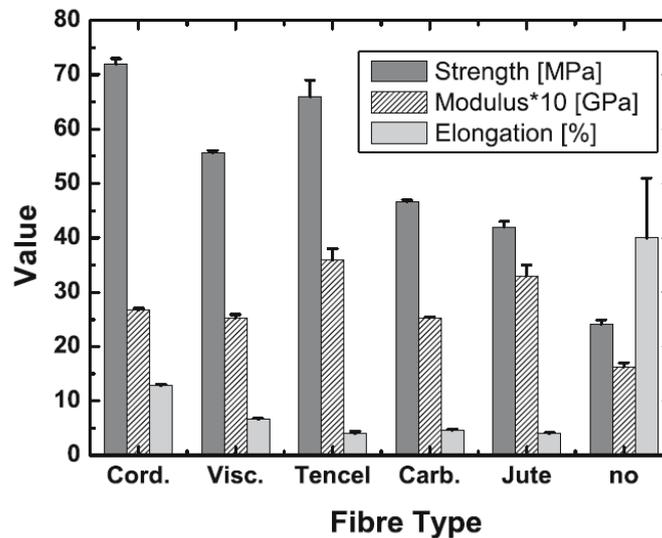
Figure 6.5

Strength, modulus and elongation for injection moulded composite test bars with 25 wt % fibre load as a function of fibre type; "no" corresponds to the neat polypropylene: Cord = Cordenka 700, Visc = Viscose, Carb = Carbamate[Ganster and Fink (2006)]

1.1.2. *Models of tensile stiffness and strength of composites*

- **Tensile stiffness**

The prediction of tensile stiffness of natural fibre-reinforced thermoplastics uses models already developed for discontinuous (short) glass or synthetic fibre composites. The model of Cox and Krenchel [Cox (1952), Krenchel (1964)] (Eq.6.1) is commonly used to predict the stiffness E_c for oriented short fibre composite, which is the case of injection moulded parts.

179

$$E_c = \xi_0 \xi_1 f E_f + (1 - f) E_m \qquad\qquad \text{[Eq.6.1]}$$

where E_f, E_m and f are the fibre Young's modulus, matrix Young's modulus and the fibre volume fraction, respectively. ξ_0 and ξ_1 are the orientation and the efficiency factors, respectively.

$$\xi_1 = \left[1 - \frac{\tanh\left(\frac{\kappa L}{2}\right)}{\frac{\beta L}{2}} \right] \qquad\qquad \text{[Eq.6.2]}$$

$$\kappa = \frac{2}{D} \left[\frac{2G_m}{E_f ln\left(\sqrt{\frac{r}{R}}\right)} \right]^{\frac{1}{2}} \qquad\qquad \text{[Eq.6.3]}$$

where L is the fibre length, G_m is the shear modulus of the matrix, χ_i is a factor depending on the geometrical packing arrangement of fibres, r is the fibre radius and R is the centre to centre spacing of fibres. The $\frac{r}{R}$ factor can be related to the fibre volume fraction f as follows:

$$Ln\left(\sqrt{\frac{r}{R}}\right) = Ln\left(\sqrt{\pi/\chi_i f}\,\right) \qquad\qquad \text{[Eq.6.4]}$$

Thomason et al. (1996) suggested $\chi_i = 4$ for glass fibre- reinforced polypropylene.

ξ_0 is actually the theoretical orientation factor of Krenchel [Krenchel (1964)] that takes into account fibre orientation as follows:

$$\xi_0 = \sum_n f_n \cos^4 \phi_n \qquad\qquad \text{[Eq.6.5]}$$

where f_n is the fraction of fibres with the orientation angle ϕ_n with respect to the tensile direction axis. It was shown by Krenchel (1964) and Folkes (1985) that $\xi_0 = 3/8$ for random planar orientation and $\xi_0 = 1/5$ for three dimensional random fibre orientation, and 1 for all fibres oriented in the direction of traction. Gharkhail et al. (2000) discussed these values and suggested that deviations may likely occur for flax fibres due to the out-of-plane oriented fibres and the bending of fibres.

- **Tensile strength**

Kelly and Tyson (1965) extended the rule of mixture to predict strength σ_c of unidirectional fibre-reinforced polymer composites as follows:

$$\sigma_c = \zeta_L f \sigma_f + (1 - f)\sigma_m \qquad\qquad\qquad\qquad \text{[Eq.6.6]}$$

where σ_f is the fibre tensile strength, σ_m is the matrix strength. ζ_L is the fibre length efficiency factor:

$$\zeta_L = \frac{1}{f}\left[\sum \frac{L_i f_i}{2L_c} + \sum f_j \left(1 - \frac{L_c}{2L_j}\right)\right] \qquad\qquad \text{[Eq.6.7]}$$

Equation 6.7 contains two parts depending on if fibre length is subcritical $L_i < L_c$ (first summation) or supercritical $L_j > L_c$ (second summation), where L_c is the critical length:

$$L_c = \frac{\sigma_f D}{2\tau} \qquad\qquad\qquad\qquad\qquad\qquad \text{[Eq.6.8]}$$

where D is the fibre diameter and τ is the fibre-matrix interfacial shear strength.

The critical length $L_c = \sigma_f \left(\frac{D}{2\tau}\right)$ can be determined either experimentally as a single fibre fragmentation test [Beckermann and Pickering (2009)] or calculated knowing the strength of the fibre σ_f. The interfacial shear strength τ are usually assessed by micromechanical tests.

Bowyer and Bader (1972) suggested a modified Kelly and Tyson model by adding an orientation factor to take into account the fibre orientation. Applied on sisal fibre composite, this model provides results that fit well the experimentally obtained tensile strengths [Li et al. (2000); Kalaprasard et al. (1997)]. Thomason et al. (1996) used an empirical orientation factor equal to 0.2 to fit the experimental measurements of glass/PP composites

1.2. Impact properties

1.2.1. *Experimental results*

Most studies related to impact properties of natural fibre-reinforced thermoplastics were not associated with injection moulding process, except those of Paunikallio et al. (2003, 2004) and Ganster and Fink (2006). Ganster and Fink (2006) focused on the composites with man-made cellulosic fibres; they showed that Tencel/PP exhibits better impact strength over jute/PP and viscose/PP but lower than Cordenka/PP at the same fibre concentration (25 wt %) (Figure 6.6). However, no correlation among composite microstructure, fibre concentration and impact properties was performed.
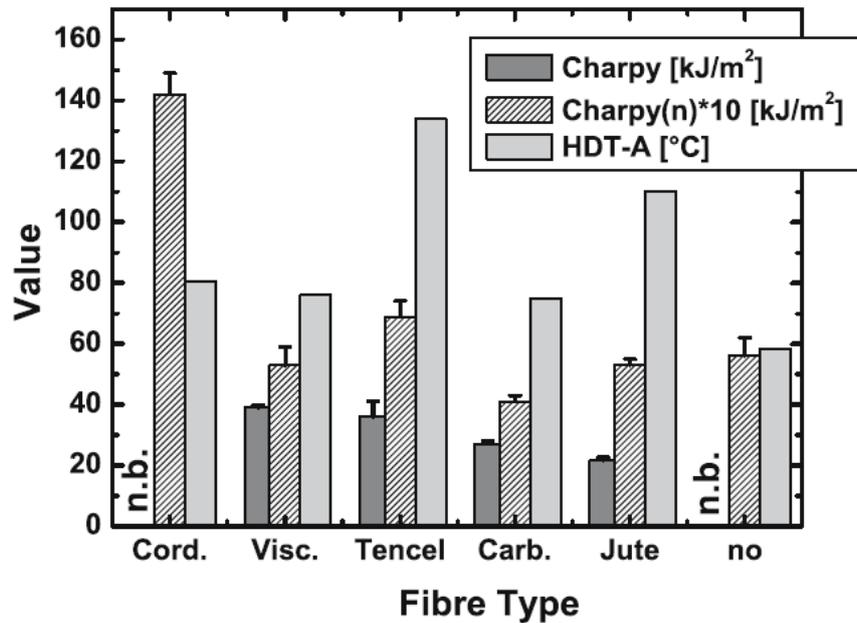
Figure 6.6

Charpy, notched Charpy "Charpy (n)" impact strength and heat distortion temperature (HDT-A) for injection moulded composite test bars with 25 wt % fibre load as a function of fibre type and for the neat PP "no" (n.b means not broken) (Cord = Cordenka 700, Visc = Viscose, Carb = Carbamate) [Ganster and fink (2006)]

For processes else than injection moulding, Wambua et al. (2003) made a comparison among Charpy impact properties of compressed randomly oriented kenaf, coir, sisal, hemp and jute fibre reinforced polypropylene. It turned out that hemp and sisal composites have better impact properties over others. Moreover, it was shown that impact strength increases with the fibre content.

Van den Oever et al. (2000) investigated mechanical properties of flax mat reinforced polypropylene and showed that while impact strength increases with increasing fibre content and fibre length, it decreases with increasing fibre-matrix adhesion. This was explained by the fact that higher adhesion results in shorter average pull-out length. Similar results were found by Gharkhail et al. (2000) for a random non-woven flax fibre mats/polypropylene and Gironès et al. (2011) for abaca/polypropylene composites. This statement was even more confirmed by Bax and Müssig (2009) for flax/PLA and Plackett et al. (2003) for jute/PLA, where fibre-

matrix adhesion is naturally good and adding fibre can unexpectedly decrease the impact strength.

Clemons et al. (2003) studied the injection moulded pulp-reinforced polypropylene and demonstrated that dynamic fracture toughness during impact test increased when fibres are oriented perpendicular to the crack direction. For the injection moulding of glass fibre-reinforced polypropylene, Thomason and Vlug (1997) demonstrated that impact strength increases when the length and the concentration of fibres get higher. Furthermore, an improved fibre-matrix interaction decreases impact strength, as found for the natural fibre case.

A small enhancement in impact strength can be obtained with a temperature decrease. Various mechanisms of energy dissipation may operate during impact test. Wells and Beaumont (1985) revealed that composite containing short fibres randomly dispersed and aligned follows a fibre pull-out, as energy dissipation mechanism preceding a fast fracture. Thomason and Vlug (1997) considered that fibre fracture is the dominant energy dissipation mechanism. The identification of the fracture mechanism is classically possible by a microscopy observation.

1.2.2. *Models of impact strength*

Cottrell (1964) developed a model for composites containing unidirectional fibres, including three possible mechanisms of energy dissipation: 1) matrix fracture, 2) fibre fracture and 3) fibre pull-out. The predicted impact energy increases with fibre length up to a critical fibre length L_c in a similar way to Kelly and Tyson (1965) model prediction for the composite strength. The maximum of impact energy was correlated with the change in the mode of fracture: from fibre pull-out for length $< L_c$ to fibre fracture for length $> L_c$. Since this model has been considered only for the unidirectional reinforcement, it is somewhat questionable to apply it for randomly oriented fibres or multi-layer oriented structure as the case of injection moulding of short fibre-reinforced composite. Therefore, Thomason and Vlug (1997) developed a simpler fibre strain energy model based on the rule of mixture as follows:

$$U_c = f \left(\frac{\sigma_f{}^2 L_d}{2E_f} \right) \left(\frac{L}{L+L_c} \right) + (1-f)U_m \qquad \text{[Eq.6.9]}$$

where U_c is composite impact strength, f is the fibre volume fraction, E_f is the fibre Young's modulus, L is the fibre length, U_m is the matrix impact strength, L_d is the length of the

debonding fibre, σ_f is the fibre strength and E_f is the fibre Young's modulus. The term $\left(\frac{\sigma_f{}^2 L_d}{2E_f}\right)$ corresponds to the total energy for the fracture of a single fibre. According to Thomason and Vlug (1997), L_d increases when L_c increases. However the effect of fibre orientation is not taken into account.

1.3. Conclusions

The mechanical performances of natural fibres reinforced thermoplastic are directly related to fibre aspect ratio and length, concentration, orientation and dispersion. The flow-induced microstructure formed in composite leads to a material with anisotropic properties. This anisotropy is directly reflected by tensile stiffness and strength. In most cases, the Young's modulus and the tensile strength are higher when specimen tensile bar is parallel to the main direction of flow than perpendicular. This stems from a different fibre alignment at the shell layer compared to the core layer. Higher fibre aspect ratio and concentration lead to better tensile and impact properties. While adding compatibilizer increases the tensile strength, it has almost no effect on the tensile stiffness and decreases the impact strength.

Models predicting the mechanical properties of composites were developed for glass fibre reinforced plastics and the same models are presently extended to the case of natural fibres. The models of the tensile properties are associated to fibre critical length; below it the contribution of fibres in composite performance is less important than above it. The value of the critical length varies from one study to other and depends on the use of compatibilizer or not. This must be one of the main reasons of the deviation of the estimated mechanical properties for natural fibre-reinforced thermoplastics. Some recent modifications of the models dedicated to tensile stiffness and strength enable to take into account fibre orientation, which makes the predicted results closer to the experimental ones. However, the existing models of prediction of the impact properties do not yet include the orientation effect.

2. Results and discussion

2.1. Tensile Properties

2.1.1. *Experimental results: influence of fibre orientation*

The location of dog-bone samples is identical to the sample used to characterize the fibre orientation, dispersion and length. This enables to correlate the tensile properties to the microstructure in the injection moulded box. All testing conditions were described in Chapter 2.
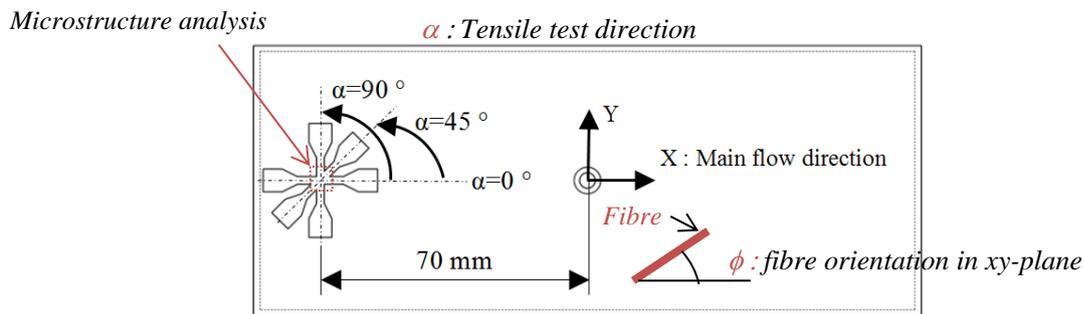

Figure 6.7

Top view of the injection moulded box in *xy*-plane, ϕ is the fibre orientation in *xy*-plane, α is the tensile test direction, three different testing directions ($\alpha = 0°$, $\alpha = 45°$ and $\alpha = 90°$) with respect to *x*-direction

Figure 6.7 shows the three orientations $\alpha = 0°$, $\alpha = 45°$ and $\alpha = 90°$ of the specimen with respect to the local flow direction. Figure 6.8 shows an example of tensile test of 20.5 vol % flax/PP for the three orientations. The best tensile properties occur for $\alpha = 0°$. In Chapter 4, we found a_{xx} is 0.8-0.9 at the shell, meaning that fibres are well oriented along the flow direction. In the core, a_{xx} is around 0.3-0.4. This corresponds to a slight orientation perpendicular to the flow direction (0 would be perfect orientation, and 0.5 means random in-plane orientation). Therefore, there is a qualitative agreement between the measured orientation and the mechanical response. Similar stress-strain curves were obtained for glass/PP and Tencel/PP (not shown).
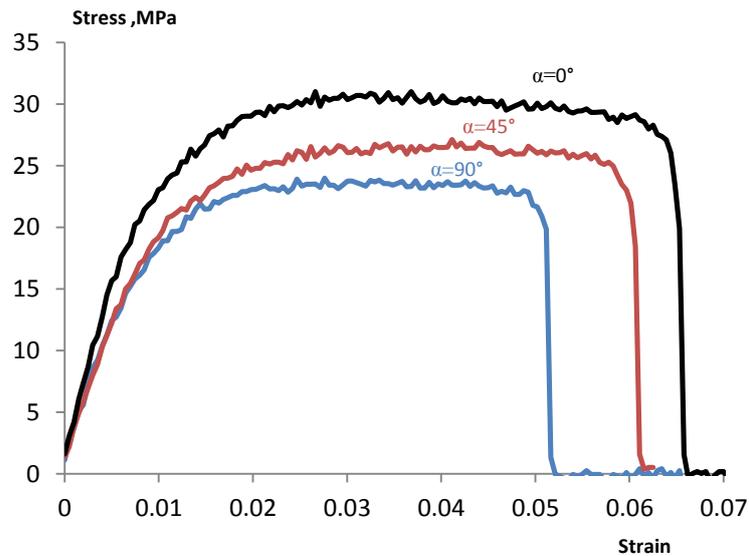
Figure 6.8

Stress-strain dependences of 20.5 vol % flax/PP for α= 0 °,45 ° and 90 °

Figures 6.9, 6.10 and 6.11 show the fracture surface after the tensile test of 20.5 vol % flax, Tencel and glass composites, respectively. For each type of composite, *zy*-plane and *zx*-plane are shown, corresponding to the traction of samples along *x*-direction (α = 0 °) and *y*-direction (α = 90 °), respectively. Two observations can be pointed out: 1) the shell layers are thicker than the core ones especially for flax and glass fibres 2) only fibres oriented in the extension direction are broken or/and pulled out. This means that fibres aligned in the tensile direction contribute marginally to the resistance against the sample extension. Moreover, thicker shell layers enable to explain more the higher tensile properties when samples are extended in *x*-direction than perpendicular. This seems reasonable because shell layers are almost aligned in the *x*-direction. The flax fibres that are pulled-out from matrix or broken during tensile testing can be elementary fibres or structured in bundles (Figure 6.9). This means that the mechanism of rupture is not dependent on the fibre morphology.
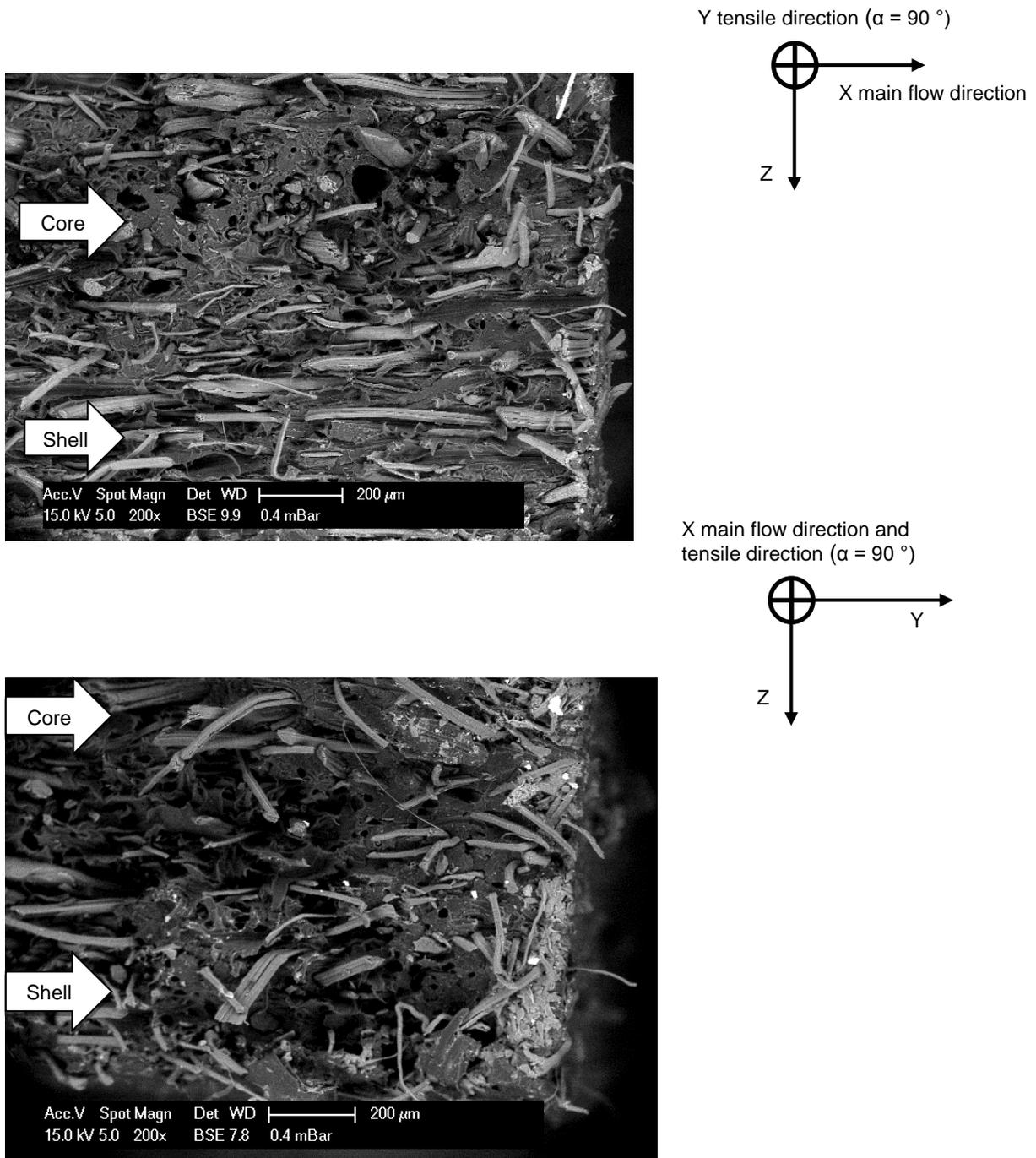
Figure 6.9

Fracture surface after tensile testing of two 20.5 vol % flax/PP samples in *xz*-plane and *yz*-plane, extended along *y*-direction (α = 90 °) and *x*-direction (α = 0 °), respectively

Figure 6.10

Fracture surface after tensile testing of two 20.5 vol % Tencel/PP samples in *xz*-plane and *yz*-plane, extended along *y*-direction (α= 90 °) and *x*-direction (α= 0 °), respectively

Y tensile direction (α = 90 °)

X main flow direction

Z
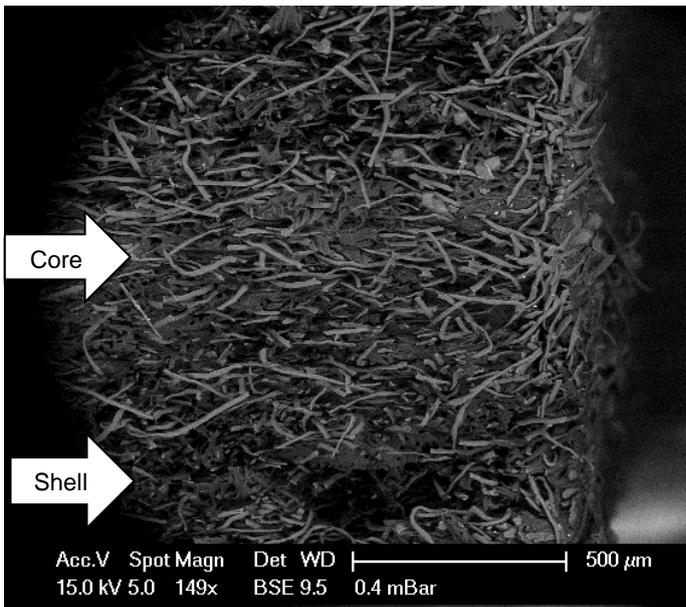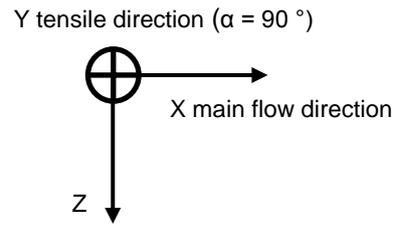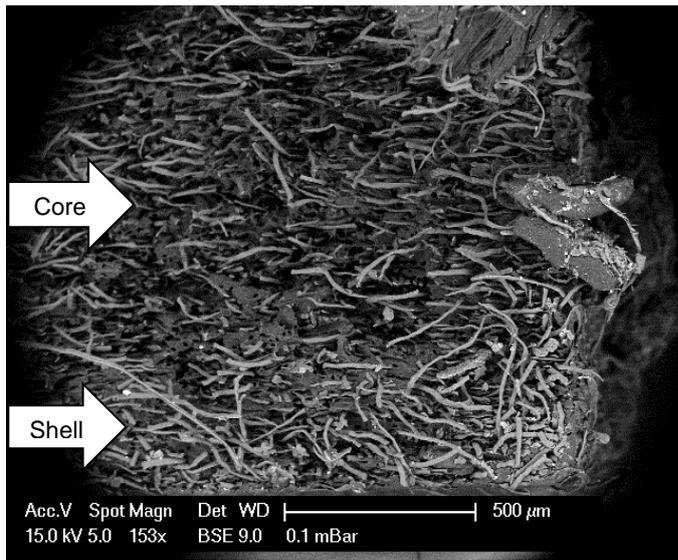
X main flow direction and
tensile direction (α = 90 °)

Y

Z
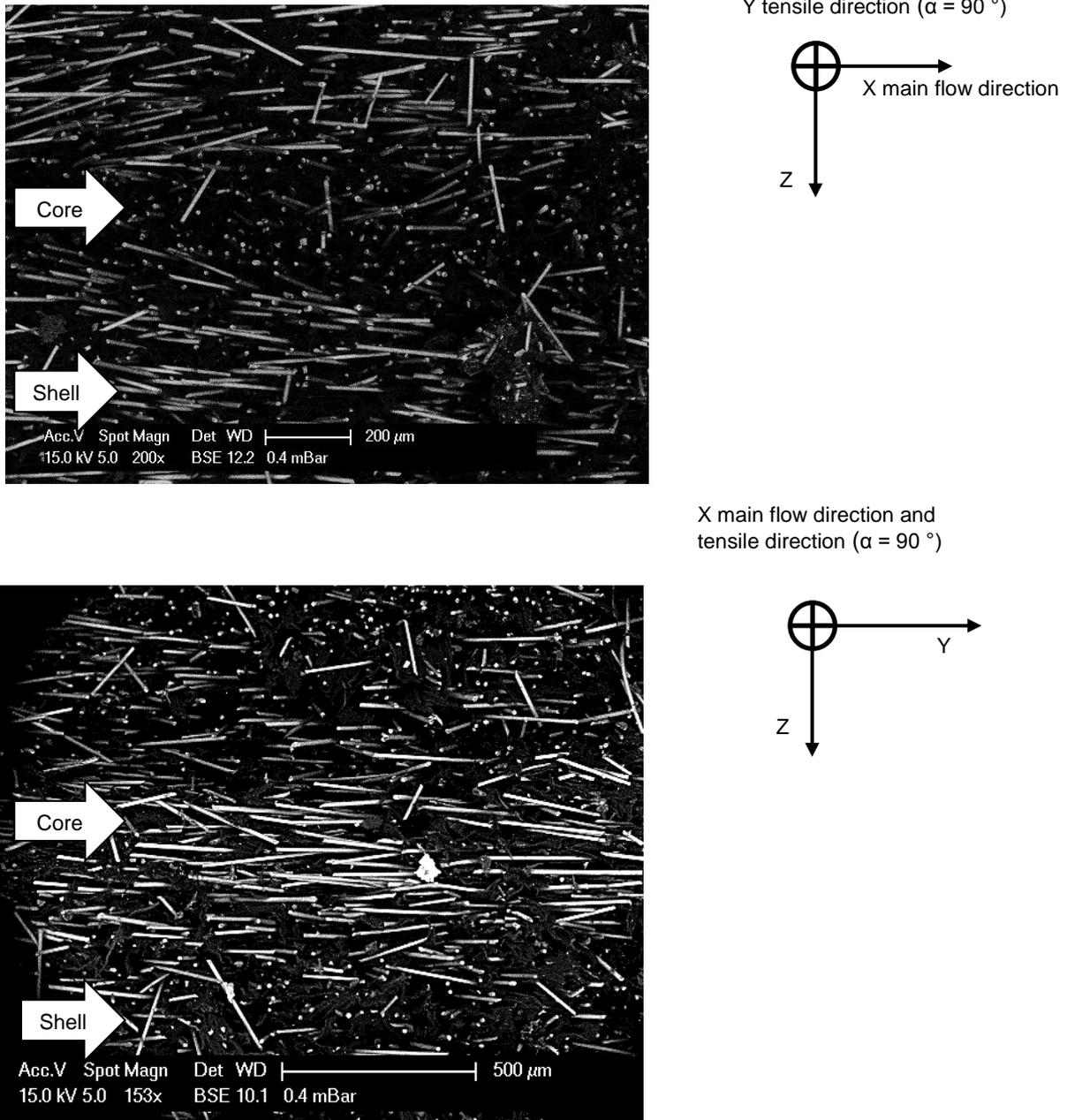
Figure 6.11

Fracture surface after tensile testing of two 20.5 vol % Tencel/PP samples in *xz*-plane and *yz*-plane, extended along *y*-direction (α= 90 °) and *x*-direction (α= 0 °), respectively

2.1.2. *Experimental results: influence of fibre type*

Figure 6.12 shows Young's moduli of 20.5 vol % composites for different fibre types and different angles α (with respect to *x*-direction). The glass composite shows the highest Young's modulus as compared to flax and Tencel ones overall angles α. As compared to the neat PP, Young's modulus of glass-reinforced composites is 116 % higher, while it is only 66

% and 43 % higher for flax and Tencel based composites, respectively. One of the reasons is that the aspect ratio of glass fibres is twice higher than that of flax and 1.5 higher than that of Tencel (see Chapter 3). Moreover, glass fibre Young's modulus is 73 GPa, whereas that of Tencel is 10-15 GPa and that of flax varies between 50 and 110 GPa depending on flax fibre diameter [Charlet et al. (2010)]. In our case, most of flax fibres are in bundles and thus their moduli should be close to 50 GPa.

The obtained moduli of composites decrease with α increasing from 0 ° to 45 ° and then remain almost constant for α from 45 ° to 90 ° overall fibre types. Moreover, when α increases, the difference in modulus between Tencel and flax composites becomes smaller. This can be explained by the fact that when the traction direction is perpendicular to the flow direction (α= 90 °), the core fibres are more effective than the shell ones, and according to results obtained in Chapter 4, Tencel fibres are more aligned than flax fibres at core ($a_{xx\ \text{(flax)}}$= 0.33 at $a_{xx\ \text{(Tencel)}}$= 0.17)
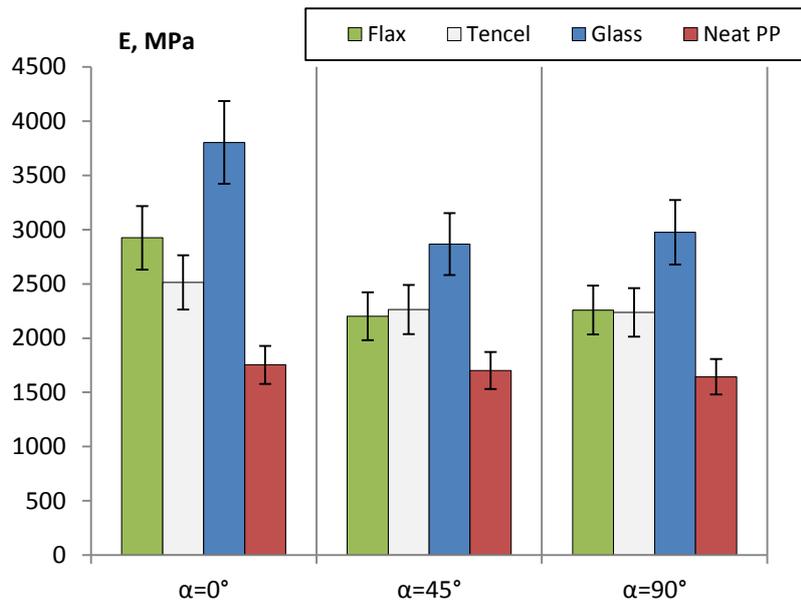
Figure 6.12

Young's modulus of 20.5 vol % composites for different types of fibres (flax, Tencel and glass) and for different loading directions (α= 0 °, α= 45 °, α= 90 °)

Figure 6.13 shows the ultimate tensile strength for composites of 20. 5 vol % for different fibre types and different angles α. Tensile strength decreases when α increases for all fibre types. The glass composite strength is higher than that of flax and Tencel. Nevertheless, the

difference in strength between glass and flax is relatively small compared to the difference in Young's modulus seen in Figure 6.11. The improvement in tensile strength relative to the neat PP is lower than the one of Young's modulus. For example at α= 0 °, the addition of fibres to PP increases strength of composite by 45 % with glass, by 40 % with and by Tencel. According to Peijis et al. (1998), Van Den Oever et al. (2000), Gharkhail et al. (2000) and Barkoula et al. (2010) compatibilizer effect is more pronounced on the tensile strength than on tensile stiffness. Therefore, the lower improvement of tensile strength of composites relative to the neat PP is due to the absence of compatibilizer.
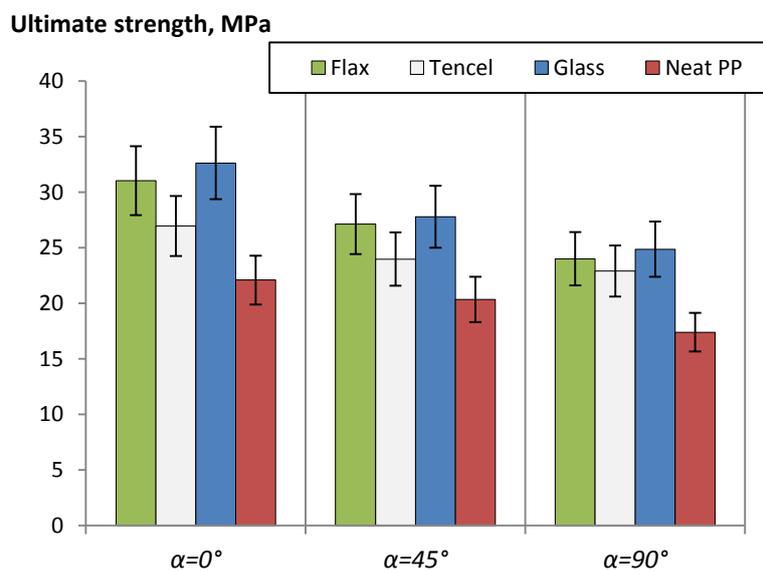
Figure 6.13

Tensile strength of 20.5 vol % composites for different types of fibres (flax, Tencel and glass) and different directions towards main flow α= 0 °, α= 45 °, α= 90 °

Figure 6.14 shows the elongation at break as a function of α and fibre type. The elongation of composites is strongly reduced compared to the neat polypropylene at α= 0 °, and it is similar at α= 90 °. The neat PP shows high elongation at break when the sample is cut as α= 0 °. This was explained by the high orientation of chains of injected PP along the main flow direction [Kalay and Bevis (1997)]. In fact, an injection-moulded neat polypropylene presents a core-shell structure appearing at the scale of the polymer chains, which leads to different properties along the flow direction and perpendicular. Tencel based composites elongation at break is twice larger as compared to flax and glass based ones. Interestingly, the elongation at break of

Tencel based composite does not depend on how the sample is positioned (and extended) with respect to the main flow direction. The most probable reason is that Tencel fibres are curved and extremely flexible so that they can be stretched under tensile force whatever the direction.
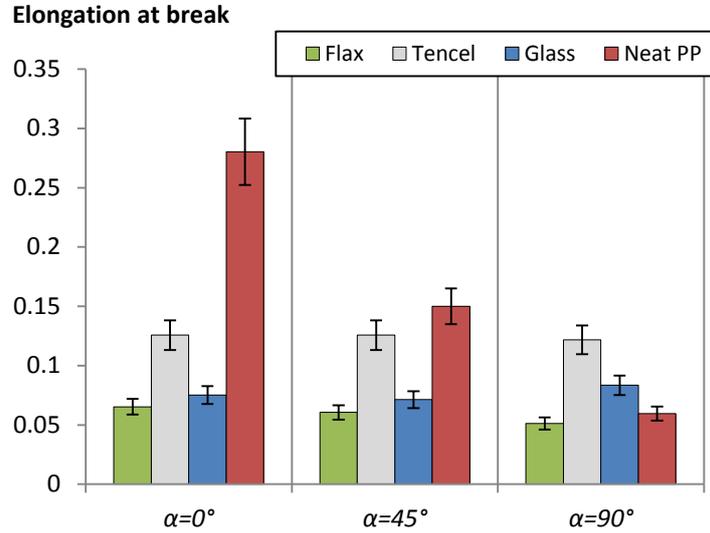

Figure 6.14

Elongation at break of 20.5 vol % composites for different types of fibres (flax, Tencel and glass) and different directions (α= 0 °, α= 45 °, α= 90 °)

2.1.3. *Predictions of composite tensile properties and comparison with experimental results*

- **Stiffness**

In this study we assume that fibre orientation is planar and symmetric with respect to the mid thickness plane. Considering that the orientation measurements were carried out for many layers at different depths across sample thickness from surface to core (Chapter 4), we approximate that a_{xx} between two successive layers does not vary and thus thickness "e" can be divided into smaller sub-thicknesses 'e_n' each with different orientation components a_{xx}. We approximate also that the orientation coefficient ξ_0 (see Eq6.5) can be calculated by a quadratic assumption such as $cos^4\varphi_n = a_{xxxx} = (a_{xx})^2$ when sample main axis (and thus extension direction) is parallel to the flow direction (α= 0 °), and $cos^4\varphi_n = a_{xxxx} = (a_{yy})^2$ when sample main axis direction is perpendicular to the flow direction (α= 90 °). a_{yy} is calculated with $a_{xx} + a_{yy} = 1$, the normalization approach of the components in the orientation tensor (see chapter 4), assuming that a_{zz} is small when compared to a_{xx} and a_{yy} . This enables to describe the core-shell orientation induced by injection moulding flow and

provides orientation factors ξ_{0x} and ξ_{0y} in *x*-direction and *y*-direction, respectively, as follows:

$$\xi_{0x} = \sum_n \frac{e_n (a_{xx_n})^2}{e} \qquad \text{[Eq.6.10]}$$

$$\text{and } \xi_{0y} = \sum_n \frac{e_n (a_{yy_n})^2}{e} \qquad \text{[Eq.6.11]}$$

We suppose that these factors remain constant with concentration variation. Table 6.1 presents the results of this approximation.

Table 6.1 Orientation factors for different composite types

	flax/PP	*Tencel/PP*	*glass/PP*
ξ_{0x}	0.38	0.28	0.34
ξ_{0y}	0.2	0.3	0.18

The efficiency factor ξ_1 [Eq.6.2] varies with fibre size that in turn varies with fibre content and fibre type. The results of fibre size during processing presented previously in Chapter 3 were used to estimate the efficiency factor ξ_1. Table 6.2 presents all calculated values.

Table 6.2 Efficiency factor variation with fibre type and fibre content

	Fibre content (vol %)	ξ_1
flax	3.6	0.39
	6.3	0.39
	13.1	0.53
	20.5	0.61
Tencel	3.6	0.82
	6.3	0.84
	13.11	0.85
	20.5	0.86
Glass	3.6	0.79
	6.3	0.76
	13.1	0.75
	20.5	0.77

Figure 6.15. a, b and c shows a comparison between experimental and predicted Young's modulus with Cox and Krenchel model as a function of fibre content for flax/PP, Tencel/PP and glass/PP, respectively. For flax composites, while the predicted moduli in *x*- and *y*-directions matche well the measured ones until 13.1 vol %, a deviation occurs at 20.5 vol %. The moduli are 20 % overestimated. The same range of deviation was found by Aurich and Mennig (2001) for 30 wt % flax/PP (which is the same fibre concentration in weight).

For Tencel based composites, the model predicts a nearly isotropic behaviour, despite a skin-core structure. The evolution with the fibre concentration is quite well predicted, but the model underestimates the measured values. Both predicted moduli of Tencel merge together towards high concentrations. Their two respective orientation factors are close, as seen in Table 6.1. Therefore, the only considerable difference to move them apart is the difference between Young's modulus of matrix in *x* and *y* directions, and this effect decreases progressively by adding fibres.

For glass composites, the *y*-direction modulus is well fitted with Cox-Krenchel prediction, whereas in the *x*-direction the modulus is overestimated and the difference between the measured and the modelled modulus gets larger with increasing the fibre content.The

measurement of orientation provided in Chapter 4 showed that $a_{xx} = 0.7$-0.4, which means that the average of a_{xx} give almost a random orientation. This is reflected in the experimental stiffness by close moduli in *x* and *y* directions, and a quite isotropic material. However, the orientation factors obtained by the quadratic assumption we adopted in Eq.6.10 and Eq. 6.11 predict a considerable anisotropy (Table 6.1), which is not in agreement with experiments. We can conclude that all *y*-direction moduli are fitted well the measured ones.
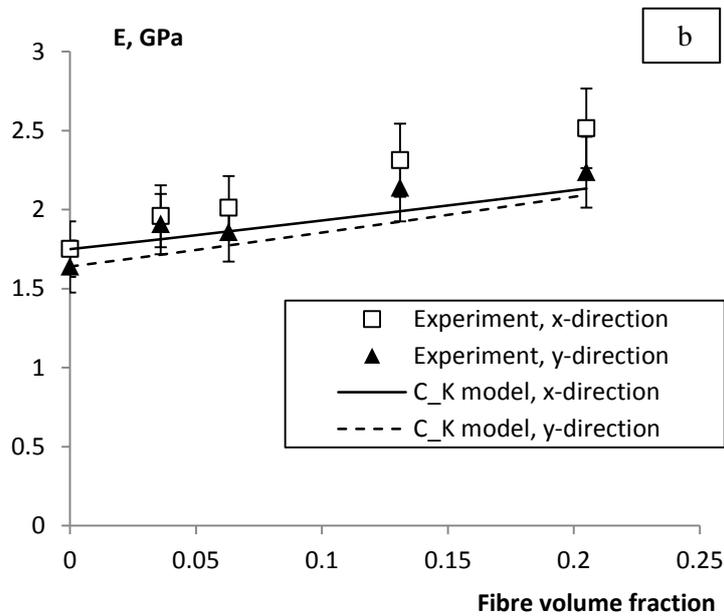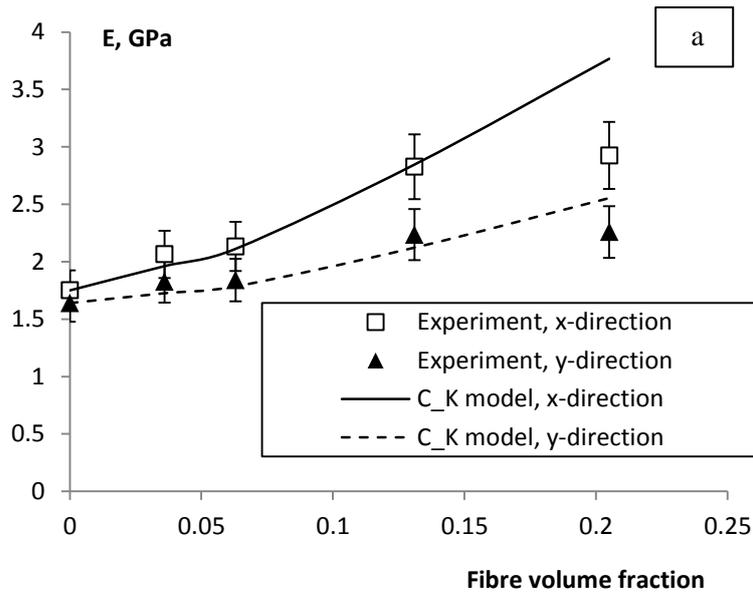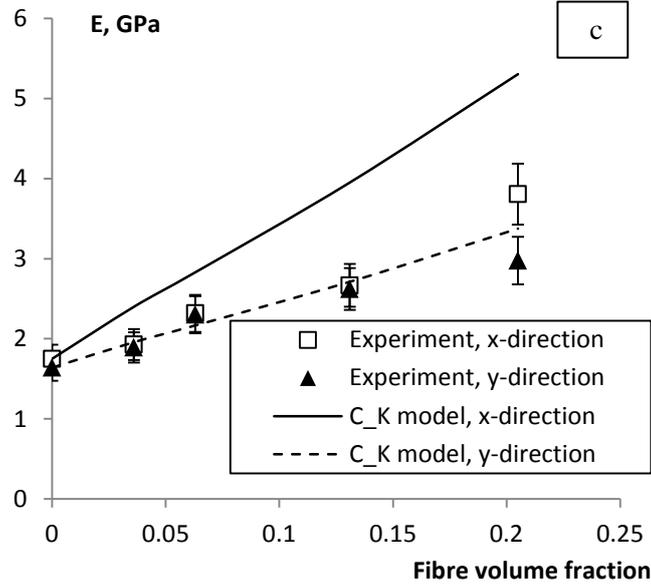
Figure 6.15

Experimental and Cox-Krenchel predicted Young's moduli (x-direction, α = 0 ° and *y*-direction, α = 90 °) as a function of fibre content, a) flax/PP b) Tencel/PP c) glass/PP

▪ **Strength**

To take into account the orientation effect for predicting tensile strength with Kelly and Tyson model [Eq. 6.6], we suggest considering the orientation coefficient in the same way as it was done for Young's modulus prediction. This results in σ_c as follows:

$$\sigma_c = \zeta_0 \zeta_L f \sigma_f + (1 - f)\sigma_m \qquad \text{[Eq.6.12]}$$

where ζ_0 is the orientation factor either denoted ξ_{0x} (Eq. 6.10) when sample is oriented along *x* (α= 0 °) or denoted ξ_{0y} (Eq. 6.10) when sample is oriented along *y* (α= 90 °). To predict the critical length, we used the results obtained on fibre size analysis and for flax/PP system without MAPP σ_f= 980 MPa and τ =13 MPa [Van Den Oever and Bos (1998)]; for Tencel σ_f = 570 MPa given by the manufacturer and τ= 5 Pa measured by Adusumalli et al. (2006 a, b), and for glass σ_f = 1818 MPa and τ= 13 MPa according to Thomason and Vlug (1997). The calculated critical length L_c, the fibre strength, the fibre-matrix interfacial shear strength τ and dimensions of fibres are shown at Table 6.3.

Table 6.3 Parameters used for tensile strength modelling

	vol %	$L_c, (\mu m)$	$\sigma_f, (MPa)$	$\tau (MPa)$	$L_n (\mu m)$	$D_n (\mu m)$
Flax	3.6	1278	980	13	428	34
	6.3	1368	980	13	407	36
	13.11	1206	980	13	420	32
	20.05	1067	980	13	388	28
Tencel	3.6	570	570	5	262	10
	6.3	570	570	5	255	10
	13.11	570	570	5	229	10
	20.05	570	570	5	211	10
Glass	3.6	6992	1818	13	494	10
	6.3	6992	1818	13	379	10
	13.11	6692	1818	13	301	10
	20.05	6692	1818	13	286	10

The calculated critical length (Table 6.3) is far higher than the fibre length in composites for the three fibre types, thus the second summation in equation 6.7 is not considered in our study.

Figure 6.16 a, b and c shows comparisons between the predicted and the measured tensile strengths as a function of fibre content for flax/PP, Tencel/PP and glass/PP, respectively. The tensile strength increases when the fibre content increases, and it is higher when sample axis (and stretching direction) is parallel to the main flow direction (*x*-direction) compared to the perpendicular (*y*-direction). The difference in strength between both directions *x* and *y* gets higher for glass composite over the other composites. For flax composites, while the predicted strength curve fits well the measured strength along *x*-direction with a small deviation at high fibre concentration, it is underestimated at α= 90 °, along *y*-direction. For Tencel composite, the predicted strength is underestimated for both *x* and *y* directions. One of the possible explanations is that Tencel fibres are flexible and can be curved, such as they can be easily interlocked and build network-like structure. A part of energy was probably dissipated to make them straight or to break this structure before rupture or pulling-out, which is not taken into account in the model of Kelly and Tyson. The effective fibre length can be shorter than it

is really, which affects the predicted strength. For glass composites, strength in *y*-direction is well predicted by the Kelly and Tyson model. However, a deviation occurs at high concentration values such as the predicted strength is higher than the measured one. The most important reasons for the deviation in strength is the incertitude in the measured σ_f that can widely vary as a function of fibre diameter, matrix properties and the presence or not of a compatibilizer. Since we have not used any compatibilizer in this study, adding MAPP to the formulation of composite can improve the obtained tensile strength.
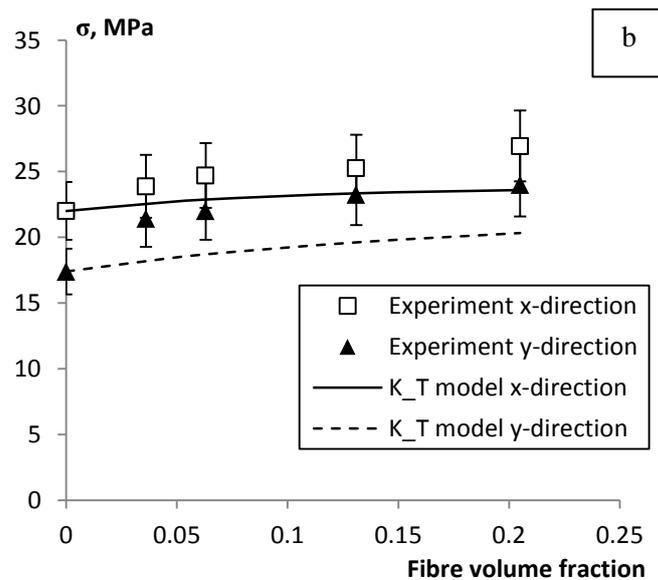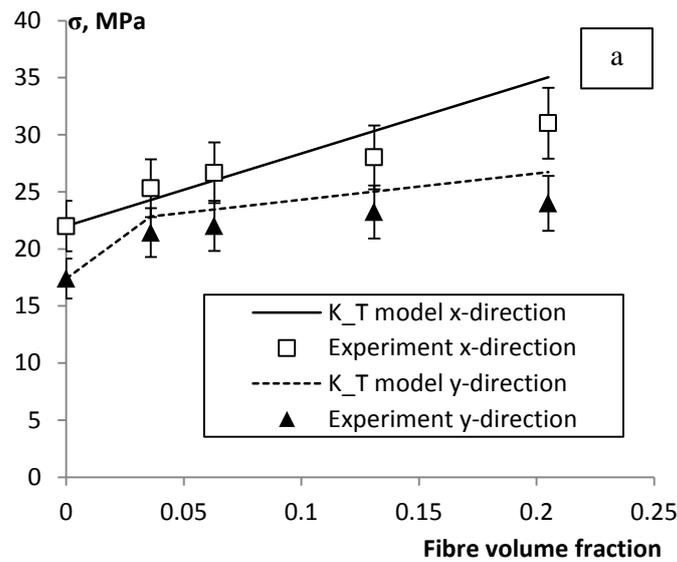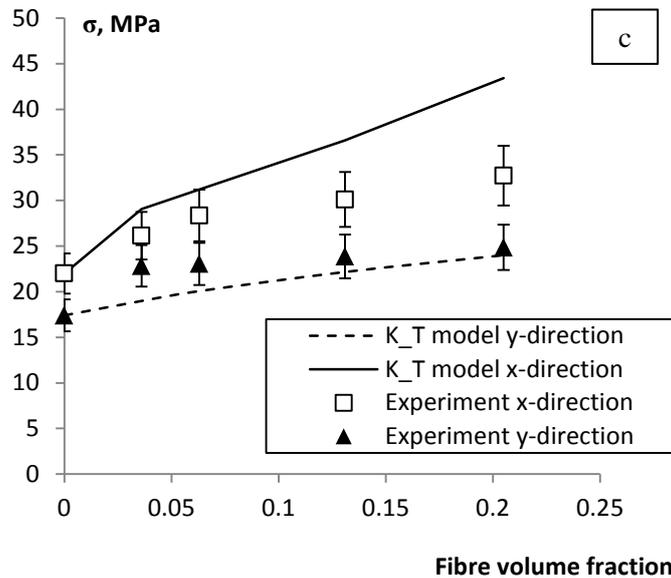
Figure 6.16

Experimental and Kelly-Tyson predicted tensile strengths (*x*-direction, α= 0 ° and *y*-direction, α= 90 °) as a function of fibre content, a) flax/PP b) Tencel/PP c) glass/PP

2.2. Impact properties

2.2.1. *Experimental results*

Figure 6.17 shows the impact strength U_c as a function of fibre volume fraction, for the neat PP and flax, Tencel and glass composites. The impact strength slightly decreases for 3.6 and 6.3 vol % of fibres compared to the neat PP, and then increases from 13.1 to 20.5 vol %, for all types of fibres used. This increase rate and the values at the highest fibre concentration is the highest for Tencel followed by glass and then by flax based composites. The decrease of reinforced polypropylene impact strength for 3.6 and 6.3 vol % can be explained by a large spacing among fibres, which probably causes an easy crack propagation. Lhymn and Schultz (1982) studied the crack morphology in injection moulded glass/PET (Polyethylene terephthalate) and demonstrated that crack path takes an irregular zig-zag shape propagating along the easiest and the weakest way around the main crack direction. Moreover, the crack tip progresses within composite by the connectivity between several discrete micro-cracks at the ends of fibres. As mentioned in Chapter 4, up to 6.3 vol % Chapter 5 fibre-fibre interactions become larger and a network-like structure starts to take place, and thus may push

the crack to get a longer way to progress prior the composite breakdown. Tencel composites exhibit a much larger number of flexible fibres as compared to glass and flax fibres, as demonstrated in Chapter 4 and 5. A more developed network of Tencel fibres creates cooperative obstacles against the crack propagation, leading to higher impact strength. This is the main plausible reason explaining that Tencel composite shows the highest impact strength at high concentration over glass and flax composites (Figure 6.17).
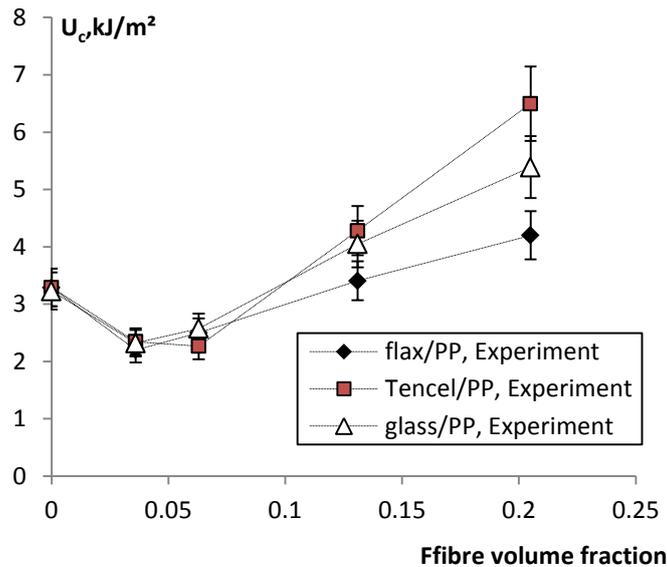
Figure 6.17

Impact strength of flax/PP, Tencel/PP and glass/PP, as a function of the fibre content. Lines are given to guide the eye

This impact strength depends also on the fibre orientation in the tested bar. Clemons et al. (2003) showed that fibres perpendicular to the crack direction enable higher impact strength. In our case, the impact samples were moulded separately and not cut from the moulded box as the way for tensile samples. The sample dimensions required for testing in agreement with the standard norms were not compatible with the dimensions of the box. The flow direction in the impact bar is perpendicular to the notch direction. By analogy to the microstructure in the box, a considerable part of fibres should be aligned along the flow direction, and thus perpendicular to the crack direction.

Basically, three rupture modes are possible, matrix fracture, fibre pull-out or debonding and fibre fracture, according to Cottrell (1964). The pull-out turned out the dominant rupture

mechanism for short fibre reinforced polymer [Cottrell (1964), Cooper (1970), Lhymn and Schultz (1982)]. To have a better understanding of the impact strength results, the rupture surfaces of 20.5 vol % composites were observed by SEM. Figure 6.18. a and c shows that the flax and glass fibres were debonded at the matrix-fibre interface (marks of fibres' tearing in the matrix), while some fibres were pulled out (black voids and empty space) and some others remain glued to the matrix. Figure 6.18.b shows that fracture can occur in the unsupported length of fibre. According to Lhymn and Schultz (1982), this is characteristically the result of fibre fatigue. Figure 6.18.e and f presents the case of Tencel, where large fibre-fibre interactions are observed. Some voids appear in Figure 6.18.f with a larger magnification, indicating fibres pull-out. Considering the SEM observations we can roughly conclude that all rupture modes are present in the rupture surface with a slight domination of the pull-out mechanism.
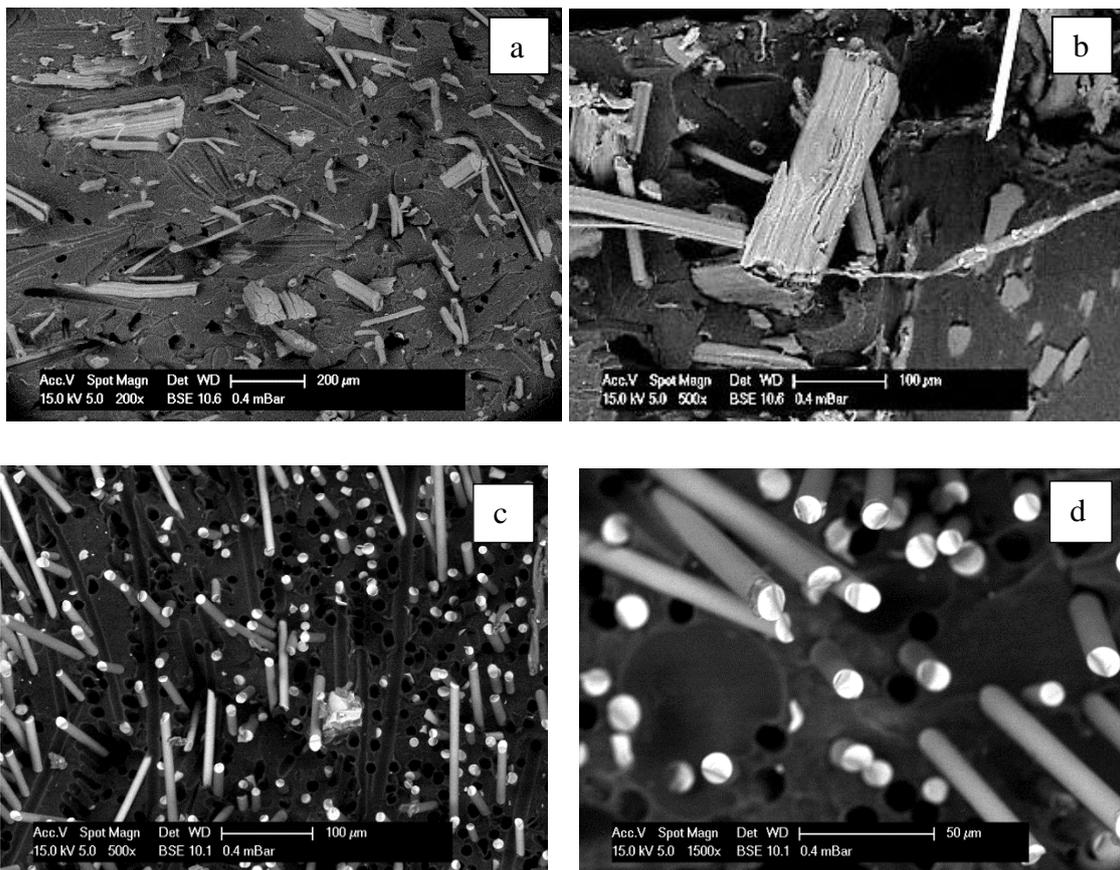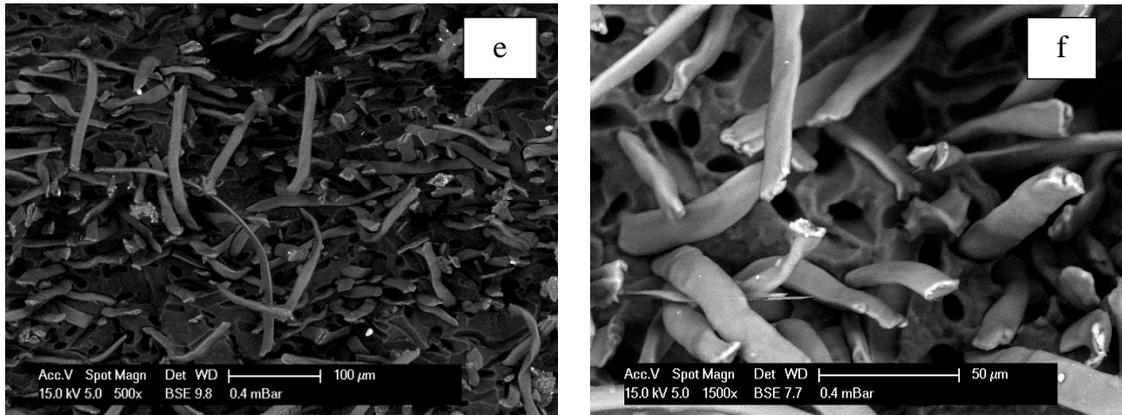
Figure 6.18

SEM images representing the fracture surfaces of 20 vol % composites for flax/PP (a,b), glass/PP (c,d) and Tencel/PP (e,f)

2.2.2. ***Predictions of composite impact properties and comparison with experimental results***

Figure 6.19 a, b and c show a comparison between the measured and calculated impact strength that is predicted by Thomason and Vlug model [Eq. 6.9] as a function of fibre content for flax/PP, Tencel/PP and glass/PP, respectively. The parameters L_c, σ_f and L are the same used earlier to model the tensile strength (Table 6.3). The debonding length L_d was determined by varying L_d in equation 6.9 to get the best fitting of the experimental curve. This results in L_d of 2.8 mm for flax, 6 mm for Tencel and 14 mm for glass fibre. According to Thomason and Vlug (1996), the debonding length obtained by fitting glass/PP composites varies between 8.7-18.2 mm to give a good agreement with experimental data. Moreover, it turned out that L_d increases as the critical length L_c increases. However, this fitting lost its physical signification, since L_d is much higher the possible fibre length in injection moulding process. Therefore the obtained results must be interpreted as a quantitative manner. The calculated impact strength of flax, glass and glass composites show an important deviation compared to experiment at low fibre concentration. That deviation becomes progressively smaller by increasing concentration until 20.5 vol % for which a good agreement with experiment is noted. The disagreement of the prediction at low concentration may be due to the low capability of the Thomas and Vlug model to predict the different mechanism of rupture within multilayer structured composite, considering that orientation of fibres was not taken into account in this model. The incertitude in fibre-matrix adhesion and fibre curvature

are also the reasons behind the deviations of the calculated values compared to experimental ones.
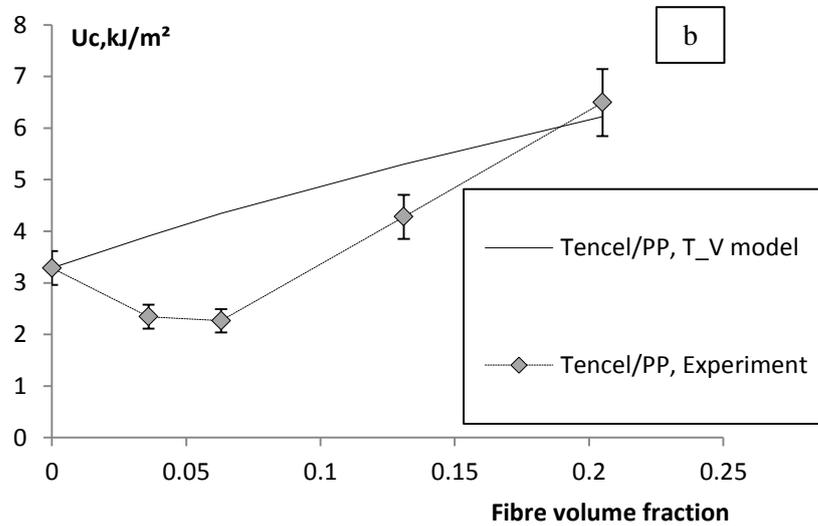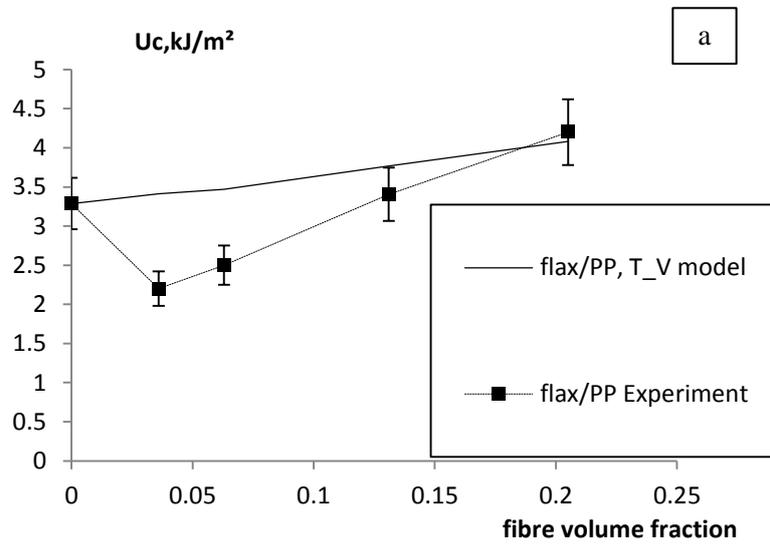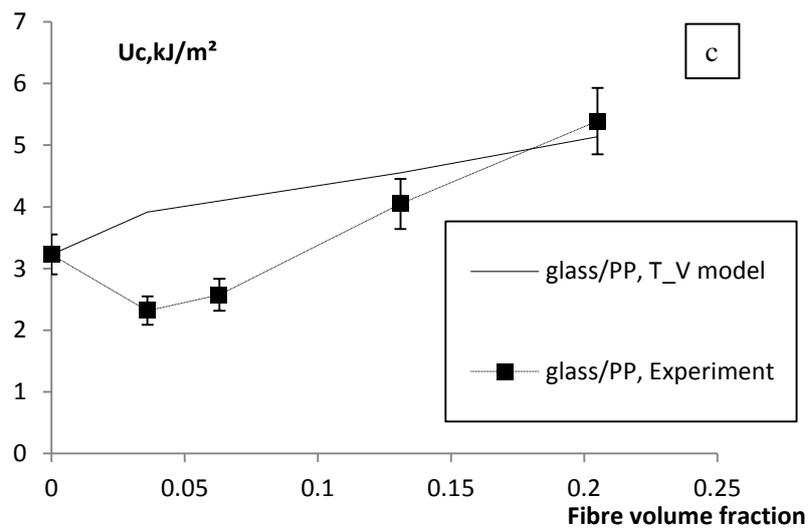
Figure 6.19

Experimental and calculated (according to Thomason and Vlug model, Eq.6.9) impact strength as a function of fibre content: a) flax/PP b) Tencel/PP and c) glass/PP

2.3. Conclusions

We investigated the tensile and impact properties of injection-moulded natural fibre reinforced polypropylene. We compared them with glass fibre composite based, using the same matrix. Fibre volume concentrations varied from 3.6 to 20.5 vol % and were the same for composites with different fibre types. The experimental values were compared to the corresponding calculated ones according to different models presented in the State of the art section. The microstructure of composites (particularly fibre orientation) was taken into account.

Tensile bars were cut from injected boxes with three orientations with respect to the main flow direction and their properties were investigated as a function of fibre type and concentration. Tensile experiments showed that all glass composites are stiffer and stronger as compared to flax and Tencel composites. Nevertheless, Tencel composites showed the highest elongation at break, around 13 %. Samples with the main axis oriented along the direction of flow exhibit higher tensile performance as compared with those oriented along 45° and 90°, for all studied composites.

Measured Young's modulus and tensile strength were compared to those predicted by Cox-Krenchel model for stiffness and Kelly and Tyson for strength. This was performed for tensile properties along the flow direction and perpendicular. We suggested a method to calculate the orientation factors in the models, based on the orientation analysis presented in Chapter 4. The predicted values increase with the fibre concentration, as experimentally. The predicted tensile stiffness and strength fit well the experimental ones in *y*-direction. The prediction overestimates the tensile properties in *x*-direction (main flow direction). The highest deviation (about 20 %) was particularly obtained for the tensile and strength at high concentration, when tensile direction is parallel to the flow. The main reasons are that no compatibilizer was used to improve fibre-matrix adhesion, the incertitude in the measurement of the fibre strength σ_f (particularly for flax fibres), the out-of-plane fibre orientation, the fibre bending and the skin fibre-free-layers. Most of these reasons were discussed in Chapter 4.

The investigation of composites' impact properties showed that Tencel based composites have the highest impact strength as compared to glass and flax reinforced composites. This was interpreted by the well-developed network structure of Tencel fibres due to their large number and flexibility that supposed to limit the crack propagation during failure. The experimental

results were compared to the impact strength calculated according to Thomason and Vlug model as a function of fibre content. A considerable deviation occurs at low fibre content and becomes smaller by increasing fibre concentration; this is true overall studied composites.

As already mentioned in the previous chapters, flax based composites are the most complex ones to be analysed. The complexity is related to the flax fibre morphology (bundles or fibres, various composition, flexibility, length and diameter) that leads to deviations between the theoretically predicted values and those experimentally obtained.

3. References

Adusumali, R. B., Reifferscheid, M., Weber, H., Roeder, T., Sixta, H., & Gindl, W. (2006, December). Mechanical properties of regenerated cellulose fibres for composites. In Macromolecular Symposia (Vol. 244, No. 1, pp. 119-125). WILEY-VCH Verlag.

Adusumalli, R. B., Müller, U., Weber, H., Roeder, T., Sixta, H., & Gindl, W. (2006, December). Tensile testing of single regenerated cellulose fibres. In Macromolecular Symposia (Vol. 244, No. 1, pp. 83-88). WILEY-VCH Verlag.

Aurich, T., & Mennig, G. (2001). Flow-induced fiber orientation in injection molded fit fiber reinforced polypropylene. Polymer composites, 22(5), 680-689.

Barkoula, N. M., Garkhail, S. K., & Peijs, T. (2009). Effect of compounding and injection moulding on the mechanical properties of flax fibre polypropylene composites. Journal of reinforced plastics and composites, 29 N9, 1366-1385.

Bax, B., & Müssig, J. (2008). Impact and tensile properties of PLA/Cordenka and PLA/flax composites. Composites Science and Technology, 68(7), 1601-1607.

Bay, R. S., & Tucker, C. L. (1992). Fiber orientation in simple injection moldings. Part II: Experimental results, Polym.Compos. 13,322-341.

Beckermann, G. W., & Pickering, K. L. (2009). Engineering and evaluation of hemp fibre reinforced polypropylene composites: Micro-mechanics and strength prediction modelling. Composites Part A: Applied Science and Manufacturing, 40(2), 210-217.

Bourmaud, A., Ausias, G., Lebrun, G., Tachon, M. L., & Baley, C. (2013). Observation of the structure of a composite polypropylene/flax and damage mechanisms under stress. Industrial Crops and Products, 43, 225-236.

Bowyer, W. H., & Bader, M. G. (1972). On the re-inforcement of thermoplastics by imperfectly aligned discontinuous fibres. Journal of Materials Science, 7(11), 1315-1321.

Charlet, K., Jernot, J. P., Eve, S., Gomina, M., & Bréard, J. (2010). Multi-scale morphological characterisation of flax: From the stem to the fibrils. Carbohydrate Polymers, 82(1), 54-61.

Clemons, C., Caulfield, D., & Giacomin, A. J. (2003). Impact toughness of cellulose-fiber reinforced polypropylene: influence of microstructure in laminates and injection molded composites. Series: Journal Articles.

Cooper, G. A. (1970). The fracture toughness of composites reinforced with weakened fibres. Journal of Materials Science, 5(8), 645-654.

Cottrell, A. H. (1964, October). Strong solids. In Proceedings of the Royal Society of London A: Mathematical, Physical and Engineering Sciences (Vol. 282, No. 1388, pp. 2-9). The Royal Society.

Cox, H. L. (1952). The elasticity and strength of paper and other fibrous materials. British journal of applied physics, 3(3), 72-79.

Folkes, M. J. (1982). Short fiber reinforced thermoplastics. JOHN WILEY & SONS, INC., 605 THIRD AVE., NEW YORK, NY 10158, 1982, 192.

Ganster, J., & Fink, H. P. (2006). Novel cellulose fibre reinforced thermoplastic materials. Cellulose, 13(3), 271-280.

Garkhail, S. K., Heijenrath, R. W. H., & Peijs, T. (2000). Mechanical properties of natural-fibre-mat-reinforced thermoplastics based on flax fibres and polypropylene. Applied Composite Materials, 7(5-6), 351-372.

Gironès, J., Lopez, J. P., Vilaseca, F., Herrera-Franco, P. J., & Mutje, P. (2011). Biocomposites from Musa textilis and polypropylene: evaluation of flexural properties and impact strength. Composites science and technology, 71(2), 122-128.

Halpin, J. C. (1969). Effects of Environmental Factors on Composite Materials (No. AFML-TR-67-423). AIR FORCE MATERIALS LAB WRIGHT-PATTERSON AFB OH.

Halpin, J. C., & Kardos, J. L. (1976). The Halpin-Tsai equations: a review. Polymer engineering and science, 16(5), 344-352.

Kalaprasad, G., Joseph, K., Thomas, S., & Pavithran, C. (1997). Theoretical modelling of tensile properties of short sisal fibre-reinforced low-density polyethylene composites. Journal of Materials Science, 32(16), 4261-4267.

Kalay, G., & Bevis, M. J. (1997). Processing and physical property relationships in injection-molded isotactic polypropylene. 2. Morphology and crystallinity. Journal of Polymer Science Part B: Polymer Physics, 35(2), 265-291.

Karmaker, A. C., & Youngquist, J. A. (1996). Injection molding of polypropylene reinforced with short jute fibers. Journal of Applied Polymer Science, 62(8), 1147-1151.

Kelly, A., & Tyson, A. W. (1965). Tensile properties of fibre-reinforced metals: copper/tungsten and copper/molybdenum. Journal of the Mechanics and Physics of Solids, 13(6), 329-350.

Krenchel, H. (1964). Fibre reinforcement; Akademisk Forlag: Copenhagen, 1964.

Landel, R. F., & Nielsen, L. E. (1993). Mechanical properties of polymers and composites. CRC Press.

Le Duc, A., Vergnes, B., & Budtova, T. (2011). Polypropylene/natural fibres composites: analysis of fibre dimensions after compounding and observations of fibre rupture by rheo-optics. Composites Part A: Applied Science and Manufacturing, 42(11), 1727-1737.

Le Moigne, N., van Den Oever, M., & Budtova, T. (2011). A statistical analysis of fibre size and shape distribution after compounding in composites reinforced by natural fibres. Composites Part A: Applied Science and Manufacturing, 42(10), 1542-1550.

Lhymn, C., & Schultz, J. M. (1983). Fracture behaviour of collimated thermoplastic poly (ethylene terephthalate) reinforced with short E-glass fibre. Journal of Materials Science, 18(7), 2029-2046.

Li, Y., Mai, Y. W., & Ye, L. (2000). Sisal fibre and its composites: a review of recent developments. Composites science and technology, 60(11), 2037-2055.

Nechwatal, A., Reußmann, T., Böhm, S., & Richter, E. (2005). The Dependence between the Process Technologies and the Effect of MAH-PP-Adhesives in Natural Fibre Reinforced Thermoplastic Composites. Advanced Engineering Materials, 7(1-2), 68-73.

Neves, N. M., Isdell, G., Pouzada, A. S., & Powell, P. C. (1998). On the effect of the fiber orientation on the flexural stiffness of injection molded short fiber reinforced polycarbonate plates. Polymer composites, 19(5), 640-651.

Papathanasiou, T. D., & Kamal, M. R. (1993). Filling of a complex-shaped mold with a viscoelastic polymer. Part I: The mathematical model. Polymer Engineering & Science, 33(7), 410-417.

Paunikallio, T., Kasanen, J., Suvanto, M., & Pakkanen, T. T. (2003). Influence of maleated polypropylene on mechanical properties of composite made of viscose fiber and polypropylene. Journal of applied polymer science, 87(12), 1895-1900.

Paunikallio, T., Suvanto, M., & Pakkanen, T. T. (2004). Composition, tensile properties, and dispersion of polypropylene composites reinforced with viscose fibers. Journal of applied polymer science, 91(4), 2676-2684.

Peijs, T., Garkhail, S., Heijenrath, R., van Den Oever, M., & Bos, H. (1998, February). Thermoplastic composites based on flax fibres and polypropylene: influence of fibre length and fibre volume fraction on mechanical properties. In Macromolecular Symposia (Vol. 127, No. 1, pp. 193-203). Hüthig & Wepf Verlag.

Plackett, D., Andersen, T. L., Pedersen, W. B., & Nielsen, L. (2003). Biodegradable composites based on L-polylactide and jute fibres. Composites Science and Technology, 63(9), 1287-1296.

Thomason, J. L., & Vlug, M. A. (1997). Influence of fibre length and concentration on the properties of glass fibre-reinforced polypropylene: Part 4. Impact properties. Composites Part A: Applied Science and Manufacturing, 28(3), 277-288.

Thomason, J. L., Vlug, M. A., Schipper, G., & Krikor, H. G. L. T. (1996). Influence of fibre length and concentration on the properties of glass fibre-reinforced polypropylene: Part 1 :Tensile and flexural, Compo.,: Part A : Applied Science and Manufacturing ,27 A (1995) 477-484.

Thomason, J. L., Vlug, M. A., Schipper, G., & Krikor, H. G. L. T. (1996). Influence of fibre length and concentration on the properties of glass fibre-reinforced polypropylene: Part 3. Strength and strain at failure. Composites Part A: Applied Science and Manufacturing, 27(11), 1075-1084.

Van den Oever, M. J. A., Bos, H. L., & Van Kemenade, M. J. J. M. (2000). Influence of the physical structure of flax fibres on the mechanical properties of flax fibre reinforced polypropylene composites. Applied Composite Materials, 7(5-6), 387-402.

Wambua, P., Ivens, J., & Verpoest, I. (2003). Natural fibres: can they replace glass in fibre reinforced plastics?. composites science and technology, 63(9), 1259-1264.

Wells, J. K., & Beaumont, P. W. R. (1988). The toughness of a composite containing short brittle fibres. Journal of materials science, 23(4), 1274-1278.

Chapter 7
Pressure and fibre orientation simulation: comparison to experiments

Numerical simulation of injection moulding is an important tool for analysing the process parameters and optimizing the final properties of parts. The main outputs of simulation software that can be experimentally evaluated are the pressure in the mould cavity and the fibre orientation. In this chapter, we will first present a brief literature review about the common computational techniques used in simulation of injection moulding, some results known from literature related to the cavity pressure and the fibre orientation models of rigid and flexible fibres. Second, we will present the experimental pressure results obtained during the injection moulding for the neat and fibre-reinforced polypropylene. The effect of viscosity variation due to the fibre type and fibre concentration will be correlated with pressure results and discussed. Third, we will compare the experimental pressure and the fibre orientation results to those numerically obtained with Rem3D®, the simulation software used in this study.

1. State of the art

1.1. Pressure in the mould cavity

Injection moulding is an intermittent cyclic process with three main stages: (1) filling, (2) packing and holding (3) cooling (Figure 7.1). These stages can be observed by following the pressure in the cavity. Filling is the stage when the melt flows into an empty cavity whose walls are held at a temperature below the solidification one. Once the cavity is full, additional material is packed into the mould to counterbalance the shrinkage caused by cooling, and thus pressure increases sharply to a plateau maintained for some time. After holding/packing step, cooling stage occurs, enabling the ejection of the component and the decrease of pressure.
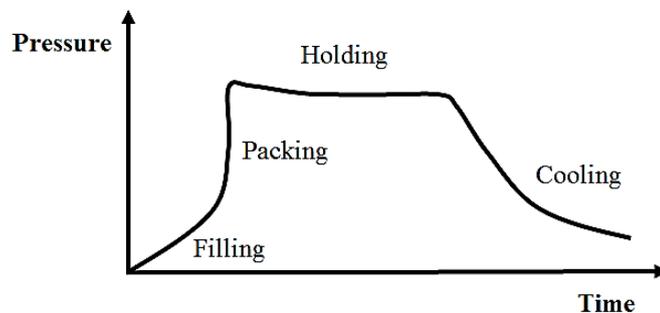
Figure 7.1

Pressure curve in the mould cavity showing the stages of a typical injection moulding cycle

Filling stage is the most comprehensively studied stage of injection moulding process [Papathanasiou and Guel (1997)]. The relevant feature of the mould filling is the existence of an advancing front. The filling stage has a great influence on the final properties of moulded fibre-reinforced thermoplastics because, as seen in Chapter 4, fibre orientation is dependent on the flow within the cavity.

1.2. Computation of injection moulding

The use of computational techniques for analysing the flow during mould filling started in the 1970s with Kamal and Kenig (1972 a,b) and Kuo and Kamal (1976). The level of sophistication increased in 1980s [Hieber and Shen 1980; Hieber et al. (1983)] with the incorporation of the finite element method to solve the Hele Shaw equations for thin gap geometry with a viscous non-Newtonian behaviour law. Shen (1984) introduced the energy equation to compute the heat transfer in the mould cavity. The consideration of viscoelasticity and fountain flow were introduced by Kamal et al. (1986) and Mavridis et al. (1988). The coupling between filling and

post-filling stages (packing, holding and cooling) was performed by Chiang et al. (1991,a,b). Further studies were performed in the two past decades to optimise the computation time by implementing sophisticated techniques. Most of today's simulation software are founded on the Hele-Shaw approach [Papathanasiou and Guell (1997)]. The reason is that injection moulded parts classically present a thickness smaller than other dimensions and there are no sudden variations of thickness, which is in agreement with Hele-Shaw assumptions. The approach of Hele-Shaw mainly consists of coupling a pressure equation to an energy equation through a temperature-dependent viscosity that can be the Arrhenius or the Williams-Landel-Ferry functions. The energy equation represents the heat convection due to the melt advancement, the heat conduction (due to the difference of temperature between cavity walls and the melt) and viscous dissipation. Manzione (1987) coupled the flow and heat transfer analysis in the cavity, the heat transfer in the mould and included the cooling channels influence. If such coupling is not possible, the boundary condition at the polymer–mould surface can be either a constant wall temperature or a heat transfer coefficient.

1.3. Experimental pressure and comparison with simulation

Few works in literature have dealt with the pressure evolution in the mould cavity. Moreover, most of the studied cases used an unreinforced polymer material. In the following, we will focus on the results that concern the neat polypropylene, because it is the polymer matrix used in the present study. Two examples of polypropylene studies, Chiang et al. (1991) and Han and Im (1997), will be presented. All conditions of injection moulding are regrouped in Table 7.1.

Table 7.1 Conditions of the injection moulding of polypropylene in Chiang et al. (1991) and Han and Im (1997) studies

	Chiang et al. (1991,b)	Han and Im (1997)
Cavity thickness (mm)	2.54	2
Melt temperature (°C)	200	180
Flow rate (cm^3/s)	26.8	7.4
Fill time (s)	0.69	1.5
Hydraulic hold pressure (MPa)	6.9	-
Holding duration (s)	>15	6
Coolant temperature (°C)	32	40

Chiang et al. (1991,b) investigated the filling and the post-filling pressure of polypropylene in a sprue-gated plaque. The pressure measurement was carried out by three transducers located in the cavity as shown in Figure 7.2.
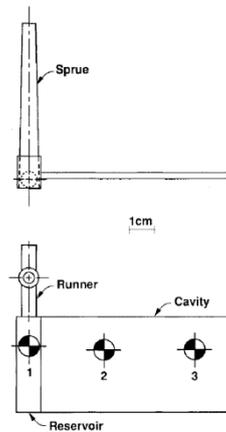
Figure 7.2

Representation of the cavity and the locations of the pressure transducers [Chiang et al. (1991,b)]

The experimental pressure measured in the transducer 1 was imposed as an input pressure for the simulation of the plaque injection moulding. A superposition of the predicted pressures at locations 2 and 3, and the experimental pressures in locations 1, 2 and 3 is presented in Figure 7.3.a. The first part of the pressure curve (0 s < t < 0. 69 s) represents the filling pressure, while the rest of the curve (t > 0.69 s) represents the post filling pressure i.e. the packing,

216

holding and cooling phases. The predicted pressures at locations 2 and 3 are in agreement with the experimental ones at the same locations, except in the cycle end, where a slight deviation happened. Silva (2007) reproduced the numerical simulation of Chiang et al. (1991,b) by using Rem3D® (the software used in this study). The pressures obtained by Rem3D® are close to the ones numerically obtained by Chiang et al. (1991,b) except pressure at location1, because the referred authors (Chiang et al. (1991,b)) used the data of this transducer as boundary conditions (Fig. 7.3b). The filling sequence of Rem3D® simulation is presented in Figure 7.4.
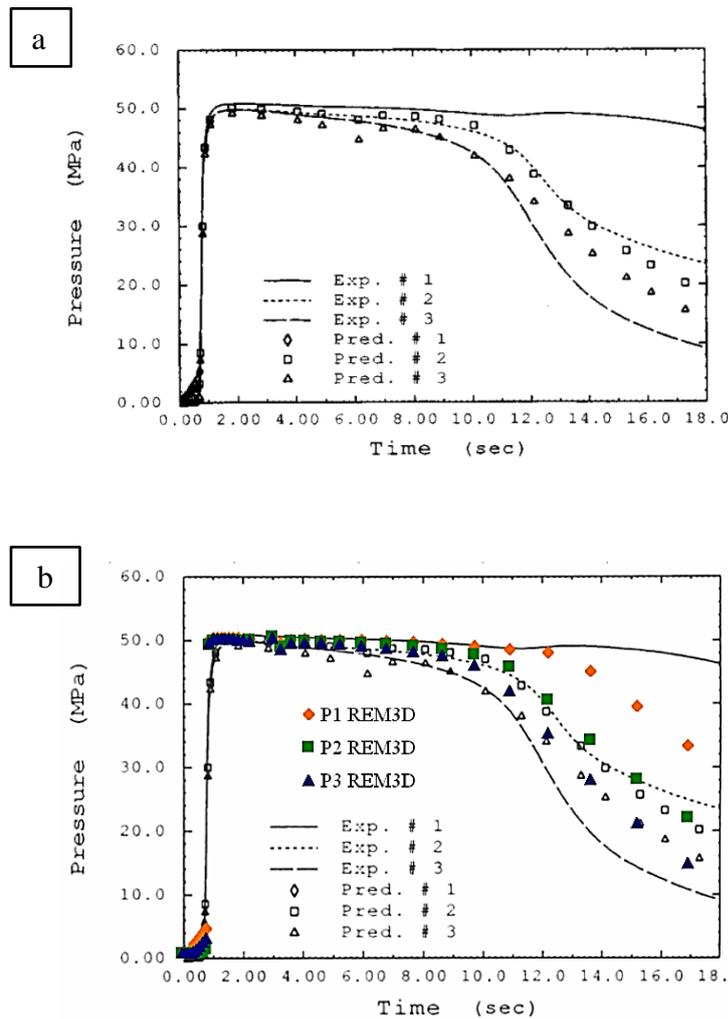
Figure 7.3

a) Pressures in experiment (solid lines) and predicted (symbols) for two transducers located in the plaque [Chiang et al. (1991)]

b) Pressures predicted by Rem3D® (coloured symbols) [(Silva 2006)]
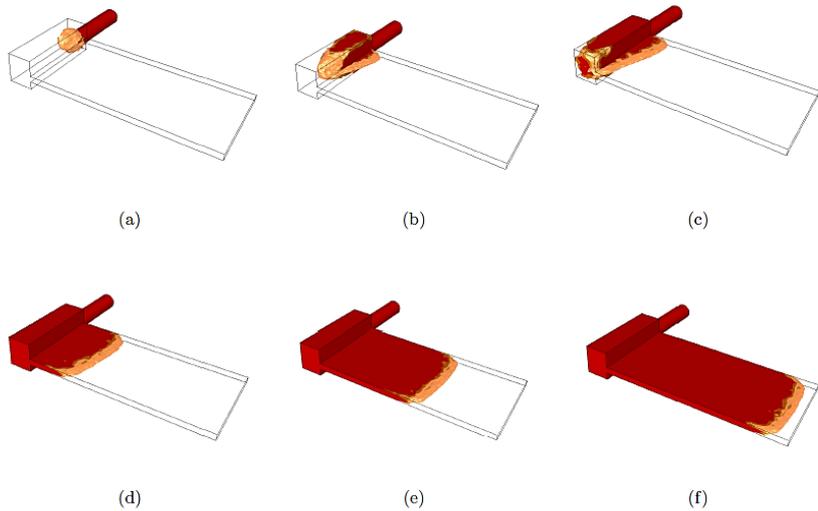
Figure 7.4

Filling of the plaque obtained by Rem3D$^{®}$ [(Silva 2006)]

Han and Im (1997) simulated the filling and the post filling phases of polypropylene within the cavity presented in Figure 7.5.a. The predicted melt front advancement is presented in Figure 7.5.b. The cavity is filled in the order: lower, upper, right and left cavities.
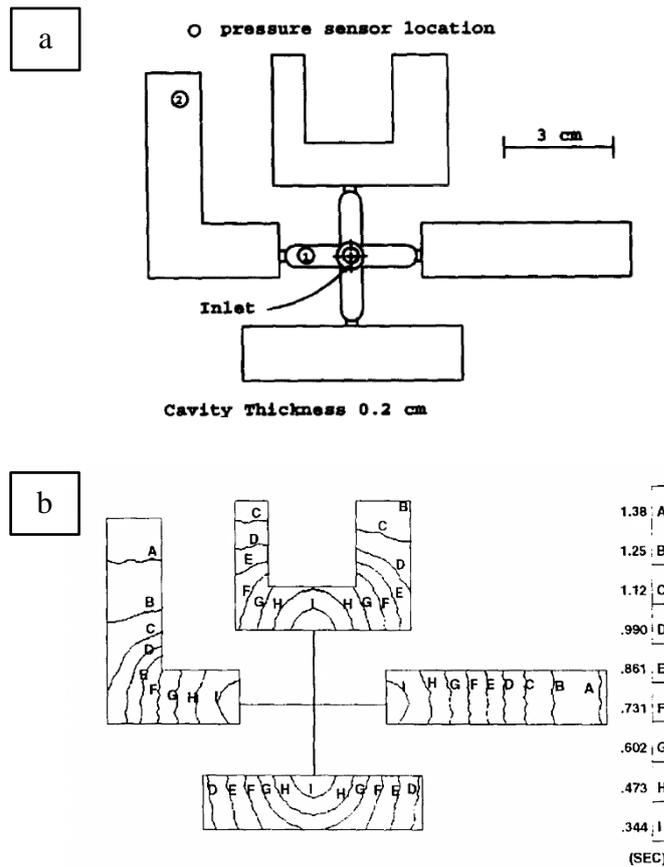
Figure 7.5

a) Sprue, runners and cavity design and the location of pressure transducers, b) the predicted melt flow advancement [Han and Im (1997)]

Figure 7.6 shows that the experimental and the predicted pressure curves are similar. The predicted pressure P1 closely fits the experimental one for filling and post filling stages. However, the predicted pressure P2 (pressure in location 2, Figure 7.5.a) exhibits a deviation at the post-filling stage by almost 20 %. The authors justified that by the inaccuracy of the thermal properties used in calculations.
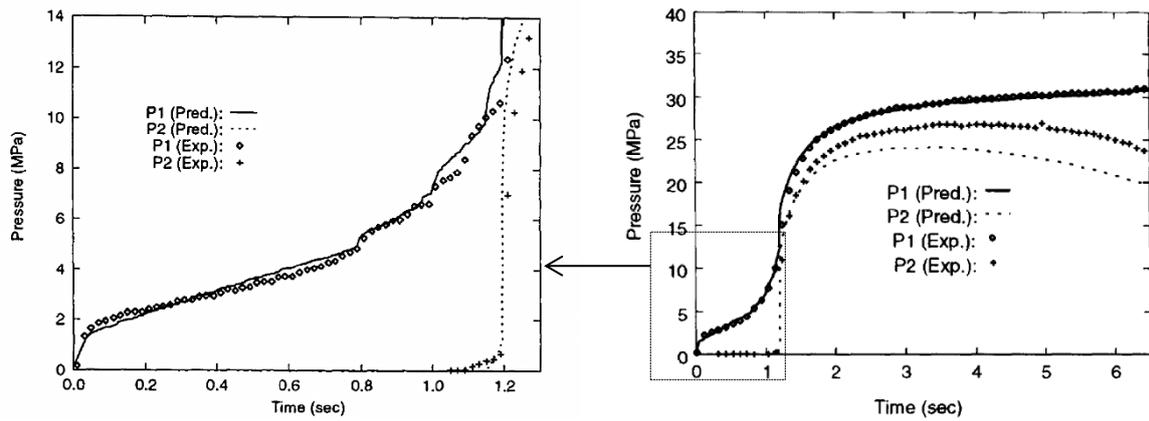
Figure 7.6

Experimental and predicted pressures in the cavity, the left hand figure is a zoom of the dashed rectangle of the right hand figure [Han and Im (1997)]

The filling phase simulation of the sprue-centre gated-box (the moulded part in this study) was performed by Agassant et al. (1996). Figure 7.7 shows the pressure isovalues in the box filling. The top side fills to some extent the big lateral sides and then the smaller lateral ones.

$t_1 = 0.09$ s

$t_2 = 0.15$ s

$t_3 = 0.21$ s

$t_4 = 0.27$ s
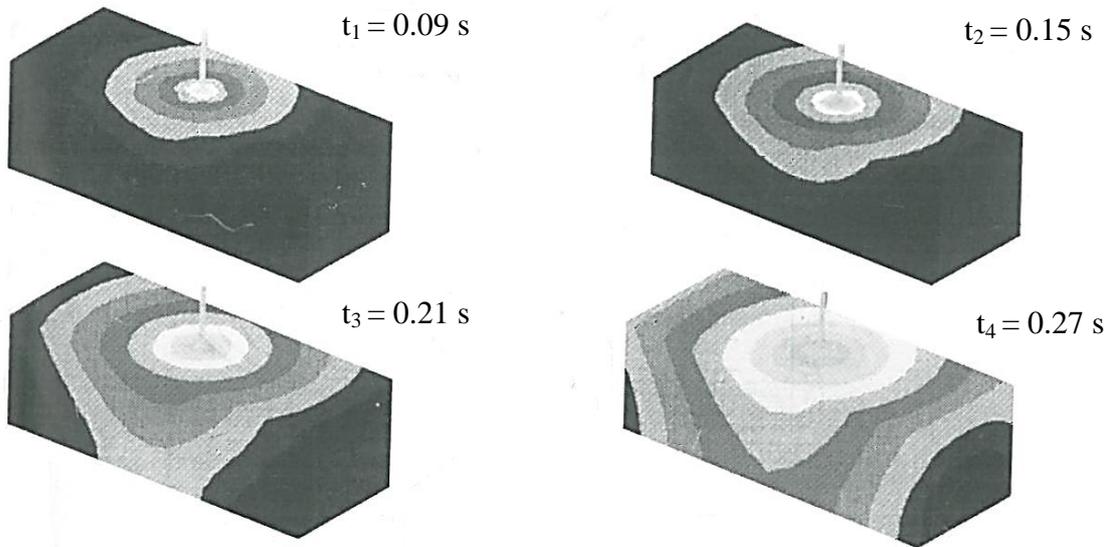
Figure 7.7

Isovalues of pressure at different filling times (t_1, t_2, t_3 and t_4) of the sprue-centre gated-box [Agassant et al. (1996)]

1.4. Prediction of fibre orientation

1.4.1. *Rigid fibres' models*

The modelling of fibre orientation began with Jeffrey equation [Jeffery (1922)], considering a single ellipsoid of aspect ratio *L/D* (in fact Jeffery considered ellipsoids with three different axes, but we will restrain here the analysis to two different axes) immersed in a Newtonian fluid. The unit vector *p* is parallel to the major axis, as shown in Figure 7.8. The orientation of p is a function of two angles θ and φ.
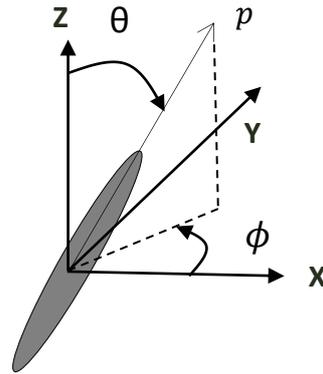
Figure 7.8

Ellipsoids orientation representation

The motion of the vector p is described as follows:

$$\dot{p} = \frac{Dp}{Dt} = \Omega.\,p + \Gamma[\dot{\boldsymbol{\varepsilon}}.\,p - \dot{\boldsymbol{\varepsilon}}{:}\,ppp] \qquad \text{[Eq. 7.1]}$$

where $\Gamma = \frac{(L/D)^2 - 1}{(L/D)^2 + 1}$, Ω and $\dot{\boldsymbol{\varepsilon}}$ are vorticity and rate of deformation tensors, respectively.

Jeffery's analysis is only valid for rigid fibres in a dilute regime. To take into account fibre-fibre interactions, Folgar and Tucker (1984) introduced the orientation tensor evolution and added a diffusion term D_r (see Eq. 7.3) such as:

$$D_r = C_I \dot{\gamma} \qquad \text{[Eq. 7.2]}$$

$$\frac{Da_{ij}}{Dt} = \Omega.\,a_{ij} + \Gamma[\dot{\boldsymbol{\varepsilon}}.\,a_{ij} - 2\dot{\boldsymbol{\varepsilon}}{:}\,a_{ijkl}] + 2\,D_r(I - 2\,a_{ij}) \qquad \text{[Eq. 7.3]}$$

$\dot{\gamma}$ is the generalized shear rate and C_I is the interaction coefficient, a dimensionless number usually taken lower than 10^{-2} to enable a good fit with experimental fibre orientation data. The evolution of the second order orientation tensor a_{ij} (Eq. 7.3) requires the knowledge of the

221

fourth order orientation tensor a_{ijkl}. To cope with this, dedicated approximations are suggested in the literature for representing the fourth order orientation tensor as a function of the second order one. The simplest closure approximations are: linear closure Hand (1962), quadratic closure Doi (1981), hybrid closure Advani and Tucker (1987) and Orthotropic closure approximation Cintra and Tucker (1995). More sophisticated approximations appeared after the latter one, and they are still a research area. New equations for the time evolution of a_{ij} have appeared, bringing a better precision for the orientation field by a strain reduction factor and/or anisotropic fibre-fibre interactions [Huynh (2001); Chung and Kwon (2002 a,b); Sepehr et al. (2004 a,b,c); Wang et al. (2008); Férec et al. (2009)]

1.4.2. *Flexible fibres' models*

The individual flexible fibre is considered as an assembly of multiple rigid parts linked to each other. The most relevant models are the bead-chain model, needle-chain model and rod-chain model. Yamamoto and Masyoka (1993; 1994) developed a bead-chain model for flexible fibre in dilute regime without hydrodynamic interactions. The flexible fibre is represented by a series of spheres lined up and bonded to each other (Figure 7.9). Yamamoto and Masyoka (1995; 1996) modified their first model to take into account the hydrodynamic interactions.
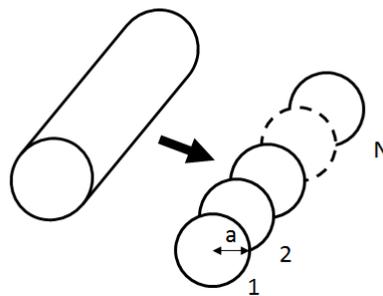
Figure 7.9

Bead chain model, a is the radius of beads

Ross and Klingenberg (1997) suggested a new representation of flexible fibres by a series of rigid spheroid connected through ball and socket joints, currently called the needle chain model (Figure 7.10). The difference from Yamamoto and Masyoka model is in the joints whose resistance can be varied to adapt the model for various flexibilities. The rotation period in shear flow of the needle chain model is in agreement with Jeffrey's equation for rigid fibres

and Forgacs and Mason (1959) experimental results for flexible fibres. However, this model did not take into account the hydrodynamic interactions, and it is limited to the dilute regime. Schmid et al. (2000) introduced the notions of the irregular fibre equilibrium and the frictional fibre interactions into the needle chain model to develop a model called the particle-level model. Further improvements in this model were carried out by Switzer (2002) to well describe the relationship between fibre properties, fibre interactions and rheological properties under a simple shear flow.
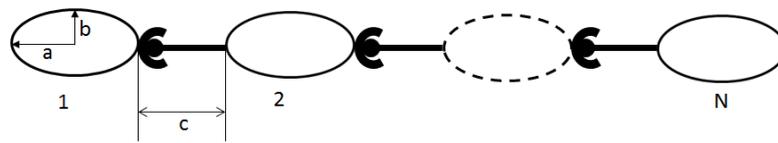
Figure 7.10

Needle chain model, a, b and c are the major and the minor axis of the ellipsoids and the distance between two successive ellipsoids, respectively.

Wang et al. (2006) proposed the rod-chain model that consists of a series of rigid rods. Each rod is itself a series of beads. The length of rod can vary with the number of beads inside, which is a way to model the extent of fibre flexibility (Figure 7.11). The rod chain model is similar to the needle chain model but used a different concept to assess the internal constraint forces.
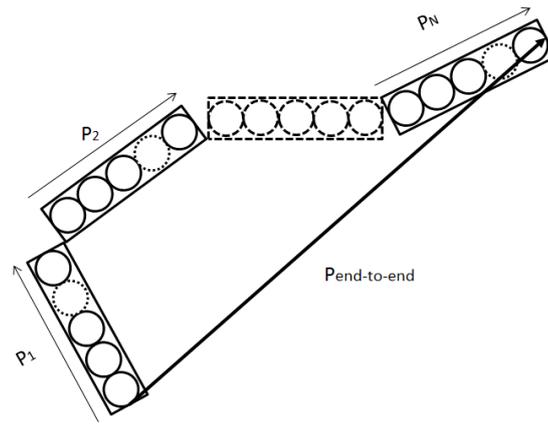
Figure 7.11

Rod-chain model, P_i are the unit vectors of each rod

1.5. Examples of simulation and comparison with experiment

The modelling of flexible fibre suspensions has not reached the level of rigid fibre suspensions. Most of the results related to flexible fibres' models have dealt with a dilute regime system. The prediction of the orientation of rigid fibres has been well developed, considering the important progress in modelling and the wide experimental studies of glass fibre-based composites. First, we will focus on Bay and Tucker (1992) study, using a modified Jeffry model, taking into account the coefficient of interaction of Folgar and Tucker (Eqs.7.2 and 7.3), without any optimisation for slowing the kinetics of fibre orientation or fibres interactions; *this is the same model used in Rem3D® software used in this study.* Second, we will present three main results using improved models that slow down the fibre orientation to closely match the experimental orientation: 1) strain reduction factor (SRF) [Huynh (2001), Wang (2007)] 2) reducing strain closure (RSC) [Wang et al. (2008)], and 3) anisotropic rotary diffusion (ARD) [Phelps and Tucker (2009)].

Bay and Tucker (1992) investigated the fibre orientation in two different injection-moulded parts (film gated strip and a centre gated disk). The composite material was 43 wt % glass/Nylon 6-6. The authors performed a comparison between the measured fibre orientation using the ellipses method (See Chapter 4) and the simulation results. Figure 7.12.a represents the predicted and the experimental orientation components (a_{xx} and a_{zz}) of the film–gated strip. x is the main flow direction and z is the direction perpendicular to the plaque plane. The value of $C_I = 0.01$ was chosen to fit the measurement. Γ was taken as 1[Eq. 7.1], meaning that the aspect ratio was considered as infinite. The inlet orientation ($a_{xx}= 0.5$, $a_{yy}= 0.2$, $a_{zz}= 0.3$

and $a_{xy} = a_{xy} = a_{xy} = 0$) that is the initial condition for the fibre orientation equation resolution was determined by experimental measurements near the gate. The computed orientation shows a typical core-shell structure that fits the experimental ones. According to the authors, the surprising rise in the predicted a_{xx} at the surface is an artefact of the calculation related to the fountain flow calculation. Figure 7.12.b represents the predicted and the experimental orientation components (a_{xx} and a_{zz}) for the centre–gated disk. The same parameters $C_I = 0.01$ and $\Gamma = 1$ are again used, since the same material has been used for the centre-gated disk and the film-gated strip. The inlet orientation was assumed to be random in space (($a_{xx} = a_{yy} = a_{zz} = 1/3$ and $a_{xy} = a_{xy} = a_{xy} = 0$). However, compared to the strip, the choice of the inlet orientation had almost no influence on the fibre orientation because the circumferential stretching flow is strong within the disk.
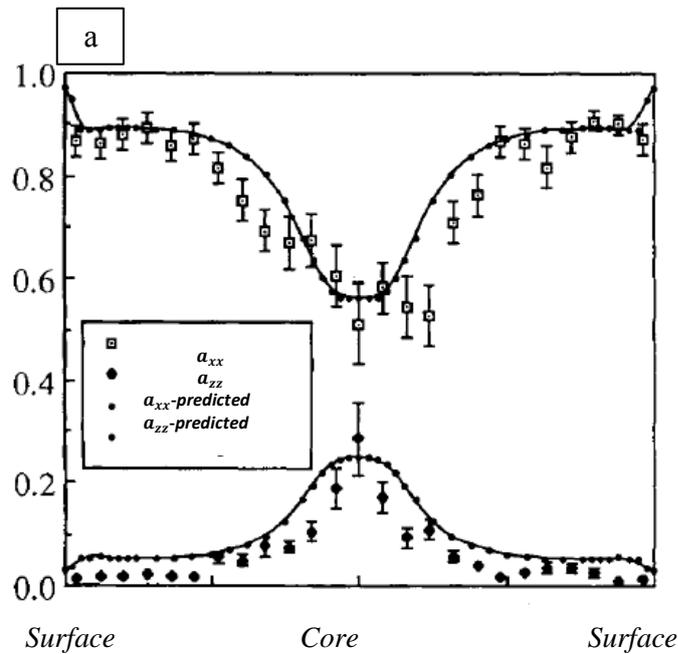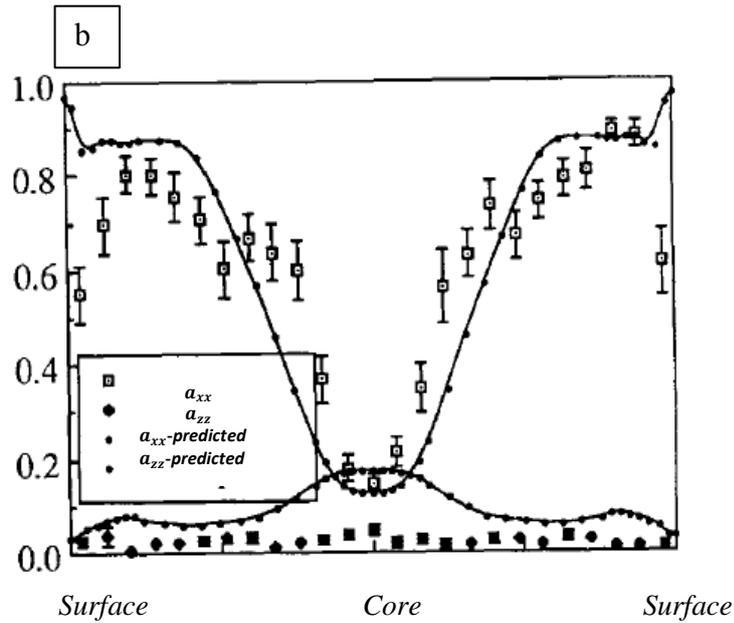
Figure 7.12

Comparison between the experimental and the predicted orientation components at a position of 5.7 times the part thickness a) in the film- gated strip b) in the centre gated disk [Bay and Tucker (1992)]

For a further position from the gate (40.4 times the disk thickness), a considerable deviation turned out between the predicted and the experimental orientation. The predicted a_{xx} at the core is much lower than the experimental one. The core, measured in experiment, gets larger compared to the position near the gate and there is preferred orientation somewhere between the shell and the core layers, which is also not well predicted by simulation. According to the authors, this is due to the circumferential stretching dominating the flow in the disk.

Bay and Tucker (1992) examined the sensitivity to the processing conditions for the same glass fibre-reinforced polyamide 6-6 in the disk mould. The obtained results showed that varying the wall temperature from 337 to 357 K and the inlet temperature from 540 to 560 K has a slight influence on the fibre orientation. The variation of the filling time controls to some extent the thickness and the orientation of each layer across the disk thickness. For example, a short filling time prevents the appearance of a skin layer (layer between shell layer and wall) and a long filling time enables a more aligned core.

Bay and Tucker (1992) examined also the effect of the coefficient of interaction C_I. They found that increasing this coefficient leads to move orientation towards random-in-space and to increase the thickness of the shell layer. Decreasing C_I makes the fibres in core more aligned perpendicular to the flow and in the shell more aligned parallel to the flow direction.

Finally the authors highlighted that the deviation in the prediction occurs at the transition between core and shell. They argued this deviation by the closure approximation used in the model. The effect of the closure approximation is to overestimate the out-of-plane orientation (greater a_{zz} and a_{xz} than expected), which results in thinner core and thicker shell as compared to experiment. In their study, Bay and Tucker (1992) used a hybrid closure approximation. A closure approximation that provides a smaller out-of-plane-orientation would give a better agreement between simulation and experiments.

Wang (2007) investigated the fibre orientation as the same geometries to Bay and Tucker (1992) (film gated strip and a centre gated disk) for 30 wt % glass/PBT (polybutylene terephtalate). Figure 7.13 shows that the improved Folgar and Tucker model including the strain reduction factor [Huynh (2001)] fits better the experimental orientation than the original Folgar and Tucker model.
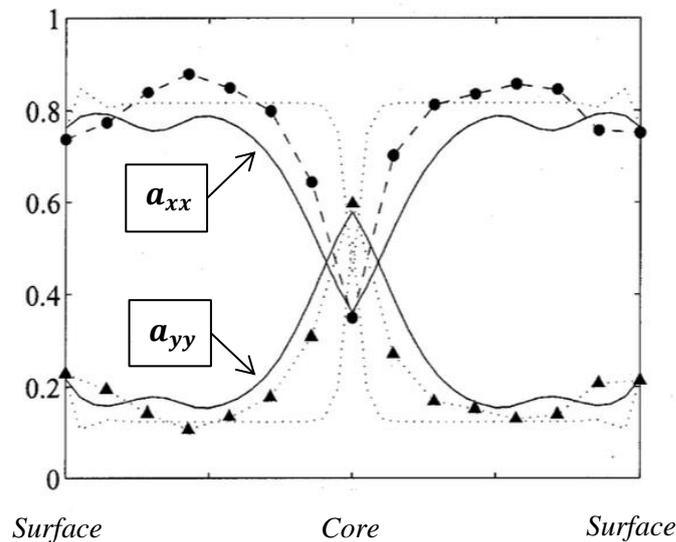
Figure 7.13

Fibre orientation comparison of experimental data (points) with predictions using standard model (dotted line) and SRF model (solid lines) for 1.5 mm thick strip [Wang (2007)]

According to Wang et al. (2008), even if the SRF provides a good match with experiment, its generalization is inconsistent because the model does not pass the rheological objectivity principle. Therefore, the authors suggested an objective model using reducing strain closure (RSC) to provide slower orientation kinetics. Another area of upgrading Folgar and Tucker family-models is the fibre interactions. Fan et al. (1998) and Phan-Thien et al. (2002) replaced the coefficient of interaction C_I by a second-order tensor C. This makes the rotary diffusion isotropic. Building on the latter work, a great improvement of this assumption was reached by Phelps and Tucker (2009) by assuming that the rotary diffusion is *anisotrocpic*. Figure 7.14 shows a comparison between orientations measured within part shaped as an end gated-strip made of 40 wt % glass/polypropylene and predicted by RSC assumption model and mixed ARD-RSC model. RSC and ARD-RSC models considerably improve the results precision. However, a deviation is still remained at the core. According to Phelps and Tucker (2009), these errors could mainly come from differences of the melt temperature.
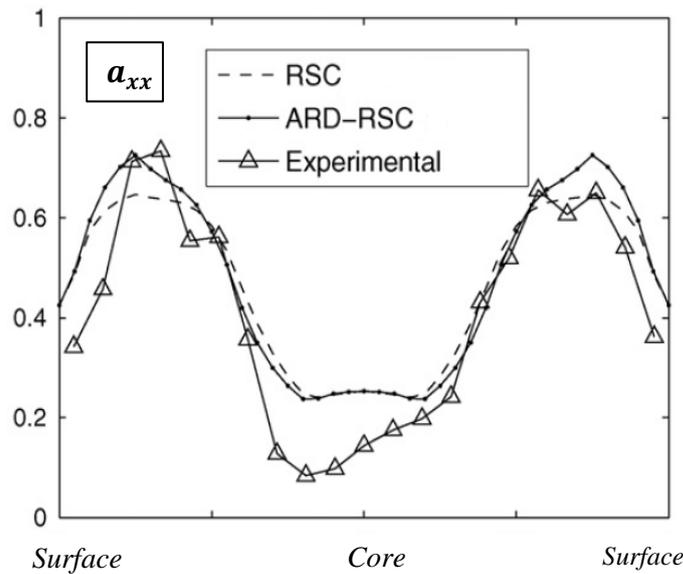

Figure 7.14

Fibre orientation comparison of experimental data (points) with predictions using standard RSC model and ARD-RSC model for 3 mm thick strip [Phelps and Tucker (2009)]

1.6. Conclusions

The state of the art presented in this section copes with the simulation of the pressure during injection moulding and the orientation of fibres in the cavity. Some studies that handled the

computation of the pressure in the filling and the post filling stages were presented. While the predicted pressure in the filling stage is close to experimental results, some deviations were noted in the post filling stages. Moreover, the investigations were limited to unfilled thermoplastics and no studies have yet emerged in literature to assess the pressure for fibre-reinforced thermoplastics. The main models classically used to compute the rigid and the flexible fibre orientation were briefly presented. Rigid fibres' models are well optimized, but more works must be done to improve the flexible fibres models. This is due to the complexity of the equations that describe the flexible fibres' orientation and calculation issues when moved from dilute regime to semi-dilute and concentrated regimes (fibre bending, fibre interactions…). Natural fibres contain elementary flexible fibres and rigid bundles. Therefore, computing the flexible fibres orientation is in our interest, but no further investigation is performed in this study, considering the lack of today's numerical tools to simulate such complex materials. The optimization of flexible fibres' models must be separately studied. We thus focused on the literature of the rigid fibres' models, which provides glass fibres orientation results in injection moulded parts, and they can be compared with experiments. The predicted results give a shell-core structure similar to the experimental one. Many factors can influence the computed orientation such as rheological and heat transfer data, the closure approximation and the interaction coefficient. Inaccuracies of these factors can probably cause some errors in the prediction.

2. Results and discussions

2.1. Experimental Pressures

The aim of this section is to understand the effect of fibre concentration and fibre type on the measured pressures. Neat PP and all the studied composites were moulded in the same conditions (summarized in Chapter 2). The experiments were repeated until reaching a stable thermal regime. The three last trials were then recorded. The range of variation in the measured pressure is around +/-10 %. We filtered the parasitic signals and averaged the measurements to get smooth pressure curves suitable for investigations.

2.1.1. *Influence of the location of pressure measurement*

The mould is equipped with three transducers located at different sites within the cavity. Transducer 1 is close to the gate, transducers 2 and 3 are placed at the end of the box top-side and at the small lateral side, respectively (Figure 7.15).
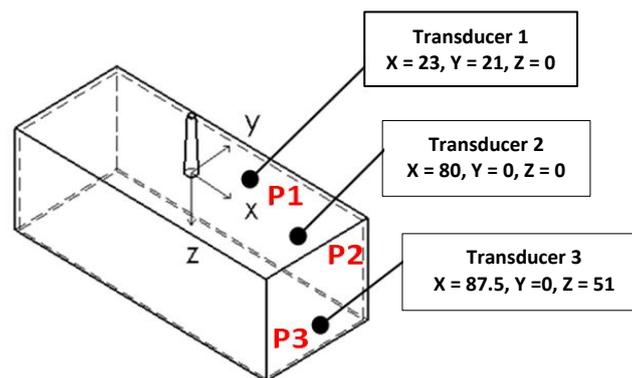
Figure 7.15

Location of the pressure transducers in the cavity (distances in mm)

Figure 7.16 shows the pressure evolution for the 20.5 vol % Tencel/PP. Similar curves were obtained for flax and glass based composites. In the filling stage, the pressure starts to rise when the flow front reaches the transducers and falls down when the melt gets frozen.

At the switch-over point, (from filling with speed control to packing with pressure control, around 0.7 s) there is a sharp increase of pressure. After the pressure overshoot, the transducer 1 shows a plateau-like curve between 1.6 and 4.2 s. Then, the pressure falls rapidly down. In fact, around 4.2 s, the polymer is solidified somewhere between the cavity entrance and the transducer. The polymer around the transducer does not feel anymore the pressure imposed by

the machine; and as it cools down, it shrinks and applies less stress on the transducer. The solidification will occur first around the thinnest area of the cavity that is located on the top box side. An order of magnitude of the cooling time is generally given by e^2/a, where "e" is the half thickness (here 0.9 mm) and "a" the thermal diffusivity (of the order of 10^{-7} m^2/s for a polymer), leading to an estimate of 8 s.

After the switch-over point, the P2 presents a "decreasing plateau-like" answer and falls down 1 s earlier than P1. P3 shows a direct pressure drop 3 s earlier than P2. The reason is that the melt solidification occurs earlier as far as the entrance is (more polymer cooling due to a longer path and less influence of new hot material coming up during the packing stage). While an important pressure drop occurs from P1 to P2, only a slight loss of pressure can be noted between P2 and P3.
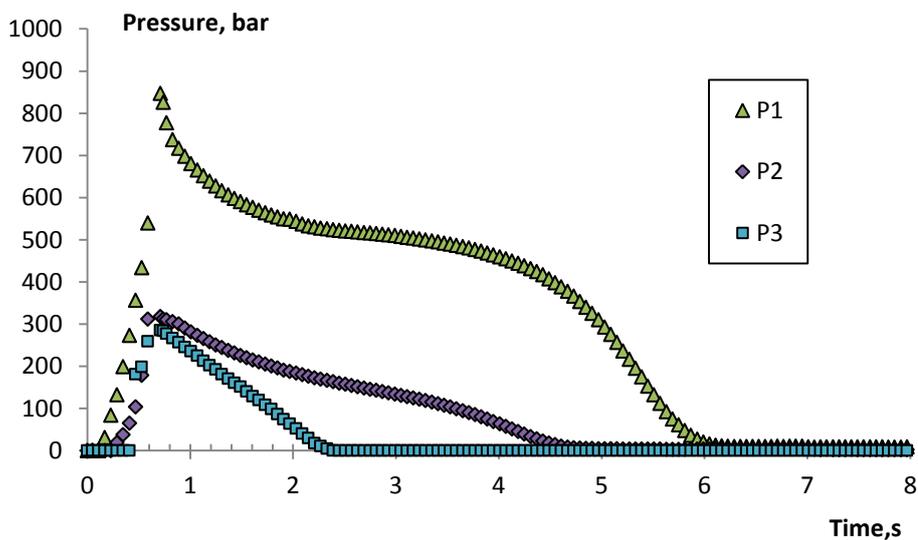
Figure 7.16

The pressures P1, P2 and P3 during the injection moulding of 20.5 vol % Tencel/PP

2.1.2. *Influence of fibre concentration*

Figure 7.17.a and b shows the evolution of the pressure (P1) throughout time for the neat polypropylene and Tencel composites with different concentrations. During the filling stage, the pressure increases as the fibre content gets larger (Fig. 7.17b). This is because of the viscosity increase when adding fibres, as discussed in Chapter 5. The level of the plateaus during the packing stage for the different composites is also correlated to the fibre content. The end of the plateau is around 5.7 s for the neat PP and 3.6 vol %, 5.3 s for 6.3 vol %, 4.7 s

for 13.1 vol % and 4 s for 20.5 vol %. We can conclude that solidification occurs earlier when the fibre concentration increases.
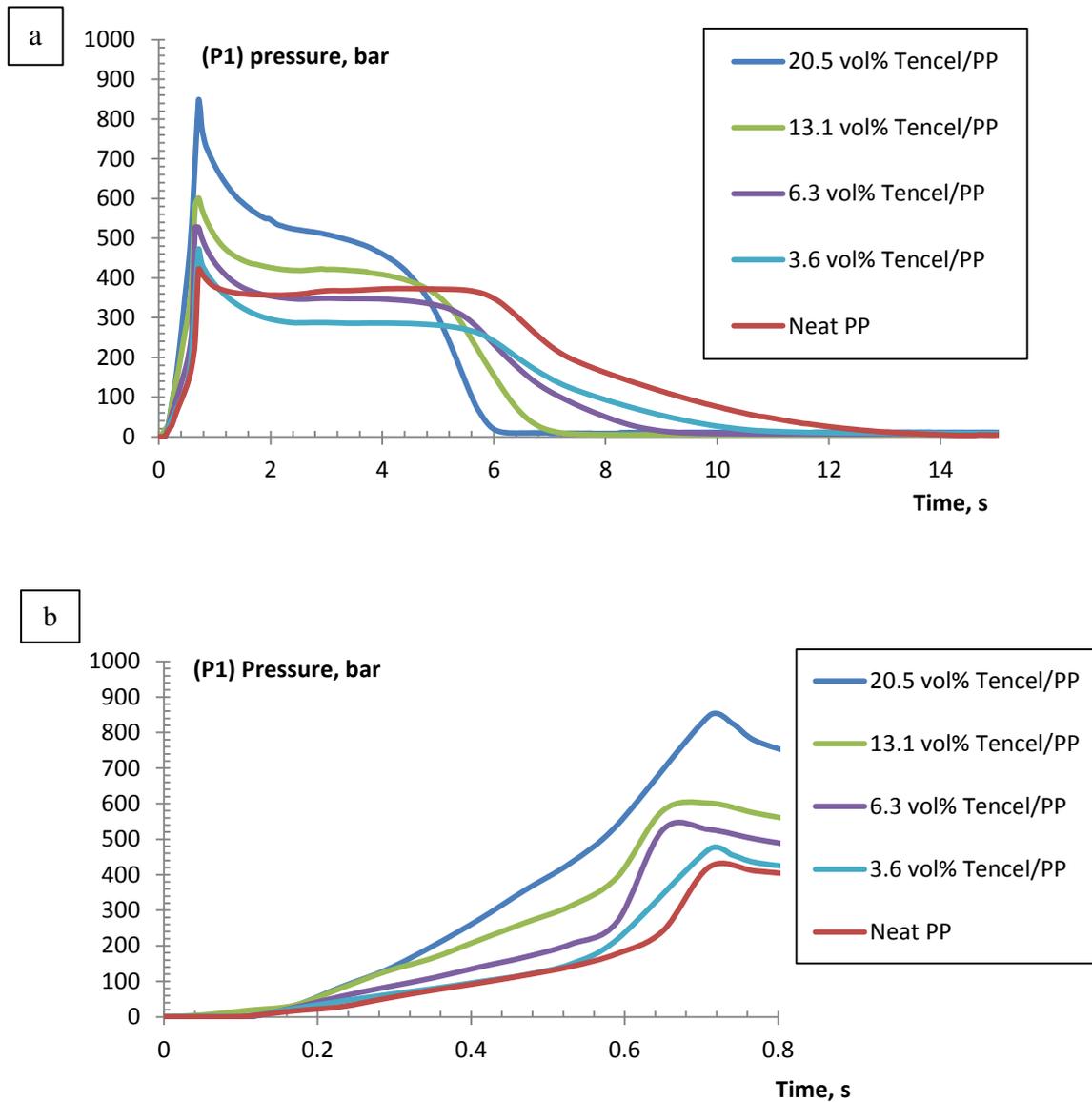
Figure 7.17

a) The overall injection pressure P1 vs time obtained (filling and post-filling stages) for different concentrations of Tencel/PP composite and the neat polypropylene

b) Zoom on the pressure during the filling stage for the same materials of figure a.

Similar trends were obtained for P2 and P3 with lower values of pressure and shorter time ranges of measurement with respect to P1, because of the pressure losses in between transducers. An example of P2 curve for Tencel composite is plotted in Figure 7.18. The

glass and flax based composites present a similar schematic fall of pressure (not shown). The effect of the fibre type on the pressure will be interpreted in the next section.
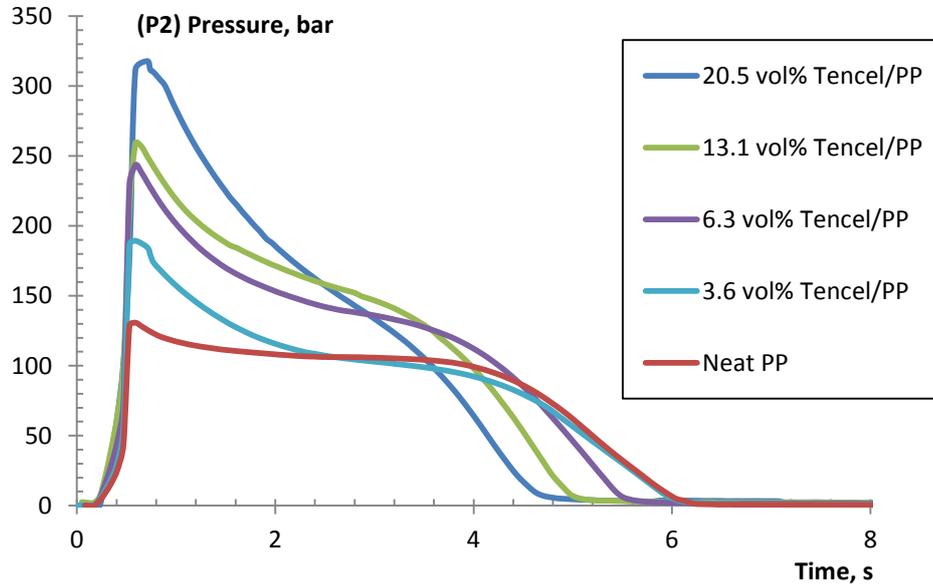
Figure 7.18

The overall injection pressure P2 vs time (filling and post-filling stages) for different concentrations of Tencel/PP composite and the neat polypropylene

2.1.3. *Influence of fibre type*

Figure 7.19 shows a comparison between the pressure P1 for Tencel, glass and flax based composites with two different concentrations 3.6 vol % and 20.5 vol %. During the filling stage, the neat PP pressure is the lowest as compared to composites (Fig. 7.19.b). At 3.6 %, up to 0.6 s, the pressure of flax composite gets higher, but around the switch-over point, Tencel pressure becomes equivalent. At 20.5 vol %, flax composite pressure becomes the lowest and those of Tencel and glass composites are similar. Around the switch-over, Tencel composite pressure shows a sharper overshoot as compared to glass composite.

The level of the plateau during the packing stage (Fig. 7.19a) for the different composites is higher for 20.5 than 3.6 vol %. For each concentration, the composites rank as follows:

- at 3.6 vol % : Tencel < glass < flax
- at 20.5 vol % : flax < glass < Tencel

233

There is no direct correlation with the viscosity, which means that the packing pressure is not only proportional to the viscosity.
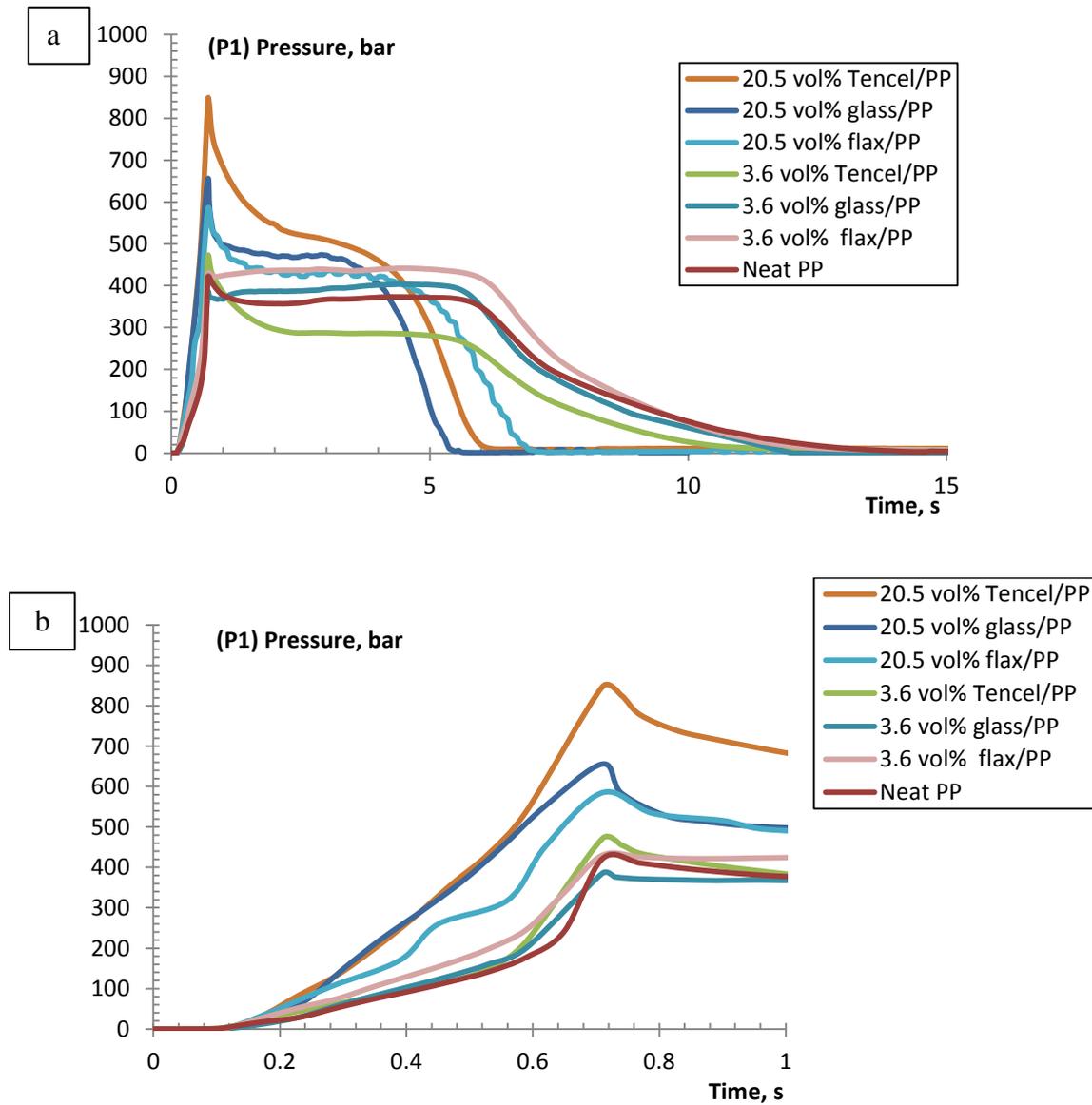
Figure 7.19

Influence of the fibre type (Tencel, flax and glass) on the pressure P1

Figure 7.20 shows the evolution of P1 and P2 at time = 0.65 s (almost 85 % of the cavity is filled) as a function of the fibre content for Tencel, glass and flax based composites. The pressure increases as the fibre contents gets greater. For both pressures P1 and P2, the Tencel composite shows higher values as compared to glass and flax composites. An important rise in P1 occurs at 20.5 vol % for Tencel composite and for glass composites with lesser extent.

234

This is similar to the results obtained in the rheology characterisation (Chapter 5) in which the viscosity of composite highly increased at 20.5 vol % fibre content, specifically for Tencel based composite. This was argued by the strong fibre-fibre interactions due to the fibre flexibility (high fibre aspect ratio and low fibre stiffness) and the local fibre dispersion. The increase in pressure is of the same magnitude of viscosity. For example, the viscosity of 20.5 vol % Tencel is 2-3 times higher than that of neat PP at high shear rate (capillary rheology range that represents the injection moulding shear rate, see Chapter 5). In Figure 7.20 the pressure of 20.5 vol % Tencel/PP is also 2-3 times larger than the pressure of neat PP. This means that any change in viscosity is directly reflected in pressure. The viscosity measured through a capillary rheometer with fibres mostly oriented along the flow direction can be even used for more complex flow and fibre orientation such those involved during injection moulding.
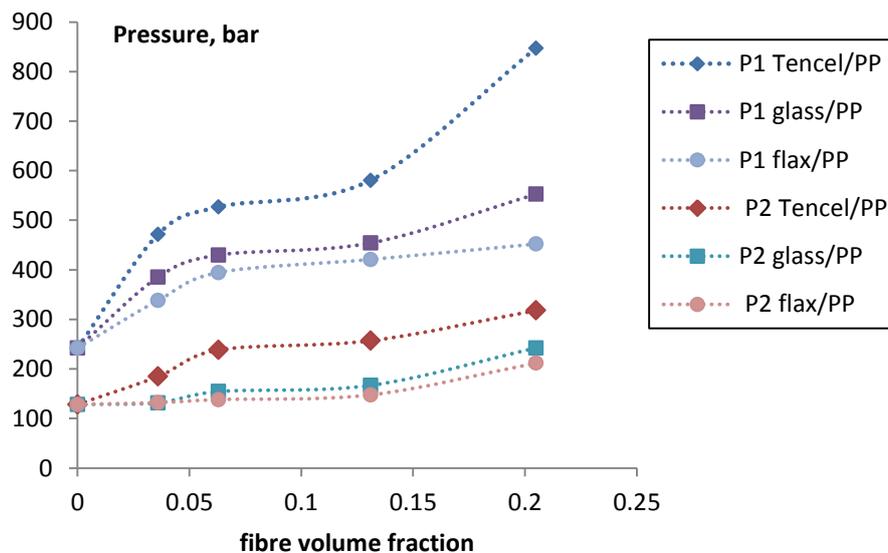
Figure 7.20

Pressures P1and P2 as a function of the fibre content for different types of fibre filled polypropylene

2.2. Simulation results and comparison with experiment

2.2.1. *Parameters of simulation*

The simulation was performed with the Rem3D® package, using a classical mixed finite element method with a decoupled approach. Three problems were solved:

- Mechanical equations (velocity, stress…), assuming a Carreau-Yasuda behaviour law and incompressible material. The flow rate is imposed at the cavity entrance and a sticking contact is used along the mould cavity walls.

- The energy equation, taking into account conduction, convection and viscous dissipation. The enthalpy of crystallization is neglected. The inlet temperature is given and the mould temperature is imposed at the wall.

- Position of the flow front: the whole cavity domain (polymer and air during the filling stage) is meshed and the position of the flow front is represented with a level set method. The latter is used to evaluate the material characteristics to be considered (polymer or air).

Additionally, the Folgar and Tucker equation (Eq. 7.3) is solved with a quadratic closure approximation. Rem3D$^{®}$ software is developed for a fixed interaction coefficient $C_I = 0.01$.

The geometry of the moulded box is symmetric with respect to both *xz* and *yz* planes. This enables to simulate the quarter of the box, leading to a considerable CPU time and memory reduction (Figure 7.21). To compare with the experimental pressures three numerical transducers were placed throughout the box, as shown in Figure 7.15.
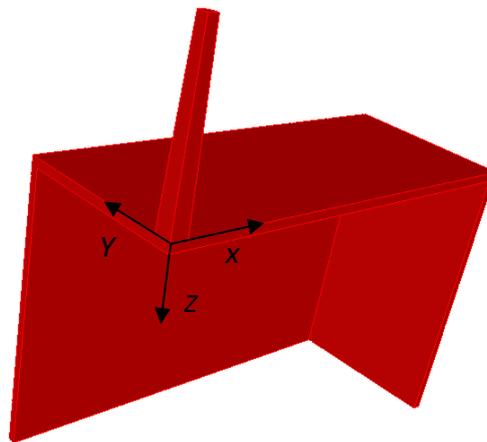

Figure 7.21

The quarter of the moulded box used for the filling stage simulation

Ten to twelve nodes through the thickness are adequate to capture velocity, temperature and orientation gradients. Moreover, the adaptive meshing of Rem3D$^{®}$ automatically refines the mesh where it is needed i.e. near the flow front, walls and gate.

To set up the simulation, we used the fitted rheological parameters except the yield stress in the modified Carreau-Yasuada model, because it concerns the low shear rate and strain range far from what expected in injection moulding. The activation energy results obtained by the time-temperature superposition principle (Chapter 5) were used. The thermal conductivity "k" and the specific heat "C_p" of polypropylene used to set up the simulation are 0.25 W.m^{-1}.°C^{-1} and 1500 J.kg^{-1}.K^{-1} [Weidenfeller al (2004)], respectively. The thermal conductivity of composites was calculated with mixture law-type equations as follows:

$$k_c = f k_f + (1 - f)k_m \hspace{4cm} \text{[Eq. 7.4]}$$

where f is the fibre volume fraction, and k_c, k_f and k_m are the thermal conductivity of composite, fibres and matrix, respectively. Other models for k_c that contain factors taking into account the fibre orientation were presented in the literature [(Nielsen (1974), Sanou et al. (1985), Papathanasiou et al. (1995)]. Since fibre orientation varies across the moulded part thickness, the investigation of the influence of each model on the predicted results seems extremely complicated.

The specific heat of composites "$(C_p)_c$" and the density "ρ_c" were also calculated by a mixture law-type, as the same manner of k_c, considering that $(C_p)_f$ and ρ_f are the specific heat and the density of fibres, respectively and "$(C_p)_m$ and ρ_m are those of the matrix. The thermal conductivity k_f and the specific heat H_f of glass fibres are 1.2 W.m^{-1}.K^{-1} and 800 J.kg^{-1}.K^{-1}, respectively according to Weidenfeller et al. (2004), and those of flax fibres are 1.2 W.m^{-1}.K^{-1} and 800 J.kg^{-1}.K^{-1} respectively according to Li et al. (2008). We assume that Tencel fibres present nearly the same properties as flax fibres, considering Tencel as a regenerated cellulose mainly based on cellulose and flax based on more than circa 70 % of cellulose. We assume also that all studied materials are incompressible, thus the density remains constant during the filling stage.

 The fibres aspect ratios experimentally calculated after injection for each fibre concentration (Chapter 3) were used for the filling stage simulation. The inlet orientation was random in space, meaning that (($a_{xx}= a_{yy}= a_{zz}= 1/3$ and $a_{xy} = a_{xy} = a_{xy} = 0$). We used an injection temperature of 190 °C (temperature of the last barrel heating rings) and a flow rate of 92.3 cm^3/s, as in experiment. In order to estimate the wall temperature, a sensor was located at 2 cm from the cavity wall. The measured temperaturevaries between 40 and 60 °C. Considering

the distance separating the cavity from the measurement point, the temperature at the cavity wall should be higher than that measured by sensor. We decided to use a wall temperature of 70 °C. This temperature is may be not accurate enough; therefore additional tests were performed concerning the effect of the wall temperature together with the composite thermal conductivity on the predicted pressure and fibre orientation. This will be shown throughout the predicted results obtained on the following.Table 7.2 summarises all the material input parameters used for simulating the filling stage

Table 7.2 The input material parameters used for simulation

	Vol %	ρ (kg.m^{-3})	k (W.m^{-1}.°C^{-1})	C_p (J.kg^{-1}.°C^{-1})	E_a (J.mol^{-1})	L/D	η_0 (Pa.s)	λ (s)	n	a
Neat PP	-	905	0.25	1377	45501	-	1201	0.04	0.38	0.85
Tencel/PP	3.6	926	0.284	1496	52354	26	2003	0.2	0.53	0.85
	6.3	942	0.31	1492	61284	25	2702	0.19	0.48	0.85
	13.1	983	0.374	1483	74458	23	3457	0.04	0.23	0.85
	20.5	1026	0.444	1474	140000	20	12025	0.15	0.23	0.85
Flax/PP	3.6	926	0.284	1496	48969	15	1500	0.05	0.4	0.85
	6.3	942	0.31	1492	61284	15	1515	0.05	0.35	0.85
	13.1	983	0.374	1483	67904	14	3055	0.07	0.3	0.85
	20.5	1026	0.444	1474	69089	15	6173	0.09	0.21	0.85
Glass/PP	3.6	962	0.284	1475	42334	49	1597	0.2	0.55	0.85
	6.3	1005	0.310	1456	45500	38	2000	0.2	0.53	0.85
	13.1	1114	0.374	1408	55617	30.2	3492	0.14	0.39	0.85
	20.5	1232	0.444	1354	55617	29	3968	0.02	0.118	0.85

Conditions for all materials:

-Flow rate = 92.3 cm^3/s

-Injection temperature = 190 °C

-Wall temperature = 70 °C

2.2.2. *Filling stage analysis and comparison with experiment*

In this section, we will primarily analyse the pressure during the filling stage for the neat polypropylene and compare with the experimental results. Second, we will present the filling stage pressure and the induced fibre orientation in composites. A comparison with the experimental results will be also discussed.

2.2.2.1. The neat polypropylene

▪ *Cavity filling*

Figure 7.22 shows the sequence of the box filling for the neat PP. The time needed to fill the entire box is 0.717 s. As the sprue is located in the centre of the box top-side (*xy*), the initial flow around the sprue is circumferential (Figure 7.22.a and b).The top side (*xy*) fills to some extent the large lateral side (*zx*) (Figure 7.22.c,d and f) that in turn feeds the small lateral side (*yz*) (Figure 7.22.h, g and i).

a

0.013 s

b

0.05 s

c

0.132 s

d

0.285 s

0.426 s   0.536 s

0.608 s   0.702 s
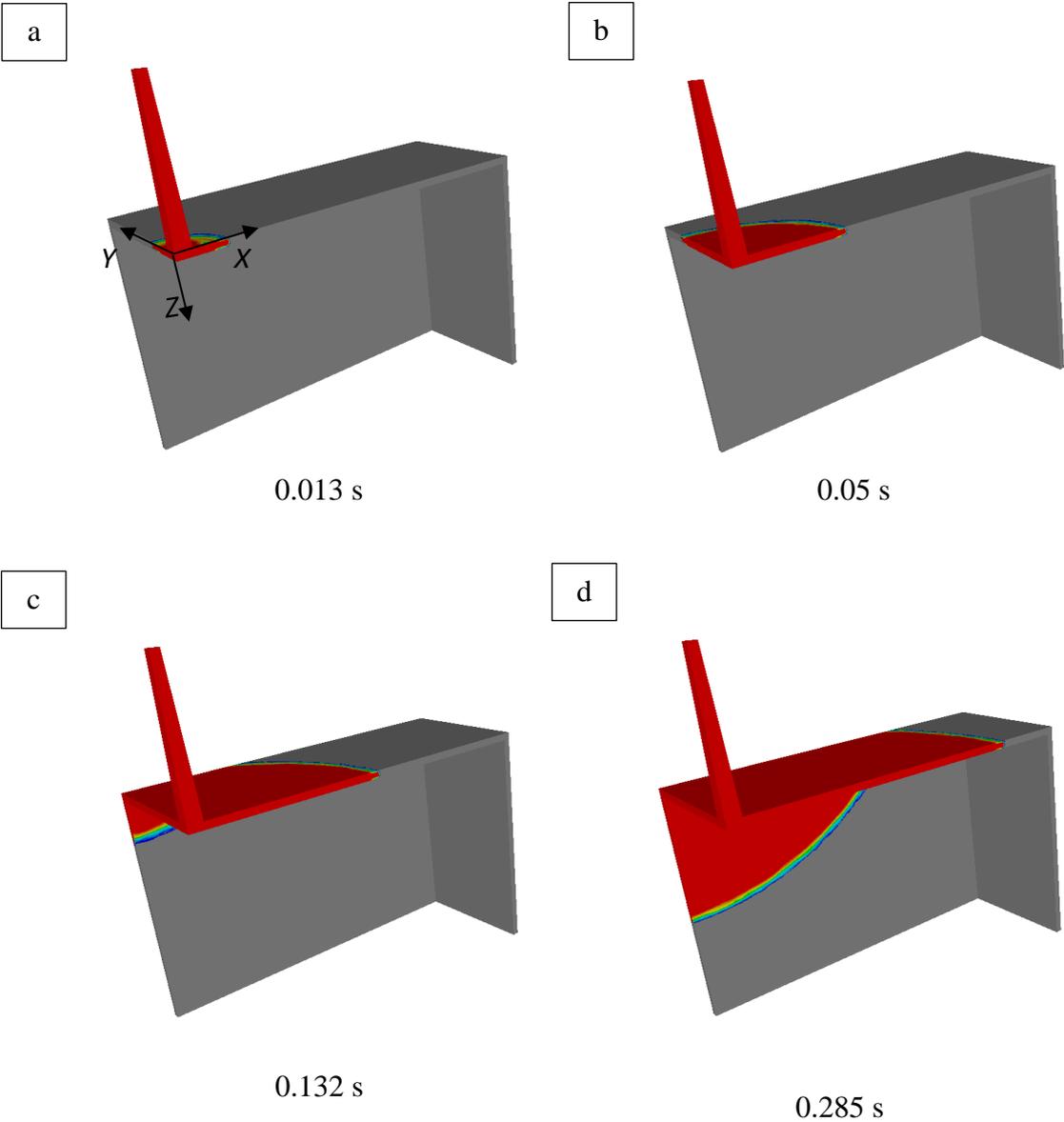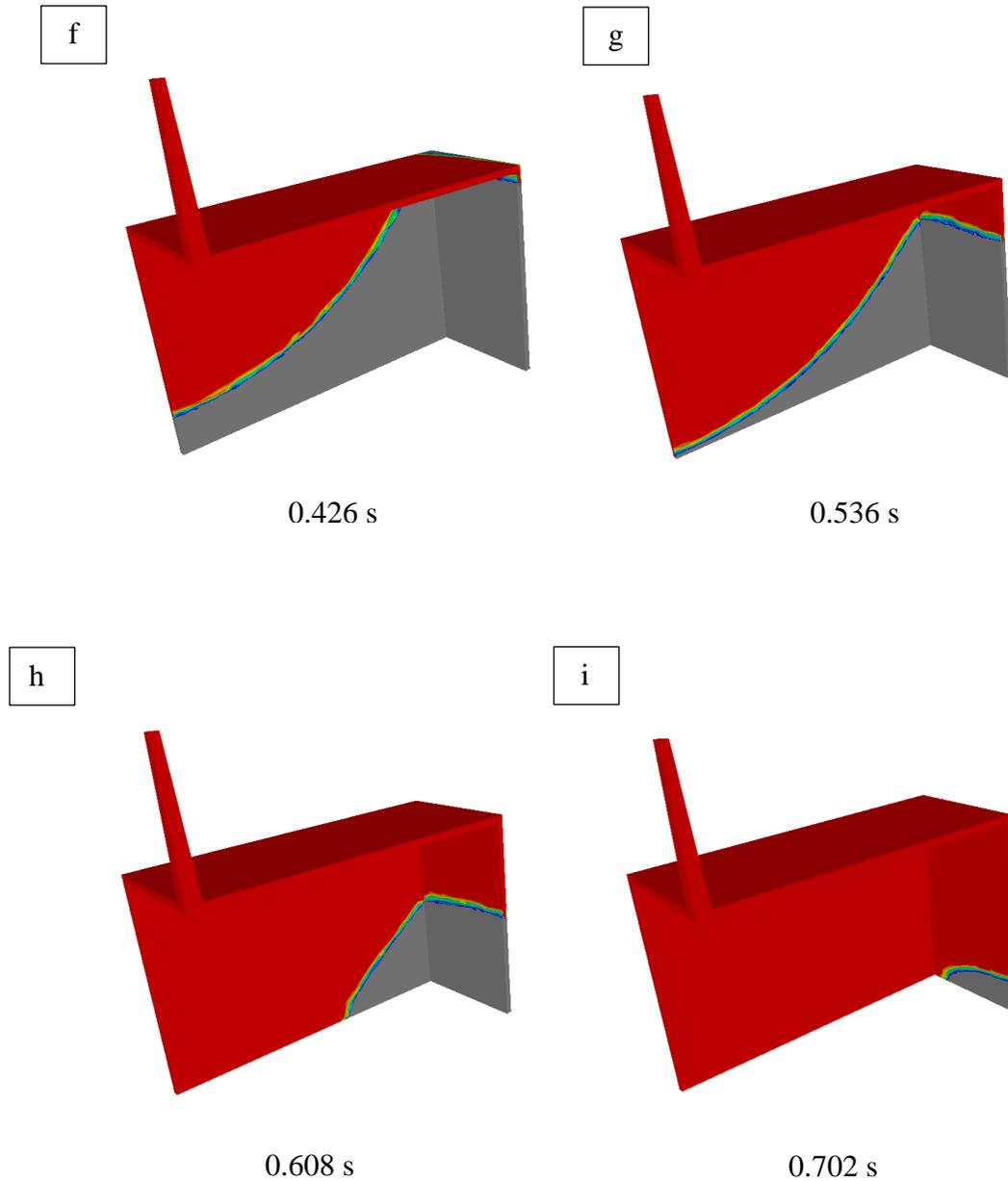
Figure 7.22

The box filling for different times

- *Pressure*

We are going to focus on the pressure (P1) to analyse the predicted results and to compare with experiment. Figure 7.23 shows a comparison between the predicted and the experimental pressure P1 during the filling stage. Considering the error due to the experiment repeatability (20 %), the prediction fits the experimental pressure except in the filling start-up where a deviation can be noticed. The overshoot in the experimental curve is due to the packing coming after the filling stage.
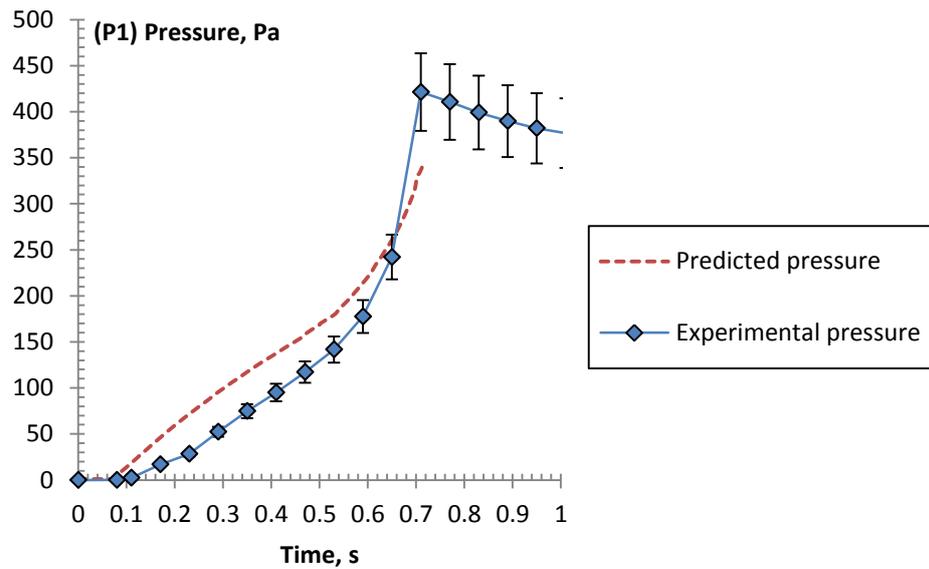
Figure 7.23

Comparison between the predicted ($k = 0.25$ W/m.°C, $T_{wall} = 70$ °C) and the experimental pressure (P1)

▪ *Thermal sensitivity*

Studying the thermal sensitivity can indicate errors in the input data, which might be responsible for the disagreement between predictions and experiments. The value of the thermal conductivity of polypropylene used in Rem3D® was taken from literature [Weidenfeller et al. (2004)] and no characterization was performed to assess its accurate value. Moreover, assuming that the cavity-wall temperature is constant (70 °C) overall the cavity is may be not precise enough to reach a well agreement with experiment. Therefore, the influence of the thermal conductivity and the wall temperature must be examined. Figures 7.24 and 7.25 show the influence of the thermal conductivity *"k"* and the wall temperature *"T_{wall}"* on the pressure of transducer P1 for the neat polypropylene, respectively. All other variables were left unchanged as in Table 7.2. The predicted pressure is higher as *"k"* increases and *"T_{wall}"*decreases, meaning that the prediction of the pressure during the filling stage is sensitive to the thermal boundary condition. While the range of deviation related to *k* and *T_{wall}* change is closely equal to the experimental error range at the filling end, it is slight and has almost no effect on the filling start-up where the predicted results overestimate experiments. This error can be associated to the assumption that the melt temperature at the cavity entrance is constant and equal to the temperature imposed in the barrel surrounding the

screw at the plasticisation unit. Viscous heating takes place due to the high shear rate in the nozzle of the injection moulding machine. Some other inaccuracies in the prediction by Rem3D® software can also be caused by the ignorance of the kinetics of the crystallinity (which is also the case of most similar software). Pantani et al. (2005) demonstrated the important influence of crystallinity on the interpretation of pressure during the injection moulding of an isostatic polypropylene. According to the authors, an increase in crystallization during flow leads to a greater pressure involved. Many studies in literature have dealt with the prediction of the development of crystallinity during injection moulding process [Manzione (1987); Lafleur and Kamal (1986); Papathanasiou et al. (1995); Hieber (2002)].
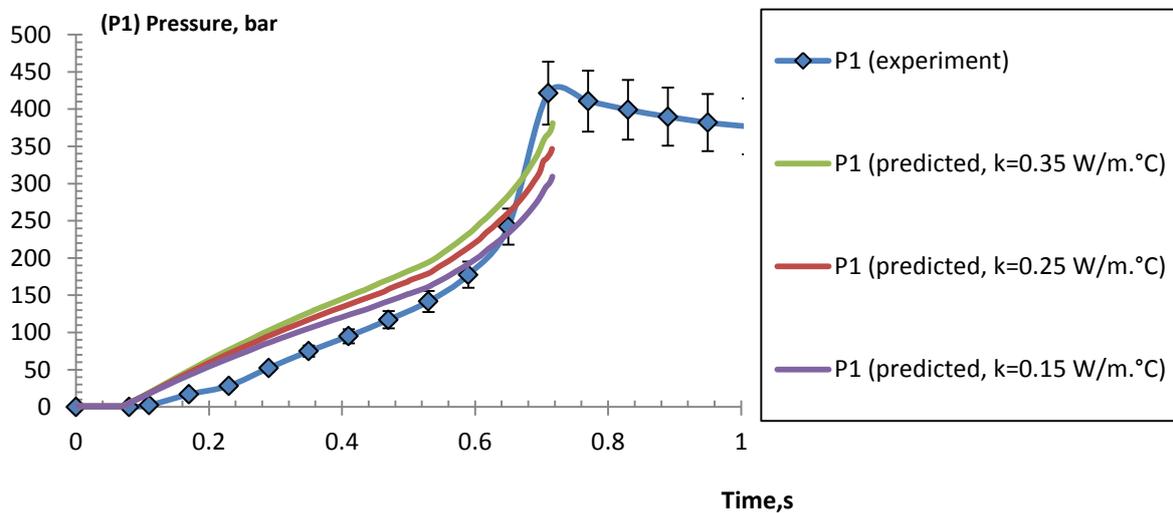
Figure 7.24

The influence of thermal conductivity "*k*" on the predicted pressure (P1) for a $T_{wall} = 70\ °C$ and comparison with the experimental pressure
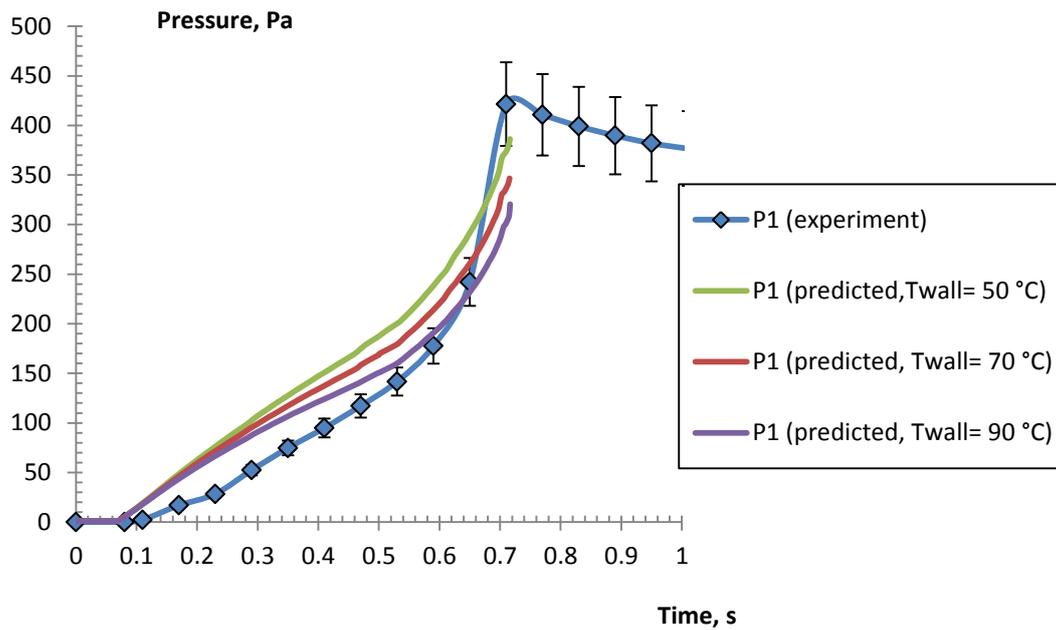
Figure 7.25

The influence of wall temperature "T_{wall}" on the predicted pressure (P1) for a k= 0.25 W/m.°C and comparison with the experimental pressure

2.2.2.2. Composites

▪ ***Pressure***

Figures 7.26, 7.27 and 7.28 show comparisons between the experimental and the predicted pressures (P1) during the filling stage, for different concentrations of Tencel, flax and glass based composites, respectively. For flax composites and to a lesser extent for glass composites the agreement is correct. Numerical results overestimate the pressure for Tencel composites especially at 20.5 vol %. For most cases, the computation overestimates the pressure at the beginning, as was observed for the neat polypropylene. The pressure at the end is correctly predicted. The increase of pressure with the fibre content is in agreement with the measurements.

The prediction of pressure is more complicated for composites than for unreinforced polymers. Flow induced microstructure affects the thermal conductivity and the rheology. This microstructure changes through time, but it is usually accounted on average (rheology for a given orientation in the rheometers, mixing law for the thermal conductivity).

Concerning moulding experiments, there are some difficulties such as material expulsion when the nozzle of the injection unit is not in contact with the mould and even if all precautions have been taken, some material thermal degradation cannot be avoided.
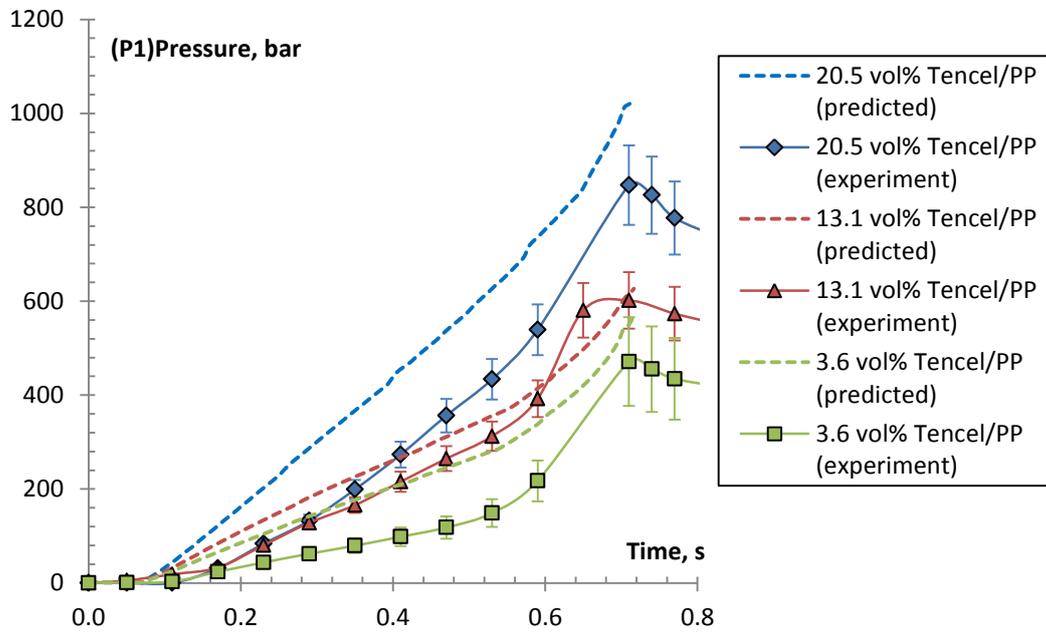
Figure 7.26

Comparison between the experimental and the predicted pressures P1 for different concentrations of Tencel/PP
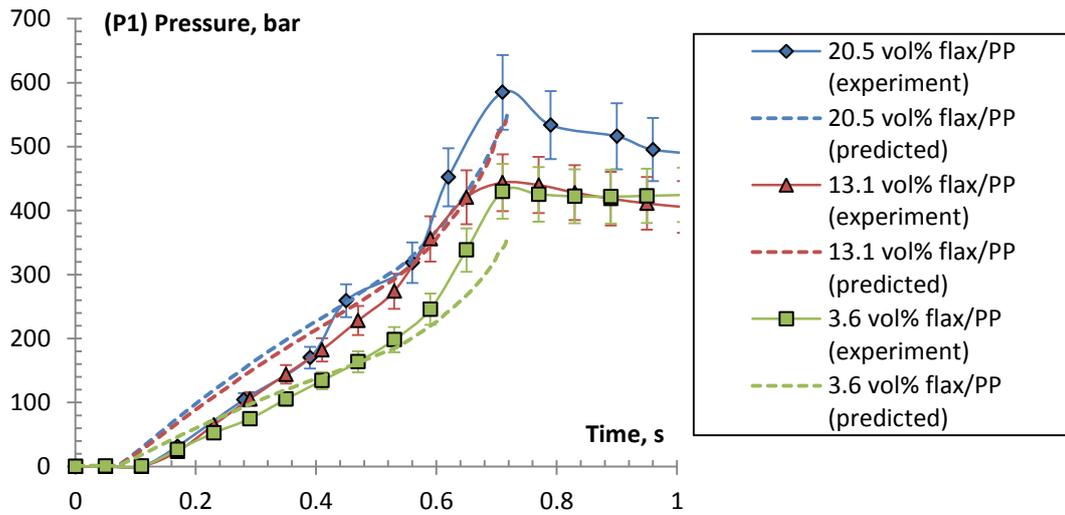
Figure 7.27

Comparison between the experimental and the predicted pressures P1 for different concentrations of flax/PP
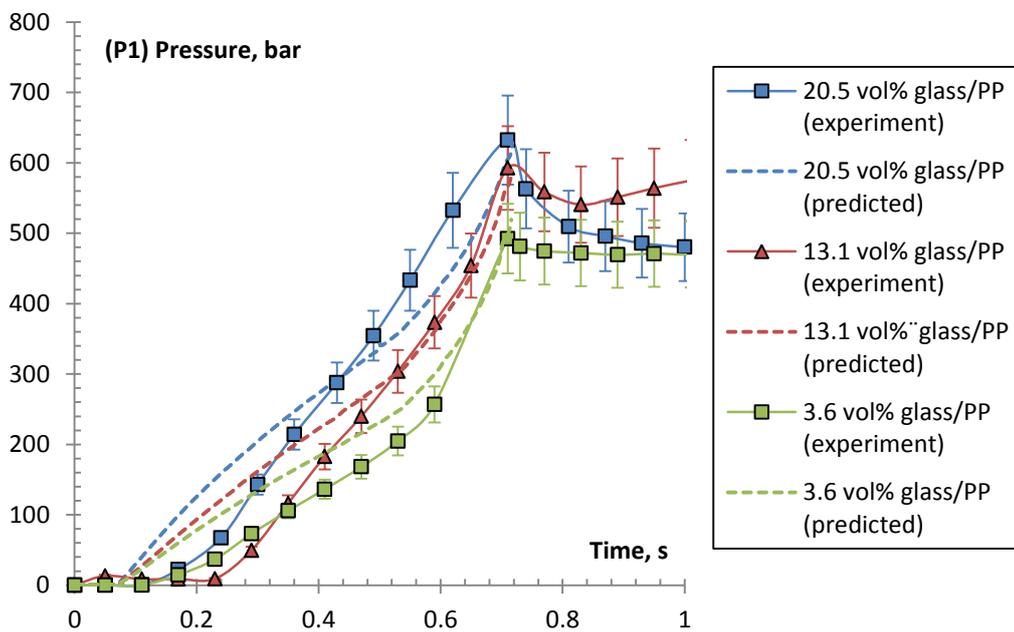
Figure 7.28

Comparison between the experimental and the predicted pressures P1 for different concentrations of glass/PP

■ *Fibre orientation*

Orientation model in Rem3D$^®$ is basically made to predict the orientation of rigid fibres. Therefore, we are going first to focus on the case of glass fibres (rigid fibres) to analyse the fibre orientation in the box after filling. We will secondly compare with the experimental results and investigate those predicted for flax and Tencel based composites. Considering the lack of orientation models taking into account the properties of natural fibres, the aim here is to estimate the precision that can be expected from a rigid fibre model.

a) Glass fibre based composite

   -*Effect of the distance from the gate*

Figure 7.29 maps out the predicted orientation component a_{xx} in several cross sections in *yz*-plane and *xz*-plane for the 20.5 vol % glass/PP. The *xz*-cross-section at *y*= 0 mm shows a core-shell structure. The core exhibits fibres well aligned to *y*-direction (blue area). They become progressively less aligned near the sprue. For *xz*-cross-section performed at *y*= 17.75 mm, in the core, fibres are aligned to *x*- direction, whereas near the surface fibres are randomly aligned (yellow and green areas). The *yz*-cross sections show that fibre alignment is different for *y* between 17.75 and *y*= 35.5 mm compared to *y* between 0 and *y*= 17.75 mm. compared to *y* between 0 and *y*= 17.75 mm.
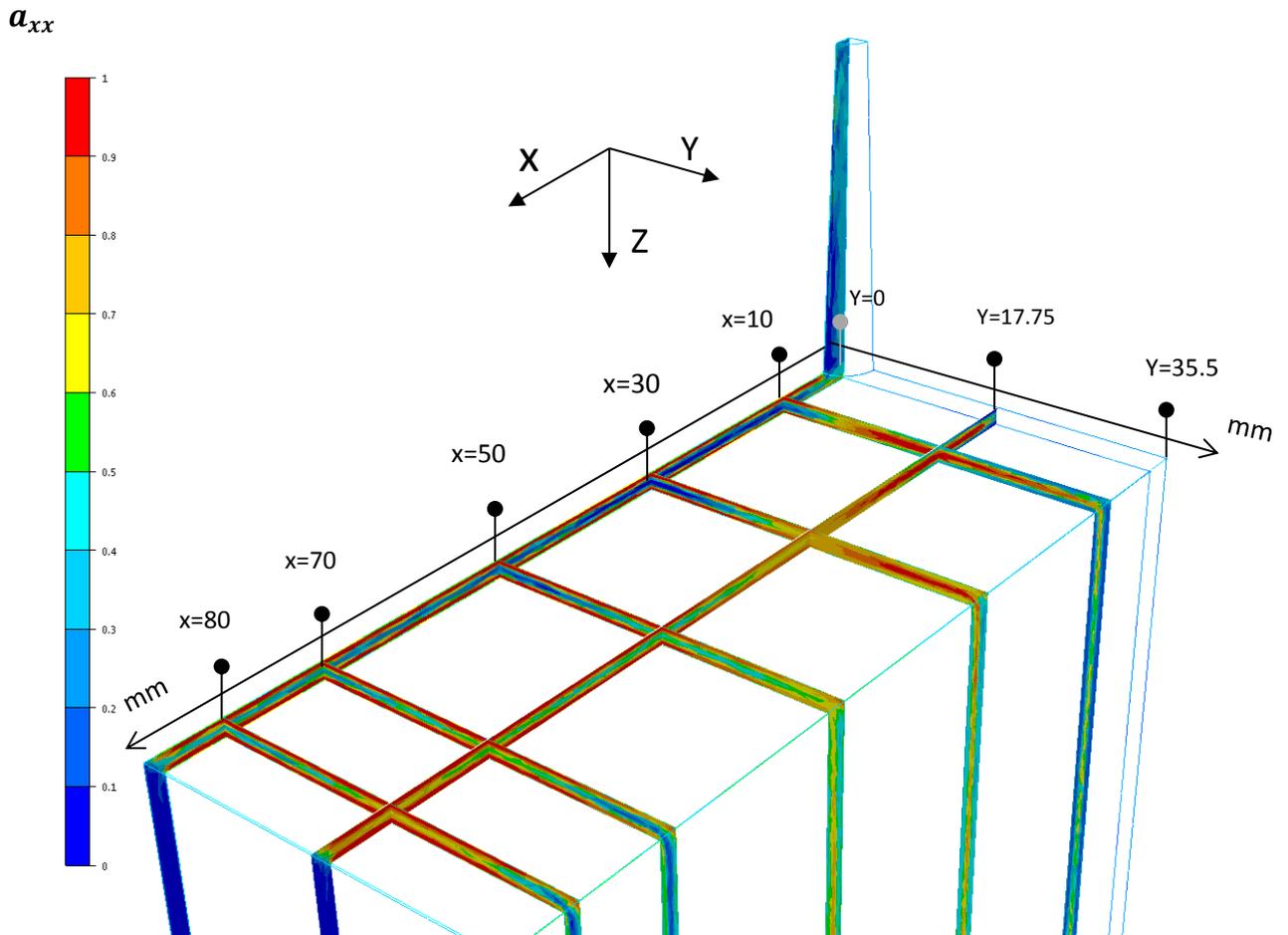
Figure 7.29

xz-and *yz*-cross-sections in different positions in the moulded box for 20.5 vol % glass/PP obtained by simulation with Rem3D® software

Figures 30 and 31 present a_{xx} evolution for different *x*-positions along *y*= 0 mm and *y*= 30 mm, respectively. For *y*= 0 mm (Figure 30), for all *x*-positions, a_{xx} is almost equal to 0.5 at surface, indicating a random orientation and signing the presence of a skin layer. a_{xx} increases rapidly to almost 0.95 at *z*= 100 µm. From *z*=100 µm to *z*= 400 µm, a_{xx} remains constant 0.9-0.95, indicating a shell layer well aligned in the *x*-direction. Then, a_{xx} decreases to reach values between 0.05 and 0.35 in the core. The difference between each *x*-position is the degree of alignment transverse to *x* and the thickness of the core layer, between *z*= 400 µm and *z*= 1500 µm. For the position *x*= 10 mm, near the sprue, the core is large (around 700 µm) with a_{xx} around 0.2. The maximum of the core alignment is obtained at the position *x*= 30

mm with a_{xx} around 0.05 and the minimum one at *x*=80 mm far from the sprue with a_{xx} around 0.35.

For *y*=30 mm near the edge, the evolution a_{xx} across thickness for different *x*-positions is very different from that of *y*=0 mm. Figure 31 shows that for the position *x*= 10 mm the core is aligned to *x*-direction and the shell is perpendicular, inversely oriented to what is known about the core-shell structure. This is caused by the central location of the sprue, resulting in a radial flow near the entrance of the cavity. The orientation in the core is perpendicular to the flow direction, which is here the *y*-direction, and parallel at the skin. Above *x*= 50 mm, the fibre alignment follows the typical shell-core structure with a shell parallel to *x*-direction, the main flow direction, and a perpendicular core. The maximum of the core and the shell alignment is reached at the position *x*= 70 mm and *x*= 80 mm, respectively.
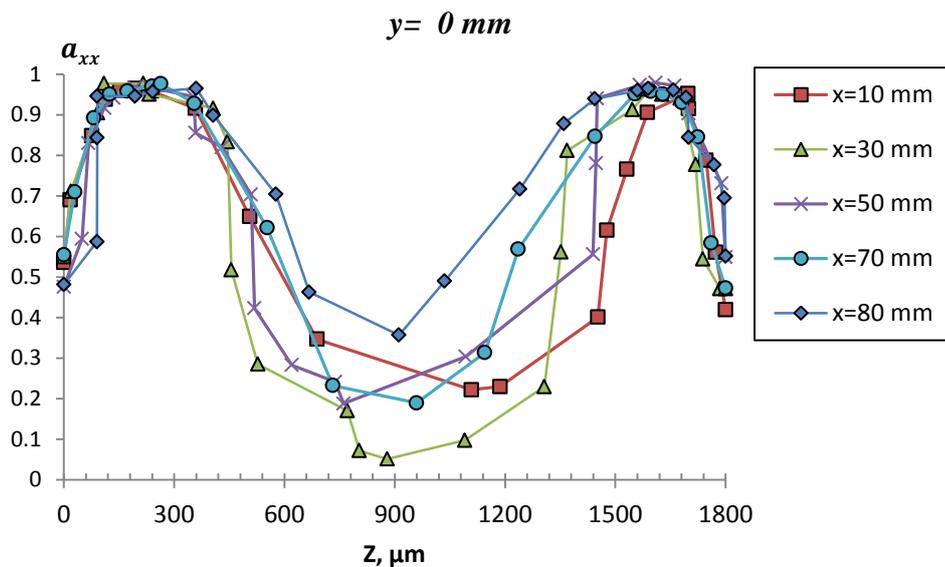
Figure 7.30

Predicted a_{xx} across thickness of 20.5 vol % glass/PP for different positions along *x*-axis, and fixed position in *y*-axis (*y*= 0 mm)
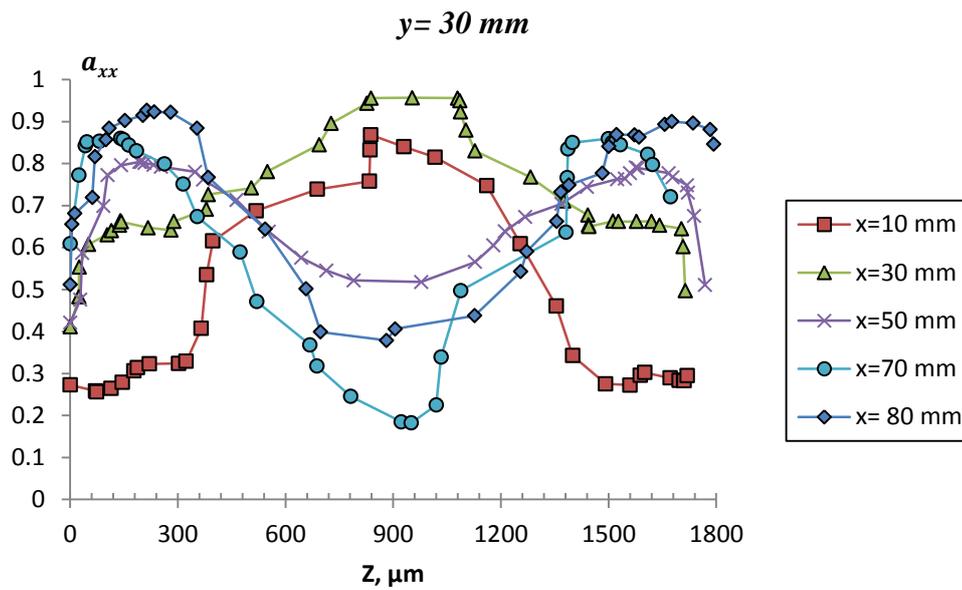
Figure 7.31

Predicted a_{xx} across thickness of 20.5 vol % glass/PP for different positions along *x*-axis, and fixed position in *y*-axis (*y*= 30 mm, *near the edge*)

-Effect of fibre content

Figure 7.32 shows the predicted a_{xx} vs thickness for different concentrations of glass/PP at the location (*x*= 70 mm, *y*= 0 mm). The orientations at the skin and the shell layers remain unchanged by increasing the fibre content. The core orientation for 3.6 to 13.1 vol % is mostly along the flow direction (a_{xx} around 0.7-0.8), whereas for 20.5 vol %, it becomes strongly perpendicular to the flow direction (a_{xx} around 0.2). Some studies in the literature [Spahr et al. (1990); Bouti et al. (1989)] concluded that increasing fibre content results in a thicker core that is highly oriented perpendicular to the main flow direction, which is in agreement with our results.
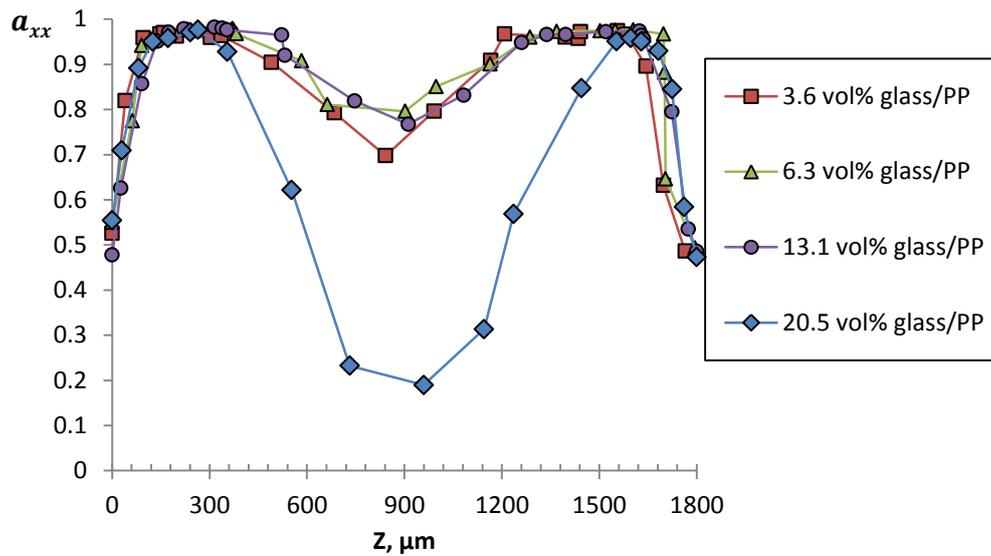
Figure 7.32

Predicted a_{xx} vs thickness for different concentrations of glass/PP at the location (x= 70 mm, y= 0 mm)

-Thermal sensitivity

We have seen earlier that the thermal boundary condition has a great influence on the pressure involved during filling. We also checked its influence on the fibre orientation state across thickness. Figures 7.33 and 7.34 show the experimental and the predicted a_{xx} for 20.5 vol % glass/PP obtained by different thermal conductivities "*k*" and wall temperatures T_{wall}, respectively. All other variables left unchanged with respect to standard conditions in Table 7.2. We can conclude that increasing *k* and decreasing T_{wall} lead to move the core orientation from well aligned perpendicular to *x*-direction to randomly oriented in *xy*-plane. This is probably related to the respective sizes of the fluid core and solidified layer near the mould walls (although there is no real solidification criteria in Rem3D, the velocity is almost zero near the walls because of the low temperature and high viscosity, mimicking the solidified layer). The shear rate (responsible for the flow direction orientation at the surface) and the elongational rate (due to the central position of the sprue, responsible for the orientation perpendicular to the flow direction in the core) repartitions are dependent on the solidified layers.

-Comparison with experimental results

As mentioned in Chapter 4, the characterization of the fibre orientation was conducted for 20.5 vol % composites at the location (x= 70 mm, y= 0 mm) for six different levels across thickness from z= 100 µm (near surface) to z= 900 µm (the mid-plane). The experimental characterization along z= 0-100 µm was not possible because the cross-section is obtained by polishing. At least a distance of 100 µm from surface is required to achieve a smooth surface of sample suitable for image processing investigation. We assume that fibre orientation is symmetric with respect to the mid-plane, thus the fibre orientation was not investigated from 900 µm to 1800 µm. Characterisation of the orientation state is essentially focused on flax and Tencel fibres. Only three levels across thickness were investigated for the glass based composite to reduce the extent of the experimental work. The predicted a_{xx} for k= 0.7 W/m.°C (Figure 7.33) or for T_{wall} = 30 °C (Figure 7.34) closely fit the experimental a_{xx} carried out at (y= 0 mm, x= 70 mm). The standard boundary conditions used for simulation in Table 7.2 (k= 0.444 W/m.°C and T_{wall}= 70 °C) overestimates the core alignment (at z= 900 µm) with respect to experiment. This reveals again the influence of the thermal boundary conditions on the pressure and the fibre orientation state, and partially clarifies the causes of the deviation between simulation and experimental results.
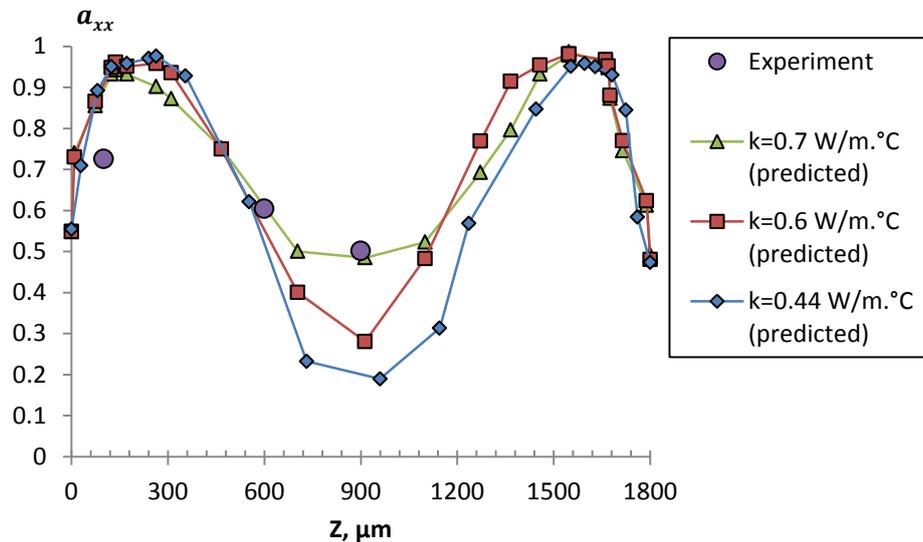
Figure 7.33

The predicted a_{xx} vs thickness for 20 vol % glass/PP with different k, compared with result obtained in experiment
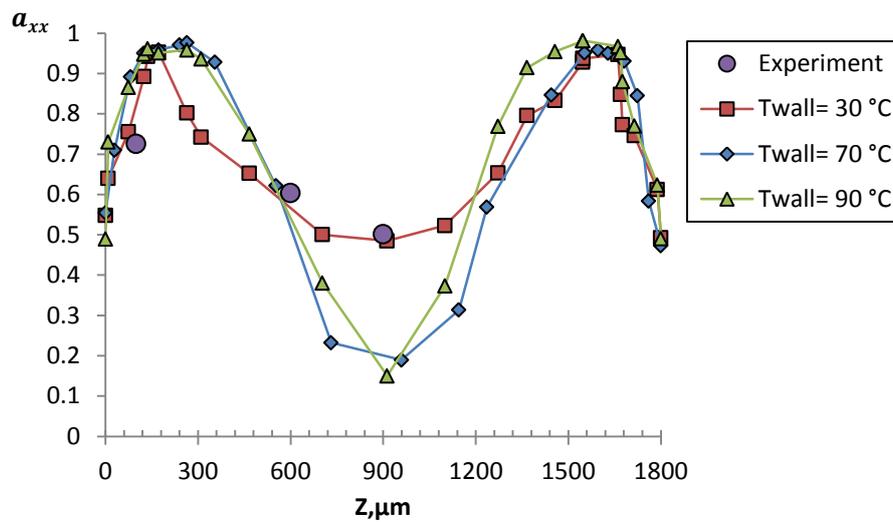
Figure 7.34

The predicted a_{xx} vs thickness for 20 vol % glass/PP with different T_{wall}, at location (*x*= 70 mm, *y*= 0), compared with result obtained in experiment

Other factors can explain the differences between experiments and computation. The first one concerns the interaction coefficient C_I (Eq.7.2). According to Folgar and Tucker (1984) and Bay and Tucker (1992), C_I is usually found by fitting predictions to experiments. However, varying only C_I would not enable to fit our experimental results. Generally, decreasing C_I leads to higher fibre alignment in both shell and core layers [Bay and Tucker (1992)]. The second factor that may explain the prediction error is the closure approximation used in the simulation. The effect of an inappropriate closure approximation is to overestimate the out-of-plane fibres (fibres that make angle to *xy*-plane), leading to a shell layer too thick and a core too thin. Rem3D® uses the simple quadratic closure approximation. A better closure approximation such as the hybrid one [Advani and Tucker (1987)] could improve the precision of the prediction. Nevertheless, by using improved models of orientation (RSC and ARD, see section 1.5), Phelps and Tucker (2009) found that the core alignment is not well estimated. The experimental measurement error can also be a source of disagreement between the experimental and the predicted fibre orientation

b) Flax and Tencel based composites

Figure 7.35 shows the experimental and the predicted a_{xx} across thickness carried out at the same location (*x*= 70 mm, *y*= 0 mm), for 20 vol % Tencel, flax and glass based composites.

The material data for the simulation are that presented in Table 7.2. The orientation state predicted for Tencel composite is extremely different from the experimental one. This was expected due to the high flexibility of Tencel fibres, considering that Rem3D$^{®}$ is basically dedicated to rigid fibres. The experimental error can also be an important reason behind this deviation, since we have approximated fibre orientation by the end-to-end vector. We can thus conclude that Rem3D$^{®}$ does not represent the real behaviour of Tencel fibres. For flax (almost rigid fibres) based composites, the predicted a_{xx} is broadly consistent with the major trends of the shell-core structure. Some experimental points were closely predicted (z= 100 μm and z= 800 μm), but for some other deviations exist, particularly in the shell/core transition. By adjusting the simulation with accurate thermal parameters, the prediction could closely fit experiment. Moreover, considering that flax fibres contain bundles, the number of fibres is smaller as compared to glass fibres (individual fibres) for the same aspect ratio and concentration, which limits the fibre-fibre interactions. Therefore a better evaluation of the interaction coefficient C_I can bring more accuracy to the predicted orientation for flax fibre composites.
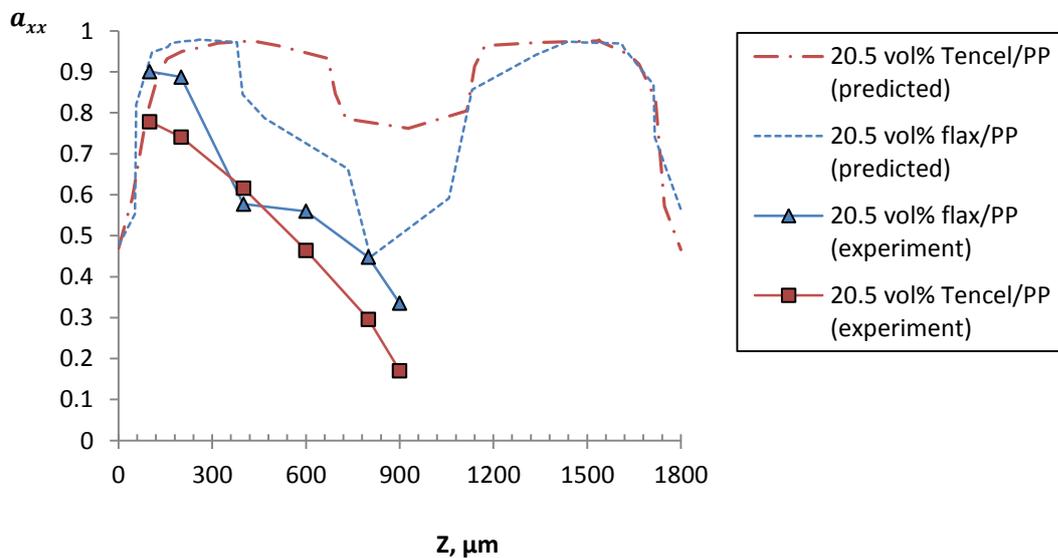

Figure 7.35

The experimental and the predicted a_{xx} across thickness at location (x= 70 mm, y= 0) for 20.5 vol % glass/PP, flax/PP and Tencel/PP

2.3. Conclusions

In this chapter we have investigated the pressure and the fibre orientation predicted by simulation of the injection moulding of glass, flax and Tencel reinforced polypropylene and compared with those experimentally obtained. We found a strong correlation between the rheology of composite and the experimental pressure. The increase of viscosity, due to either the fibre concentration or the fibre aspect ratio/flexibility increase, leads to enhance the pressure in cavity. It turned out that pressure increase is of the same magnitude to the viscosity increase. The simulation of the filling stage overestimates the experimental pressure around the start-up of the pressure evolution. The difference reduces when the melt progresses into the cavity. This is for the neat polypropylene and overall the studied composites. Thermal boundary conditions parameters have a large influence on the predicted pressure.

Since the software Rem3D$^®$ uses a computational model adapted to rigid fibres, we have conducted a detailed investigation of glass fibres orientation in the moulded box. A core-shell structure across the thickness dominates the moulded part. The evolution of the orientation tensor component a_{xx} across the thickness is nearly the same for concentrations between 3.6 and 13.1 vol %. It turned out that the core layer with fibres oriented perpendicular to the flow direction appears only for 20.5 vol %.

According experimental data performed for glass fibre reinforced polypropylene, only partial conclusions can be drawn concerning the accuracy of the simulation. The simulation predicts well the experimental orientation except in the core layer in which the simulation overestimates the degree of alignment perpendicular to the flow direction. The thermal boundary conditions can be modified to get a good agreement.

The simulation of orientation of flax and Tencel fibre cases were carried out. The purpose is to test to what extent a rigid fibres' model can simulate both types of natural fibres. It turned out that the predicted flax fibres' orientation matches correctly the experimental results, while that of Tencel fibre is extremely far from experiment. The flax fibres contain partially rigid bundles. An accurate set-up of the thermal conditions input could clearly improve the obtained results. However, Tencel fibres are very flexible and their behaviour during the flow cannot be modelled by a rigid fibres model. A specific flexible fibre model is required to get more promising results. Our work is one of the first investigations about the prediction of the orientation of natural fibres based composites. This could be a contribution to the ongoing

discussions about which models are suitable to predict the microstructure of natural fibres in injection moulded parts.

3. References

Advani, S. G., & Tucker III, C. L. (1987). The use of tensors to describe and predict fiber orientation in short fiber composites. Journal of Rheology (1978-present), 31(8), 751-784.

Agassant, J. F., Avenas, P., Sergent, J. P., Vergnes, B., & Vincent, M. (1996). La mise en forme des matières plastiques.

Bay, R. S., & Tucker, C. L. (1992). Fiber orientation in simple injection moldings. Part II: Experimental results. Polymer composites, 13, 332-342.

Chiang, H. H., Hieber, C. A., & Wang, K. K. (1991, a). A unified simulation of the filling and postfilling stages in injection molding. Part I: Formulation. Polymer Engineering & Science, 31(2), 116-124.

Chiang, H. H., Hieber, C. A., & Wang, K. K. (1991, b). A unified simulation of the filling and postfilling stages in injection molding. Part II: Experimental verification. Polymer Engineering & Science, 31(2), 125-139.

Chung, D. H., & Kwon, T. H. (2002, a). Invariant-based optimal fitting closure approximation for the numerical prediction of flow-induced fiber orientation. Journal of Rheology (1978-present), 46(1), 169-194.

Chung, D. H., & Kwon, T. H. (2002, b). Fiber orientation in the processing of polymer composites. Korea-Australia Rheology Journal, 14(4), 175-188.

Cintra Jr, J. S., & Tucker III, C. L. (1995). Orthotropic closure approximations for flow-induced fiber orientation. Journal of Rheology (1978-present), 39(6), 1095-1122.

Doi, M. (1981). Molecular-dynamics and rheological properties of concentrated-solutions of rodlike polymers in isotropic and liquid-crystalline phases. Journal of Polymer Science Part B-Polymer Physics, 19(2), 229-243.

Fan, X., Phan-Thien, N., & Zheng, R. (1998). A direct simulation of fibre suspensions. Journal of Non-Newtonian Fluid Mechanics, 74(1), 113-135.

Férec, J., Ausias, G., Heuzey, M. C., & Carreau, P. J. (2009). Modeling fiber interactions in semiconcentrated fiber suspensions. Journal of Rheology (1978-present), 53(1), 49-72.

Folgar, F., & Tucker, C. L. (1984). Orientation behavior of fibers in concentrated suspensions. Journal of Reinforced Plastics and Composites, 3(2), 98-119.

Forgacs, O. L., & Mason, S. G. (1959). Particle motions in sheared suspensions: IX. Spin and deformation of threadlike particles. Journal of colloid science, 14(5), 457-472.

Han, K. H., & Im, Y. T. (1997). Compressible flow analysis of filling and postfilling in injection molding with phase-change effect. Composite Structures, 38(1), 179-190.

Hand, G. L. (1962). A theory of anisotropic fluids. Journal of Fluid Mechanics, 13(01), 33-46.

Hieber, C. A. (2002). Modeling/simulating the injection molding of isotactic polypropylene. Polymer Engineering & Science, 42(7), 1387-1409.

Hieber, C. A., & Shen, S. F. (1980). A finite-element/finite-difference simulation of the injection-molding filling process. Journal of Non-Newtonian Fluid Mechanics, 7(1), 1-31.

Hieber, C. A., Socha, L. S., Shen, S. F., Wang, K. K., & Isayev, A. I. (1983). Filling thin cavities of variable gap thickness: A numerical and experimental investigation. Polymer Engineering & Science, 23(1), 20-26.

Huynh, H. M. (2001). Improved fiber orientation predictions for injection-molded composites

Jeffery, G. B. (1922, November). The motion of ellipsoidal particles immersed in a viscous fluid. In Proceedings of the Royal Society of London A: Mathematical, Physical and Engineering Sciences (Vol. 102, No. 715, pp. 161-179). The Royal Society.

Kamal, M. R., & Kenig, S. (1972). The injection molding of thermoplastics part I: Theoretical model. Polymer Engineering & Science, 12(4), 294-301.

Kamal, M. R., & Kenig, S. (1972). The injection molding of thermoplastics part II: experimental test of the model. Polymer Engineering & Science, 12(4), 302-308.

Kamal, M. R., Chu, E., Lafleur, P. G., & Ryan, M. E. (1986). Computer simulation of injection mold filling for viscoelastic melts with fountain flow. Polymer Engineering & Science, 26(3), 190-196.

Kuo, Y., & Kamal, M. R. (1976). The fluid mechanics and heat transfer of injection mold filling of thermoplastic materials. AIChE Journal, 22(4), 661-669.

Landel, R. F., & Nielsen, L. E. (1974). Mechanical properties of polymers and composites. Vol. 2, Marcel Dekker, New York.

Li, X., Tabil, L. G., Oguocha, I. N., & Panigrahi, S. (2008). Thermal diffusivity, thermal conductivity, and specific heat of flax fiber–HDPE biocomposites at processing temperatures. Composites science and technology, 68(7), 1753-1758.

Manzione, L. T. (1987). Applications of computer aided engineering in injection molding. Carl Hanser Verlag, Kolbergerstrasse 22, D-8000 Munchen 80, FRG, 1987.

Mavridis, H., Hrymak, A. N., & Vlachopoulos, J. (1988). The effect of fountain flow on molecular orientation in injection molding. Journal of Rheology (1978-present), 32(6), 639-663.

Pantani, R., Coccorullo, I., Speranza, V., & Titomanlio, G. (2005). Modeling of morphology evolution in the injection molding process of thermoplastic polymers. Progress in Polymer Science, 30(12), 1185-1222.

Papathanasiou, T. D. (1997). Flow-induced alignment in injection molding of fiber-reinforced polymer composites. Flow-induced alignment in composite materials, 112.

Papathanasiou, T. D., Ingber, M. S., & Guell, D. C. (1995). Stiffness enhancement in aligned, short-fibre composites: a computational and experimental investigation. Composites science and technology, 54(1), 1-9.

Phan-Thien, N., Fan, X. J., Tanner, R. I., & Zheng, R. (2002). Folgar–Tucker constant for a fibre suspension in a Newtonian fluid. Journal of Non-Newtonian Fluid Mechanics, 103(2), 251-260.

Phelps, J. H., & Tucker, C. L. (2009). An anisotropic rotary diffusion model for fiber orientation in short-and long-fiber thermoplastics. Journal of Non-Newtonian Fluid Mechanics, 156(3), 165-176.

Ross, R. F., & Klingenberg, D. J. (1997). Dynamic simulation of flexible fibers composed of linked rigid bodies. The Journal of chemical physics, 106(7), 2949-2960.

Sanou, M., Chung, B., & Cohen, C. (1985). Glass fiber- filled thermoplastics. II. Cavity filling and fiber orientation in injection molding. Polymer Engineering & Science, 25(16), 1008-1016.

Schmid, C. F., Switzer, L. H., & Klingenberg, D. J. (2000). Simulations of fiber flocculation: Effects of fiber properties and interfiber friction. Journal of Rheology (1978-present), 44(4), 781-809.

Sepehr, M., Ausias, G., & Carreau, P. J. (2004 a). Rheological properties of short fiber filled polypropylene in transient shear flow. Journal of Non-Newtonian Fluid Mechanics, 123(1), 19-32.

Sepehr, M., Carreau, P. J., Grmela, M., Ausias, G., & Lafleur, P. G. (2004 b). Comparison of rheological properties of fiber suspensions with model predictions. Journal of polymer engineering, 24(6), 579-610.

Sepehr, M., Carreau, P. J., Moan, M., & Ausias, G. (2004 c). Rheological properties of short fiber model suspensions. Journal of Rheology (1978-present), 48(5), 1023-1048.

Shen, S. F. (1984). Simulation of polymeric flows in the injection moulding process. International journal for numerical methods in fluids, 4(2), 171-183.

Silva, L. (2004). Viscoelastic compressible flow and applications in 3D injection molding simulation. Mines Paristech, Paris, Phd Thesis.

Singh, P., & Kamal, M. R. (1989). The effect of processing variables on microstructure of injection molded short fiber reinforced polypropylene composites. Polymer composites, 10(5), 344-351.

Wang, G., Yu, W., & Zhou, C. (2006). Optimization of the rod chain model to simulate the motions of a long flexible fiber in simple shear flows. European Journal of Mechanics-B/Fluids, 25(3), 337-347.

Wang, J., O'Gara, J. F., & Tucker III, C. L. (2008). An objective model for slow orientation kinetics in concentrated fiber suspensions: Theory and rheological evidence. Journal of Rheology (1978-present), 52(5), 1179-1200.

Weidenfeller, B., Höfer, M., & Schilling, F. R. (2004). Thermal conductivity, thermal diffusivity, and specific heat capacity of particle filled polypropylene. Composites Part A: applied science and manufacturing, 35(4), 423-429.

Yamamoto, S., & Matsuoka, T. (1993). A method for dynamic simulation of rigid and flexible fibers in a flow field. The Journal of chemical physics, 98(1), 644-650.

Yamamoto, S., & Matsuoka, T. (1994). Viscosity of dilute suspensions of rodlike particles: A numerical simulation method. The Journal of chemical physics, 100(4), 3317-3324.

Yamamoto, S., & Matsuoka, T. (1995). Dynamic simulation of fiber suspensions in shear flow. The Journal of chemical physics, 102(5), 2254-2260.

Yamamoto, S., & Matsuoka, T. (1996). Dynamic simulation of microstructure and rheology of fiber suspensions. Polymer Engineering & Science, 36(19), 2396-2403.

.

General conclusions and prospects

1. Conclusions

The work undertaken has provided an in-depth analysis of processing-microstructure-properties relationships in injection moulding of natural fibre-reinforced polypropylene. This type of composites are quickly developing and have several advantages compared to glass fibre based composites such as lower density, reduced environmental foot print and low cost. We have conducted our work with two types of cellulose-based fibres, Tencel and flax which have different intrinsic structures: flax is a mixture of semi-rigid thin elementary fibres and thick rigid bundles and Tencel is thin elementary flexible fibre. Classical rigid glass fibres were also used for comparison. A variety of experimental techniques has been used and some were developed to assess the microstructure and mechanical and rheological properties of composites. A simulation of the filling stage during injection moulding has been performed, enabling to compare the predicted pressure and fibre orientation with those experimentally obtained. A summary of the main results obtained is presented below.

1- Influence of compounding and injection on fibre size distribution

The influences of compounding and injection moulding have revealed the dissimilarities in fibre breakage between glass, flax and Tencel fibres. Glass fibres, which are rigid rods, are submitted to large breakage during compounding and an additional slight breakage during injection moulding. For Tencel fibres, which are individual and flexible, their length after processing is shortened by 30 % and fibres break more with the increase of fibre content. For flax fibres, both length <u>and</u> diameter are reduced during processing, but the resulting aspect ratio remains almost unchanged when compared to its initial value. Some bundles persist even after injection moulding, giving an aspect ratio lower than those of glass and Tencel fibres, despite that the length of flax fibres is higher than that of Tencel. This bundle's structure is a

specific feature of a typical natural fibre, which leads to a different rupture mechanism during processing compared to glass fibres.

2- Microstructure of Tencel and flax composites

A novel experimental approach has been developed to study in details the microstructure of the injection moulded flax and Tencel reinforced polypropylene. Cross-sections parallel to the part plane (*xy*-plane) were analysed by optical microscopy in reflection mode and image analysis for several levels in the thickness.

Depending on their apparent shapes, fibres were classified into four categories: straight, C-shaped, S-shaped and short particles or out-of-plane fibres. We demonstrated that because of flexibility difference between flax and Tencel (flexibility being proportional to aspect ratio over Young's modulus), Tencel fibres can be bent in two conformations: C-shaped and S-shaped, whereas elementary flax fibres are bent only in C-shaped conformation. We showed that as in glass fibres based composites, flax and Tencel composites generally show a core-shell structure where fibres are aligned along the main flow direction near the surface and perpendicular to it in the core.

Some differences between flax and Tencel fibres in terms of the spatial distribution and bending conformation were identified. The number of Tencel fibres is three times larger than that of flax for the same volume concentration. This was explained by the presence of bundles in flax containing several elementary fibres "glued together" that remained after processing. Moreover, as for glass fibres, the concentration of flax increases from surface to core, while Tencel concentration is practically independent on thickness.

3- Composite rheological properties

The dynamic rheological measurements have shown that the increase of fibre content and flexibility (case of Tencel) lead to enhanced complex viscosity and viscous and elastic moduli. An apparent yield stress was recorded at low frequencies when fibre volume fraction reaches the concentrated regime. This is due to fibre-fibre interactions which become more pronounced as the fibre content increases, and they are further increased when fibre flexibility increases. For the same volume fraction, because of the larger number of fibres and their high flexibility, Tencel-based composites show a viscosity and an apparent yield stress that are

moderately higher than those of the glass based composites and further higher than of the flax ones.

The influence of temperature on composite viscosity was analysed using Arrhenius law, enabling the calculation of composite activation energy. For the three types of composites, the activation energy increases as the fibre content increases. Adding fibres to polypropylene seems to increase composite "resistance" to flow. Tencel composites exhibit higher activation energy compared to flax and glass ones. We suggest that additional restrictions of polymer chains motion may be caused by the strong network-like structure of flexible fibres. The superposition dynamic/capillary rheology obeyed the Cox-Merz approximation. The overall curves including dynamic and capillary measurement were fitted with the yield stress Carreau-Yasuda model. The obtained data, which give the viscosity evolution throughout a large range of shear rate, are important input for the simulation of the pressure during injection and of the fibre orientation within the filling stage.

4- Composite tensile properties

The influence of the microstructure on composite tensile properties was investigated by testing specimen cut-out in the moulded part at different angles with respect to the main flow direction. Samples aligned with the main flow direction exhibit larger tensile performance compared to those oriented at 45° and 90°, for all studied composites. All glass-based composites with different fibre concentrations are stiffer and stronger compared to flax and Tencel composites. Tencel composites show higher elongation at break compared to glass and flax. Cox-Krenchel and Kelly-Tyson models were used to analyse composites tensile stiffness and strength using orientation factors that were calculated on the basis of experimentally obtained fibre orientation. Some deviations occurs when predicting the tensile properties along the main flow direction, which were associated to the inaccuracy of the fibre strength values, the out-of-plane fibre orientation, the fibre bending and the skin fibre-free-layers.

5- Composite impact properties

The investigation of composites' impact properties showed that Tencel based composites have the highest impact strength compared to glass and flax reinforced composites. This was interpreted by the well-developed network of Tencel fibres because of their largest number and flexibility. The analysis of the impact strength was performed using Thomason and Vlug

model; it was demonstrated that the predicted impact strength fits well the experimental and high concentration but deviation occurs at low concentrations.

6- Analysis of pressure during injection: experiment vs model prediction

Pressure evolution during injection was measured and calculated using Rem3D® software. The experimental analysis of the pressure involved during the injection moulding cycle showed that higher melt viscosity (due to the increase in either fibre concentration or fibre aspect ratio or flexibility) increased the pressure in the cavity. The range of the pressure increase is close to that of viscosity when fibre content gets larger. The pressure during the filling stage, predicted with Rem3D® software, matches experimental pressure with a deviation mostly at the start-up of the pressure evolution, for neat polypropylene and over all studied composites. This error is reduced when the melt progresses into the cavity for the neat polypropylene and for all the studied composites. The deviation was explained by the inaccuracy of the thermal parameters required for setting-up the calculations.

7- Fibre orientation: theoretical prediction vs experiment

The prediction of glass fibre orientation after filling performed with Rem3D® fits well the experimental one, except in the core layer where the fibre alignment is overestimated. The errors were related to thermal conditions set-up in the model, but the orientation model itself may be questionable.

The prediction of the orientation of flax and Tencel fibres in the moulded part was carried out. The goal was to examine if rigid fibres' model can predict the orientation of both types of natural fibres which have very different structure compared to rigid glass fibres. Considering that flax fibres contain rigid bundles, we found that their predicted orientation approximately matches the experimental results; an accurate set-up of the calculation parameters would bring improvements to the obtained orientation. The predicted orientation of Tencel fibres is extremely far from what was obtained in experiment. Tencel fibres are very flexible and their behaviour during the flow cannot be modelled by a typical rigid fibres model. Therefore, a flexible fibre model is required for Tencel based composites to reach adequate orientation results.

2. Prospects

Because this work is one of the first investigations of the microstructure of natural fibre reinforced composites and its correlation with composite processing and properties, a lot of points still need clarifications.

1. In our study a semi-automated method was used to quantify the microstructure across the thickness of the injection moulded part. Development of a fully automated image analysis of fibre size and orientation would enormously help in reducing this time-consuming experimental work. X-ray microtomography will be also a possibility, if applicable to fibres whose contrast regarding the matrix is low.

2. We demonstrated that cellulosic fibres are broken during compounding and injection moulding. Despite some progress in the understanding of the mechanisms of fibres breakage during processing (work in Cemef using rheo-optics), some questions remain opened. For example, till now, there is no clear answer on what is the main parameter controlling fibre rupture: is it specific mechanical energy, or cumulated strain, or a combination of both? Does it depend on fibre type and flexibility? These answers are needed to predict fibre sizes in the final composite.

3. A simple sprue-gated box was used in this work for the analysis of the microstructure of Tencel and flax based composites. Other mould and gate geometries need to be used to confirm (or not) the results obtained and to reach further advance in the understanding of natural fibre composite microstructure.

4. The experiments that we conducted were with unique injection moulding conditions. Nothing is known about their influence (flow rate, mould temperature, packing parameters) on the microstructure of natural fibre reinforced composites. These studies would open-up discussions and comparison with the results known for glass fibre based composites.

5. We performed the analysis of composites microstructure and structure-properties correlations for two types of fibres, flax and Tencel. This work should be extended to other types of cellulosic fibres. For example, the results obtained on Tencel should be checked on cotton fibres that are also based on pure cellulose and are flexible elementary fibres. The results obtained on flax should be checked on hemp or sisal that are similar to flax with semi-rigid elementary fibres and bundles.

6. To predict the orientation of natural fibres within an injected part we used Rem3D® software that is developed for rigid fibres. We demonstrated that it does not work for Tencel fibres. Thus numerical modelling of microstructure during injection of composites based on fibres with different flexibility and different diameters is strongly needed, if willing to further develop natural fibre reinforced composites. This is not an easy task that should be undertaken step by step from simple to complex cases.

Injection de Polypropylène Renforcé de Fibres Naturelles : Procédé, Microstructure et Propriétés

Resumé. Les fibres naturelles sont une alternative aux fibres de verre pour renforcer les polymères. Lors de la mise en œuvre par injection, la taille, l'orientation et la distribution de fibres évoluent en fonction de l'écoulement, et cela conditionne les propriétés des pièces injectées. L'objectif de cette thèse est de caractériser la microstructure de composites à base de deux types de fibres, le lin et Tencel, et d'établir une corrélation avec leurs propriétés.

Les fibres et matrice ont été mélangés en extrusion bivis et les composites obtenus injectés. La rupture de fibres est plus importante lorsque leur concentration augmente. La casse est principalement pendant la phase de mélange. Une nouvelle approche de caractérisation permettant la quantification des orientation, distribution et courbure de fibres a été développée. Les composites présentent une structure cœur-peau dans l'épaisseur de la pièce injectée. Les propriétés rhéologiques des composites ont été étudiées en modes dynamique et capillaire. Les fibres Tencel, qui sont les plus flexibles, conduisent à une augmentation plus grande des viscosités, modules et seuil d'écoulement. Les propriétés mécaniques en traction et au choc ont été déterminées dans des éprouvettes prélevées dans des boites injectées avec différentes orientation par rapport à l'axe d'écoulement. Les propriétés d'impact des composites à fibres Tencel sont supérieures à celles à base de lin et de verre. Des modèles ont été testés en prenant en compte l'orientation de fibres. Lors des campagnes d'injection, les pressions sur des capteurs situés dans la cavité ont été mesurées. Les pressions calculées avec le logiciel Rem3D$^®$ sont en assez bon accord avec la mesure. Le modèle d'orientation de fibre rigide utilisé dans Rem3D$^®$ donne des résultats corrects pour les fibres de lin, mais il s'est avéré inapproprié pour prédire l'orientation des fibres Tencel extrêmement flexibles.

Ce travail est réalisé dans le cadre de la Chaire Industrielle Bioplastiques financée par Mines ParisTech et Arkema, l'Oréal, Nestlé, PSA et Schneider Electric.

Mots clefs : fibres naturelles, composites, rhéologie, injection, microstructure, modélisation

Injection Moulding of Natural Fibre Reinforced Polypropylene: Process, Microstructure and Properties

Abstract. Natural fibres are an alternative to glass fibres for reinforcing polymers. During injection, fibre size, orientation and distribution evolve as a function of flow and determine composite properties. The goal of this thesis is to characterize the microstructure of composites based on two types of fibres, flax and Tencel, and to correlate with composite properties.

The composites were prepared by extrusion and injection. Fibre rupture was higher at higher fibre concentrations. There was practically no breakage during injection. A new approach allowing quantification of fibre orientation, distribution and curvature was developed. The composites with cellulosic fibres have core-skin structure along the part thickness. The rheological properties of composites were studied in dynamic and capillary modes. Tencel fibres, which are the most flexible, showed the highest viscosity, moduli and yield stress. Tension and impact were measured for samples cut from the moulded part at different orientations towards the main flow direction. Impact properties of Tencel-based composites were the highest compared to flax and glass fibre composites. Models taking into account fibre orientation were tested. Pressure in the mould during injection was recorded. Pressure calculated with Rem3D$^®$ software showed a reasonable agreement with the experiment. Modelling of fibre orientation with Rem3D$^®$ gave results comparable with experiment for flax but turned out to be not applicable for Tencel which are flexible.

The work was performed within the Industrial Chair in Bioplastics supported by MINES ParisTech and Arkema, L'Oréal, Nestlé, PSA and Schneider Electric.

Key-words: Natural fibres, composites, rheology, injection, microstructure, modelling.